Erasmus+

Erasmus+

TL-IRMP

A book "Applications of ionizing radiation in materials processing" has been published within the Erasmus+ program on "Cooperation for innovation and the exchange of good practices – Strategic Partnerships for higher education". It is a result of the Erasmus project (TL-IRMP) on the "Joint innovative training and teaching/ learning program for enhancing the development and transfer of knowledge on the application of ionizing radiation in materials processing". Seven institutions have participated in this program. This book was reviewed by Anthony Berejka, consultant to the IAEA on the effects of ionizing radiation on materials, reviewer for the US National Academies of its publication "Radiation source use and replacement" and for its operating arm, the National Research Council, of standards laboratories; co-founder and Past-President of the Council on Ionizing Radiation Standards and Measurements and of RadTech International North America, having over 42 years of industrial experience in radiation processing including conducting technology assessments for industrial companies.
This book is co-funded by the Polish Ministry of Science and Higher Education.

APPLICATIONS OF IONIZING RADIATION IN MATERIALS PROCESSING

edited by
Yongxia Sun and Andrzej G. Chmielewski

VOLUME 1

INSTITUTE OF NUCLEAR CHEMISTRY AND TECHNOLOGY

WARSZAWA 2017

iPCB ISTITUTO PER I POLIMERI COMPOSITI E BIOMATERIALI

ktu kaunas university of technology 1922

ichtj

HACETTEPE UNIVERSITY

UNIVERSITÉ DE REIMS CHAMPAGNE-ARDENNE

PETRU PONI INSTITUTE

Erasmus+

APPLICATIONS
OF IONIZING RADIATION
IN MATERIALS PROCESSING

edited by

Yongxia Sun and Andrzej G. Chmielewski

VOLUME 1

Institute of Nuclear Chemistry and Technology

Warszawa 2017

Istituto per i Polimeri, Compositi e Biomateriali, Consiglio Nazionale delle Ricerche

Kaunas University of Technology

Institute of Nuclear Chemistry and Technology

Università degli Studi di Palermo

Hacettepe University

Université de Reims Champagne-Ardenne

"Petru Poni" Institute of Macromolecular Chemistry

CONTENTS

PREFACE

"Applications of ionizing radiation in materials processing" is a result of the project "Joint innovative training and teaching/learning program in enhancing development and transfer knowledge of application of ionizing radiation in materials processing" (acronym: TL-IRMP, Agreement number 2014-1-PL01-KA203-003611), which is within the framework of the Erasmus+ program "Cooperation for innovation and the exchange of good practices – Strategic Partnerships for higher education". This book is co-funded by the Polish Ministry of Science and Higher Education. Twenty seven professors and researchers from seven organizations in six countries (Poland, Italy, Lithuania, Romania, Turkey and France) have contributed to this book. The text of each chapter was first internally reviewed amongst the authors, and then it was given a global review by Anthony J. Berejka who is familiar with the effects of ionizing radiation on materials and its use in commercial processes. Mr. Berejka also smoothed out the language of the book using his professional style of scientific English, his native language.

This book consists of two volumes. It starts with the basic theory of radiation and its interactions with materials, and then goes into the radiation chemistry of liquid and solid systems, radiation-induced grafting, crosslinking, polymerization, polymer degradation and oxidation. Analytical methods for characterization of irradiated materials and applications of radiation processing to polymers are then covered. The text ends with opportunities for future developments in radiation processing. This book can be used as teaching material in material science or engineering by university professors, or as a self-learning material by students. It is also very useful for materials scientists, chemical engineers, chemistry students, or for anyone else interested in material processing technologies.

Assoc. Prof. Yongxia Sun, Ph.D., D.Sc.
Project coordinator of TL-IRMP

BASIC RADIATION PHYSICS AND SOURCES OF RADIATION

Diana Adlienė
Kaunas University of Technology, Physics Department, Studentų g. 50,
LT-51368 Kaunas, Lithuania

1. INTRODUCTION

Treatment of materials and products with radiation in order to modify their physical, chemical and biological properties is defined as radiation processing of materials. Radiation processing can be controlled and used for the development of the novel materials and products with desirable properties.

The knowledge of the basic radiation physics, including the structure of matter, elements of nuclear physics, the nature of electromagnetic radiation, and radiation interaction with matter is required to understand irradiation processing and its potential in material sciences.

1.1. CLASSIFICATION OF RADIATION

Radiation-induced changes in materials depend on the origin and type of radiation and the deposited energy (Fig.1).

Energy deposition processes in turn depend on the origin of the radiation:
- particulate radiation, including electrons, positrons, protons, neutrons, ions;
- electromagnetic radiation, which covers a broad wavelength range, including infrared, visible and ultraviolet radiation and X-rays and gamma rays.

The following Table 1 gives approximate wavelengths, frequencies, and energies for selected regions of the electromagnetic spectrum.

Deposition of kinetic energy of accelerated particles in a target is considered when discussing the interaction of particulates with matter. In the case of electromagnetic radiation, interaction with matter, in general, energy transferred by the individual quanta, known as photons, is taken into account. The energy of photon (quantum energy), E, is given by:
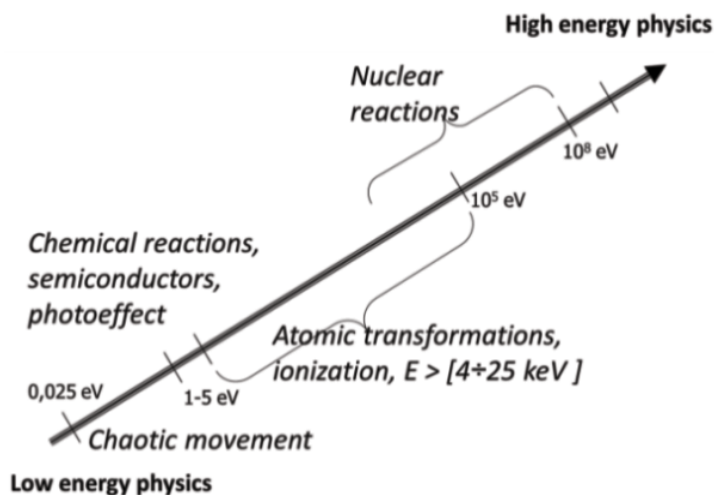
Fig.1. Comparison of energies.

Table 1. Spectrum of the electromagnetic radiation.

Wave region	Wavelength [m]	Frequency [Hz]	Energy [eV]
Radio	> 0.1	$< 3 \times 10^9$	$< 10^{-5}$
Microwave	$0.1\text{-}10^{-4}$	$3 \times 10^9\text{-}3 \times 10^{12}$	$10^{-5}\text{-}0.01$
Infrared	$10^{-4}\text{-}7 \times 10^{-7}$	$3 \times 10^{12}\text{-}4.3 \times 10^{14}$	0.01-2
Visible	$7 \times 10^{-7}\text{-}4 \times 10^{-7}$	$4.3 \times 10^{14}\text{-}7.5 \times 10^{14}$	2-3
Ultraviolet	$4 \times 10^{-7}\text{-}10^{-9}$	$7.5 \times 10^{14}\text{-}3 \times 10^{17}$	$3\text{-}10^3$
X-rays	$10^{-9}\text{-}10^{-13}$	$3 \times 10^{17}\text{-}3 \times 10^{21}$	$10^3\text{-}10^7$
Gamma rays	$< 10^{-11}$	$> 3 \times 10^{19}$	$> 10^5$
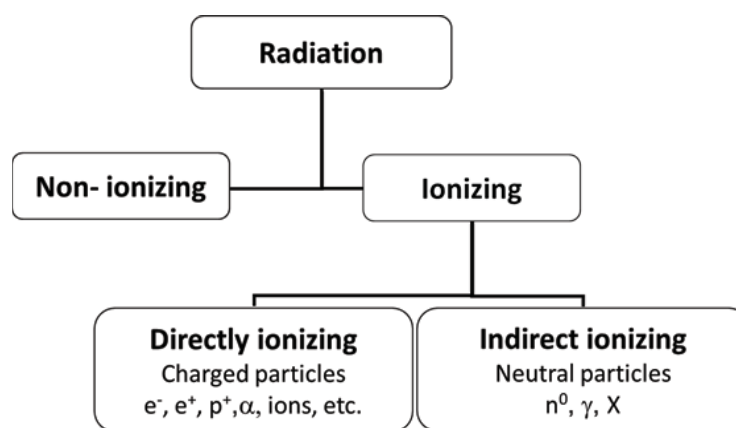
Fig.2. Classification of radiation.

$$E = h\nu = h\frac{c}{\lambda} \tag{1}$$

where: the constant h is known as Planck's constant, ν – a frequency, c – a speed of light in vacuum, λ – wavelength.

Radiation is classified in two main categories, non-ionizing and ionizing radiation depending on its ability to ionize matter (Fig.2):

- Direct ionizing radiation corresponds to the energy deposition in the material by energetic charged particle which have Coulomb interaction with an orbital electron of a target atom.
- Indirect ionizing radiation is realized in two steps. First, fast charged particles (electrons and positrons) are released in the material due to the photon energy deposition or due to kinetic energy deposition by neutrons, protons or heavier ions. Second, the released charged particles deposit their energy directly in the material through Coulomb interactions between these particles and orbital electrons of an atom.

2. ATOMIC AND NUCLEAR STRUCTURE

2.1. BASIC DEFINITIONS FOR ATOMIC STRUCTURE

The atom is composed of a central nucleus surrounded by a cloud of negatively charged electrons. An atomic nucleus consists of Z protons, and N neutrons. The main characteristics of the constituents of an atom are shown in Table 2.

Table 2. Main characteristics of the atom constituents.

Particle	Symbol	Mass [kg]	Energy [MeV]	Charge
Proton	p	1.672×10^{-27}	938.2	+
Neutron	n	1.675×10^{-27}	939.2	0
Electron	e	0.911×10^{-30}	0.511	–

The radius of an atom is $\sim 10^{-10}$ m, the radius of the nucleus is about 10^{-14} m.

Protons and neutrons are commonly referred to as nucleons.

The number of protons in atom is known as the atomic number, Z. It equals the number of electrons in a non-ionized atom, thus making an atom neutral.

Atomic mass number, A, equals to the number of protons plus neutrons in the nucleus.

Atomic mass, M, might be expressed in mass units – g or in atomic mass units – u, where u is equal to 1/12 of the mass of the ^{12}C atom or 931.5 MeV/c².

Some binding energy is required to keep the nucleons within the nucleus. Thus the atomic mass of particular nuclide is smaller than the sum of the individual masses of constituent particles.

Number of atoms, N_a, per mass of an element is:

$$\frac{N_a}{m} = \frac{N_A}{A} \tag{2}$$

where N_A is Avogadro's number ($N_A = 6.022 \times 10^{23}$ atoms/g-atom).

Number of electrons, N_e, per mass of element is:

$$\frac{N_e}{m} = Z\frac{N_a}{m} = \frac{Z}{A}N_A \tag{3}$$

Number of electrons, N_e, per volume, V, of an element is:

$$\frac{N_e}{V} = \rho Z\frac{N_a}{m} = \rho Z\frac{N_A}{A} \tag{4}$$

In nuclear physics, a nucleus X with atomic mass number A and atomic number Z is denoted as $^A_Z X$, for example $^{60}_{27}Co$ and $^{137}_{55}Cs$.

An atomic nucleus identified by its atomic element and its mass number is defined as nuclide.

Atoms having an identical atomic number, Z, but different atomic mass numbers, A, related to different numbers of neutrons in the nucleus are called isotopes of a given element, for example: $^{11}_6C$, $^{12}_6C$, $^{13}_6C$, $^{14}_6C$.

In ion physics it is usual to provide ions with superscripts +/–. For example, $^4_2He^{2+}$ stands for a doubly ionized He atom which is the alpha particle [1].

2.2. ATOMIC STRUCTURE

The currently accepted simplified atom model relies on the 1913 Bohr theory [2, 3] and his famous postulates that combine classical non-relativistic mechanics with quantum mechanics adding the concept of angular momentum quantization. A variety of postulated formulations (physical content being the same) are provided in the literature [4-6]. Here is a summary of Bohr's postulates, as noted in Ref. [7]:

• Postulate 1: Electrons revolve about the Rutherford nucleus in well-defined, allowed orbits (planetary-like motion):

$$F_{coul} = \frac{1}{4\pi\varepsilon_0}\frac{Ze^2}{r_e} \equiv F_{cent} = \frac{m_e v_e^2}{r_e} \tag{5}$$

• Postulate 2: While in orbit, the electron does not lose any energy despite being constantly accelerated (no energy loss while electron is in an allowed orbit).

- Postulate 3: The angular momentum $L = m_e vr$ of the electron in an allowed orbit is quantized and given as $L = n\hbar$, where n is an integer referred to as a principal quantum number, $\hbar = h/2\pi$ and h is Planck's constant.
- Postulate 4: An atom emits radiation only when an electron makes a transition from the initial orbit with a quantum number n_i to final orbit with a quantum number n_f (energy emission during orbital transitions).

$$h\nu = E_i - E_f \tag{6}$$

Electron transitions result in the emission of photons. The wavenumber k of the emitted photon is given by:

$$k = \frac{1}{\lambda} R_\infty \left(\frac{1}{n_f^2} - \frac{1}{n_i^2} \right) \equiv 109737 \text{ cm}^{-1} Z^2 \left(\frac{1}{n_f^2} - \frac{1}{n_i^2} \right) \tag{7}$$

where R_∞ is the Rydberg constant.

The radius r_n of one-electron Bohr atom is given by:

$$r_n = a_0 \left(\frac{n^2}{Z} \right) = 0.529 \text{ Å} \left(\frac{n^2}{Z} \right) \tag{8}$$

where $a_0 = 0.529$ Å is the Bohr's radius.

The energy levels for orbital electron shells in one-electron atomic structure are given by:

$$E_n = -E_R \left(\frac{Z}{n} \right)^2 = -13.6 \text{ eV} \left(\frac{Z}{n} \right)^2 \tag{9}$$

where: E_R – the Rydberg energy, n – the principal quantum number (n = 1, ground state, n > 1, excited state), Z – atomic number of one-electron atomic structure.

An energy level diagram for the hydrogen (H) atom is shown in Fig.3A.

Bohr's theory works well for one-electron structures (hydrogen atom, singly ionized helium atom and doubly ionized lithium atom, *etc.*), but it does not apply directly to multi-electron atoms because of the repulsive Coulomb interactions among the atomic electrons. Development of the theory of quantum mechanics by Heisenberg, Schrödinger, Dirac, Pauli and others, contributed significantly to the explanation of possible energy levels (states) that might be occupied by electrons in a multi-electron atom. In this theory, individual energy states are defined by four quantum numbers as follows [8]:

- the principal quantum number, n, which specifies the ground (main) energy shell and can take integer values;
- the azimuthal quantum number, l, which specifies the total rotational angular momentum for the electron and can take integer values between 0 and n − 1;
- the magnetic quantum number, m, which specifies a component of the angular momentum and can take integer values between –l and +l;
- the spin quantum number, s, which specifies a component of the spin angular momentum of the electron and takes values –½ or +½.
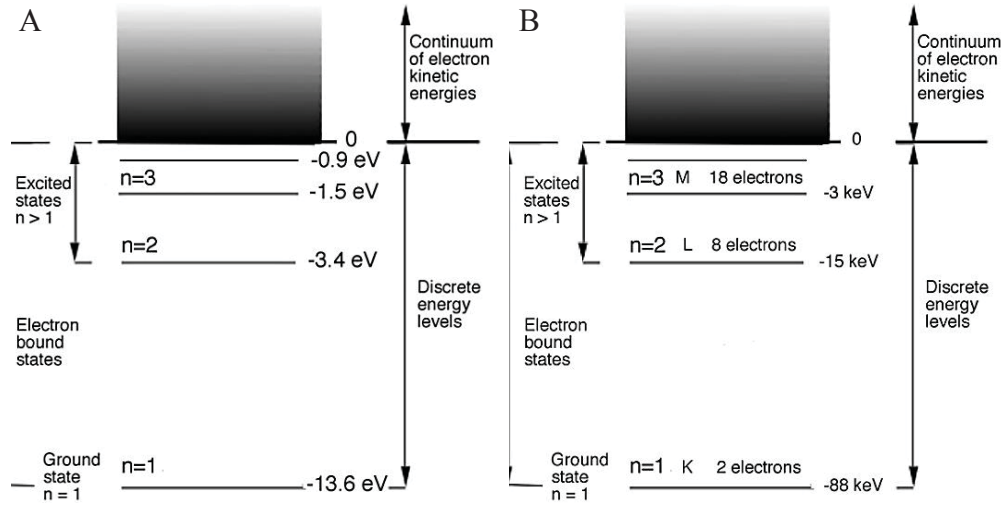
Fig.3. Energy level diagrams: A – for a hydrogen atom, B – for a lead atom. (Adapted from Ref. [7]).

Electrons occupy allowed shells; however, the number of electrons per shell according to the Pauli exclusion principle is limited to $2n^2$.

The distribution of energy levels in a multi-electron atom (Pb) is shown in Fig.3B.

The energy levels associated with the various electron orbits (not drawn to scale) increase with Z and decrease with quantum number n and the average distance from the nucleus. The outer electronic shell (the valence shell) determines the chemical properties of the element. The energy bands associated with n = 1, 2, 3, *etc.*, are known as the K, L, M, *etc.*, bands. The structure of each band arises from small differences in energy associated with both the l and s quantum numbers.

In a multi-electron atom, inner shell electrons are bound with much larger energies E_n than E_R in single-electron model: $E_n = -E_R(Z^2_{eff}/n^2)$, and the corresponding atomic radius is: $r_n = a_0(n^2/Z_{eff})$, where Z_{eff} is the effective atomic number, given by $Z_{eff} = Z - s_c$, with s_c as the screening constant, which equals to 2 for K-shell electrons.

There are two main processes when an electron is removed from a given shell in the atom: excitation and ionization. Both of them occur within the atom through various possible interactions (energy transition) which will be discussed in Chapter 2.

Excitation of an atom is present when an electron is moved from a given shell to a higher n shell which is empty or is not filled by corresponding number of electrons. Excitation energy (excitation potential) is a minimum energy required to excite an atom from its ground state to a higher state (Fig.4A).

Ionization of an atom occurs when an electron is removed from the atom (a certain amount of energy is transferred to the electron which is sufficient to
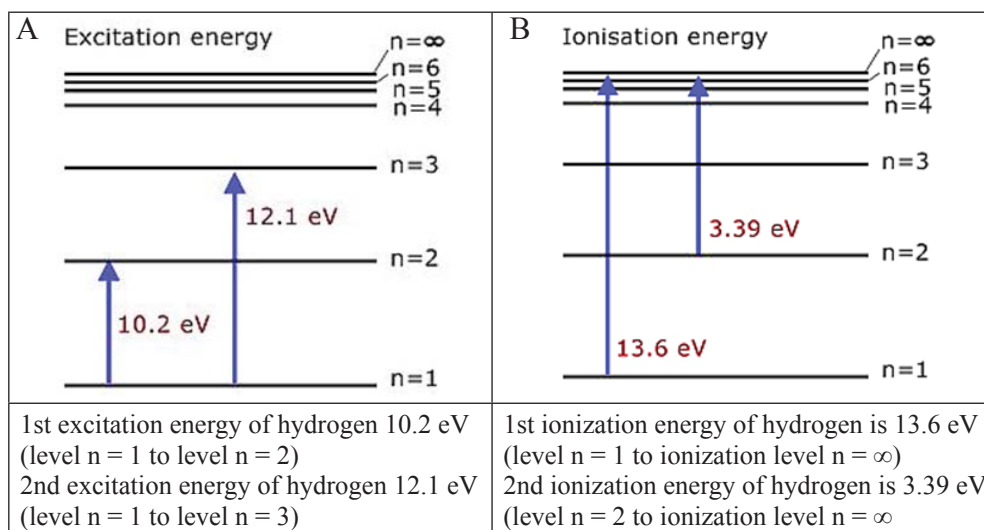
Fig.4. Excitation scheme (A) and ionization scheme (B) of hydrogen atom.

overcome its binding energy in the shell). Ionization energy (ionization potential) is a minimum energy required to release electron from atom or ion (Fig.4B).

An orbital electron from a higher n shell will fill the electron vacancy in a lower n atomic shell. The energy difference between two shells will be either emitted as a (fluorescent) photon or it will be transferred to the higher n-shell electron, which will be ejected from the atom as an Auger electron.

The minimum energy required to ionize the atom (ionization potential) ranges from a few (alkali elements) to 24.5 eV (helium) [9].

2.3. NUCLEAR STRUCTURE

Most of the mass of an atom is concentrated in the atomic nucleus, consisting of Z protons and $N = (A - Z)$ neutrons and having radius:

$$r = r_0 \sqrt[3]{A} \tag{10}$$

where r_0 is a constant (~1.4 fm) assumed equal to ½ of r_e, the classical electron radius.

The constituents of the nucleus, protons and neutrons (nucleons), are bound in the nucleus with a strong force. This short-range (10^{-15} m) force exceeds not only the long-range electromagnetic force between charged nucleons (protons), which is repulsive and tends to disrupt the nucleus, but also other known natural forces (gravitational, weak interaction) by several orders of magnitude and holds different nucleons (protons-neutrons) together in the nucleus. The energy associated with the strong force is called binding energy.
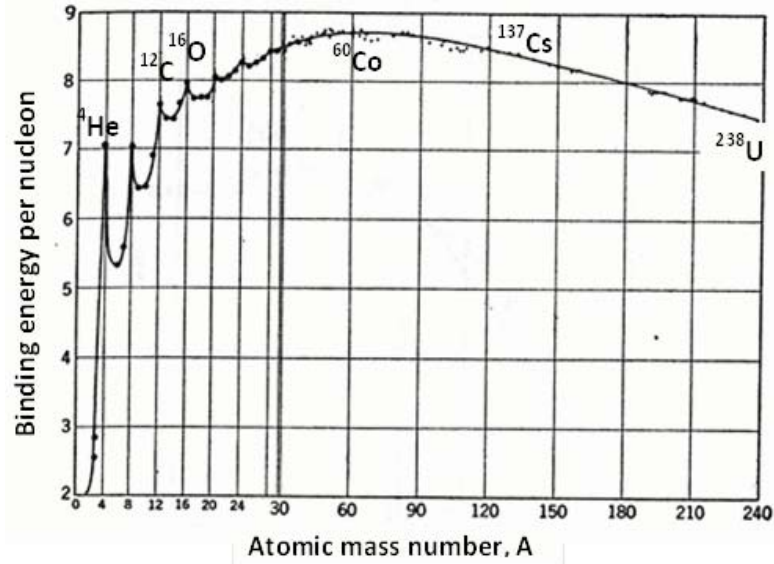
Fig.5. Binding energy per nucleon for different elements. (Adapted from Ref. [10]).

The binding energy per nucleon, E_B/A, in a nucleus varies gradually with the number of nucleons, A (Fig.5). It may be calculated from the energy equivalent of the mass deficit (defect), Δ_m, of a given nucleus as:
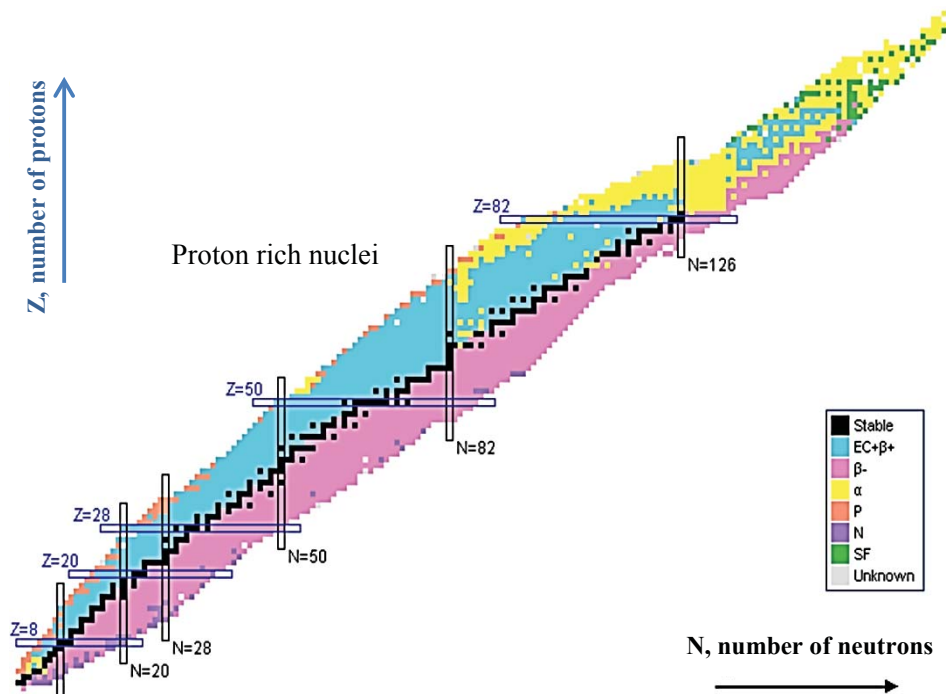
Fig.6. Nuclear stability chart. The stability line is indicated in black. (Adapted from Ref. [11]).

$$\frac{E_B}{A} = \frac{\Delta mc^2}{A} = \frac{Zm_pc^2 + (A - Z)m_nc^2 - Mc^2}{A} \qquad (11)$$

where: M – the nuclear mass, expressed in atomic mass units – u ($Mc^2 = 931.5$ MeV); m_pc^2 – the proton rest energy; m_nc^2 – the neutron rest energy.

A stable nucleus has enough binding energy to hold the nucleons together permanently. There is no basic relation between the atomic mass number A and atomic number Z of a nucleus, but an empirical relationship:

$$Z = \frac{A}{1.98 + 0.0155A^{2/3}} \qquad (12)$$

gives a good approximation for a stable nucleus.

Strong nuclear forces and the associated binding energy in the nucleus determine the stability of the nucleus (balance of protons and neutrons). Too many neutrons or too many protons upset this balance disrupting the binding energy of the strong nuclear forces making the nucleus unstable (Fig.6).

3. NUCLEAR TRANSFORMATIONS

The nuclear transformations (transmutations) play a significant role in the development of new materials. Materials in which nuclear transformation processes take place are known as natural radiation sources. They represent a powerful tool for radiation-induced modification of materials (especially in nuclear energy and in the biomedical field), since the result of every transmutation process is an energy release [12]. Nuclear transmutation energy is released as:
- Kinetic energy of the product particles.
- Almost immediate emission of very high energy photons, *i.e.* prompt gamma rays, or it is a postponed energy release through gamma decay to the ground state of the nucleus, which is present, when nucleus is firstly transformed to a metastable state.
- A small amount of energy may also emerge in the form of X-rays. (Generally, the product nucleus has a modified atomic number, so the configuration of its electron shells is destroyed. As the electrons rearrange themselves and drop to lower energy levels, X-rays, due to internal transitions, may be emitted).
   There are four major types of nuclear transmutation [4]:
- Radioactive decay, in which nuclei spontaneously eject one or more particles and lose energy to become the nuclei of lighter atoms. Examples are alpha, beta and gamma decays.
- Fission, which is the splitting of a nucleus into two "daughter" nuclei, *e.g.* $n + {}^{235}_{92}U \rightarrow {}^{236}_{92}U \rightarrow {}^{141}_{56}Ba + {}^{92}_{36}Kr + 3n$.

- Fusion of two parent nuclei into one daughter nucleus, *e.g.* $^1_1N + {}^1_1N \rightarrow {}^2_1N$ + $e^+ + \nu_e$, where ν_e stands for (electron) neutrino – which is an elementary particle holding no electrical charge, travelling at nearly the speed of light, and passing through ordinary matter with virtually no interaction.
- Neutron capture, in which the nuclear charge (Z, the atomic number) is unchanged, the nuclear mass (A = number of protons + neutrons, the atomic mass) increases by one, and the number of neutrons (N) increases by one.

The simplified overview of nuclear transmutations is provided in Fig.7.
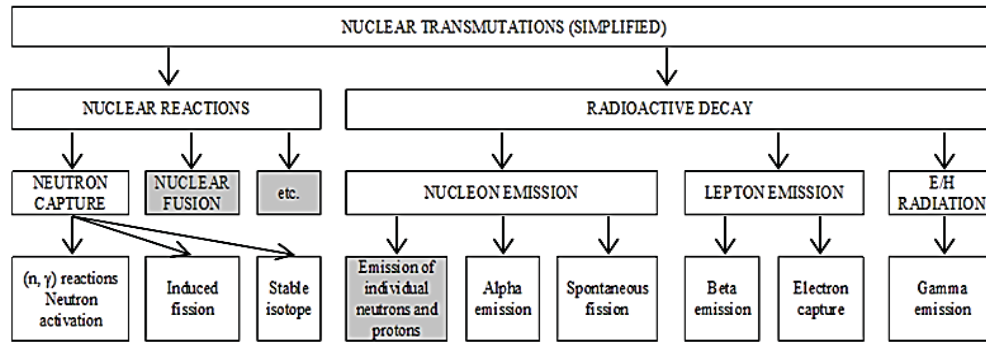
Fig.7. Nucler transmutation processes. Processes indicated in gray boxes are not considered for discussion in this book.

3.1. RADIOACTIVITY

Radioactivity is a process characterized by a transformation of an unstable nucleus into more stable state that may also be unstable and will decay further through a chain of decays until a stable nuclear configuration is reached. The energy difference between the two quantum states is called the decay energy, Q, and is emitted from the nucleus in the form of electromagnetic radiation (gamma rays) or in the form of kinetic energy of the reaction products.

All radioactive processes are governed by the same formalism based on:
- substance related characteristic parameter called the decay constant λ;
- activity, A(t), which represents the total number of disintegrations (decays) of nuclei per unit time and is defined as:

$$A(t) = \lambda N(t) \tag{13}$$

where N(t) is the number of radioactive nuclei at time t.

The SI unit of activity is the becquerel, Bq (1 Bq = 1 s^{-1}), but the older unit of activity, the curie, Ci (1 Ci = 3.7 × 10^{10} Bq), originally defined as the activity of 1 g of ^{226}Ra, is also used.

The simplest radioactive decay involves a transition with a decay constant λ_p from a quantum state of the unstable parent nucleus, P, to the quantum state of the stable daughter nucleus, D: $P \xrightarrow{\lambda_P} D$.

The rate of depletion of the number of radioactive parent nuclei, N_P, is equal to the activity of radioactive parent, $A_P(t)$, at time t:

$$\frac{dN_P(t)}{dt} = -A_P(t) = -\lambda_P N_P(t), \quad \int_{N_P(0)}^{N_P(t)} \frac{dN_P}{N_P} = -\int_0^t \lambda_P dt \qquad (14)$$

where $N_P(0)$ is the initial number of parent nuclei at time t = 0.

The number of radioactive parent nuclei $N_P(t)$ in radioactive substance and the activity of radioactive parent $A_P(t)$ as a function of time (Fig.8) may be defined as:

$$N_P(t) = N_P(0)e^{-\lambda_P t}$$
$$A_P(t) = \lambda_P N_P(t) = \lambda_P N_P(0)e^{-\lambda_P t} = A_P(0)e^{-\lambda_P t} \qquad (15)$$

where $A_P(0)$ is the initial activity at time t = 0.
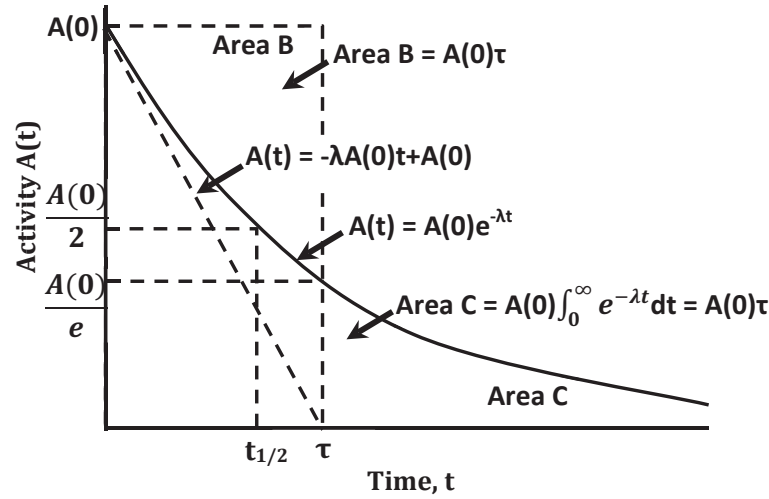
Fig.8. Plot of activity as a function of time.

The half-life, $(t_{1/2})_P$, of radioactive parent, P, is the time during which the number of radioactive parent nuclei decay from the initial value $N_P(0)$ at time t = 0 to half of the initial value:

$$N_P(t = t_{1/2}) = \frac{N_P(0)}{2} = N_P(0)e^{-\lambda_P (t_{1/2})_P} \qquad (16)$$

The same relationship is valid for the activity.

The average (mean) lifetime, τ_P, of a radioactive substance is the average life expectancy of all parent radioactive nuclei in the substance at time t = 0:

$$A_P(0)\tau = \int_0^\infty A_P(0)e^{\lambda_P t}dt = \frac{A_P(0)}{\lambda_P} \qquad (17)$$

The decay constant λ_P, the half-life $(t_{1/2})_P$ and average lifetime τ_P of a radioactive substance are related to each other as follows:

$$\lambda_P = \frac{\ln 2}{(t_{1/2})_P} = \frac{1}{\tau_P}, \quad (t_{1/2})_P = \tau_P \ln 2 \tag{18}$$

Specific activity a is the activity per unit mass:

$$a = \frac{A(t)}{M} = \frac{\lambda N(t)}{M} = \frac{\lambda N_A}{A} = \frac{N_A \ln 2}{A(\tau_{1/2})_P} \tag{19}$$

where N_A stands for Avogadro's number and A is the atomic mass number.

A more complicated radioactive decay occurs when a radioactive parent nucleus, P, decays with its decay constant λ_p into unstable daughter nucleus, D, which in turn decays with a decay constant λ_D into a stable granddaughter, G: $P \xrightarrow{\lambda_P} D \xrightarrow{\lambda_D} G$.

Time-dependent parent and daughter activities are shown in Fig.9.
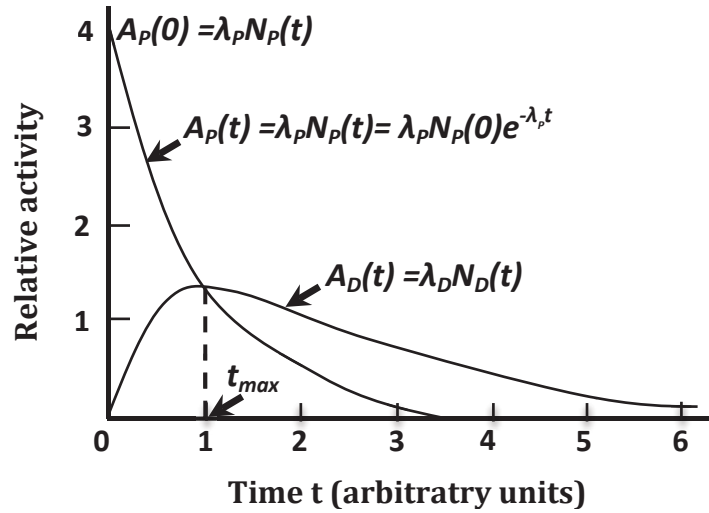
Fig.9. Parent and daughter activities plotted as a functions of time.

The activity of the daughter nuclei is expressed as:

$$A_D = \frac{\lambda_D}{\lambda_D - \lambda_P} A(0)(e^{-\lambda_P t} - e^{-\lambda_D t}) \tag{20}$$

The maximum activity of daughter nuclei occurs at time t_{max}:

$$t_{max} = \frac{\ln(\lambda_D / \lambda_P)}{\lambda_D - \lambda_P} \tag{21}$$

under condition, that $N_D = 0$ at time $t = 0$.

There are some special considerations in the parent-daughter-granddaughter relationship:

• for non-equilibrium:

$$\lambda_D < \lambda_P \quad \text{or} \quad (t_{1/2})_D > (t_{1/2})_P, \quad \frac{A_D}{A_P} = \frac{\lambda_D}{\lambda_D - \lambda_P}\left[1 - e^{-(\lambda_D - \lambda_P)t}\right] \tag{22}$$

• for transient equilibrium:

$$\lambda_D > \lambda_P \quad \text{or} \quad (t_{1/2})_D < (t_{1/2})_P, \quad \frac{A_D}{A_P} = \frac{\lambda_D}{\lambda_D - \lambda_P}, \text{ for } t \gg t_{max} \tag{23}$$

• for secular equilibrium:

$$\lambda_D \gg \lambda_P \quad \text{or} \quad (t_{1/2})_D \ll (t_{1/2})_P, \quad A_D/A_P \approx 1 \tag{24}$$

3.2. ACTIVATION OF NUCLIDES

Activation of nuclides is possible when a parent nuclide, P, interacts with thermal neutrons in a nuclear reactor. This interaction is followed by occurance of a radioactive daughter nuclide, D, that decays into a granddaughter nuclide, G: $P \xrightarrow{\sigma\dot{\varphi}} D \xrightarrow{\lambda_D} G$, where $\dot{\varphi}$ (in $cm^{-2} \cdot s^{-1}$) indicates neutron fluence rate.

The probability for the parent nuclei activation is determined by nuclear reaction cross section, σ, expressed in barn/atom (1 barn = 10^{-24} cm^2). In the case of parent nuclei activation, the expression for daughter activity is given in Eq. (21) where λ_P is replaced by the $\sigma\dot{\varphi}$:

$$A_D(t) = \frac{\sigma\dot{\varphi}\lambda_D}{\lambda_D - \sigma\dot{\varphi}} N_P(0)(e^{-\sigma\dot{\varphi}t} - e^{-\lambda_D t}) \tag{25}$$

In the activation process the maximum activity of daughter nuclei occurs at time:

$$t_{max} = \frac{\ln\lambda_D / \sigma\dot{\varphi}}{\lambda_D - \sigma\dot{\varphi}} \tag{26}$$

When $\sigma\dot{\varphi} \ll \lambda_D$, the daughter activity expression transforms into:

$$A_D(t) = \sigma\dot{\varphi}\lambda_D N_P(0)(1 - e^{-\lambda_D t}) \tag{27}$$

$^{60}_{27}$Co being one of the most important radionuclides for industrial and medical irradiators is also produced artificially by bombarding stable $^{59}_{27}$Co with thermal neutrons in a nuclear reactor:

$$^{59}_{27}Co + n \rightarrow {}^{60}_{27}Co + \gamma, \quad \text{or} \quad {}^{59}_{27}Co(n, \gamma){}^{60}_{27}Co \tag{28}$$
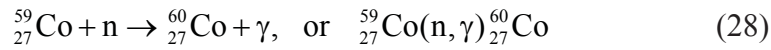
Estimated cross section for this process is $\sigma = 37$ barn/atom. The typical neutron fluence rate $\dot{\varphi}$ is of the order of 10^{14} cm$^{-2} \cdot$s^{-1} [13, 14].

3.3. RADIOACTIVE DECAY MODES. NATURAL RADIATION SOURCES

Radioactive decay is a process in which an unstable parent nucleus, P, reaches a more stable daughter nucleus, D, through possible decay modes. The most important radioactive decay modes are: alpha (α) decay, β^+ decay, β^- decay, electron capture (ε), and isomeric transition (IT) which is also called internal conversion (IC), spontaneous fission (sf), proton (p) decay, neutron (n) decay and special mixed beta-decay processes. Most of the decay processes are followed by gamma emissions.

Total energy of particles released from the decaying nucleus equals the decrease in the rest energy:

$$Q = [M_P - (M_D + m)]c^2 \tag{29}$$

where M_P, M_D and m are the nuclear rest masses of the parent, daughter and emitted particle, respectively.

Radioactive decay processes are described in detail in Ref. [4]. Information on radionuclide decay data are found in special databases [11, 13, 14].

Alpha decay is a nuclear transformation in which an energetic alpha particle ($_2^4$He nucleus) is emitted: $_Z^A P \to {}_{Z-2}^{A-4}D + {}_2^4He$.

The process of alpha decay is found mainly in proton rich, high atom number (Z > 83) nuclides (see Fig.6). The reason for alpha decay is an unbalance between two competing forces in the nucleus: electrostatic repulsion (Coulomb) force between protons and the strong interaction force between protons and neutrons.

The binding energy of alpha particle (potential barrier in the nucleus) is very high (EB = 28.3 MeV).

The kinetic energy of alpha particles released by naturally occurring radionuclides is between 4 and 9 MeV.

An example of alpha decay for $_{88}^{226}$Ra is provided in Fig.10.
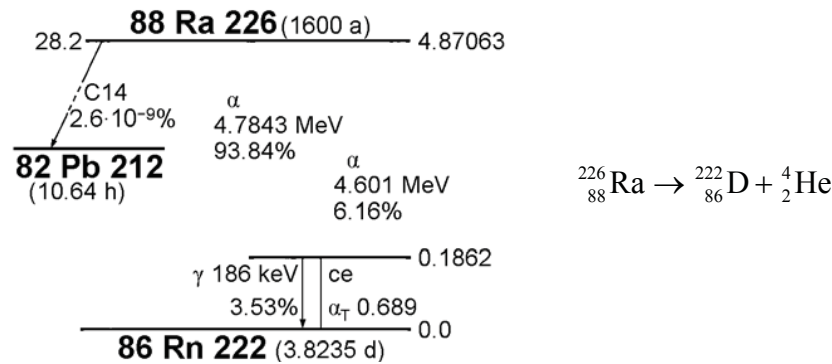
Fig.10. Alpha decay of $_{88}^{226}$Ra. Most important processes are: α1 decay (4.7843 MeV, 93.84%) and α2 decay (4.601 MeV, 6.16%) followed by gamma emission (186 keV, 3.53%). (Adapted from database [15], 2012).

Beta decay is a nuclear transformation in which an electron or positron is emitted. There are no electrons in nucleus. The reason for beta decay is quite different as compared to alpha decay. Weak interaction forces are responsible for beta decay, since the weak interaction causes transmutation of quarks, that are constituents of nucleons [16]. Six types of quarks are known, but nucleons are constructed from *up* and *down* quarks: a neutron consists of one *up* (+2/3e) and two *down* (–1/3e) quarks; a proton – two *up* (+2/3e) and one *down* (–1/3e) quarks. Weak interaction is the only process in which a quark can change to another quark.

In **neutron decay,** one *down* quark is changed to an *up* quark, transforming the neutron into a proton:

$$d \rightarrow u + e^- + \overline{\nu}_e \tag{30}$$

In **proton decay,** one *up* quark is changed to the *down* quark, transforming the proton into the neutron:

$$u \rightarrow d + e^+ + \nu_e \tag{31}$$

The number of nucleons and total charge are conserved in the beta decay process and the daughter, D, can be referred to as an isobar of the parent, P. This transformation is only possible, if $M_P > M_D + m_e$.

- β^+ decay occurs when, in a proton rich radioactive parent nucleus, a proton is converted into a neutron and a positron and neutrino. Sharing the available energy, positrons and neutrinos are ejected from parent nucleus:

$$p \rightarrow n + e^+ + \nu_e, \quad \text{and} \quad {}_Z^A P \rightarrow {}_{Z-1}^A D + \beta^+ + \nu_e \tag{32}$$

An example of β^+ decay for ${}_9^{18}F$ is provided in Fig.11. The radionuclide ${}_9^{18}F$ is a widely used tracer in nuclear medicine.
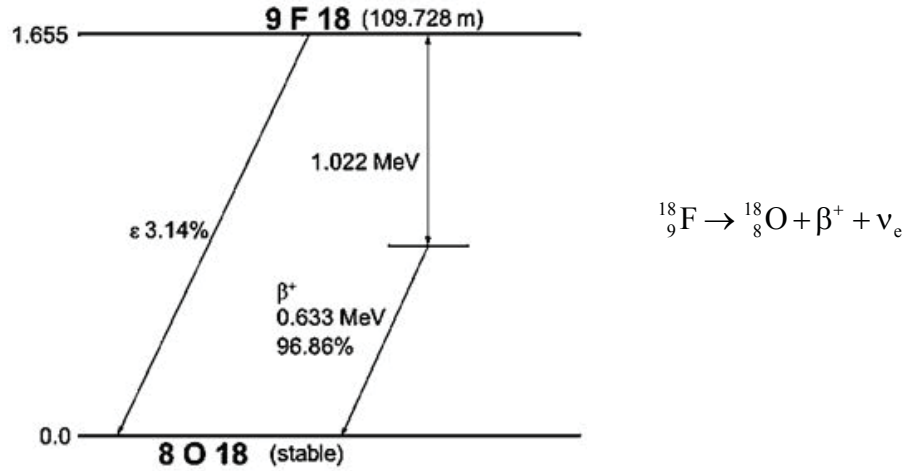
Fig.11. β^+ decay of ${}_9^{18}F$. The main decay mode is positron emission (0.633 MeV, branching ratio 96.86%). Branching ratio for electron capture is 3.14%. No gamma emissions are observed. (Adapted from database [15], 2013).
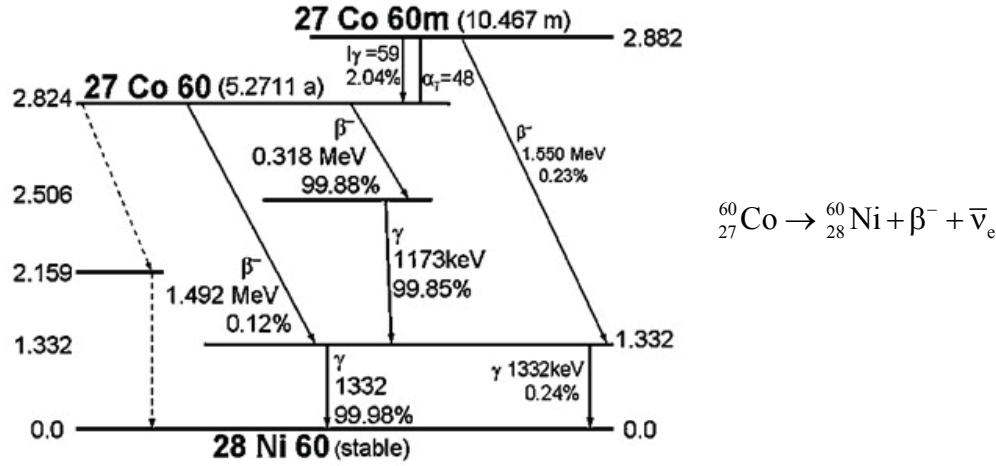
Fig.12. β⁻ decay of $_{27}^{60}$Co. In 99.88% cases electrons with a maximum energy of 0.318 MeV are emitted, the rest – 0.12% electrons – with a maximum energy of 1.492 MeV. β⁻ decay is followed by gamma emissions: $E_{\gamma 1}$ = 1.173 MeV, 99.85% and $E_{\gamma 2}$ = 1.332 MeV, 99.98%. A metastable state ^{60m}Co is also indicated. The transition from metastable state to the ground state of ^{60}Co occurs primary through electronic capture. (Adapted from database [15], 2012).

- β⁻ decay occurs when in a neutron-rich radioactive parent nucleus a neutron is converted into a proton and an electron and anti-neutrino, that share the available energy, are ejected from the parent nucleus:

$$n \rightarrow p + e^- + \overline{\nu}_e, \quad \text{and} \quad _Z^A P \rightarrow _{Z+1}^A D + \beta^- + \overline{\nu}_e \qquad (33)$$
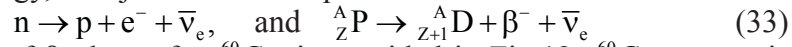
An example of β⁻ decay for $_{27}^{60}$Co is provided in Fig.12. $_{27}^{60}$Co source is widely used in different industrial and medical applications. One gram of $_{27}^{60}$Co has an activity of *ca.* 43 TBq.

Electron capture is a process in which a neutron deficient nucleus captures an atomic electron from the inner K or L shells of the atomic orbits. As a result, a proton in the nucleus transforms into a neutron and neutrino is ejected:

$$p + e_K^- = n + \nu_e, \quad \text{and} \quad _Z^A P + e_K^- = _{Z-1}^A D + \nu_e \qquad (34)$$
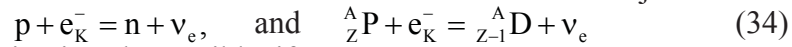
This transformation is only possible, if $M_P + m_e > M_D$.
An example of electron capture process is provided in Fig.13.

Gamma emission is present when excited daughter nucleus, D, generally produced through alpha decay, β⁻ or β⁺ decay, attains its ground state:

$$_Z^A P \rightarrow _{Z+1}^A D^* \rightarrow _{Z+1}^A D + \gamma \qquad (35)$$

If the daughter nucleus de-excites with a time delay, the excited state of the daughter is referred to as a metastable, *, state. The nucleus in metastable state is called an isomer and the process of de-excitation is called an isomeric transition, with the emission of gamma photons. Radioactive decay related spontaneously emitted photons are from the range 5 keV-1.5 MeV, but in some cases also higher photon energies (6-7 MeV) are possible.
An example of gamma decay scheme of $_{55}^{137}$Cs source, is provided in Fig.14.
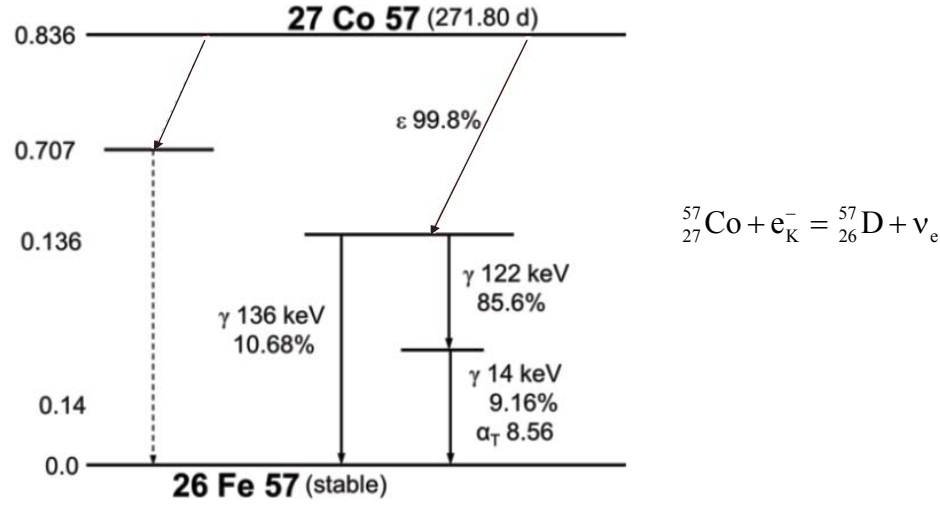
Fig.13. $_{27}^{57}$Co decay by electron capture. Electron capture (99.8%) is prevailing process when $_{27}^{57}$Co nuclei (0.836 MeV) transforms into the $_{26}^{57m}$Fe in the excited state (0.136 MeV). This transformation is caused by the fact that the Q value (0.836 MeV) is not sufficient for β$^+$ decay (threshold energy for positron emission is 1.022 MeV). The process is followed by gamma emissions. (Adapted from database [15], 2012).

$_{55}^{137}$Cs is used as irradiation/calibration source in medical and industrial applications. One gram of $_{55}^{137}$Cs has an activity of *ca.* 3.215 TBq.

Internal conversion is a process in which the nuclear excitation energy may be transferred to a K- or L-shell orbital electron that is ejected instead of gamma photon emission:
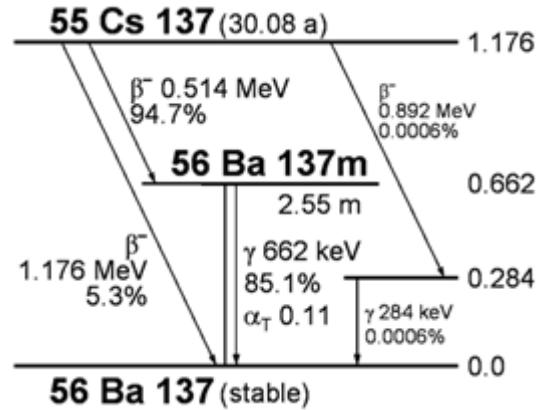
Fig.14. Metastable transition $_{55}^{137}$Cs → $_{56}^{137}$Ba. 94.7% of $_{55}^{137}$Cs nuclei possess β$^-$ decay to a metastable short-lived nuclear isomer of barium, $_{56}^{137m}$Ba ($t_{1/2}$ = 153 s); the 5.3% of $_{55}^{137}$Cs nuclei through β$^-$ decay are transformed directly to the ground state of $_{56}^{137}$Ba, which is stable. $_{56}^{137m}$Ba is responsible for the emissions of gamma rays with the energy of 0.662 MeV (85.1%). The emission of conversion electrons is also possible: 7.8% – K shell, 1.8% – L and M shells. (Adapted from database [15], 2012).

$$^A_Z D^* = {}^A_Z D + e^-_K \qquad (36)$$

The kinetic energy of ejected electron equals to the difference between the excitation energy and the orbital electron binding energy. The resulting K-shell vacancy is filled with a higher level orbital electron and the transition energy is emitted in the form of characteristic photons or Auger electrons.

An example of internal conversion is the decay of metastable $^{137\mathrm{m}}_{56}\mathrm{Ba}$ (Fig.14), which results from β^- decay of $^{137}_{55}\mathrm{Cs}$, into stable $^{137}_{56}\mathrm{Ba}$ through emission of gamma rays and internal conversion electrons.

4. ELECTRICAL (ARTIFICIAL) RADIATION SOURCES

Fundamentals of radiation physics have been discussed in previous sections with the aim of introducing a basic knowledge of atomic and nuclear structures and their radioactive transformation processes. This knowledge is necessary to understand the origin and behaviour of natural radiation sources, which might be used for materials modification and in the radiation processing of materials. However radioactive decay of naturally occurring radionuclides has a probabilistic character. Even if the energies of the released particles might be relative high: up to 5 MeV for alpha particles and up to 3 MeV for beta particles, their scientific and especially industrial applications are limited by the difficulties in maintaining radioactive sources, their lack of purity for chemical processing, low intensity, poor geometry and sometimes uncontrolled broad range of energies. Radioactive sources can be expensive and require replenishment. This makes electrical (artificial) sources, beams of accelerated particles, produced using different physical phenomena and techniques, very attractive. These particles may additionally produce beams of secondary particles. Photons (X-rays, gamma rays, visible light) might be generated by the interaction of accelerated electrons with matter, while neutrons are generated by accelerated proton beams in neutron spallation sources. Primary and secondary beams are used for radiation processing of materials and in the analysis of material properties, or for the treatment and diagnosis of patients.

4.1. PRODUCTION OF X-RAYS

Particle interaction processes with matter are discussed in detail in Chapter 2. In order to have a full scope of particles that are produced within an atom, a physical background of X-ray production must be introduced.

Inelastic interactions between incident electrons and orbital electrons or nuclei result in production of X-rays of two types: characteristic X-rays, and

"bremsstrahlung" X-rays (braking radiation). X-rays may be of natural origin, but intensive X-ray beams that are used as radiation sources in medical, industrial and research applications, are generated electricity: low energy (kilovoltage range) X-rays are produced in conventional X-ray tubes, and megavoltage X-rays are produced by particle accelerators.

Bremsstrahlung X-rays are produced when a high energy electron beam strikes a target, letting the incident electron interact with a nucleus of the absorbing material (Fig.15A). Due to deceleration in the E/H field of the nucleus, the electron loses its energy. This results in the appearance of the continuous spectrum of X-ray photons, that are emitted from the target material, with the energies ranging from zero to the kinetic energy of the incident electron.

Characteristic X-rays are produced when the high energy incident electron interacts with an orbital electron and ejects it from the absorber atom (ionization). This action results in appearance of a vacancy, which is filled by an orbital electron (secondary electron) from a higher level shell. The energy difference between the two shells, $h\nu = W_2 - W_1$, is well defined and is specific for each element in the periodic table. This energy may be either emitted in the form of characteristic X-rays or transferred to another orbital electron that is ejected from the atom as an Auger electron (Fig.15B).
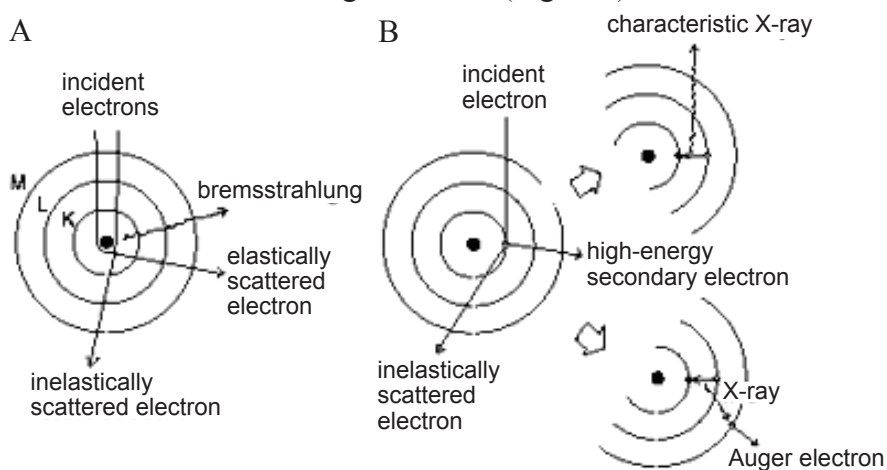
Fig.15. X-ray production schemes and related scattering: A – bremsstrahlung X-rays, B – characteristic X-rays.

The bremsstrahlung spectrum produced by a given X-ray target depends upon the kinetic energy of the incident electron, the atomic number of the target and the thickness of the target. A typical X-ray spectrum, consisting of continuous bremsstrahlung spectrum and superimposed onto it linear characteristic X-ray spectrum, is shown in Fig.16.
The relative proportion of the number of characteristic photons to bremsstrahlung photons in an X-ray beam spectrum varies with the kinetic energy of the electron beam striking the X-ray target and the atomic number of the target.
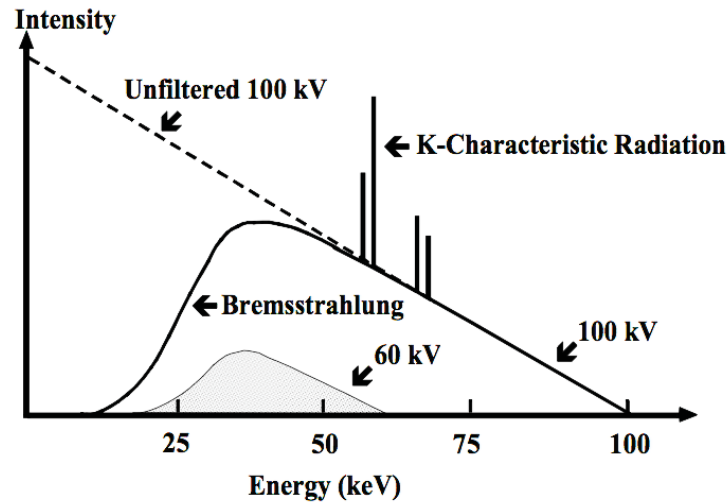
Fig.16. Typical X-ray spectrum.

For example, X-ray beams produced by a tungsten target by 100 keV electrons contain *ca.* 20% in characteristic photons and *ca.* 80% in bremsstrahlung photons. In the megavoltage range the contribution of characteristic photons to the total spectrum is negligible.

5. APPLICATION OF RADIATION SOURCES IN MATERIALS PROCESSING

It was estimated in 2013 [17] that more than 20 000 particle accelerators producing charged particle beams were used in the industrial processes. This number does not include the more than 11 000 particle accelerators that have been produced exclusively for medical therapy with electrons, ions, neutrons, or X-rays, and accelerators for physics research. An overview on industrial application of accelerated particles in different fields is shown in Fig.17.
Production of accelerated particle beams for different purposes is defined by the physical process of particle generation and operational parameters of generating equipment (Fig.18).
   Accelerators for industrial applications, including radiation processing of materials are classified according to the particle generation processes:
- Direct voltage accelerators (accelerate either electrons or ions):
  – Dynamitrons™ and Cockcroft Walton accelerators (energies to 5 MeV and currents up to 100 mA),
  – Van de Graaff accelerators (energies from 1 to 15 MeV at currents of a few nA to a few mA),
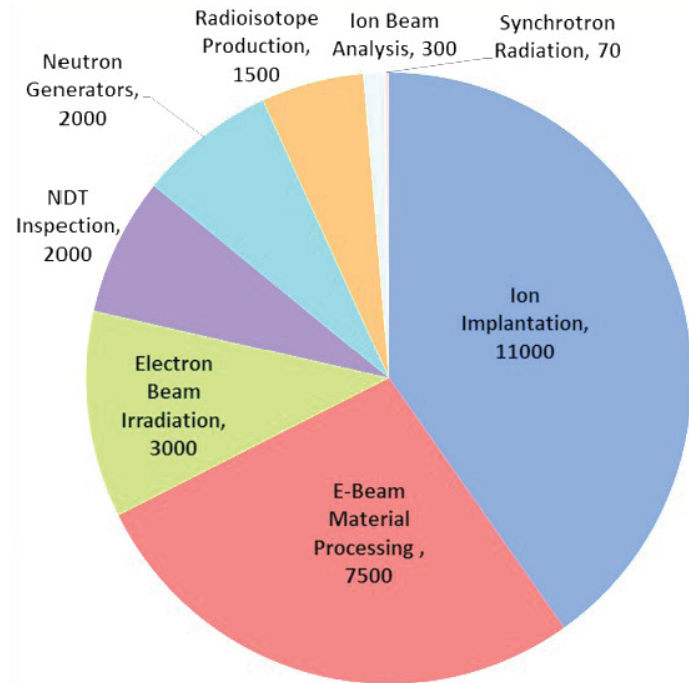
Fig.17. Number of particle accelerators in operation and fields of their industrial applications in 2013. (Adapted from Ref. [17]).

- – inductive core transformers (ICT) (energies to 2.5 MeV at currents to 50 mA);
- • RF linacs (within a wide range of operating RF frequencies for charged particles):
    - – electron linacs (standing wave and travelling wave cavities from 0.8 to 9.0 GHz, energies from 1 to 16 MeV at beam powers to 50 kW),
    - – ion linacs (RF from 100 to 600 MHz, energies from 1 to 70 MeV at beam currents to > 1 mA);
- • circular accelerators:
    - – betatrons (electron energies to 15 MeV at a few kW beam power),
    - – cyclotrons (ion energies from 10 to 70 MeV at beam currents to several mA),
    - – Rhodotrons™ (electron energies from 5 to 10 MeV at beam powers up to 700 kW),
    - – synchrotrons (electron energies to 3 GeV and ion energies to 300 MeV/amu).

Useful and detailed information on industrial irradiators can be found in the textbooks edited by R.W. Hamm and M.E. Hamm [18], A. Chao *et al.* [19], and A. Sessler and E. Wilson [20].

In this book we will concentrate on electron, gamma (high activity ^{60}Co and ^{137}Cs sources) and X-ray applications for materials processing (Table 3).

Electron beam processing applications fall into two broad categories: modifications of materials (welding, melting, cutting, drilling and hardening)
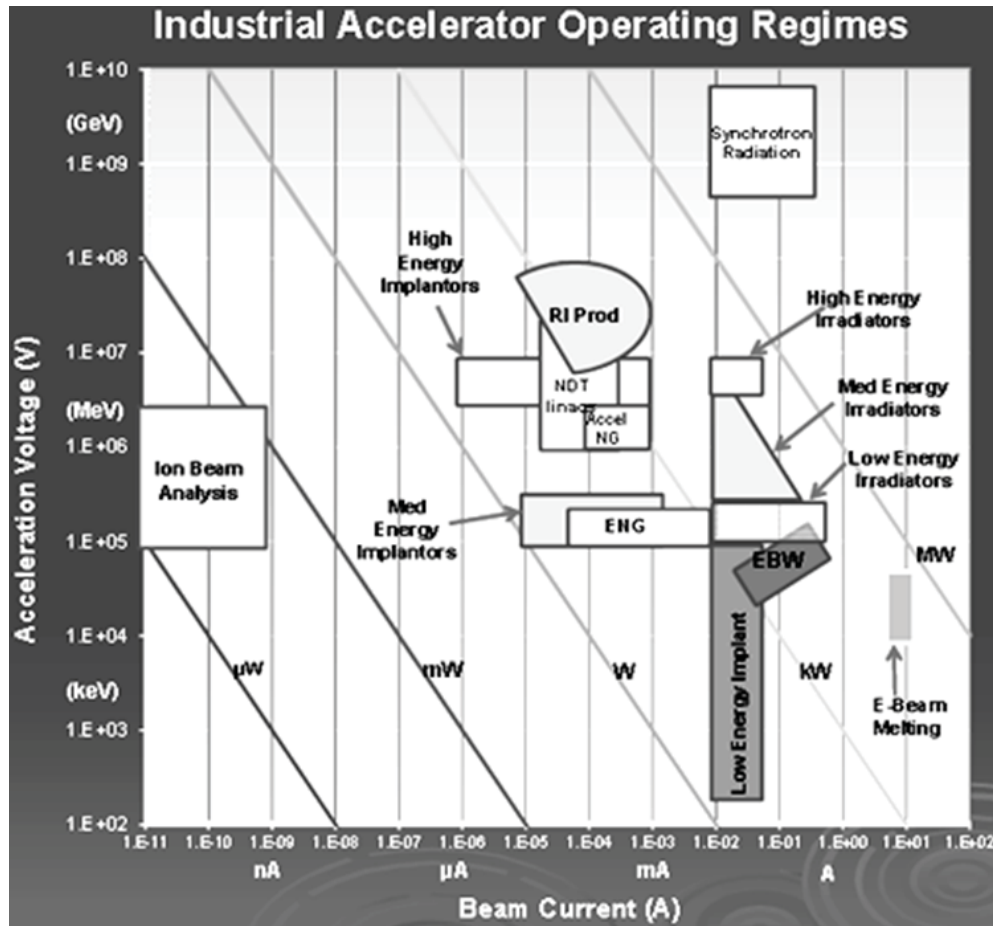
Fig.18. Operational regimes of industrial accelerators. (Adapted from Ref. [17]).

Table 3. Comparison of ionizing radiation sources. (Adapted from Ref. [21]).

	Electron beam	X-rays	Gamma rays
Power source	Electricity	Electricity	Radioactive isotope (mainly ^{60}Co)
Power activity	Electrical on-off	Electrical on-off	Half-life: 5.27 year
Properties	Electrons	Photons	Photons
Charge	1.16×10^{-19} C	$\lambda = 4.1 \times 10^{-3}$ nm	$\lambda = 1.0 \times 10^{-3}$ nm
Emission	Unidirectional (can be scanned and bent by magnets)	Forwards peaked	Isotropic
Penetration	Finite range	Exponential attenuation	Exponential attenuation
Dose rate	100 kGy/s	2.7×10^{-2} kGy/s	2.8×10^{-3} kGy/s (fresh source)

and irradiation, which includes radiation processing of polymers, monomers and oligomers used in inks, coatings and adhesives or for composite matrices, food preservation, product sterilization and waste treatment.

Bombarding a material with energetic electrons can promote chemical processes by generating ions and slow electrons which modify the material's atomic bonds through interactions with the free radicals. This can alter both its chemical and physical properties. Applications of such radiation processing can be divided into four main categories: polymerization-crosslinking of inks, coatings and adhesives; production of crosslinked, scissioned and grafted polymers; sterilization and food preservation; and wastewater and gas treatment. There are other applications such as the curing composite matrices, viscose production, and thermo-mechanical pulp production that have been demonstrated but are not yet in wide-spread use [21].

The electron beam energy needed in these applications is determined by the thickness and density of the material being processed. The accelerators used cover a wide range of beam energies and can be classified as low (80 to 300 keV), medium (300 to 1000 keV) and high (1 to 10 MeV).

Low energy electron beam accelerators are used for the polymerization--crosslinking of thin film coatings on sheets of material, for the crosslinking of plastic laminates and for thin gauged, single strand wire. Medium energy systems are mainly used for crosslinking, as for wire insulation and heat shrinkable products and in the partial crosslinking of components used in tire manufacture.

High energy accelerators are used for the crosslinking or treatment of thicker materials and for the sterilization of medical products. High energy, high current accelerators are used with water cooled tantalum targets for medical device sterilization, as an alternative to the use of radioactive isotopes, and for bio-hazard elimination. High energy accelerators with a water-cooled tungsten target generate high energy X-rays that can be used for food irradiation, wastewater remediation, and gemstone colour enhancement, particularly topaz and diamonds. The energy limit of 10 MeV is set to avoid activation in the processed material of any metal into a radioactive isotope. For food irradiation, the regulatory approved upper energy limit is 7.5 MeV.

Radioactive isotope emitted gamma rays and electrically sourced X-rays are mainly used for food preservation and for the sterilization of packaged medical devices. Gamma rays and X-rays have the same penetration depth, but X-rays are one order higher in dose rate. High through-put industrial processes use high beam current accelerators. Low dose rate, small isotope sources have historically been used for research purposes, with medical device sterilization being the only major industrial market. Recent developments in modular beam tube technology have enabled small, self-shielded laboratory units to become available. The decision to use either electron beam or X-ray or gamma-ray treatment is made depending the size of the object being treated and industry

demands for product through-put. Many of the industrial applications using electron beam and X-ray processing have been described in Ref. [21].

REFERENCES

[1]. Burcham, W.E., & Jobes, M. (1995). *Nuclear and particle physics*. New York: John Wiley & Sons.
[2]. Bohr, N. (1913). On the constitution of atoms and molecules. Part I. *Philos. Mag.*, *26*, 1-25.
[3]. Bohr, N. (1913). On the constitution of atoms and molecules. Part II. *Philos. Mag.*, *26*, 476-502.
[4]. Magill, J., & Galy, J. (2005). *Radioactivity – radionuclides – radiation.* Berlin, Heidelberg, New York: Springer.
[5]. Turner, J.E. (2007). *Atoms, radiation and radiation protection* (3rd ed.). Weinheim: Wiley-VCH Verlag GmbH & Co KGaA.
[6]. Sharma, Sh. (2008). *Atomic and nuclear physics*. India: Dorling Kindersley.
[7]. Podgorsak, E.B. (2005). *Radiation oncology physics: A handbook for teachers and students*. Vienna: IAEA.
[8]. Yang, F., & Hamilton, J.H. (2010). *Modern atomic and nuclear physics*. New Jersey: World Scientific.
[9]. Smith, F.A. (2000). *A primer in applied radiation physics*. Singapore: World Scientific.
[10]. Evans, R.D. (1955). *The atomic nucleus*. New York: McGraw-Hill.
[11]. Brookhaven National Laboratory. *Chart of nuclides*. Retrieved March 30, 2016, from www.nndc.bnl.gov/chart.
[12]. Paver, N. (Ed.). (2008). Nuclear physics and data for material analysis. *ICTP Lect. Notes*, *22*.
[13]. Magill, J., Pfennig, G., Dreher, R., & Sóti, Z. (2015). *Karlsruher Nuklidkarte* (9. Auflage). Karlsruhe: Nucleonica GmbH.
[14]. IAEA Nuclear Data Section. *Live chart of nuclides*. Retrieved March 30, 2016, from https://www-nds.iaea.org/relnsd/vcharthtml/VChartHTML.html.
[15]. European Atomic Energy Community. (2007-2016). *Nucleonica – a nuclear science internet portal*. Retrieved March 30, 2016, from http://www.nucleonica.com.
[16]. Povh, B., Rith, K., Scolz, Ch., Zetsche, F., & Rodejohann, W. (2015). *Particles and nuclei: An introduction to the physical concepts* (7th ed.). Berlin, Heidelberg, New York: Springer.
[17]. Hamm, R.W. (2013). *Industrial accelerators*. IPAC2013: 4th International Particle Accelerator Conference, 12-17 May 2013, Shanghai, China. Retrieved March 30, 2016, from http://accelconf.web.cern.ch/accelconf/ipac2013/talks/weib201_talk.pdf.
[18]. Hamm, R.W., & Hamm, M.E. (Eds.). (2012). *Industrial accelerators and their applications*. Singapore: World Scientific.
[19]. Chao, A.W., Mess, K.H., Tigner, M., & Zimmermann, F. (Eds). (2013). *Handbook of accelerator physics and engineering* (2nd ed.). Singapore: World Scientific.

[20]. Sessler, A., & Wilson, E. (2014). *Engines of discovery: A century of particle accelerators* (Rev. & exp. ed.). Singapore: World Scientific.

[21]. IAEA/iiA. (2011). *Industrial radiation processing with electron beams and X-rays* (6th revision). International Atomic Energy Agency, International Irradiation Association. Retrieved March 30, 2016, from http://www.cirms.org/pdf/Industrial%20 Radiation%20Processing%20-%20May%202011%20-%20Revision%206.pdf.

RADIATION INTERACTION WITH CONDENSED MATTER

Diana Adlienė

Kaunas University of Technology, Physics Department, Studentų g. 50, LT-51368 Kaunas, Lithuania

1. INTRODUCTION

Radiation processing of materials is conducted with the aim of modification of material properties (bulk, surface) and the creation of new materials and structures. Radiation that can alter material properties and structures are energetic fundamental particles, ions and electromagnetic waves.
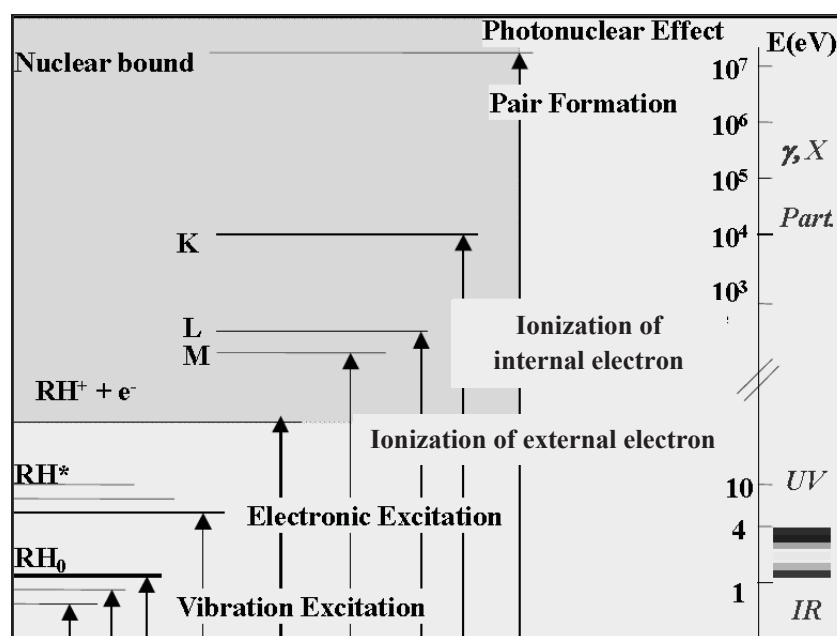
Fig.1. Energy-dependent radiation-induced processes in matter [1].

Radiation interaction mechanisms with matter depend on the type and energy of the bombarding particles, on the target material and energy imparted,

and on other physical and technical parameters. The most important parameter in discussing radiation-induced processes in matter is the energy of radiation. The energy dependency of different radiation-induced processes in materials is schematically shown in Fig.1.

Interaction mechanisms are distinguished between heavy charged particles (protons, alpha particles and heavy ions), heavy neutral particles (neutrons), charged particles (electrons and positrons) and virtual particles/electromagnetic waves (gamma and X-ray photons). Depending on the energy imparted radiation interaction with matter may lead to:

- initiation of chemical reactions,
- excitation of electrons and molecules,
- ionization of matter,
- nuclear reactions (this topic was covered in the Chapter 1).

Knowledge of the radiation interaction processes related to the energy transfer to the irradiated target is fundamental to radiation detection, measurement, and control, as well as to understanding the biological effects of radiation, when working with biomaterials.

2. INTERACTIONS OF CHARGED PARTICLES WITH MATTER

2.1. INTERACTIONS OF HEAVY CHARGED PARTICLES WITH MATTER

2.1.1. Ion beams

Ion beam interactions with matter (ion implantation, ion beam mixing, plasma assisted ion implantation or ion beam assisted deposition, *etc.*) are very complex processes that cover a broad area of different phenomena initiated by penetrating ions (Fig.2).

The energy transfer mechanisms are common for all charged particles, but ion beam induced radiation processes are quite different from those observed when fundamental particles such as electrons, protons or neutrons interact with matter. Many radiation defects are produced along a path of penetrating ions that contribute significantly to the properties of irradiated materials. Ion beam induced phenomena provides an important link to the application of energetic ions for the modification and creation of new materials.

This book is aimed at providing knowledge on material processing and modification using energetic electron or photon beams, so the energy deposition processes of heavy ions will be covered in this chapter without going into details on further processes induced in matter by bombarding it with ions.
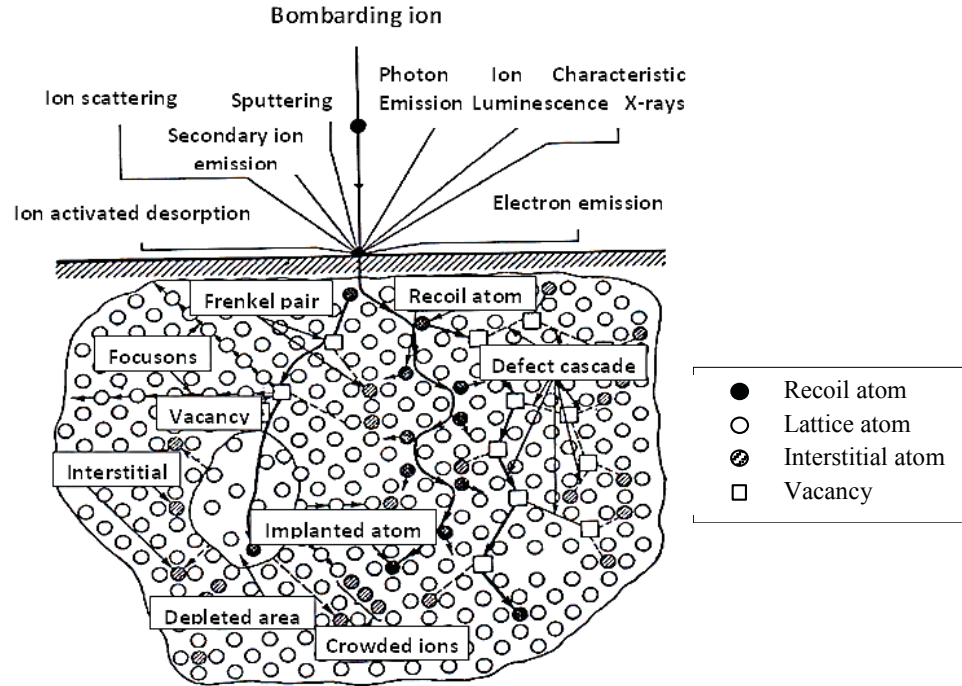
Fig.2. Primary processes induced in matter due to its bombardment with ions. (Adapted from Ref. [2]).

Useful information on ion beam interaction processes and ion beam applications can be found in Refs. [3-5].

2.1.2. Interactions mechanisms

A heavy charged particle traversing matter loses energy primarily through the ionization and excitation of atoms. The moving charged particle, being surrounded by its Coulomb electric force field, interacts with one or more electrons or with the nucleus of practically every atom it passes. In most of these interactions only a very small fraction of the incident particle's kinetic energy is transferred. For example: a 1 MeV charged particle would typically undergo 10^5 interactions with electrons before losing all of its kinetic energy. Heavy charged particles travel an almost straight path through matter since any deflection in electron collisions, which is most probable, is negligible. Nevertheless the energy transferred may be sufficient to knock an electron out of an atom and thus ionize it, or it may leave the atom in an excited state when the electron is moved to the higher energy level.

The following approximate empirical formulas can be used to estimate the mean excitation energies, $\bar{I}$, for the element with atomic number Z [6]:

- $\bar{I} \approx 19.0$ eV, Z = 1 (hydrogen);
- $\bar{I} \approx 11.2 + 11.7 \times Z$ eV, $2 \leq Z \leq 13$;
- $\bar{I} \approx 52.8 + 8.71 \times Z$ eV, Z > 13.

The mean excitation potential, $\bar{I}$, is the geometric-mean value of all the ionization and excitation potentials of an atom of the absorbing medium.

Assuming that the particle moves rapidly compared with the electron and that the energy transferred is large compared with the binding energy of the electron in the atom, the electron is free and at rest and the collision is elastic. The simplest way to calculate the maximum energy transfer is:

$$Q_{max} = \frac{4mME_k}{(M+m)^2} \tag{1}$$

But the exact relativistic expression for the maximum energy transfer, with m and M denoting the rest masses of the electron and the heavy particle, is:

$$Q_{max} = \frac{2\gamma^2 mv^2}{1 + 2\gamma m / M + m^2 / M^2} \tag{2}$$

where $E_k = Mv^2/2$ is the initial kinetic energy of the incident particle, $\gamma = 1/\sqrt{1-\beta^2}$, $\beta = v/c$, c is a speed of light.

Since the electrons are bound in the discrete energy states of the medium, the minimum, or threshold, energy transfer $Q_{min} \geq \bar{I}$ is required, which is sufficient to ionize or excite the atom when heavy particle interacts with a bound electron.

The average linear rate of energy loss of a heavy charged particle passing through matter is of fundamental importance in radiation physics and dosimetry. This quantity, designated S = dE/dx, is called the stopping power of the medium for the particle, where dE is the loss in kinetic energy of the particle as it travels a distance dx.

For a given type of charged particle at a given energy, the stopping power is given by:

$$-\frac{dE}{dx} = \mu Q_{avg} = \mu \int_{Q_{min}}^{Q_{max}} QW(Q)dQ \tag{3}$$

where μ is the probability per unit distance of travel that an electron collision occurs (also called macroscopic cross section, attenuation coefficient) and Q_{avg} is the average energy loss per collision, expressed as a product of energy loss and probability W(Q)dQ, that a given collision will result in an energy loss between Q and Q + dQ.

Stopping power, S, depends upon the type of particle, its energy and the medium traversed. It is common to express the distance in terms of mass per unit area of the material, giving the mass stopping power, S/ρ:

$$\frac{S}{\rho} = \frac{1}{\rho}\frac{dE}{dx} \tag{4}$$

where ρ is the mass density of material.

Using relativistic quantum mechanics, Bethe derived the following expression (as it is provided in Ref. [6]) for the stopping power of a uniform medium for a heavy charged particle:

$$-\frac{dE}{dx} = \frac{4\pi k_0^2 Z^2 e^4 n}{mc^2\beta^2}\left[\ln\frac{2mc^2\beta^2}{\bar{I}(1-\beta^2)} - \beta^2\right] \tag{5}$$

where: $k_0 = 8.99 \times 10^9$ Nm²·C⁻², Z – the atomic number of the heavy particle, e = 1.6 × 10⁻¹⁹ C, n – the electron concentration in medium, m – the rest mass of electron, c – speed of light in vacuum, β = v/c, $\bar{I}$ – mean excitation energy of the medium. The multiplicative factor in the formula can be written with the help of constants [5]:

$$\frac{4\pi k_0^2 Z^2 e^4 n}{mc^2\beta^2} = 5.08 \times 10^{-31}\frac{Z^2 n}{\beta^2}\left[\text{MeV}\cdot\text{cm}^{-2}\right] \tag{6}$$

When the material is a compound or mixture, the stopping power can be calculated as follows:

$$n\ln I = \sum_i N_i Z_i \ln \bar{I}_i \tag{7}$$

where: n – the total number of electrons/cm³ in the material (n = $\Sigma_i N_i Z_i$), N_i – the number of atoms/cm³ of an element with atomic number Z_i, $\bar{I}_i$ – mean excitation energy.

General formula for calculation of the stopping power for any heavy charged particle in any medium is:

$$-\frac{dE}{dx} = \frac{5.08\times10^{-31}Z^2 n}{\beta^2}\left[F(\beta) - \ln I_{eV}\right] \tag{8}$$

where in the dimensionless $\ln I_{eV}$, the excitation energy values (in eV) are inserted; and $F(\beta)$ is calculated as:

$$F(\beta) = \ln\frac{1.02\times10^6\beta^2}{1-\beta^2} - \beta^2 \tag{9}$$

The reciprocal of the stopping power gives the distance of the heavy charged particle travelled per unit energy loss. The integral of this quantity down to zero kinetic energy defines an absolute travelling distance of the particle before coming to rest. This distance is called particle range in material:

$$R(E_k) = \int_0^{E_k}\left(-\frac{dE}{dx}\right)^{-1} dE \tag{10}$$

The Bethe (stopping power) formula for heavy charged particles is valid at high energies, as long as inequality γm/M << 1 (see Eq. (2)) holds, but there are some limitations for low and very high energies.

2.2. INTERACTIONS OF ELECTRONS AND POSITRONS WITH MATTER

Electron and proton interaction processes and interaction products (Fig.3) are different as compared with ion interaction processes (see also Fig.2). Electron and positron energy loss processes are usually treated together, referring to both particles as "electrons" or "beta particles" and distinguishing between them only where it is necessary.
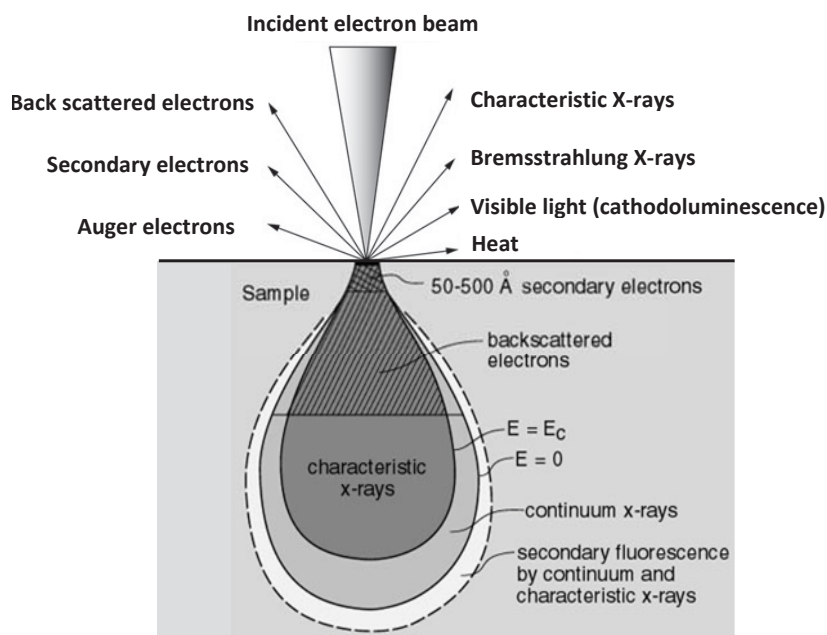
Fig.3. Schematic illustration of interaction volumes for various electron-specimen interactions (E_c – the energy required to produce X-rays in a bombarded target of interest).

Energetic electrons lose their kinetic energy in matter almost continuously through Coulomb interactions with atomic orbital electrons and atomic nuclei (collision and radiative losses) or change their direction of motion (scattering). In contrast to heavy charged particles, beta particles do not generally travel through matter in straight lines. The interactions between incident electron and an orbital electron or nucleus may be elastic and inelastic.

In an elastic interaction the incident electron is deflected from its original path but no energy loss occurs. This process has a significant effect on electron penetration and diffusion in matter at low energies.

The type of inelastic interaction that an electron undergoes with a particular atom of radius a, depends on the impact parameter of the interaction, b (distance between the trajectory of the electron and nucleus) [7]:

- b >> a, soft collisions of electrons with the whole atom; small amount of its kinetic energy (a few per cent) transferred to orbital electrons;

- b ≈ a, hard collision of electron with an orbital electron and a significant fraction of its kinetic energy (up to 50%) transferred to the orbital electron;
- b << a, radiation collision of an electron with the atomic nucleus; emission of a bremsstrahlung photon with energy between 0 and the incident electron kinetic energy.

In an inelastic collision with orbital electron the incident electron is deflected from its original path and loses part of its kinetic energy which is used for ionization or excitation of absorbing atoms [8]. As it was already discussed in Chapter 1, ionization is related to the ejection of an orbital electron from the absorber atom (Fig.4A) and excitation is related to the transfer of an orbital electron of the absorber atom from an allowed orbit to the higher one (higher shell) (Fig.4B). Atomic ionization and excitation result in collision energy losses and are characterized by collision stopping power.

A – ionization e⁻ e⁻ B – excitation e⁻ X-ray X-ray
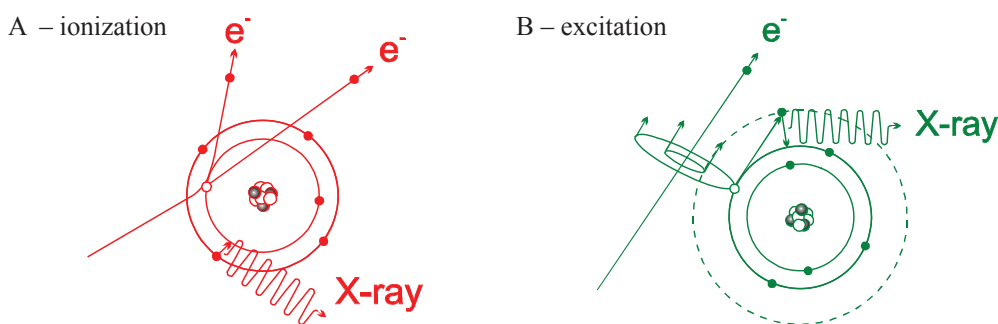
Fig.4. Inelastic collision schemes for the incident electron [9].

Elastic scattering is the dominant process at the lowest energies. Slow electrons undergo almost a random diffusion, changing direction through frequent elastic collisions without energy loss. Eventually, the occasional competing inelastic excitation and ionization collisions bring the energies of the electrons down into the region where they can react chemically with water molecules or became hydrated. At about 200 eV, ionization and the elastic scattering are comparable and considerably more probable than excitation. The attenuation coefficient curves do not cross. Elastically scattered electrons (which include backscattered electrons) are generally scattered through larger angles than are inelastically scattered electrons. At the highest energies, elastic scattering occurs increasingly in the forward direction. While elastic scattering affects electron transport through redirection of the electron paths, it does not contribute to the stopping power, because there is no associated energy loss.

The relative importance of ionization, excitation, and elastic scattering for electrons in water at energies up to 1 MeV are shown in Fig.5.

In an inelastic collision with an atomic nucleus the incident electron is deflected from its original path (scattered electron) and loses part of its kinetic energy in the form of X-ray photons (bremsstrahlung). This type energy loss is characterized by a radiative stopping power.
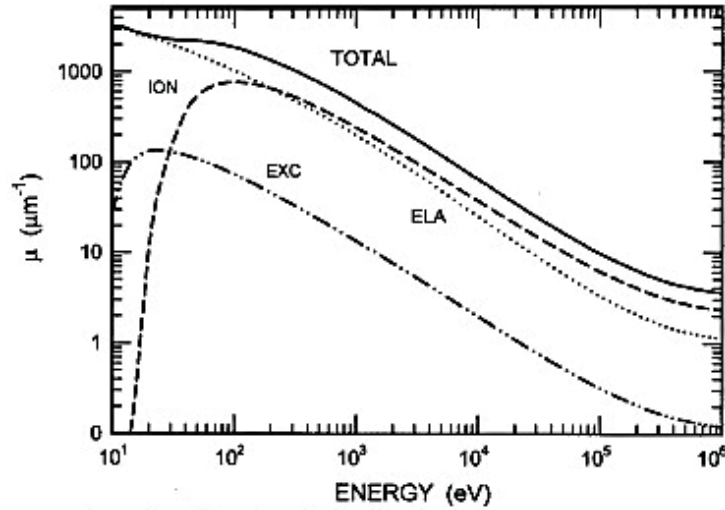
Fig.5. Attenuation coefficients μ (see Eq. (3)) for excitation (EXC), ionization (ION), elastic scattering (ELA) and total interaction for electrons in liquid water as a function of energy. (Adapted from Ref. [6]).

Coulomb interactions with the bound atomic electrons are the principal way that charged particles lose energy in the materials and energies of interest. The particle creates a trail of ionizations and excitations along its path as it is shown in Fig.6.
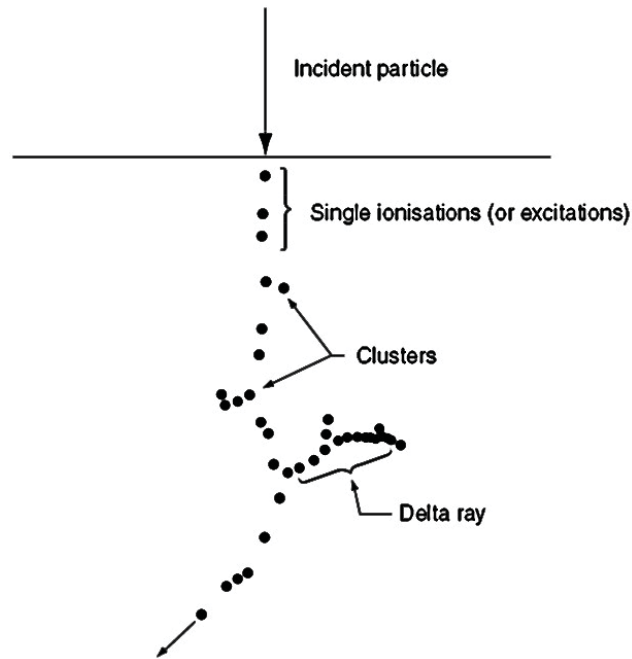
Fig.6. Schematic representation of the track of a charged particle in matter. (Adapted from Ref. [10]).

Occasionally, the energy transfer to the atomic electron is sufficient to create a so-called delta ray (or δ-ray). Delta rays are defined as (secondary) electrons that acquire sufficiently high kinetic energies through hard collisions which enables them to carry this energy a significant distance away from the track of the primary particle and produce their own ionization of absorber atoms.

The inelastic energy losses by electrons travelling through material are described by a total mass stopping power, which represents the kinetic energy loss by electron per unit path length, divided by the density of material (see Eq. (4)). The mass collision stopping power expresses the average rate of energy loss by a charged particle in all hard, as well as soft, collisions. Collision stopping power plays an important role in radiation dosimetry, since it is related to the dose absorbed in medium [11]:

$$D = \Phi \left(\frac{S}{\rho} \right)_{col} \tag{11}$$

where Φ is the fluence of electrons.

The delta rays resulting from hard collisions may be energetic enough to carry kinetic energy a significant distance away from the track of the primary particle. In this case, the use of mass collision stopping power may lead to an overestimation of the dose. To overcome this problem the restricted stopping power defined as a fraction of the collision stopping power that includes all the soft collisions plus those hard collisions resulting in delta rays with energies less than a cut-off value Δ shall be applied [12]:

$$\left(\frac{S}{\rho} \right)_{\Delta} = \left(\frac{1}{\rho} \frac{dE}{dx} \right)_{\Delta} \tag{12}$$

The full quantum-mechanical expression for the electron mass collision stopping power [13] is given by:

$$\left(-\frac{dE}{dx} \right)_{col}^{\pm} = \frac{4\pi k_0^2 2e^4 n}{\beta^2} \left[\ln \frac{mc^2 \tau \sqrt{\tau+2}}{\sqrt{2I}} + F^{\pm}(\tau) - \delta \right] \tag{13}$$

where for electrons:

$$F^-(\beta) = \frac{1-\beta^2}{2} \left[1 + \frac{\tau^2}{8} - (2\tau+1)\ln I \right] \tag{14}$$

and for positrons:

$$F^+(\beta) = \ln \left[23 + \frac{14}{\tau+2} + \frac{10}{(\tau+2)^2} + \frac{4}{(\tau+2)^3} \right] \tag{15}$$

where $\tau = E/mc^2$ with E as kinetic energy of the β^+ or β^- particle, and δ is the density effect correction factor. The other symbols in these equations are the same as it was defined in the Eq. (5).

The total mass stopping power consists of two components: the mass stopping power related to electron-orbital electron interactions (ionization and excitation) and the radiative mass stopping power related to electron-nucleus interactions (bremsstrahlung):

$$(S/\rho)_{tot} = (S/\rho)_{col} + (S/\rho)_{rad} \qquad (16)$$

Both stopping powers are competing: within a broad range of kinetic energies below 10 MeV collision (ionization) losses are dominant $(S/\rho)_{col} > (S/\rho)_{rad}$, but at high kinetic energies the situation is reversed (Fig.7).
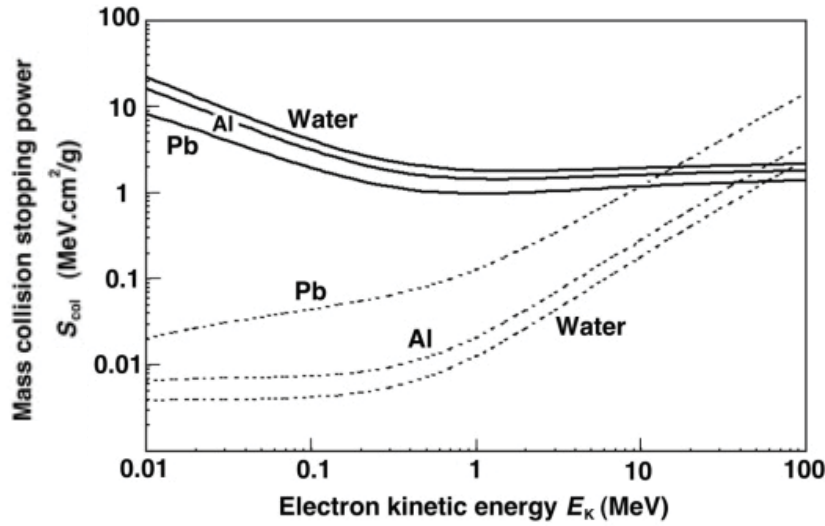
Fig.7. Mass stopping powers for electron in medium: solid lines – mass collision stopping power, dotted lines – mass radiation stopping power. (Adapted from Ref. [14]).

The energy loss rate in collision interactions depends on the kinetic energy of the electron and the electron density of the absorber. It is greater for low atomic number Z absorbers than for high Z absorbers because of lower electron density in high Z absorbers.

The energy loss rate in radiation interactions (followed by bremsstrahlung) is approximately proportional to the kinetic energy of the electron and Z^2 of the absorber. Bremsstrahlung production is more efficient for higher energy electrons and higher atomic number absorbers.

Radiative yield, also known as radiation efficiency, is expressed as:

$$Y = \frac{1}{E_i} \int_0^{E_i} \frac{(S/\rho)_{rad}}{(S/\rho)_{tot}} \, dE \qquad (17)$$

The radiative yield increases directly with atomic number Z and kinetic energy of electrons. The radiation yield for low energy range electrons (~100 keV) is ~1% and for megavoltage region ~0%.

For heavy charged particles the radiation stopping power is negligible thus $(S/\rho)_{tot} \approx (S/\rho)_{col}$.

When the energetic electron travels through matter it has interactions (electron-electron or electron-nucleus) with every atom it encounters. Due to Coulomb interactions electron loses its kinetic energy and comes to the rest at a certain depth in the absorbing medium called electron (particle) range.

Since the stopping of particles in an absorber is a statistical process, several definitions of the range are possible. According to Attix [15], distinctions are made between the path length, the projected path range and the mean path length for the electron entering material with a certain amount of kinetic energy:

- The path length of an electron is the total distance travelled along its actual trajectory until the electron comes to rest.
- The projected path range of an electron is the sum of individual path length, projected onto the incident beam direction.
- The mean path length of an electron of initial kinetic energy E_0 is defined as:

$$R_{CSDA} = \int_0^{E_0} \left(\frac{S(E)}{\rho} \right)_{tot}^{-1} dE \qquad (18)$$

The mean path length is called also CSDA range taking into account that the fractions of electron's kinetic energy transferred to matter in each single interaction is very small and it is convenient to assume that the electron is losing its energy gradually and continuously in a process referred to as continuous slowing down approximation (CSDA) [16]. CSDA range is purely calculated quantity representing the mean path length along electron's trajectory but not the depth of penetration in the defined direction.
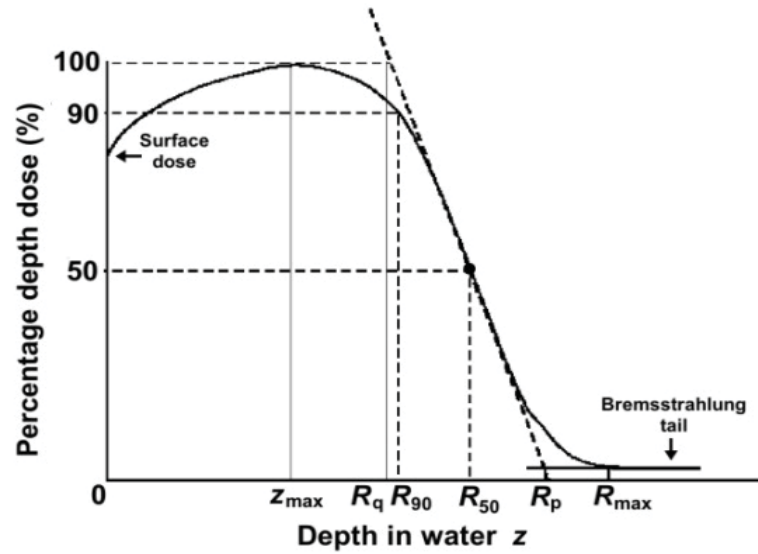
Fig.8. Typical electron beam depth-dose distribution curve with indicated penetration ranges. (Adapted from Ref. [17]). <u>Note</u>: Percentage depth dose (PDD) is defined as the quotient, expressed as a percentage, of the absorbed dose at any depth z to the absorbed dose at a fixed reference depth z_0, along the central axis of the beam.

Also other beam ranges are in use to define penetration depth of electron beams (Fig.8):

- The maximum range R_{max} (in cm or g/cm^2) is the largest penetration depth of an electron in an absorber. Being extrapolated from the depth-dose curve, this point is not well defined.
- The practical range R_p (in cm or g/cm^2) is defined as the depth at which the tangent plotted through the steepest section of the electron depth-dose curve intersects with the extrapolation line of the bremsstrahlung tail.
- R_{90} (most important for medical applications) and R_{50} are the depths at which the percentage depth dose values beyond the depth of dose maximum z_{max} attain of 90 and 50%, respectively.
- The depth R_q is defined as the depth where the tangent through the dose inflection point intersects the maximum dose level.

3. INTERACTION OF PHOTONS WITH MATTER

3.1. PHOTON INTERACTION PROCESSES

There are four categories of indirectly ionizing photon radiation:
- bremsstrahlung (electron-nucleus Coulomb interaction),
- characteristic X-rays (electron-orbital electron interaction),
- gamma rays (originates in nuclear gamma decay),
- annihilation radiation (positron annihilation).

If photons penetrate an absorbing medium, they may interact with the atoms of the absorbing material, with atomic nuclei or with orbital electrons. Each interaction is described by the probability or cross section which depends on the energy hν of the photon and on the atomic number Z of the attenuating material.

Direct photon-nucleus interactions lead to photodisintegration but photon interaction with an electrostatic field of the nucleus results in pair production. Thomson scattering and Compton scattering are present when photon interacts with loosely bound orbital (free) electron ($E_B \ll h\nu$), but the interaction between photon and tightly bound orbital electron ($E_B \leq h\nu$) is described by photoelectric effect and Rayleigh scattering [18].

During the interaction the photon may completely disappear (photoelectric effect, pair production, triplet production) or it may be scattered coherently (Rayleigh scattering) or incoherently (Compton scattering). Light charged particles (electrons, positrons) that might be produced in the absorbing medium through photon interactions behave in the way, as discussed in this chapter. A summary of photon interactions with matter is shown in Fig.9.
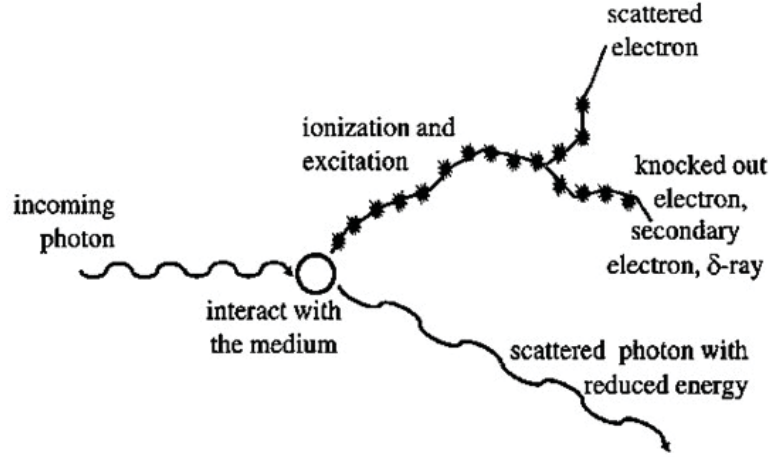
Fig.9. Schematic presentation of photon interaction processes with matter.

Photon beam is attenuated, when travelling through matter. The linear attenuation coefficient, μ, is the most important parameter used for characterization of X-ray or gamma-ray penetration into absorbing media. It is defined as the probability per unit path length that a photon will have an interaction with the absorber. It is related to the exponential decrease of the narrow monoenergetic photon beam intensity when travelling through material of the thickness x:

$$I(x) = I(0)e^{-\mu(h\nu,Z)x} \qquad (19)$$

where I(0) is the original intensity of the unattenuated beam and μ(hν,Z) is the linear attenuation coefficient which depends on photon energy hν and attenuator atomic number Z.

Several specific thicknesses are used for characterization of monoenergetic photon beams in narrow beam geometry:

- Half-value layer (HVL or $x_{1/2}$) corresponds to the absorber thickness which attenuates the original beam intensity to 50%.
- Mean free path (MFP or $\overline{x}$) is the absorber thickness which attenuates the beam intensity to 1/e = 36.8%.
- Tenth-value layer (TVL or $x_{1/10}$) equals to the absorber thickness which attenuates the beam intensity to 10%.

In addition to the linear attenuation coefficient, μ (in cm^{-1}), other related attenuation coefficients and cross sections are used for describing photon beam attenuation: mass attenuation coefficient, μ_m (in cm^2/g), atomic cross section, $_a\mu$, and electronic cross section, $_e\mu$:

$$\mu_m = \frac{\mu}{\rho}; \ \ \mu = \rho\mu_m = \frac{\rho N_A}{A}\,_a\mu = \frac{\rho N_A Z}{A}\,_e\mu \qquad (20)$$

where ρ, Z, N_A and A are the density, atomic number, Avogadro's number and atomic mass number, respectively.

Two additional attenuation coefficients distinguish between energy transfer coefficient, μ_{tr}:

$$\mu_{tr} = \mu \frac{\overline{E}_{tr}}{h\nu} \qquad (21)$$

and energy absorption coefficient, μ_{ab}:

$$\mu_{ab} = \mu \frac{\overline{E}_{ab}}{h\nu} \qquad (22)$$

where $\overline{E}_{tr}$ is the average energy transferred to charged particles (electrons and positrons), and $\overline{E}_{ab}$ is the average energy deposited by charged particles in the attenuator.

Both coefficients are related through radiative fraction g as follows:

$$\mu_{ab} = \mu_{tr}(1 - g) \qquad (23)$$

Usually mass attenuation coefficients, μ_m, obtained by dividing the linear attenuation coefficient by the mass density of absorber material, are used to describe photon interaction processes.

Photoelectric effect, Compton scattering, pair production (including triplet production) and photonuclear reactions are the most important photon interaction processes in materials.

In the photoelectric effect (Fig.10A) photon interacts with a tightly bound electron of absorber (from inner shells of atom mainly) and disappears, while the orbital electron is ejected from the atom as a photoelectron with a kinetic energy $E_K = h\nu - E_B$ ($h\nu$ – the incident photon energy, E_B – the binding energy of electron). Characteristic X-rays and/or Auger electrons might be also produced.

The average energy transferred from a photon of energy $h\nu > (E_B)_K$ to electrons $(\overline{E}_K)_{tr}^{PE}$ is given as:

$$(\overline{E}_K)_{tr}^{PE} = h\nu - P_K\omega_K(E_B)_K \qquad (24)$$

where: $(E_B)_K$ – the binding energy of the K-shell electron (photoelectron); P_K – the fraction of all photoelectric interactions in the K shell, as compared to the total number of photoelectric events in the whole atom; ω_K – the fluorescent yield for the K shell which is defined as the number of photons emitted per vacancy in a given atomic shell. The same evaluation mechanism is valid for L-shell electrons (Fig.10B), if the incident photon energies range from $(E_B)_L < h\nu < (E_B)_K$. The fraction of Auger electrons equals to: $1 - \omega$.

The atomic attenuation coefficient, $_a\tau$, for photoelectric effect is proportional to $Z^4/(h\nu)^3$, while the mass attenuation coefficient, τ_m, for photoelectric effect is proportional to $Z^3/(h\nu)^3$, where Z is the atomic number of absorber.

In the Compton effect (incoherent scattering) (Fig.11) a photon with energy $h\nu$ interacts with loosely bound electron (from outer shells of atom). Part of the incident photon energy is transferred to a "free" orbital electron which is emitted from the atom as the Compton (recoil) electron under the angle φ. The photon is scattered through a scattering angle θ and its energy $h\nu'$ is lower
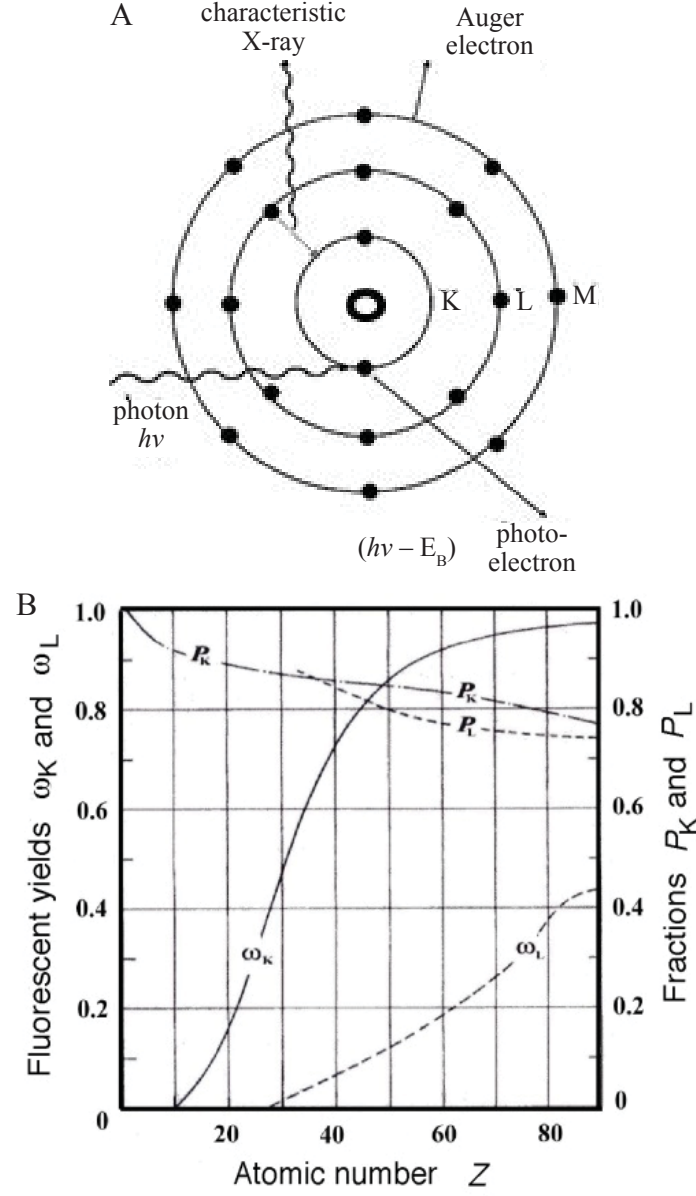
Fig.10. A – Schematic presentation of photoeffect; B – X-shell related fluorescence yields ω_X and P_X fractions against the atomic number of absorber. (Adapted from Ref. [15]).

than the incident photon energy hν resulting in the photon wavelength change after interaction:

$$\Delta\lambda = \lambda_C(1 - \cos\theta) \qquad (25)$$

with $\lambda_C = 0.024$ Å as the Compton wavelength of the electron.

Taking into account energy and momentum conservation in the Compton process the scattered photon energy hν' and the kinetic energy of Compton electron E_K are given as follows:
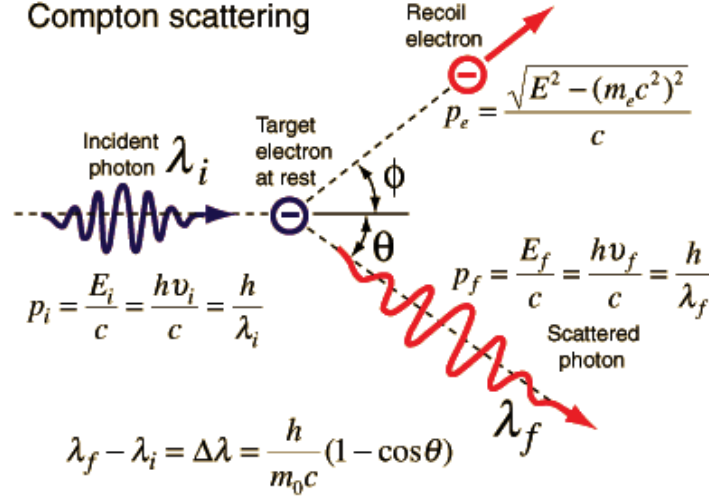
Fig.11. Schematic diagram of Compton scattering. (Adapted from Ref. [19]).

$$\nu' = h\nu \frac{1}{1 + \dfrac{h\nu}{m_e c^2}(1 - \cos\theta)}, \quad E_K = h\nu \frac{\dfrac{h\nu}{m_e c^2}(1 - \cos\theta)}{1 + \dfrac{h\nu}{m_e c^2}(1 - \cos\theta)} \qquad (26)$$

where m_e is the rest mass of electron.

Maximum and mean fractions of incident photon energy transferred to a Compton recoil electron, $(\overline{E}_K)_{tr}^{CE} = (\overline{E}_K)$, and to scattered photon are presented in Fig.12. The atomic Compton attenuation coefficient, $_a\sigma_C$, depends linearly on
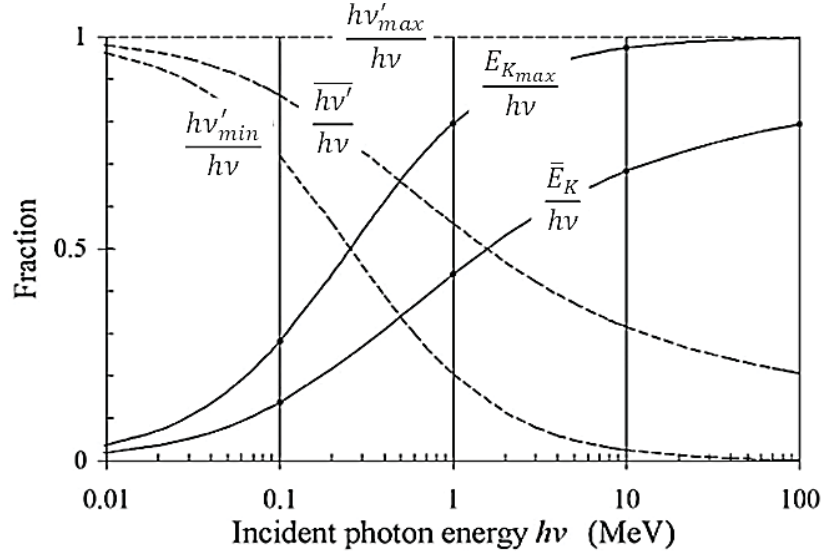
Fig.12. Fractions of incident photon energy transferred to a recoil electron, E_K, and to scattered photon, $h\nu'$, during Compton process. (Data are obtained from Ref. [19]).
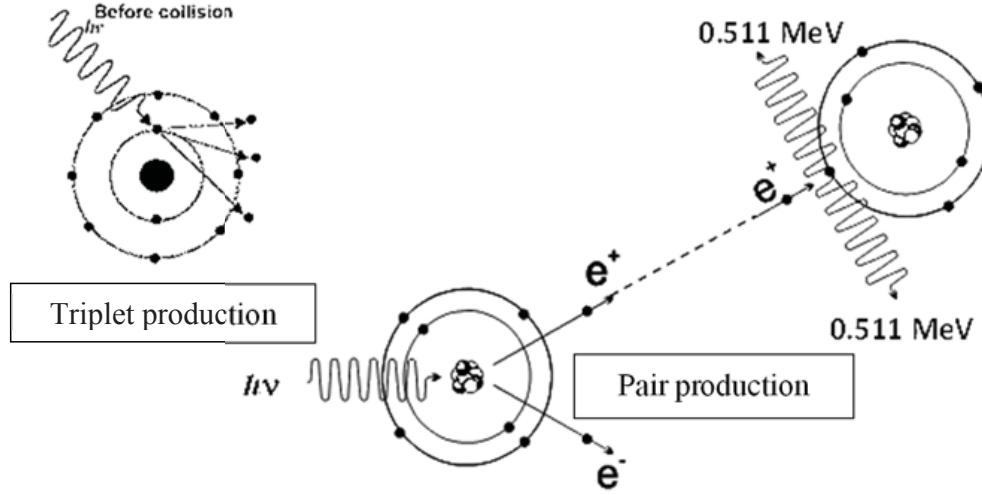
Fig.13. A scheme for pair/triplet production. (Adapted from Ref. [9]).

the atomic number Z of absorber material, while $_e\sigma_C$ and $(\sigma_C)_m$ – electronic and mass Compton attenuation coefficients, respectively, are independent of Z.

In pair production the photon disappears and the electron-positron pair with a combined energy $(\overline{E}_K)_{tr}^{PP} = h\nu - 2m_ec^2$ is produced in the nuclear Coulomb field [7]. Since this is an energy to mass conversion process, pair production has an energy threshold of $2m_ec^2 = 1.02$ MeV. The process is followed by positron annihilation with a "free" and stationary electron, producing two annihilation quanta, most commonly with energies of 0.511 MeV each and emitted at 180° from each other to satisfy the conservation of charge, momentum and energy (Fig.13). When pair production occurs in the field of an orbital electron, triplet (an electron-positron pair and the orbital electron) production is possible. The threshold for this effect is $4m_ec^2$. The atomic attenuation coefficient for pair production, $_a\kappa$, and the mass attenuation coefficient for pair production, κ_m, vary approximately as Z^2 and Z, respectively. The attenuation coefficient for pair production exceeds significantly the attenuation coefficient for triplet production at same photon energy and atomic number of absorber.

Photonuclear reactions (photodisintegration reactions) occur when a high energy photon is absorbed by the nucleus of an atom resulting in emission of neutron ((x, n) reaction) or proton ((x, p) reaction) and transformation of the nucleus into a radioactive reaction product. The threshold for a particular photonuclear reaction depends on the reaction type and nucleus and is of the order of 10 MeV for most nuclei. Photodisintegration is responsible for the nucleosynthesis of at least some heavy, proton rich elements, but the probability for photonuclear reactions is much smaller than that for other photon atomic interactions.

The probability for a photon to undergo any one of various interaction processes depends on the energy $h\nu$ of the photon and on the atomic number Z
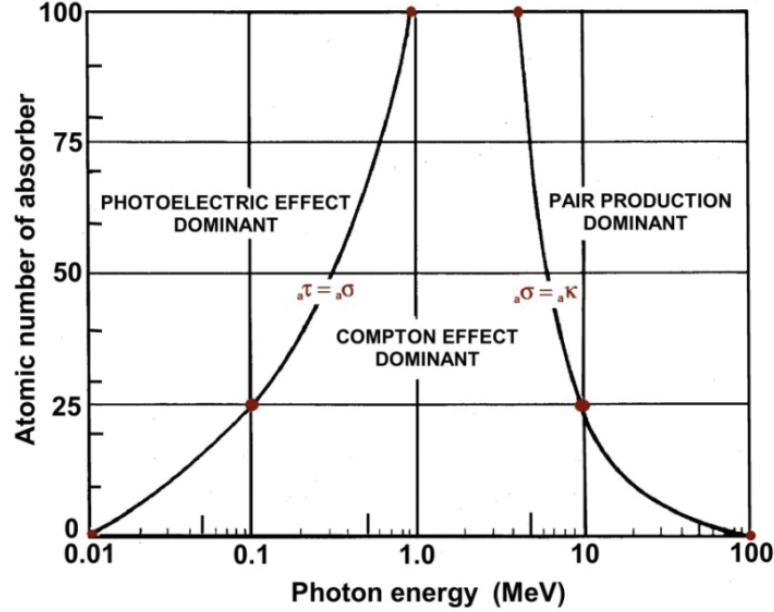
Fig.14. Regions of relative predominance of the three main forms of photon interaction with matter. (Adapted from Ref. [14]).

of the attenuating material. In general the regions of relative predominance of the most important effects are known, as it is shown in Fig.14.

3.2. PHOTON ATTENUATION IN MATTER

Earlier in this chapter it was noted that mass attenuation coefficient, μ_m, is the main parameter used for the characterization of photons attenuation in matter. This is defined as a sum of mass attenuation coefficients for individual photon interaction events (Eq. (7)). The same is applicable for energy transfer coefficient, μ_{tr} (Eq. (28)).

$$\mu_m = \frac{\mu}{\rho} = \frac{\tau}{\rho} + \frac{\sigma_R}{\rho} + \frac{\sigma_C}{\rho} + \frac{\kappa}{\rho} \qquad (27)$$

$$\frac{\mu_{tr}}{\rho} = \frac{1}{\rho}\left(\tau \frac{h\nu - P_K \omega_K E_B(K)}{h\nu} + \sigma_C \frac{(\overline{E}_K)_C}{h\nu} + \kappa \frac{h\nu - 2m_e c^2}{h\nu} \right) \qquad (28)$$

$$\frac{\mu_{ab}}{\rho} = \frac{\mu_{tr}}{\rho}(1-g) \qquad (29)$$

where: τ, σ_R, σ_C and κ – attenuation coefficients related to photoelectric effect, Rayleigh scattering, Compton scattering and pair production, respectively; $(\overline{E}_K)_{tr}^{CE}$ – the averaged energy transferred to charged particles (electrons and
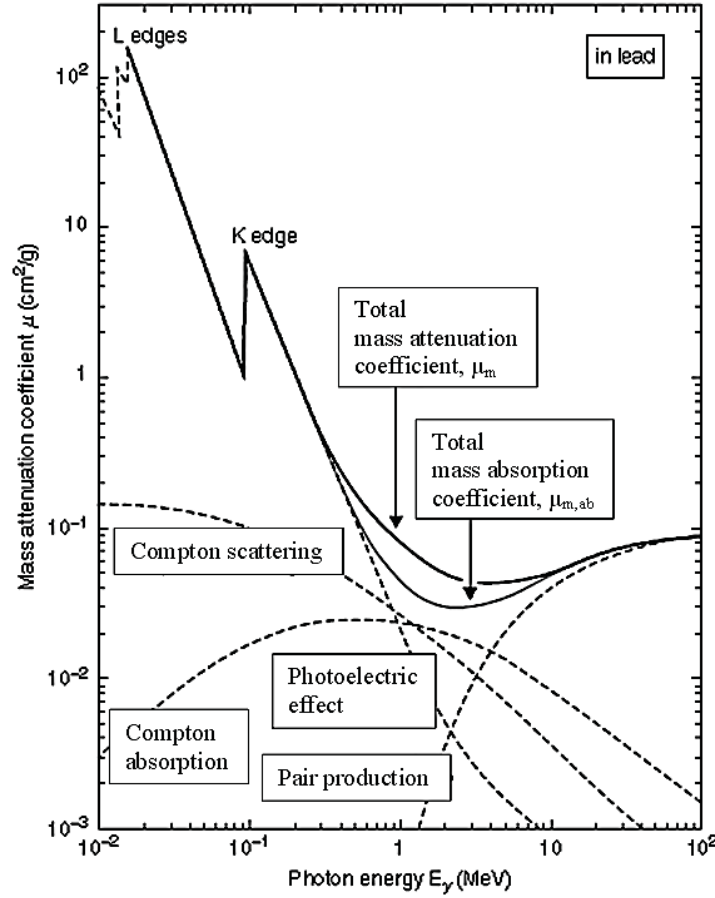
Fig.15. Mass attenuation coefficients in lead (Pb). (Data are obtained from Ref. [19]).

positrons) due to Compton effect; $E_B(K)$ – the binding energy of the K-shell orbital electron; P_K – the fraction of all photoelectric effect interaction occurring in the K shell; ω_K – the fluorescent yield of the K shell.

Mass attenuation coefficients in Pb with indicated K and L absorption edges are presented in Fig.15.

It is to notice, that the mass attenuation coefficient, corresponding to Rayleigh scattering should be also included, when calculating total mass attenuation coefficient. However Rayleigh scattering is present at low energies only; no energy transfer occurs and therefore Rayleigh scattering contributes neither to energy transfer nor to energy absorption coefficient.

3.3. PHOTON PENETRATION

Interaction processes of neutral particles (photons, neutrons) with matter are different from those of electrons or ions. Travelling through matter, neutral
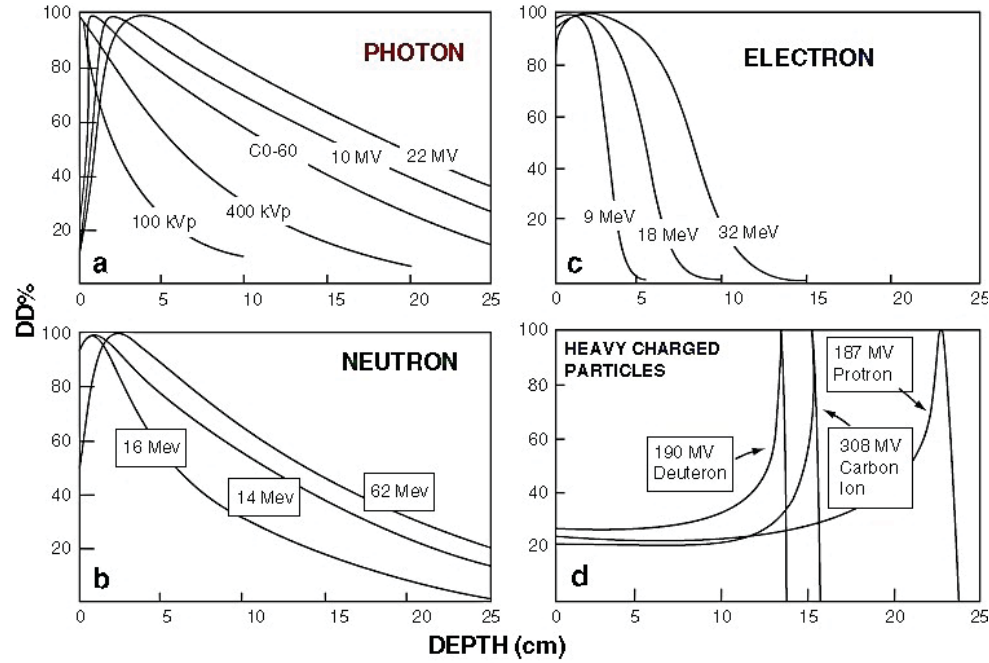
Fig.16. Typical depth-dose distribution curves for different particles with indicated penetration ranges [21].

particles are not effected by atomic Coulomb forces. Photons, representing deeply penetrating radiation, transfer their energy to the irradiated material when being attenuated in it. Photon penetration depth is limited by attenuating properties of the material and depends on the initial energy of photons. The main result of each interaction is the amount of energy imparted by ionizing radiation to matter of mass, m, in a finite volume, which is expressed as an absorbed dose, D [20]:

$$D = \frac{d\overline{\epsilon}}{dm} \qquad (30)$$

Typical dose-depth distribution curves for different energetic particles are provided in Fig.16.

Useful and more detailed information on radiation interaction with matter can be found in Refs. [22-24].

REFERENCES

[1].   Mostafavi, M. (2009). *Ionizing radiation and condensed mater interaction. Slide set*. IAEA Training Course "Nanomaterials and radiation: synthesis, characterization, applications", November 30-December 4, 2009, Reims, France.

[2]. Galdikas, A., & Pranevičius, L. (2000). *Interaction of ions with condensed matter.* N.Y.: Nova Science Publishers, Inc. (Series: Horizonts in World Physics, Vol. 229).

[3]. Utke, I., Moshkalev, S., & Russell, Ph. (2012). *Nanofabrication using focused ion and electron beams: Principles and applications*. Oxford, New York: Oxford University Press. (Oxford series on nanomanufacturing).

[4]. Goorsky, M. (Ed.). (2012). *Ion implantation*. InTech.

[5]. Hellborg, R., Whitlow, H.J., & Zhang, Y. (Eds.). (2010). *Ion beams in nano-science and technology*. Berlin, Heidelberg: Springer.

[6]. Turner, J.E. (2007). *Atoms, radiation and radiation protection* (3rd ed.). Weinheim: Wiley-VCH Verlag GmbH & Co KGaA.

[7]. Podgorsak, E.B. (2005). *Radiation oncology physics: A handbook for teachers and students*. Vienna: IAEA.

[8]. Dance, D.R., Christofides, S., Maidment, A.D.A., McLean, I.D., & Ng, K.H. (2014). *Diagnostic radiology physics: A handbook for teachers and students*. Vienna: IAEA.

[9]. Miglierini, M. (2007). *Detectors of radiation*. Lecture for the E. Wigner course. Retrieved March 30, 2016, from http://www.nuc.elf.stuba.sk/bruno/presentations/detectors/Det_1_static_files/frame.htm.

[10]. ICRU. (1970). *Linear energy transfer*. Bethesda, MD: ICRU. (ICRU Report 16).

[11]. IAEA. (1987). *Absorbed dose determination in photon and electron beams. An international code of practice*. Vienna: IAEA. (IAEA Technical Report Series No. 277).

[12]. ICRU. (1980). *Radiation quantities and units*. Washington, DC: ICRU. (ICRU Report 33).

[13]. ICRU. (1984). *Stopping powers for electrons and positrons*. Bethesda, MD: ICRU. (ICRU Report 37).

[14]. Podgorsak, E.B. (2010). *Radiation physics for medical physicists*. Berlin, Heidelberg, New York: Springer.

[15]. Attix, F.H. (1986). *Introduction to radiological physics and radiation dosimetry*. New York: Wiley-VCH Verlag GmbH & Co KGaA.

[16]. Berger, M.J., & Seltzer, S.M. (1983). *Stopping powers and ranges of electrons and positrons*. Washington, DC: National Bureau of Standards. (NBSIR 82-2550-A).

[17]. Podgorsak, E.B. (2012). *Set of 91 slides based on the chapter authored by W. Strydom, W. Parker, and M. Olivares of the IAEA publication (ISBN 92-0-107304-6): Radiation oncology physics: A handbook for teachers and students. Chapter 8: Electron beams: physical and clinical aspects* (Ver. 2012). Retrieved March 30, 2016, from www-naweb.iaea.org/nahu/DMRP/documents/slides/Chapter_08_Electron_beams.pdf.

[18]. Johns, H.E., & Cunningham, J.R. (1985). *The physics of radiology*. Springfield, IL: Charles C. Thomas Publisher.

[19]. Berger, M.J., Hubbell, J.H., Seltzer, S.M., Chang, J., Coursey, J.S., Sukumar, R., Zucker, D.S., & Olsen, K. (2010). *XCOM: Photon Cross Section Database* (ver. 1.5) [online]. Retrieved March 30, 2016, from http://physics.nist.gov/xcom.

[20]. ICRU. (1998). *Fundamental quantities and units for ionizing radiation*. Bethesda, MD: ICRU. (ICRU Report 60).

[21]. Beyzadeoglu, M., Ozygit, G., & Ebruli, C. (2010). *Basic radiation oncology*. Berlin, Heidelberg: Springer.

[22]. Kharisov, B.I., & Kharissova, O.V. (2013). Main ionizing radiation types and their interaction with matter. In: B. Kharisov, O. Kharissova & U. Ortiz-Mendez (Eds.). *Radiation synthesis of materials and compounds* (pp. 1-25). Boca Raton: CRC Press.

[23]. Leroy, C., & Rancoita, P.-G. (2004). *Principles of radiation interaction in matter and detection*. Singapore: World Scientific.

[24]. Nikjoo, H., Uehara, Sh., & Emfietzoglou, D. (2012). *Interaction of radiation with matter*. Boca Raton: CRC Press.

DOSIMETRY PRINCIPLES, DOSE MEASUREMENTS AND RADIATION PROTECTION

Diana Adlienė[1], Rūta Adlytė[2]

[1] *Kaunas University of Technology, Physics Department, Studentų g. 50, LT-51368 Kaunas, Lithuania*
[2] *Kaunas University of Technology, Accounting Department, Gedimino g. 50, LT-44239 Kaunas, Lithuania*

1. INTRODUCTION

In radiation processing dosimetry is used to quantify the energy deposited in a material or absorbed by a human from radiation sources.

Different dosimetry systems are used for different purposes in industry and research irradiation facilities, which have different requirements for dose determinations. Radiation safety standards and issues involving the radiation protection of humans against radiation exposure have their own dosimetry metrology.

Radiation dosimetry is a branch of physical science exploring different methods for the quantitative determination of energy, which is deposited in a given material by ionizing radiation, either through direct or indirect exposure. Dosimetry deals with determinations and calculations of quantities (dose) that describe the energy absorbed in a material and to some extent its rate of deposition (dose rate). Dosimetry determinations that are performed by exposing a dosimeter to a radiation source help in evaluating the radiation-induced effects, physical, chemical, and/or biological, on an irradiated material [1].

To assure that the desired radiation effects (biological, chemical, and/or physical) are achieved and that the irradiation process is performed safely, validation and process control procedures are implemented. Process controls rely on the establishment of a relationship between the source parameters and the absorbed dose in an irradiated object (for isotropic radioactive source irradiators: dwell time, position in the source rack, and conveyance speed; for accelerator sources: beam voltage, beam current, scanning width, scanned uniformity and conveyance speed). Absorbed dose and dose distribution is

inferred from determinations made with a suitable dosimetry system having some level of accuracy and precision [2].

Many dosimetry systems used in the radiation processing of materials are implemented in accordance with corresponding ISO/ASTM international standards (www.astm.org): ISO/ASTM 52628:2013 (general issues) [3], ISO/ASTM 51261:2013 (calibration) [4], ISO/ASTM 52701:2013 (characterization) [5], ISO/ASTM 52303:2015 (dose mapping) [6], ISO/ASTM 51707:2015 (uncertainties) [7], ASTM E2232-10 (mathematical modelling) [8], taking into account that the irradiation facilities also fulfil the standard requirements: ISO/ASTM 51649:2015 (high energy electron beam) [9], ISO/ASTM 51818:2013 (low energy electron beam) [10], ISO/ASTM 51608:2015 (X-ray beam) [11], ISO/ASTM 51702:2013 (gamma facility) [12]. These standards for dosimetry systems will be referenced in the appropriate sections below.

2. DOSIMETRIC QUANTITIES

A quantitative radiation dose is used:
- to predict associated radiation effects and possible material transformation and modification caused by irradiation;
- to ensure that overall radiation protection and safety are implemented when working with ionizing radiation.

A number of quantities and units have been defined by the International Commission of Radiation Units and Measurements (ICRU Report 60) [13] for describing the radiation sources. The most commonly used quantities in dosimetry and their units are listed in Table 1.

It was already noted in Chapter 2 "Radiation interaction with condensed matter" that absorbed dose is the main characteristic that allows the evaluation of radiation processing's impact on an irradiated material.

The absorbed dose is related to the stochastic quantity of the energy imparted by a source which is the sum of all energies entering the volume of interest, minus all of the energy leaving this volume, taking into account any mass energy conversion within this volume [14] and is defined as follows:

$$D = \frac{d\overline{\varepsilon}}{dm} \qquad (1)$$

where: $\overline{\varepsilon}$ is the mean energy imparted, and dm is the mass of a finite volume, V. The unit of absorbed dose is joule per kilogram (J/kg), or gray (Gy).

In the case of uncharged radiation (photons and indirect ionizing radiation), energy is imparted to matter in a two-step process.

Table 1. Radiation beam quantities (dN – a number of particles incident on a sphere of a cross-sectional area dA; E – the energy of particle; $\Phi_E(E)$ and $\Psi_E(E)$ – short notations for the particle fluence spectrum and the energy fluence spectrum differential in energy E, respectively).

Monoenergetic beam	Polyenergetic beam
Particle fluence, Φ [m^{-2}]	
$\Phi = \dfrac{dN}{dA}$	$\Phi_E(E) = \dfrac{d\Phi}{dE}(E)$
Energy fluence, Ψ [J/m^{-2}]	
$\Psi = \dfrac{dE}{dA} = \dfrac{dN}{dA}E = \Phi E$	$\Psi_E(E) = \dfrac{d\Psi}{dE}(E) = \dfrac{d\Phi}{dE}(E)E$
Particle fluence rate, $\dot{\Phi}$ [m$^{-2}\cdot$s^{-1}]	
$\dot{\Phi} = \dfrac{d\Phi}{dt}$	
Energy fluence rate (intensity), $\dot{\Psi}$ [J/m$^2\cdot$s]	
$\dot{\Psi} = \dfrac{d\Psi}{dt}$	

In the first step, the indirect ionizing radiation transfers energy to secondary charged particles. The mean energy transferred from indirectly ionizing radiation to charged particles (electrons) per unit mass of the material is defined as kerma (an acronym from: kinetic energy released per unit mass) [15]:

$$K = \frac{d\overline{E}_\alpha}{dm} \tag{2}$$

In the second step, these charged particles transfer some of their kinetic energy to the material (resulting in absorbed dose) and lose some of their energy in the form of radiative losses (bremsstrahlung, annihilation).

Different possibilities of energy absorption in the volume due to photon interactions with material are shown in Fig.1.

Energy absorbed in the volume V of matter is expressed as:

$$E_{ab} = \left(\sum \varepsilon_i\right)_1 + \left(\sum \varepsilon_i\right)_2 + \left(\sum \varepsilon_i\right)_3 + \left(\sum \varepsilon_i\right)_4 \tag{3}$$

where $(\Sigma\varepsilon_i)_1$ is the sum of energy lost by collisions along the track of the secondary particles within the volume, V.

Secondary electrons are losing their energy along their tracks (blackened parts of the tracks shown in Fig.1). Energy is not absorbed at the same location where it was first transferred to an electron.
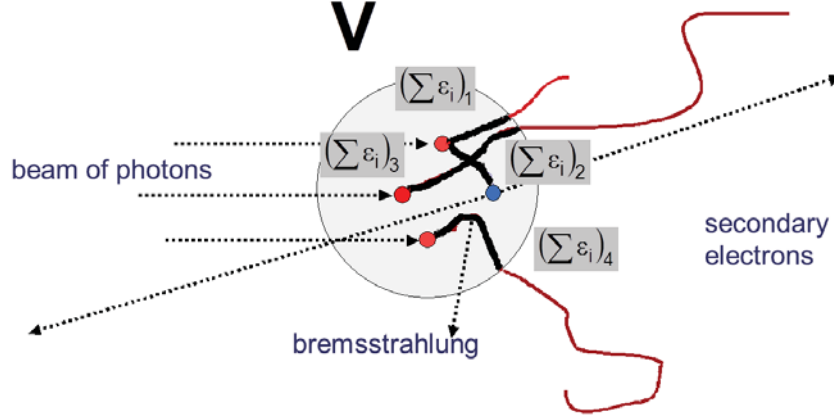
Fig.1. Illustration for the energy absorbed in volume. (Adapted from Ref. [16]).

In the case of the charged particles beam (electrons), most of the energy is directly absorbed at the place within the volume where it was deposited (energy absorption). The absorbed dose to a material or medium is related to electron fluence in the material or medium:

$$D_{med} = \Phi_{med} \left(\frac{S_{col}}{\rho} \right)_{med} \tag{4}$$

where $(S_{col}/\rho)_{med}$ is mass collision stopping power of the material or medium for the electrons penetrating material or medium with a certain energy.

Due to the slowing down of electrons in the material or medium, a primary fluence spectrum, $\Phi_{med,E}$, that ranges from the kinetic energy, E_k, down to zero, will be always present, even if the electron beam is defined as mono-energetic. So absorbed dose to the material or medium is an integral of D_{med}, (Eq. (4)):

$$D_{med} = \int_{0}^{E_{max}} \Phi_{med,E} \left(\frac{S_{col}}{\rho} \right)_{med} (E)dE = \Phi_{med,E} \left(\frac{\overline{S}_{col}}{\rho} \right)_{med} \tag{5}$$

The dose rate, which is another important parameter in materials processing, may be obtained by differentiation of absorbed dose:

$$\dot{D} = \frac{dD}{dt} \tag{6}$$

In materials processing, one should take into account dose rate effects. High dose rates lead to the creation of high free radical concentrations → back reactions → reduced effect; low dose rates lead to the consumption of dissolved oxygen → less peroxy radicals → reduced effect [1]. The same reduction of effects may be obtained by irradiating materials in an oxygen-free atmosphere.

It is possible to calculate the dose rate from the natural radioactive sources (^{60}Co, ^{137}Cs, *etc.*) that are used in different applications such as medical product sterilization. The calculation is based on the evaluation of the exposure at a certain distance from the source and followed by the conversion of the exposure to absorbed dose.

The exposure, X, is usually defined as the sum of the electric charges on all ions of one sign that are produced when all electrons liberated by the radiation in a volume of air are completely stopped, divided by the mass of air in that volume: $X = dQ/dm_{air}$. An exposure X of 1 C/kg provides an absorbed dose in air, D_{air}, of 33.97 Gy [13]:

$$D_{air} \; [Gy] = \frac{W_{air}}{e} X \tag{7}$$

with W_{air}/e = 33.97 J/C, where W_{air} is the average energy, expended in air to produce ion pair.

The dose to a material or medium, D_{med}, is related to the dose in air, D_{air}, at the same location:

$$D_{med} = 33.97 \frac{\left(\dfrac{\mu_{en}}{\rho}\right)_{med}}{\left(\dfrac{\mu_{en}}{\rho}\right)_{air}} X \tag{8}$$

The exposure rate in air, $\dot{X}$, is inversely proportional to the squared distance from the point source of activity, A(t) [17]:

$$\dot{X} = \frac{\Gamma A(t)}{r^2} \tag{9}$$

where Γ is the specific exposure gamma-ray constant at 1 m distance from the source.

Specific exposure gamma-ray constants for the nuclides, most commonly used in radiation processing, are: $\Gamma(^{60}\text{Co})$ = 2.50 × 10^{12} Cm^2/kg·MBq·s and $\Gamma(^{137}\text{Cs})$ = 6.64 × 10^{13} Cm^2/kg·MBq·s [18]. Γ values, provided in different literature sources, differ slightly due to new recalculations of the radionuclide properties. Instead of a specific exposure gamma-ray constant, a specific dose gamma-ray constant might also be used when exposure is converted to absorbed dose. The formulae used are valid only for point sources. Field arrangements and geometry factors must be taken into account if calculating the dose from the complex sources, such as pencil sources in gamma cell, or sources in the racks of the ^{60}Co unit.

3. DOSE DETERMINATIONS

3.1. STANDARDS

Radiation measurements cover a broad area of instruments and methods focusing on assessing different parameters of radiation processing. A radiation dosimeter is a device, instrument or system that measures or evaluates, either directly or indirectly, dosimetric quantities. A dosimeter along with its reader is referred to as a dosimetry system. The inference of dose is extremely important in industrial and research uses as well as in clinical applications, which are not covered in this book.

Validation, verification and radiation process control depend on the assessment of absorbed dose. The main requirements for performing proper assessments of absorbed dose and related quantities) should be fulfilled [3, 5, 19-21]:

- Assessments of absorbed dose shall be performed using a dosimetry system or systems having some level of accuracy and precision.
- The calibration of each dosimetry system shall be traceable. Traceability is defined as a property of the result of a test that can be related to stated references, usually national or international standards, through an unbroken chain of comparisons, all having stated uncertainties. For example, certificates issued by a national metrology laboratory in compliance with the International Committee on Weights and Measures (CIPM; Bureau International des Poids et Mesures – BIPM) Mutual Recognition Arrangement (MRA) or any other laboratory accredited to ISO/IEC 17025:2005 can be taken as proof of traceability and no further action is required by the user [22].

Accurate, traceable dose determinations provide independent, inexpensive means for quality control in radiation processing.

The classification of dosimetry systems (ISO/ASTM 52701:2013) [5] is based on the metrological properties of a dosimetry system (Type I and Type II) and field of its application. Reference or standard systems are Type I. Systems for routine use are Type II.

- Type I dosimeter – a dosimeter of high metrological quality; its response is affected by individual influence quantities in a well-defined way so, that it can be expressed in terms of independent correction factors.
- Type II dosimeter – a dosimeter, the response of which is affected by influence quantities in a complex way that cannot practically be expressed in terms of independent correction factors.
- Reference standard systems (Type I) are used to calibrate dosimeters for routine use and therefore require high metrological quality; low uncertainty and traceability to appropriate national or international standards are needed.

- Routine systems (Type II) are used for routine absorbed dose assessments, such as dose mapping and process monitoring. Traceability to national or international standards is needed.

The hierarchy of standard dosimetry systems as well as particular ISO standards for radiation processing are shown in Fig.2.

PSDL: Standards laboratory – national standards

Calorimeters, ionization chambers [D_w, Gy (±1%) D_w, kGy (±2%)]

|

SSDL: Reference standard dosimetry systems (±3%), k = 2

*Fricke, ceric, dichromate, alanine, calorimeters,
ethanol-monochlorobenzene (ECB), ionization chambers*

|

Routine dosimetry systems (±6%), k = 2

Films, plastics, dyed plastics, TLD, OSLD, semiconductor devices…
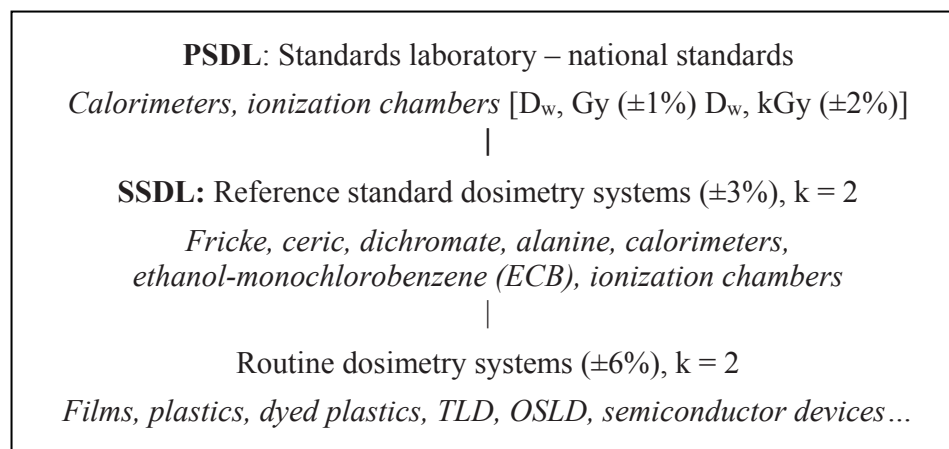
Fig.2. Dosimetry standards hierarchy.

Primary standards are instruments of the highest metrological quality that permit determination of the unit of a quantity from its definition. The accuracy of primary standards has been verified by comparison with standards of other institutions operating at the same metrological level. Primary standards are recognized by the primary standards dosimetry laboratories (PSDLs) in about 20 countries worldwide. Regular international comparisons between the PSDLs and with the CIPM (BIPM) ensure international consistency of the primary dosimetry standards. Radiation detectors used for the calibration of radiation sources for industry, research or medicine, must have a calibration coefficient traceable (directly or indirectly) to a primary standard. Primary standards are not used for routine calibrations, since they represent the unit for the quantity at all times. Instead, the PSDLs calibrate dosimeters for secondary standards dosimetry laboratories (SSDLs) that in turn are used for calibrating the reference instruments of users, such as therapy level ionization chambers (hospitals) or calorimeters (radiation processing). This allows for the transfer of information from an accredited standards laboratory to an irradiation facility with established traceability (comparing absorbed dose assessments). Reference dosimeters are further used for calibration of dosimetry systems for the routine determination of absorbed dose.

The result of a dose determination is only an approximation or estimate of the dose value and is complete only when accompanied by a quantitative statement of its uncertainty. In dosimetry, the uncertainty associated with the determinations is often expressed in terms of accuracy and precision (Fig.3).

High precision	High precision	Low precision	Low precision
High accuracy	Low accuracy	High accuracy	Low accuracy
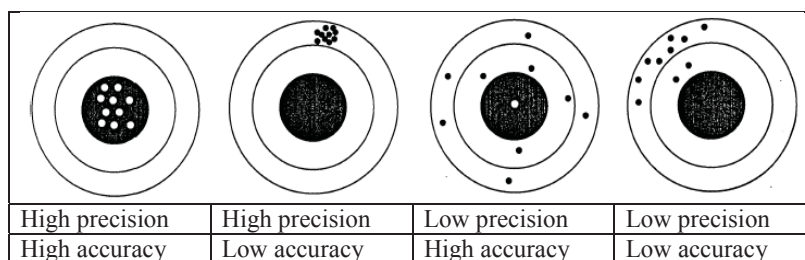
Fig.3. Illustration of precision and accuracy. (Adapted from Ref. [16]).

Accuracy specifies the proximity of the mean value of a measurement to the specified value.

Precision specifies the degree of reproducibility of a determination. High precision is associated with a small standard deviation of the distribution of determination results.

3.2. CALIBRATION AND VERIFICATION OF DOSIMETRY SYSTEMS

In radiation processing, validation and process control (as for sterilization, food irradiation, *etc.*) and the whole irradiation performance depend on the assessment of absorbed dose. This is performed using dosimetry systems having an acknowledged level of accuracy and precision. In dosimetry, accuracy is associated primarily with a quantity, which can be directly traceable to a primary standard system. Traceability is achieved by the calibration of a dosimetry system. Calibration is performed by determining the relationship between dosimeter response and the absorbed dose of reference or a primary standard. The effects of the influence factors, such as dose rate, temperature, storage time, storage conditions, humidity and light, should be minimized to attain optimal calibration conditions. Calibration is needed for reference standard dosimeters as performed in national or accredited laboratory; for transfer standard dosimeters, as performed according to class distinction requirements; and for routine dosimeters, as performed in a calibration laboratory, or in-plant facility. Primary standard dosimeters do not require any calibration.

Both components of a dosimetry system – dosimeters and the measuring or read-out equipment – shall be calibrated and traceable to internationally recognized standards:
• Calibration of measurement equipment is performed measuring certain parameters of the equipment and comparing them with a set of reference values. If measurement equipment cannot be calibrated (*e.g.* signal amplitude from an EPR (electron paramagnetic resonance) spectrometer), the stability of the equipment has to be demonstrated by the use of measurement standards (*e.g.* stable EPR spin standards).

- Calibration of dosimeter is performed by following a sequence of steps: a) irradiate the dosimeters, b) read the information provided by the dosimeters using a calibrated instrument, c) generate a calibration curve or response curve, d) compare the response curve with an initial calibration verification having periodic confirmation of validity, and e) compliance with a traceability chain that provides consistency of the performed measurements with the appropriate national or international standard.

More details on calibration procedures are found in ISO/ASTM 51261:2013 [4], and NPL Report CIRM 29 [23].

In order to verify the calibration, calibration curves prepared for routine dosimeters in a calibration laboratory or in an in-house calibration facility should be verified for the actual conditions of use in the irradiation production facility. Routine dosimeters should be irradiated together with reference or transfer standard dosimeters to at least three different absorbed doses. Absorbed dose results given by two types of dosimeters should be analysed with respect to any systematic trends for potential corrections if needed.

3.3. UNCERTAINTIES

The current methodology for estimating measurement uncertainty is given in the document "Evaluation of measurement data – Guide to the expression of uncertainty in measurement" (JCGM 100:2008) [24]. This is referred to as the "GUM", which defines the uncertainty as a parameter associated with the result of a measurement that characterizes the dispersion of measured values (= range of the values) that could reasonably be attributed to the measurand (= absorbed dose). This document is prepared in line with a standard ISO/ASTM 51707:2015 [7]. Uncertainties are based on probabilities and are often expressed as standard deviations (standard uncertainties), σ. The distribution of possible values often approximates a Gaussian or normal distribution (Fig.4).

There two types of uncertainties are investigated in performing measurements: type A (random) and type B (non-random, systematic):

- Type A standard uncertainties, u_A, are evaluated by statistical analysis of series of measurements (*e.g.* standard deviation of the mean) and are related mainly to some precision of the dosimeter response.

  If a measurement of a dosimetric quantity x is repeated N times, then the best estimate for x is the arithmetic mean of all measurements x_i:

$$\mu = \overline{x} = \frac{1}{N} \sum_{i=1}^{N} x_i \tag{10}$$

  The standard deviation σ_x is used to express the uncertainty for an individual result x_i:
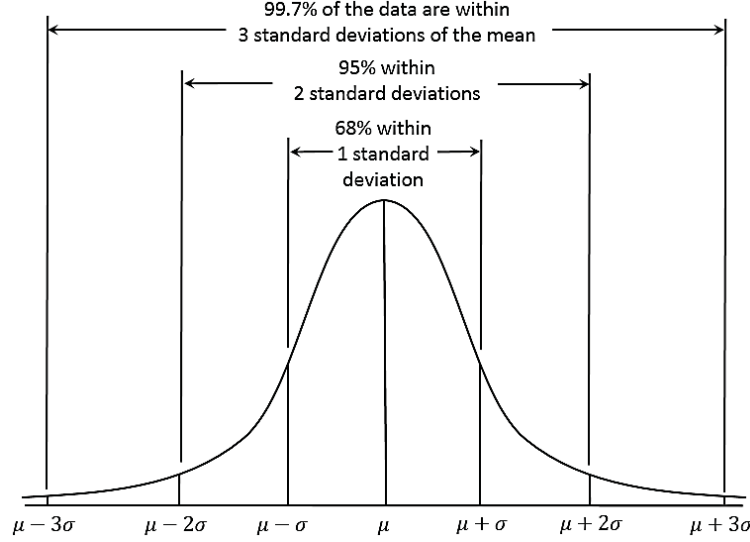
Fig.4. Gaussian distribution of measurement probability. Values μ corresponds to the arithmetic mean of all measurements; σ is standard deviation. The probability of a value being within ±1σ is ~68% (coverage factor k = 1); the probability of a value being within ±2σ is ~95% (k = 2); the probability of a value being within ±3σ is ~99.7% (k = 3). (Adapted from Ref. [25]).

$$\sigma_x = \sqrt{\frac{1}{N-1}\sum_{i=1}^{N}(x_i - \mu)^2} \qquad (11)$$

The standard deviation of the mean value is used to express the uncertainty for the best estimate:

$$u_A = \sigma_{\bar{x}} = \frac{1}{\sqrt{N}}\sigma_x = \sqrt{\frac{1}{N(N-1)}\sum_{i=1}^{N}(x_i - \mu)^2} \qquad (12)$$

- Type B standard uncertainties, u_B, cannot be estimated by repeated measurements and are evaluated by means other than statistical analysis (based on judgement and previous experimental data). Type B uncertainties include influences on the measuring process, the application of correction factors or physical data taken from the literature and are related to a calibration (accuracy). Type B evaluations vary, but their outcomes should be converted into a standard uncertainty in order to allow for the mathematical combination of all components of uncertainty.

  Having evaluated standard uncertainties associated with each component of a measurement, the combined uncertainty, u_C, associated with a particular measurement is obtained by summing in quadrature standard uncertainties of the individual component, *i.e.* by taking the square root of the sum of the squares of the individual components:

$$u_C = (u_1^2 + u_2^2 + u_3^2 + ...)^{1/2} \qquad (13)$$

The results of such analyses are often presented in a table, known as an uncertainty budget. An example of uncertainty budget of routine polystyrene calorimetric dosimetry system is provided in Table 2.

Table 2. Measurement uncertainties of routine polystyrene calorimetric dosimetry systems from Risø High Dose Reference Laboratory, at k = 2. (Data are adapted from Ref. [26]).

Component of uncertainty	Type A [%]	Type B [%]
Calibration of irradiation dose		3.2
Temperature measurement of calorimeter (at 3 kGy)	1.0	
Temperature extrapolation of calorimeter (at 3 kGy)	1.0	
Change of temperature sensitivity of specific heat of polystyrene		0.5
Heating effects	0.5	
Quadrature sum	1.5	3.2
Overall quadrature sum	3.5	

The combined uncertainty u_C is assumed to exhibit a Gaussian distribution (confidence level of 68%).

The expanded uncertainty, $U = k \times u_C$, with a coverage factor k = 2, corresponding to 95% confidence level, is often used to represent overall uncertainty, which relates to the accuracy of the measurement of a certain quantity.

4. DOSIMETRY SYSTEMS

Quality assurance programmes and implemented quality control measures are aimed to prove that the irradiation process was carried out within prescribed dose limits. This requires careful selection of the dosimetry system and its proper use after selection. The scope of application is one of the most important criteria for the selection of a suitable dosimetry system:
- field (industry, medicine, research and development),
- process to be controlled,
- standard (primary standard, reference, transfer, routine dosimetry),
- measured quantity (absorbed dose, dose rate and other dosimetric quantities, dose mapping and others),
- physical properties of dosimeter (radiation-induced physical and chemical processes in detector material that are related to the measured or evaluated dosimetric quantity),

- physical state (solid, liquid, gaseous, combined),
- measurement type (internal, external),
- measurement mode (*in-situ* or *ex-situ*),
- target substance related measurement (*in vivo*, *in vitro*).

   Dosimetry systems are based on measurement of radiation-induced physical or chemical changes in the detector material which can then be attributed to the absorbed dose. Thus, dosimetry methods are classified as:

- ionization based (ionization chambers),
- temperature change related (calorimeters),
- thermoluminescence (LiF),
- colour change related (Perspex™, radiochromic systems),
- free radical concentration change related (alanine),
- conductivity change related (ECB, alanine solution),

Table 3. Dosimeter system standards. (Compiled on basis of Ref. [28]).

Dosimeter system	Method of analysis	Useful dose range [Gy]	Nominal precision limits [%]	References
Fricke solution	UV spectrophotometry	$3 \times 10\text{-}4 \times 10^2$	1	ASTM E 1026-04 [29]
Ceric-cerous sulphate	UV spectrophotometry	$10^3\text{-}10^6$	3	ISO/ASTM 51205:2009 [30]
Potassium dichromate	UV-VIS spectrophotometry	$5 \times 10^3\text{-}4 \times 10^4$	1	ISO/ASTM 51401:2013 [31]
Ethanol-mono-chlorobenzene	Titration, or HF oscillometry	$4 \times 10^2\text{-}3 \times 10^5$	3	ISO/ASTM 51538:2009 [32]
L-alanine	EPR	$1\text{-}10^5$	0.5	ISO/ASTM 51607:2013 [33]
Perspex systems	VIS spectrophotometry	$10^3\text{-}5 \times 10^4$	4	ISO/ASTM 51276:2012 [34]
FWT-60 film	VIS spectrophotometry	$10^3\text{-}10^5$	3	ISO/ASTM 51275:2013 [35]
B3/GEX film	VIS spectrophotometry	$10^3\text{-}10^5$	3	ISO/ASTM 51275:2013 [35]
Cellulose triacetate	UV spectrophotometry	$10^4\text{-}10^6$	3	ISO/ASTM 51650:2013 [36]
Calorimetry	Resistance/temperature	$1.5 \times 10^3\text{-}5 \times 10^4$	2	ISO/ASTM 51631:2013 [37]
LiF (Sunna film)	Optically stimulated luminescence	$50\text{-}3 \times 10^3$	3	ASTM E2304-03 [38]
TLD	Thermoluminescence	$1\text{-}10^4$	2	ISO/ASTM 51956:2013 [39]

- radiation chemical oxidation based (Fricke),
- radiation chemical reduction based (dichromate, ceric-cerous),
- optically stimulated luminescence (OSL, Al_2O_3, Sunna),
- production of radiation defects in semiconductors (diodes, MOSFETs),
- others.

Information on standards applicable for dosimetry systems used in radiation processing is presented in the Table 3. It can be also found on the web pages: www.iso.org, and www.astm.org/COMMITTEE/E61.htm. Essential and very useful information on the dosimetry systems used in materials processing is found in Refs. [2] and [27]. Table 3 summarizes the description of most of the important dosimetry systems.

Primary standard dosimetry systems

Calorimetry and ionization chambers are considered as primary standard methods to determine dose. Calorimeters are used when establishing standards for dose in the radiation processing of materials. Calorimeters and ionization chambers are used to establish dose for medical applications. Dosimeters for medical applications, not discussed here, are described in detail in several publications including Refs. [15, 40-43].

Calorimetry is the most fundamental method used as a primary standard for absorbed dose, since the measured rise in temperature is the most direct consequence of energy absorption (energy-to-heat conversion) in a thermally isolated mass. Measured energy per unit mass or the average dose to the medium assuming no heat loss is:

$$\bar{D} = \frac{h\Delta T}{1-\delta} \qquad (14)$$

where h is specific heat capacity of the medium, and δ is the thermal defect (this small fraction of the energy that does not appear eventually as thermal energy because of a chemical reaction).

The principle of calorimetry is illustrated in Fig.5.

A graphite calorimeter is used by several PSDLs as a primary instrument to determine absorbed dose. Graphite is an ideal material for calorimetry. Gaphite has a low atomic number, Z, so that all of the absorbed energy reappears as heat, without any loss of heat in other mechanisms (such as heat defection) and its specific heat capacity is 7.1×10^2 J/K, so that temperature changes of a few μ°C can be measured.

Water calorimeter is also used by PSLDs as a primary standard to determine the absorbed dose to water in a water phantom. An example of a water calorimeter is shown in Fig.6.

Water calorimeter at Physicalisch Technische Bundesanstalt [44], is able to determine D_w for ^{60}Co radiation under reference conditions with a standard measured uncertainty of approximately 0.2%. Highly purified water is used due to low operationing temperature of 4°C.
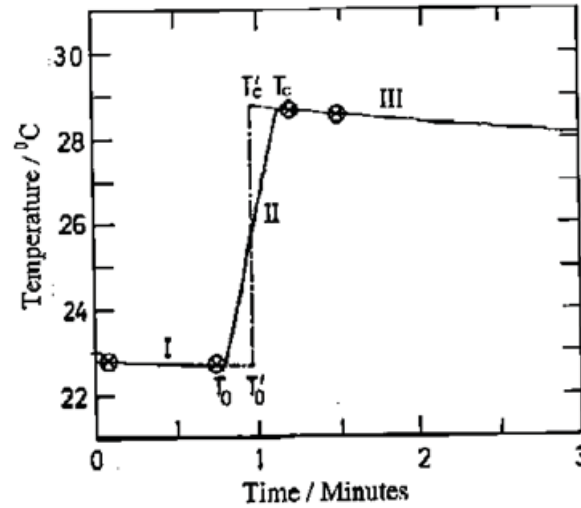
Fig.5. The temperature curves were extrapolated from T_0 and T_c to mid-point of the irradiation time at T_0' and T_c', respectively. $\Delta T = T_c' - T_0'$ is used for dose calculation. Regions I, II and III are before, during and after the irradiation, respectively. (Adapted from Ref. [15]).

The advantage of using graphite instead of water is a lack of thermal defects.

Graphite, water and polystyrene calorimeters, classified as Type II detectors (ISO/ASTM 52628:2013) [3], are also defined as *process calorimeters*. These calorimeters may be used as internal standards at an electron beam irradiation facility, including their application as transfer standard dosimetry systems for calibration of other dosimetry systems, or they may be used as routine dosimeters provided they are used under static, non-moving conditions. Calorimeters are highly sensitive (water calorimeter – 3.4 kGy/°C, polystyrene calorimeter – 1.4 kGy/°C, graphite calorimeter – 0.75 kGy/°C) to absorbed dose within the range of 1.5-60.0 kGy measured using 4-10 MeV electron beams.

A   B   C
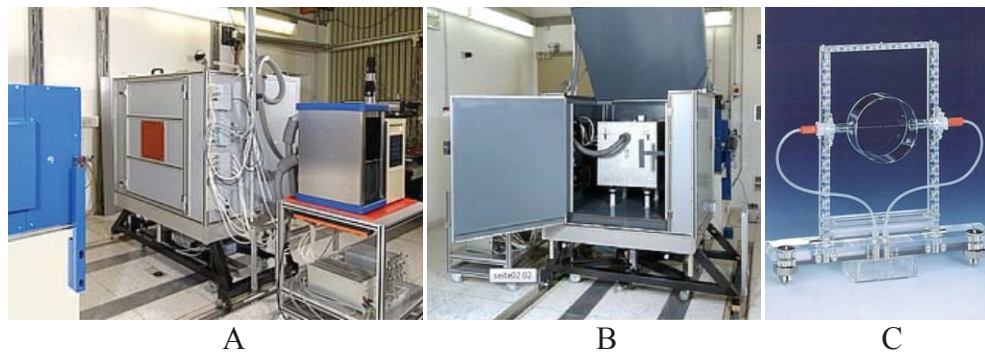
Fig.6. Water calorimeter at Physicalisch Technische Bundesanstalt (PTB, Germany): A – an overall view of the construction, B – cubic water phantom surrounded by polystyrene containing walls, C – calorimetric detector filled with highly purified water. (Adapted from Ref. [44]).

However, calorimetry has not been conducted under the high speed operating conditions common to electron beam processing.

Special polystyrene calorimeters are used for dose measurements at 1.5-4 MeV electron beam energies and that the development of a calorimeter for low energy (80-120 keV) electron beams under static, non-moving conditions is ongoing [28].

Reference standard chemical dosimetry systems

(Fricke, ceric-cerous, potassium dichromate, alanine, ECB dosimeters)

In chemical dosimetry systems, the dose is determined by evaluating the chemical change produced by radiation in the sensitive volume of the dosimeter.

Fricke dosimeters use a water solution of $FeSO_4(7H_2O)$ or $Fe(NH_4)_2(SO_4)_2(6H_2O)$ with additives of sulphuric acid (H_2SO_4) and sodium chloride (NaCl), and are the most widely used chemical dosimetry standard (Fig.7).

| A | B |

Fig.7. Fricke dosimeters: (A) as prepared Fricke solutions, (B) application of Fricke dosimeter in research related to food irradiation. (Adapted from Ref. [28]).

When irradiated, ferrous ions Fe^{2+} are oxidized into ferric ions Fe^{3+}, that exhibit a strong absorption peak at a wavelength of 304 nm, whereas ferrous ions Fe^{2+} do not show any absorption at this wavelength. The response of Fricke dosimeter is expressed in terms of the yield of ferric ions Fe^{3+}. It is nearly independent of the photon and electron energy in the range of 5-16 MeV. The average dose to Fricke solution is given by a change in optical density at 304 nm:

$$\overline{D}_F = \frac{\Delta OD}{\varepsilon G \rho L} \tag{15}$$

where: ε – the molar extinction coefficient (217.4 l/mol·cm at 25°C), G – the yield of ferric ions Fe^{3+} (1.617 × 10^{-6} mol/J), ρ – the density of Fricke solution (1.023 kg/dm^3 at 25°C), L – the path length over which the optical signal was red (typically 2-4 cm). The absorbed dose within the range of 40-400 Gy can be measured using Fricke dosimeter.

Potassium dichromate is known as reference dosimetry system for gamma facilities. It uses a potassium dichromate ($K_2Cr_2O_7$) and silver dichromate ($Ag_2Cr_2O_7$) solution in perchloric acid ($HClO_4$). Dose measurements within the range of 10-50 kGy are based on colour changes in the solution at a wavelength of 440 nm due to the radiolytic reduction of dichromate ions to chromic ions. The $Ag_2Cr_2O_7$ solution in $HClO_4$ allows the determination of doses down to 2 Gy, but the dose response then (colour change) is observed at 350 nm (Fig.8).

A   B
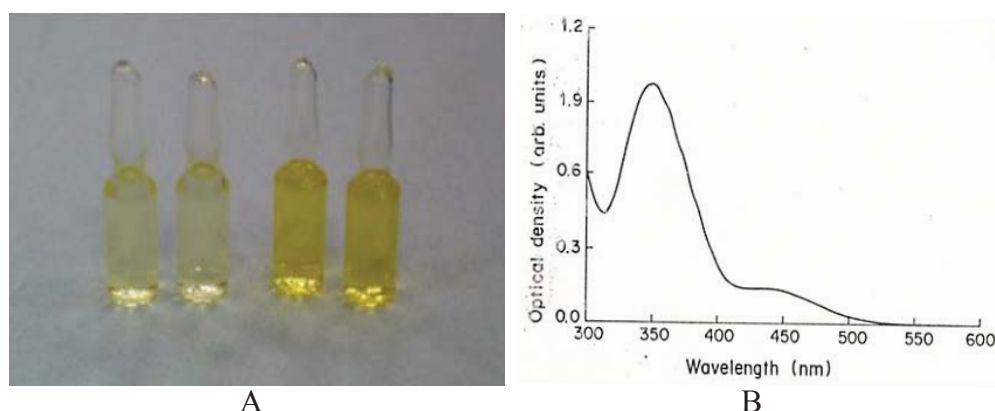
Fig.8. Dichromate dosimeters: A – as prepared (left) and irradiated (right) dosimeters, B – UV-VIS absorbance spectrum of irradiated potassium dichromate. (Adapted from Ref. [28]).

Ethanol-monochlorobenzene dosimeter contains monochlorobenzene (C_6H_5Cl) in an aerated ethanol-water solution. The concentration of mono-chlorobenzene may vary between 4 and 40 vol% based upon request, but in radiation processing a solution containing 24 vol% of monochlorobenzene is used. This dosimeter is based on the formation of hydrochloric acid (HCl) upon irradiation *via* dissociative electron attachment, since monochlorobenzene is a good electron scavenger and reacts with "dry" and solvated electrons. The determination of absorbed dose is carried out by measuring the concentration of HCl using alkalimetric or mercurimetric titration [45]. This dosimeter is used in reference (also transfer) dosimetry systems for dose measurements at electron and X-ray facilities. Doses from the range of 10 Gy-200 kGy can be measured when the electron beam energy is higher than 4 MeV, while the doses measured at X-ray beams (> 2 MeV) can be from the range of 10 Gy-2 MGy. This do-simeter is nearly independent of irradiation temperature.

Alanine dosimeters (pellets or films) are based on an amino acid which forms stable free radicals when irradiated:
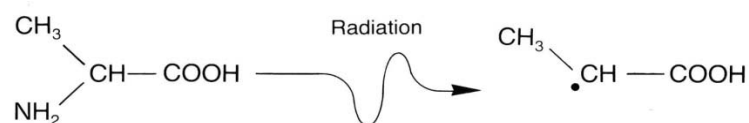
The concentration of free radicals is measured using EPR spectroscopy (Fig.9) and is proportional to the absorbed dose, which can be determined within the range of 10 Gy-100 kGy. Alanine is used for gamma and electron reference dosimetry. However dose response dependency on environmental conditions (humidity, temperature) should be considered when performing measurements.
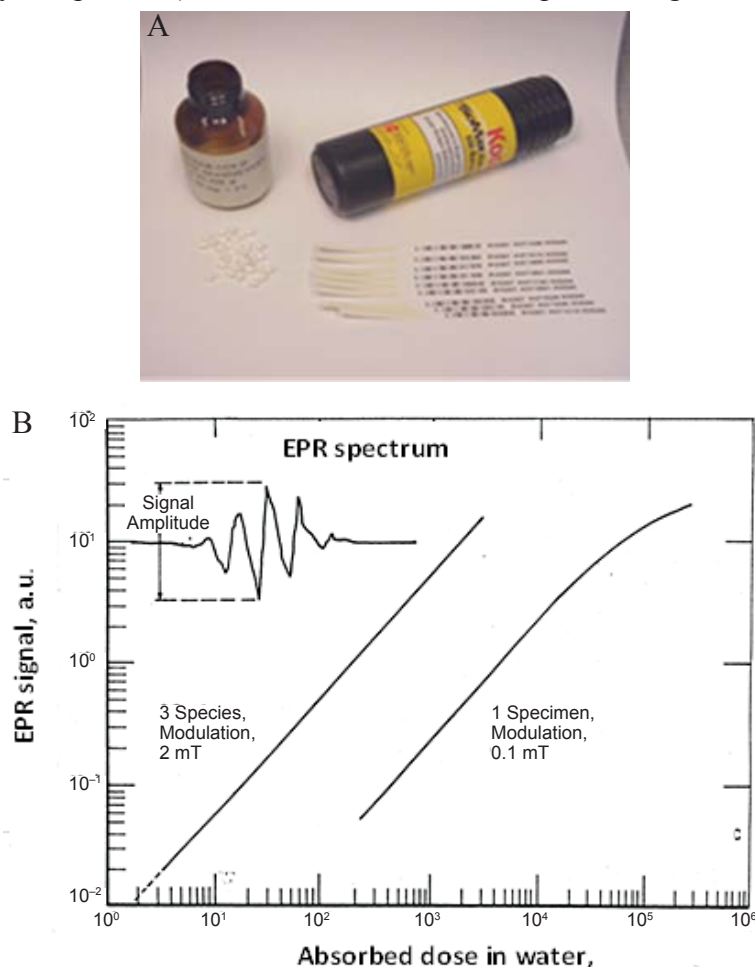
Fig.9. Alanine dosimeters: A – a variety of alanine dosimeters, B – EPR spectrum and measured value: peak to peak signal. (Adapted from Ref. [2]).

Routine dosimetry systems
(Perspex™, films, ECB, ceric-cerous solutions, process calorimeters)
    These systems are used in radiation processing facilities for absorbed dose mapping and process monitoring. They require calibration.
    Perspex™ is the trade name of poly(methyl methacrylate) $(C_5O_2H_8)_n$. Certain dyes are responsible for the colour of Perspex (red, amber, gammachrome YR). *Perspex dosimeters* darken when irradiated (Fig.10). The increased absorption is a result of radiation-induced free radicals that initially react with
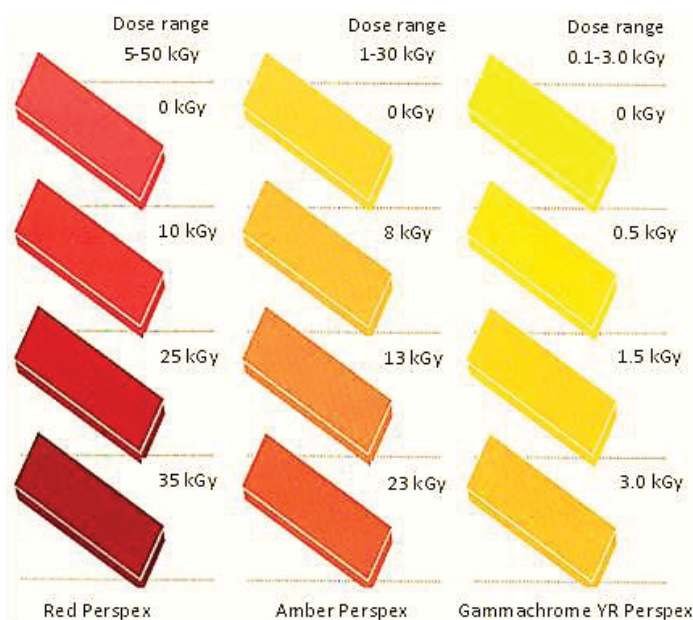
Fig.10. Different types of Perspex dosimeters and their reaction to irradiation. (Adapted from Ref. [28]).

oxygen present in the polymer to yield peroxy radicals. Radiation-induced colour changes can be accurately measured by means of a spectrophotometer and are related to the absorbed dose. Absorbed doses within the interval of 0.1-3.0 kGy can be determined at 530 nm by the Gammachrome YR Perspex, within interval of 1-30 kGy – at 603 nm by the Amber Perspex and within interval of 5-50 kGy – 640 nm by the Red Perspex dosimeter. Perspex dosimeters are used in routine gamma dosimetry.

Film dosimeters are mainly used for absorbed dose mapping and process monitoring at an irradiation facility. Most important film dosimeters are:

• FTR-125 – cellulose triacetate dosimeters are used for routine dosimetry in electron beam, gamma-ray and ion beam irradiation facilities, mainly for dose mapping. Absorbed dose within the range of 5-300 kGy can be evaluated according to radiation-induced absorbance changes at 280 nm.

Fig.11. A – irradiated Risø B3 film; B and C – GEX DoseStix and WinDose dosimeters made from Risø B3 film, respectively. (Adapted from Ref. [19]).

- FTW-60 is a colourless radiochromic film containing hexa (hydroxyethyl) pararosaniline cyanide in a nylon matrix. Radiation induces a film colour changes toward a deep blue. Absorbed dose can be estimated for the range of 3-30 kGy, if spectrophotometric optical density measurements are carried out at 605 nm, and for the range of 30-150 kGy, if spectrophotometric optical density measurements are carried out at 510 nm. Film response is independent of the energy and type of radiation (electron beam, gamma ray or X-ray) and of the dose rate up to about 10^{13} Gy/s. These dosimeters are used for process control for gamma as well as for electron beam irradiation.

- Risø B3 (GEX) radiochromic film (Fig.11) is colourless polyvinyl butyral film containing the leucocyanide of pararosaniline. Radiation induces film colour changes to deep pink. Heating at 60°C for 5 to 10 min after irradiation helps stabilize the colour. Absorbed dose can be estimated within the range of 2-100 kGy performing spectrophotometric measurements at 544 nm. Films are widely used in gamma and electron beam radiation processing.

- Gafchromic films are radiochromic films consisting of colourless transparent coatings of polycrystalline substituted diacetylene sensor layers on a clear polyester base. Radiation induces film colour changes to deep blue. Absorbed doses within the range of 1 Gy-40 kGy can be evaluated. Spectrophotometric readings are performed at different wavelengths (670, 633, 600, 500 and 400 nm) depending on the absorbed dose. Films are applicable as a routine dosimeters in medical applications, industrial radiation processing and food irradiation.

- Sunna film [46] is a novel OSL dosimetry system and is made by LiF uniformly dispersed in a polyethylene matrix (Fig.12).
  Irradiation stimulates formation of colour centres in LiF (F-, M-, N-, R-centre) that correspond to discrete optical absorption bands in the UV-VIS region. The information related to the absorbed dose can be inferred by excitation of the irradiated dosimeter with a light at the wavelength of the colour centre absorption and measurement of a characteristic luminescence at a significantly higher wavelength. The range of the evaluated absorbed dose depends on the absorption wavelength:
  – for the evaluation of UV absorbance at 240 nm, the dose range is between 5 and 100 kGy;
  – for the evaluation of green OSL at 530 nm, the dose range is between 200 Gy and 250 kGy;
  – for the evaluation of near infrared OSL at 670 and 1100 nm, the dose range is between 10 Gy and 10 kGy.
  The Sunna films are used in both gamma and electron beam processing for dose distribution measurements, as well as for routine process control.

- Tetrazolium films [47] are also based on the colour changes after irradiation. The main component of the film, a tetrazolium salt, is a heterocyclic organic compound which yields highly coloured water insoluble formazans
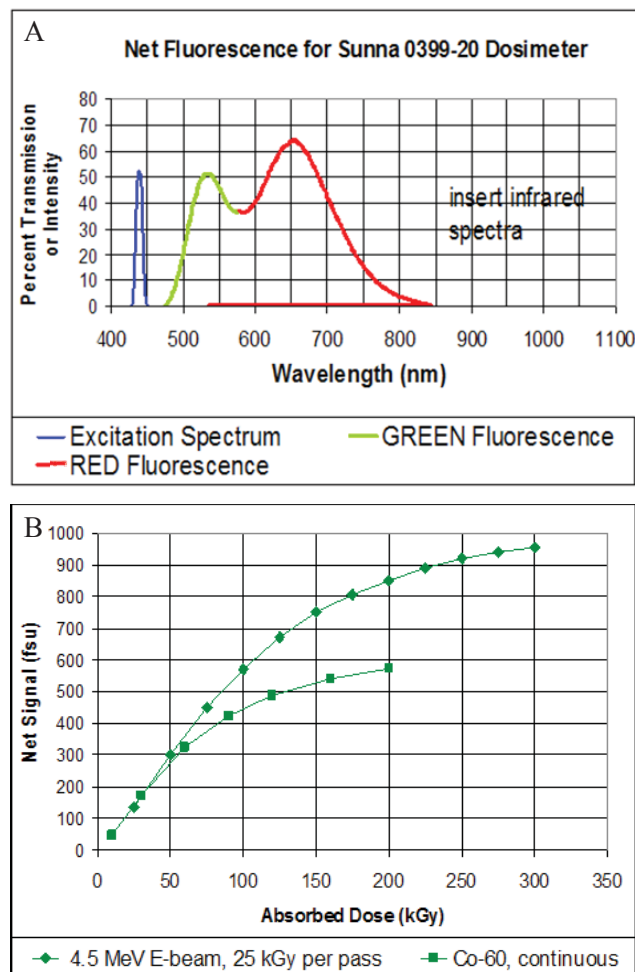
Fig.12. A – Sunna films UV, green or red (IR) OSL absorption bands; B – sensibility of Sunna film (green range) to different irradiations. (Adapted from Ref. [28]).

due to radiolytic reduction. The range of the inference of absorbed dose depends on the measured wavelength at which the absorption peak was identified:

– for tetrazolium violet (TV): 525 nm measured absorbance corresponds to the dose range of 10 Gy-30 kGy;
– for tetrazolium red (TTC): 490 nm measured absorbance corresponds to the dose range of 10 Gy-100 kGy;
– for tetrazolium blue (TB): 520 nm measured absorbance corresponds to the dose range of 10 Gy-10 kGy;
– For nitro blue tetrazolium (NBT): 522 and 612 nm measured absorbance correspond to the dose range of 10 Gy-25 kGy.

Some additional information related to Gafchromic films, Sunna dosimeters, tetrazolium films and other novel dosimetry systems could be found in Ref. [14].

5. RADIATION SAFETY AND RADIATION PROTECTION

Mankind greatly benefits from the use of electron beam, gamma rays and X-rays in industrial processing and in research and development. Radioisotopes and fissionable materials are used in medicine, research, and power generation. These uses involve potential exposure of personel to radiation. Accidental exposure is also possible. Since radiation exposure presumably involves some risk to the individuals, the levels of exposure allowed should be worth the result that is achieved. The overall objective of radiation protection is to balance the risks and benefits from activities that involve radiation even if these risks and benefits are hardly measurable directly [48].

The IAEA recommendations for radiation protection are provided in the Basic Safety Standards (BSS) books [49, 50]. These basic safety standards represent internationally agreed standards that set out the requirements for a framework to regulate radiation safety in each country and that, in principle, have been accepted by all member states. They are based on knowledge of radiation effects and on established principles of radiation protection, recommended by the ICRP (International Commission on Radiological Protection):

• Benefit of practices must offset radiation detriment.
• Exposures and likelihood of exposure should be kept as low as reasonably achievable (ALARA principle).
• Dose limits should be set to ensure that no individual faces an unacceptable risk under normal circumstances.

The ICRP has proposed safety standards to protect the health of workers and the general public against the dangers arising from ionizing radiation (last upgraded version: ICRP publication 103 [51]). These recommendations were laid down in a European Directive: EU Council Directive 2013/59/EURATOM [52], which has been accepted by the Member States of the European Community.

The Directive has defined safety standards for the exposed workers in the following way:

• The limit on the effective dose is 100 mSv in a consecutive five year period, subject to a maximum effective dose of 50 mSv in any single year. In accordance with this, most Member States have defined an annual limit of 20 mSv. (Sievert, Sv, is equal to 1 joule of energy deposited in a kilogram of human tissue).
• The annual limit on the equivalent dose for the lens of the eye is 20 mSv.
• The annual limit on the equivalent dose for the skin is 500 mSv.
• The annual limit on the equivalent dose for the hands, forearms, feet, and ankles is 500 mSv.

The annual limit for the whole-body dose for the general population, is 1 mSv in most countries.

The ICRU has defined radiation protection quantities for dose limitations to the potentially exposed workers that are different from those described above in the introduction of this chapter: the equivalent dose (accounts for radiation type) and the effective dose (accounts radiosensitivity of different organs and tissues) [13].

Equivalent dose is the dose absorbed in an organ or tissue and multiplied by the relevant radiation weighting factor, w_R:

$$H_{T,R} = w_R D_{T,R} \tag{16}$$

where $D_{T,R}$ is the average absorbed dose in the organ or tissue T, and w_R is the radiation weighting factor for radiation R (alpha particles, electrons, photons, neutrons).

Effective dose is a summation of the tissue equivalent doses, each multiplied by the appropriate tissue/organ weighting factor, w_T:

$$E = \sum_T w_T H_T \tag{17}$$

where H_T is the equivalent dose in tissue T, and w_T is the tissue weighting factor for tissue T.

The unit of equivalent and also effective dose is J/kg, termed the sievert (Sv).

In order to minimize radiation risks to personnel working in potential exposure conditions, relevant radiation protection measures should be imple-

Table 4. Typical personal dosimeters [42].

Dosimeter	Principle of operation	Radiation type, measurement range	Advantages and disadvantages
Film badge	Photochemical blackening	γ, β 0.1 mSv-5.0 Sv	Can be documented, insensitive for low-energy rays
Pen-type pocket dosimeter	Ionization chamber	γ 0.03-2.00 mSv	Very sensitive, permanently readable, insensive for α- and β-rays, cannot be documented
Permanently readable dosimeter (pocket dosimeter)	Ionization or proportional chambers and GM counters	γ 0.1 μSv-10.0 Sv	Permanently readable, cannot be documented
TLD dosimeter	Thermoluminescence measurement	γ, (β) 0.1 mSv-10.0 Sv	Suitable for low dose measurements, cannot be documented
Phosphate glass dosimeter	Photoluminescence measurement	γ 0.1 mSv-10.0 Sv	Can be documented, can be read repeatedly
Albedo neutron dosimeter	Neutron moderation by the carrier	n, γ 0.1 mSv-10.0 Sv	Calibration depends on human carrier

mented in the work environment and the doses to workers must be permanently controlled and measured using the appropriate dosimeters.

Typical applications of different measurement techniques for personal dosimetry are listed in Table 4. More detailed information on personal dosimeters can be found in Refs. [41, 42, 53].

REFERENCES

[1]. Greening, J.R., Green, S., Charles, M.W. (2010). *Fundamentals of radiation dosimetry* (3rd ed.). London: Taylor & Francis.

[2]. IAEA. (2013). *Guidelines for development, validation and routine control of industrial radiation processes.* Vienna: IAEA. (IAEA Radiation Technology Series No. 4).

[3]. ISO. (2013). *Practice for dosimetry in radiation processing.* ISO/ASTM 52628:2013.

[4]. ISO. (2013). *Practice for calibration of routine dosimetry systems for radiation processing.* ISO/ASTM 51261:2013.

[5]. ISO. (2013). *Guide for performance characterization of dosimeters and dosimetry systems for use in radiation processing.* ISO/ASTM 52701:2013.

[6]. ISO. (2015). *Guide for absorbed-dose mapping in radiation processing facilities.* ISO/ASTM 52303:2015.

[7]. ISO. (2015). *Guide for estimation of measurement uncertainty in dosimetry for radiation processing.* ISO/ASTM 51707:2015.

[8]. ASTM International. (2010). *Standard guide for selection and use of mathematical methods for calculating absorbed dose in radiation processing applications.* ASTM E2232-10. West Conshohocken, PA.

[9]. ISO. (2015). *Practice for dosimetry in an electron beam facility for radiation processing at energies between 300 keV and 25 MeV.* ISO/ASTM 51649:2015.

[10]. ISO. (2013). *Practice for dosimetry in an electron beam facility for radiation processing at energies between 80 and 300 keV.* ISO/ASTM 51818:2013.

[11]. ISO. (2015). *Practice for dosimetry in an X-ray (bremsstrahlung) facility for radiation processing at energies between 50 keV and 7.5 MeV.* ISO/ASTM 51608:2015.

[12]. ISO. (2013). *Standard practice for dosimetry in gamma irradiation facility for radiation processing.* ISO/ASTM 51702:2013.

[13]. ICRU. (1998). *Fundamental quantities and units for ionizing radiation.* Bethesda, MD: ICRU. (ICRU Report 60).

[14]. Podgorsak, E.B. (2005). *Radiation oncology physics: A handbook for teachers and students*. Vienna: IAEA.

[15]. Attix, F.H. (1986). *Introduction to radiological physics and radiation dosimetry*. Weinheim: Wiley-VCH Verlag GmbH & Co KGaA.

[16]. Seuntjens, J.P., Strydom, W., & Shortt, K.R. (2005). Chapter 2. Dosimetric principles, quantities and units. In E.B. Podgorsak (Ed.), *Radiation oncology physics: A handbook for teachers and students* (pp. 45-70). Vienna: IAEA. Retrieved March, 30, 2016, from http://www-naweb.iaea.org/nahu/DMRP/documents/Chapter2.pdf.

[17]. Turner, J.E. (2007). *Atoms, radiation and radiation protection* (3rd ed.). Weinheim: Wiley-VCH Verlag GmbH & Co KGaA.

[18]. Smith, D.S., & Stabin, M.G. (2012). Exposure rate constants and lead shielding values for over 1,100 radionuclides. *Health Phys., 102*, 3, 271-291.

[19]. IAEA. (1987). *Absorbed dose determination in photon and electron beams*. Vienna: IAEA. (IAEA Technical Report Series No. 277).

[20]. IAEA/iiA. (2011). *Industrial radiation processing with electron beams and X-rays* (6th revision). International Atomic Energy Agency, International Irradiation Association. Retrieved March 30, 2016, from http://www.cirms.org/pdf/Industrial%20Radiation%20Processing%20-%20May%202011%20-%20Revision%206.pdf.

[21]. ICRU. (2008). *Dosimetry systems for use in radiation processing.* Bethesda, MD: ICRU. (ICRU Report 80).

[22]. ISO. (2005). *General requirements for the competence of testing and calibration laboratories*. ISO/IEC 17025:2005.

[23]. Sharpe, P., & Miller, A. (2009). *Guidelines for the calibration of routine dosimetry systems for use in radiation processing*. U.K: Queens Printer and Controller of HMSO. (NPL Report CIRM 29).

[24]. JCGM. (2008). *Evaluation of measurement data — Guide to the expression of uncertainty in measurement*. JCGM 100:2008.

[25]. Wheeler, D.J., & Chambers, D.S. (1992). *Understanding statistical process control* (2nd ed.). SPC Press.

[26]. IAEA Regional Workshop "Use of uncertainty in conformity assessment in radiation processing", 9-11 November, 2015. Budapest: Centre for Energy Research of the Hungarian Academy of Sciences. [unpublished training materials].

[27]. Zaman, K., & Dahlan, H.M. (2008). Radiation processing. In *Physical methods, instruments and measurements* (Vol. 4). (Encyclopedia of Life Support Systems (EOLSS)). Developed under the Auspices of the UNESCO, Paris, France: Eolss Publishers. [http://www.eolss.net].

[28]. IAEA Regional Training Course "Dosimetry at electron beam facilities", 11-15 May, 2015. Warsaw: Institute of Nuclear Research and Technology. [unpublished training materials].

[29]. ASTM International. (2004). *Standard practice for using the Fricke reference standard dosimetry system*. ASTM E1026-04. Conshohocken, PA.

[30]. ISO. (2009). *Standard practice for use of the ceric-cerous sulphate dosimetry system*. ISO/ASTM 51205:2009.

[31]. ISO. (2013). *Practice for use of a dichromate dosimetry system*. ISO/ASTM 51401:2013.

[32]. ISO. (2009). *Practice for use of the ethanol-chlorobenzene dosimetry system*. ISO/ASTM 51538:2009.

[33]. ISO. (2013). *Practice for use of the alanine-EPR dosimetry system*. ISO/ASTM Standard 51607:2013.

[34]. ISO. (2012). *Standard practice for use of a polymethylmethacrylate dosimetry system*. ISO/ASTM 51276:2012.

[35]. ISO. (2013). *Practice for use of a radiochromic film dosimetry system*. ISO/ASTM 51275:2013.

[36]. ISO. (2013). *Standard practice for use of cellulose acetate dosimetry systems*. ISO/ASTM 51650:2013.

[37]. ISO. (2013). *Practice for use of calorimetric dosimetry systems for electron beam dose measurements and dosimeter calibrations*. ISO/ASTM 51631:2013.

[38]. ASTM International. (2004). *Standard practice for use of a LiF photo-fluorescent film dosimetry system*. ASTM E2304-03(2011). Conshohocken, PA.

[39]. ISO. (2013). *Practice for use of a thermoluminescence – dosimetry system (TLD system) for radiation processing*. ISO/ASTM 51956:2013.

[40]. Del Guerra, A. (2004). *Ionizing radiation detectors for medical imaging*. Singapore: World Scientific.

[41]. Knoll, G.F. (2010). *Radiation detection and measurement* (4th ed.). New York: Wiley.

[42]. Seco, J., Clasie, B., & Partridge, M. (2014). Review on the characteristics of radiation detectors for dosimetry and imaging. *Phys. Med. Biol.*, *59*, R303-R347.

[43]. Grupen, C., & Buvat, I. (Eds.). (2012). *Handbook of particle detection and imaging*. Berlin, Heidelberg: Springer.

[44]. Physikalisch-Technische Bundesanstalt (2010). Water calorimeter: EUR-RAD--PTB-1004. *Primary standard measuring for Co-60 radiation (calorimeter, detector)*. Retrieved March 7, 2016, from https://www.ptb.de/cms/en/ptb/fach-abteilungen/abt6/fb-62/623-unit-of-absorbed-dose-to-water/water-calorimeter--primary-standard.html.

[45]. Doric, I. (1970). The ethanol-chlorobenzene dosimeter. In N.W. Holm & R.J. Berry (Eds.). *Manual on radiation dosimetry* (Part 2, pp. 345-349). New York: Marcel Dekker.

[46]. Kovács, A., Baranyai, M., Wojnárovits, L., McLaughlin, W.L., Miller, S.D., Miller, A., Fouchi, P.G., & Lavalle, M. (2000). Application of the Sunna dosimeter film in gamma and electron beam radiation processing. *Radiat. Phys. Chem.*, *57*, 691-695.

[47]. Kovács, A., Baranyai, M., Wojnárovits, L., Slezsák, I., McLaughlin, W.L., Miller, A., & Moussa, A. (2000). Dose determination with nitro blue tetrazolium containing radiochromic dye films by measuring absorbed and reflected light. *Radiat. Phys. Chem.*, *57*, 711-716.

[48]. Shapiro, J. (2002). *Radiation protection. A guide for scientists, regulators, and physicians* (4th ed.). Harvard University Press.

[49]. IAEA. (2010). *Radiation safety of gamma, electron and X ray irradiation facilities*. Vienna: IAEA. (IAEA Safety Standards Series No. SSG-8).

[50]. IAEA. (2011). *Radiation protection and safety of radiation sources: International basic safety standards*. Vienna: IAEA. (IAEA Safety Standards Series No. GSR Part 3).

[51]. ICRP. (2007). The 2007 recommendations of the International Commission on Radiological Protection. ICRP Publication 103. *Ann. ICRP*, 37 (2-4).

[52]. Council of the European Union. (2014). Council Directive 2013/59/EURATOM of 5 December 2013 laying down basic safety standards for protection against the dangers arising from exposure to ionising radiation, and repealing Directives 89/618/Euratom, 90/641/Euratom, 96/29/Euratom, 97/43/Euratom and 2003/122/Euratom. *Official Journal of the European Union*, L13/1, 17.01.2014.

[53]. Podgorsak, E.B. (2010). *Radiation physics for medical physicists* (2nd ed.). Berlin, Heidelberg, New York: Springer.

RADIATION CHEMISTRY OF LIQUID SYSTEMS

Krzysztof Bobrowski
Institute of Nuclear Chemistry and Technology, Dorodna 16, 03-195 Warszawa, Poland

1. INTRODUCTION

The radiation chemistry of liquid systems illustrates a versatile use of high energy ionizing radiation [1-4]. Radiolysis, the initiation of reactions by high energy radiation, is a very valuable and powerful chemical tool for inducing and studying radical reactions in liquids. In many cases radiolysis offers a convenient and relatively easy way of initiating radical reactions in all phases (including liquid phase) that cannot be or can be performed with some limitations by chemical, electrochemical and photolytic methods. Radiolysis of most liquids produces solvated electrons and relatively simple free radicals, some of which can oxidize and/or reduce materials [5]. This chapter is divided into four main sections: "Introduction", "Radiolysis of water", "Radiolysis of organic solvents", and "Radiolysis of ionic liquids". The first section summarizes the mechanisms and features of radiation energy deposition along with a quantification of chemical effects induced by radiation, and techniques used in radiation chemical studies. The second section focuses on radiation-induced radical reactions in water and aqueous solutions using low and high linear energy transfer (LET) irradiation at ambient and high temperatures, and high pressures. Relevant examples include radical reactions initiated by primary and secondary radicals from water radiolysis with a variety of compounds. The third section describes the most important features of radiolysis in organic liquids using common solvents for inducing and studying radical reactions. Relevant examples include radical reactions connected with the selective formation of radical cations, radical anions and excited states. The last section briefly summarizes the most commonly use ionic liquid (IL) systems and highlights radiation-induced radical reactions in IL, a new matrix used for the radiation generation of radicals and radical ions in the liquid phase [6].

The chemical changes that commonly involve radiation-induced radical reactions are the consequences of the absorption of energy of high energy radiation by matter [7-13].

1.1. MECHANISMS OF RADIATION ENERGY DEPOSITION

The mechanisms by which radiation energy is deposited in matter depend upon the type of radiation. There are three types of ionizing radiation: (i) electromagnetic radiation (X- and γ-rays), (ii) charged particles (electrons and heavy positive ions), and (iii) neutral particles (neutrons). There are three important processes by which electromagnetic radiation interacts with matter. These processes are the photoelectric effect, the Compton effect, and pair production, probabilities of which vary with the energy of radiation and the atomic number, Z, of the material involved [7-13]. Charged particles interact with matter *via* three main processes, *i.e.* emission of "bremsstrahlung" or braking radiation, inelastic and elastic collisions. Their relative importance depends upon the energy of the particles and also on the nature of the material which they pass through (see Chapter 2). In the case of neutrons there are four main processes by which they interact in collisions with atomic nuclei: elastic and inelastic scatterings, nuclear reactions, and neutron capture.

The absorption of the energy in a medium, M, causes ionization of molecules and/or formation of excited and super-excited states represented by Eqs. (1) and (2), respectively:

$$M \xrightarrow{\quad\wedge\wedge\wedge\wedge\quad} M^{\bullet+} + e^- \tag{1}$$

$$M \xrightarrow{\quad\wedge\wedge\wedge\wedge\quad} M^*/M^{**} \tag{2}$$
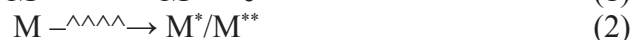
The electrons produced in ionization (Eq. (1)) can cause further ionization and excitation. Thus, the primary effect of any type of ionizing radiation on matter is the production of radical ions, ions, excited states and electrons [14].

1.2. FEATURES OF RADIATION ENERGY DEPOSITION

Radiation energy deposition is spatially inhomogeneous and creates sites of dense ionization, called spurs. The mean rate of energy loss by a particle per unit path length, called linear energy transfer (LET), increases in the sequence of electron, proton and α-particle, for the same particle energy, E. This is, according to the Bethe equations, because the value of LET increases with decreasing particle velocity, v, which decreases with increasing particle mass, M, for the same E since LET increases as the square of the particle charge, Z [11, 15-17]. At sub-picoseconds time scales, local inhomogeneous distribution of ions and radical ions, excited states and electrons in small and widely separated volumes called spurs are produced by high energy electromagnetic ra-

diation or by the charged particles (including electrons) resulting in a high local concentration of reactive species (ion pairs) and promoting their recombination. In liquids, the fate of ion pairs is strongly dependent on the properties of the liquid. In non-polar liquids (*e.g.* hydrocarbons), characterized by low permittivity, most of the ejected electrons return to the initiating radical cation. On the other hand, in polar liquids (water, alcohols) most of the ejected electrons have sufficient energy to escape from the positive radical ions and, after thermalization (loss of their excess energy), are trapped by surrounding molecules forming solvated electrons (e^-_{solv}) [5].

An important feature of high energy radiation is also its non-selective absorption in matter. This means that molecules are ionized according to their relative abundance in the irradiated medium, *i.e.* partition of energy among the components of a sample is controlled by the contribution of each component and to the density of electrons. The concept of a direct effect of the radiation on the solute and an indirect effect, in which excited states and ions derived from the solvent subsequently react with the solute refers to this phenomenon. In studies of dilute solutions, any direct effect on the solute molecules will be negligible in comparison with the indirect effect. The radiolysis mechanisms of the solvent are of paramount importance for radical reactions initiated by high energy radiation. The radical reactions observed are essentially those resulting from the interactions of excited states and/or ions from the solvent with themselves, or with any solute present. One potential disadvantage of the latter situation is that the limiting rate of intermediate formation derived from the solute is usually controlled by its concentration.

1.3. QUANTIFICATION OF RADIATION CHEMICAL EFFECTS

Radiation chemical effects are quantified by the radiation chemical yield, G(X) [18], defined as the quotient of the amount n(X) of a substance X, either produced or destroyed and the energy, E, absorbed in the medium (Eq. (3)):

$$G(X) = n(X)/E \qquad (3)$$

The SI unit of the G-value is $mol \cdot J^{-1}$. For practical purposes $\mu mol \cdot J^{-1}$ unit is used. In the earlier literature, the G-values were expressed as the number of molecules produced or destroyed per 100 eV of energy absorbed. The mutual conversions of these units are as follows:

$$1 \; \mu mol \cdot J^{-1} = 9.65 \; molecules \; (100 \; eV)^{-1}$$
$$1 \; molecule \; (100 \; eV)^{-1} = 0.1036 \; \mu mol \cdot J^{-1}$$

Since the absorbed fraction of the radiation energy can only induce physical and chemical changes, the absorbed energy (the absorbed dose) is an important parameter. The absorbed dose (dose), D, is defined as the mean energy, dE, deposited in an incremental quantity of matter, divided by the mass of that matter (Eq. (4)):

$$D = dE/dm \qquad (4)$$

The preferred SI unit of the absorbed dose is the gray (Gy) which expresses the energy in joules (J) absorbed in the unit mass – kg: 1 Gy = 1 J·kg^{-1}. The former unit of the absorbed unit, rad, was defined as 100 erg·g^{-1}. Hence, 1 Gy = 100 rad.

1.4. TECHNIQUES OF RADIATION CHEMISTRY

Two main types of approaches are commonly used in applying radiation chemistry to investigate radical reactions in liquids. First, radiolysis can involve exposure to a steady radiation source, usually a ^{60}Co source for a desired amount of time and the stable products are analyzed after the end of the radiolysis period. Modern analytical techniques (including high performance liquid chromatography for separation of products, with spectrophotometric, fluorescence, electrochemical, mass spectrometric or nuclear magnetic resonance detections) are used for qualitative and quantitative determination of the final products [5, 19].

The second approach involves exposure of a selected chemical system to pulsed sources, usually electron accelerators, where sufficiently high concentration of radicals is desired in a short time in order to follow their reactions directly [5, 19]. This technique, pulse radiolysis, has been the main source of a quantitative information concerning reaction kinetics of free radicals in solutions [20-24]. For radicals in solutions the most common used technique is time-resolved UV-Vis spectroscopy [22, 23, 25], but time-resolved conductivity [23, 26], electron paramagnetic resonance [27], vibrational resonance Raman spectroscopy [28], microwave absorption spectroscopy [29], polarography [30], circular dichroism [31], and recently infrared spectroscopy [32], although less widely employed, can also provide kinetic, spectral, and mechanistic details that are not accessible *via* optical measurements.

Due to space limitations, a comprehensive overview of basics of radiation-induced phenomena in liquids cannot be given here. There are many excellent and comprehensive discussions of this [7, 10, 12, 33-35], and books which address the topics mentioned above in a more detailed manner [11, 13, 15, 36-40].

2. RADIOLYSIS OF WATER

The radiolysis of water has been studied extensively since the beginning of radiation chemistry. Excellent critical reviews of the spectral and kinetic properties, methods of production, and compilations of reaction rate constants of

the primary water radiolysis transients with inorganic and organic substrates have been written over the years [2, 11, 18, 41-49]. Most of radiation-induced radical reactions have been studied in aqueous solutions because they are readily available and not difficult to work with. Moreover, the radiolysis of water is a relatively easy and convenient way to produce an enormous variety of highly reactive radical species which otherwise cannot readily be generated by thermal or photochemical methods. There were several motivations for undertaking and pursuing these studies: (i) to gain a knowledge about chemical processes in general (*e.g.* redox and polymerization processes); (ii) to understand effect of high energy radiation on biologically relevant molecules (water is a main constituent in living organisms and plays a key role in biological systems); (iii) to produce and study the reactions of reactive short-lived species that are also produced in living organisms, *e.g.* hydroxyl radicals ($^{\bullet}OH$), peroxyl radicals ($ROO^{\bullet}$), and superoxide radical anions ($O_2^{\bullet-}$); and (iv) to control and predict precisely effects of water radiolysis in water cooled nuclear reactors in order to avoid unwanted effects such as radiation-induced stress corrosion cracking.

2.1. RADIOLYSIS OF WATER AT AMBIENT TEMPERATURES WITH LOW LET IRRADIATION

2.1.1. Primary transients: formation, spur reactions, radiation chemical yields, acid-base equilibria, spectral and redox properties

Formation of the radical cation ($H_2O^{\bullet+}$) and pre-hydrated electrons (e^-_{prehyd}) is a consequence of the ionization of water molecules and represents the primary process in the radiolysis of water (Eq. (5)). There is no unequivocal evidence that electronic excitation of water molecules (Eq. (6)) plays any significant role in radiolysis.

$$H_2O \xrightarrow{\wedge\wedge\wedge\wedge\wedge} H_2O^{\bullet+} + e^-_{prehyd} \tag{5}$$
$$H_2O \xrightarrow{\wedge\wedge\wedge\wedge\wedge} H_2O^* \tag{6}$$

Both reactions occur on the time scale of electronic transition, *i.e.* $\sim 10^{-16}$ s. The water radical cation ($H_2O^{\bullet+}$) is a very strong acid and immediately loses a proton (in $\sim 10^{-14}$ s) to neighboring water molecules forming hydroxyl radical (Eq. (7)):

$$H_2O^{\bullet+} + H_2O \rightarrow {}^{\bullet}OH + H_3O^+ \tag{7}$$
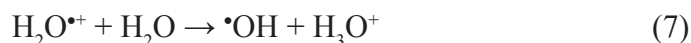
The lifetime of $H_2O^{\bullet+}$ was recently measured to be around 200 fs using polarization anisotropy technique [50]. The yield of $H_2O^{\bullet+}$ at few tens of fs was estimated to be around 0.53 μmol·J^{-1} [51]. The electronically excited water molecules (H_2O^*) may undergo homolytic dissociation (Eq. (8)) in $\sim 10^{-13}$ s and the electrons ejected in an ionization process (Eq. (5)) undergo hydration by $\sim 10^{-12}$ s, after thermalization (Eq. (9)):

$$H_2O^* \rightarrow {}^{\bullet}H + {}^{\bullet}OH \tag{8}$$

$$e^-_{prehyd} + nH_2O \rightarrow e^-_{aq} \tag{9}$$
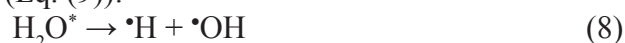
At this time, the products of reactions depicted in Eqs. (7)-(9) are distributed inhomogeneously and located together in spurs. Subsequently, these products start to diffuse randomly. Some of them interact with one another within spurs, before diffusing apart into the bulk water, forming molecular and secondary radical products. These spur reactions (Eqs. (10)-(17)) together with their respective rate constants are listed in Table 1.

Table 1. Spur reactions in water and their rate constants [46].

Spur reaction (number)	k [dm$^3 \cdot$mol$^{-1} \cdot$s^{-1}]
$e^-_{aq} + e^-_{aq} \rightarrow H_2 + 2^-OH$ (10)[a]	5.4×10^9
$e^-_{aq} + {}^{\bullet}OH \rightarrow {}^-OH$ (11)	3.0×10^{10}
$e^-_{aq} + H_3O^+ \leftrightarrows {}^{\bullet}H + H_2O$ (12)	2.3×10^{10}
$e^-_{aq} + {}^{\bullet}H \rightarrow H_2 + {}^-OH$ (13)[a]	2.5×10^{10}
${}^{\bullet}H + {}^{\bullet}H \rightarrow H_2$ (14)	1.3×10^{10}
${}^{\bullet}OH + {}^{\bullet}OH \rightarrow H_2O_2$ (15)	5.3×10^9
${}^{\bullet}OH + {}^{\bullet}H \rightarrow H_2O$ (16)	3.2×10^{10}
$H_3O^+ + {}^-OH \rightarrow 2H_2O$ (17)	1.4×10^{11}

[a] The mass balance is ensured by hydration water.

Those products, which diffuse outside the spurs, become homogeneously distributed and may react with added solutes (acting as scavengers). All spur reactions and diffusion of reactants leading to their homogeneity are completed within 10^{-7} s.

The radiolysis of water (for low LET irradiation ~0.23 eV·nm^{-1}) is summarized by Eq. (18), where the numbers in parentheses represent radiation chemical yields (G-values) in units μmol·J^{-1} [4, 14]:

$$H_2O \xrightarrow{\wedge\wedge\wedge\wedge\wedge} {}^{\bullet}OH\ (0.28),\ e^-_{aq}\ (0.28),\ {}^{\bullet}H\ (0.062),\ H_2\ (0.047),$$
$$H_2O_2\ (0.073),\ H_3O^+\ (0.28) \tag{18}$$
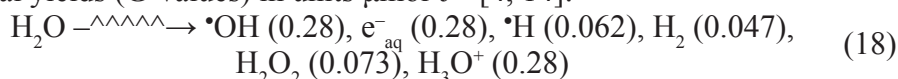
The primary transients from water radiolysis (Eq. (18)) are involved in the following acid-base equilibria represented by Eqs. (19) and (20):

$$^{\bullet}H + HO^- \leftrightarrows e^-_{aq} + H_2O \tag{19}$$
$$^{\bullet}OH + HO^- \leftrightarrows O^{\bullet -} + H_2O \tag{20}$$
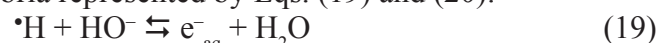
Hydrogen atoms (${}^{\bullet}H$) and hydrated electrons (e^-_{aq}) exist in the acid-base equilibrium (Eq. (19)) with pK_a = 9.1 (${}^{\bullet}H$ atom is a conjugate acid of e^-_{aq}). The lifetime of e^-_{aq} in pure water is quite long since its protonation by water is slow. However, at pH < 4, the diffusion-controlled reaction of e^-_{aq} with bulk protons (Eq. (12), Table 1) is important in causing an increase of the yield of ${}^{\bullet}H$ atoms

with decreasing pH and thus their radiation chemical yield in acidic solutions can be as high as 0.34 $\mu mol \cdot J^{-1}$. On the other hand, in very basic solutions $^{\bullet}H$ atoms are converted into e^-_{aq} with $k_{forward}$ (in equilibrium represented by Eq. (19)) = $2.2 \times 10^7 \, dm^3 \cdot mol^{-1} \cdot s^{-1}$ [46].

Hydroxyl radicals ($^{\bullet}OH$) exist in the acid-base equilibrium (Eq. (20)) with $pK_a = 11.8$ ($^{\bullet}OH$ is a conjugate acid of the oxide radical ion ($O^{\bullet-}$)), with $k_{forward}$ (in equilibrium represented by Eq. (20)) = $1.3 \times 10^{10} \, dm^3 \cdot mol^{-1} \cdot s^{-1}$ and $k_{reverse}$ (in equilibrium represented by Eq. (20)) = $7.9 \times 10^7 \, s^{-1}$ [52]. Since $O^{\bullet-}$ radical anion is very rapidly protonated by water, its radical reactions occur in a significant extent only at a pH > 12.

Spectral properties of the primary transients from water radiolysis are summarized in Table 2.

Table 2. Spectral parameters and reduction potentials of primary transients in water radiolysis [49, 53].

Transient	λ_{max} [nm]	ε_{max} [$dm^3 \cdot mol^{-1} \cdot cm^{-1}$] [49]	E^0 *vs.* NHE [V] [53]
$^{\bullet}OH$	230	530	+2.72 (for the redox couple: $^{\bullet}OH$, H^+/H_2O) +1.90 (for the redox couple: $^{\bullet}OH/^-OH$)
$O^{\bullet-}$	240	240 (for pH 13)	+1.78 (for the redox couple: $O^{\bullet-}$, $H_2O/2^-HO$)
e^-_{aq}	720	19 000	−2.87
$^{\bullet}H$	< 200	1 620 (for λ_{max} = 188 nm)	−2.31

The hydrated electron is characterized by its strong absorption at 720 nm and the majority of oscillating strength is derived from optical transitions from the equilibrated *s* state to the *p*-like excited state. The 720-nm absorption is used for the determination of reaction rate constants with the vast variety of compounds. On the other hand, both the $^{\bullet}H$ atoms and $^{\bullet}OH(O^{\bullet-})$ radicals absorb in the far UV region, which has made their distinction and observation very difficult, if not impossible. Therefore, their reaction rate constants with the variety of compounds have been determined either by observation of the respective products or competition techniques [46].

Redox properties of the primary transients from water radiolysis can be summarized as follows: (i) the $^{\bullet}OH$ radical is a powerful one-electron oxidant with a reduction potential varying with the pH, (ii) the hydrated electron is a

powerful reductant in neutral and alkaline solutions while the •H atom becomes the major reductant in acidic solutions [46, 53].

The radical cation $H_2O^{•+}$ absorbs light in the visible spectral domain [54], and its reduction potential has been estimated as ~ +4.0 V *vs.* NHE [51].

2.1.2. Selective generation of primary transients

Since the primary transients formed in the radiolysis of aqueous solutions are characterized either by oxidizing (•OH) or reducing (e^-_{aq}, •H) properties, it is desirable to study their reactions in conditions when only one type of radical is present. These conditions can be achieved *via* an appropriate design of the reaction system which subsequently will be exposed to high energy irradiation [18].

To eliminate the contribution of e^-_{aq} in the reaction system, the solution is saturated with nitrous oxide (N_2O). Hydrated electrons are rapidly scavenged by N_2O generating additional amount of •OH radicals (Eq. (21)) with $k_{21} = 9.1 \times 10^9$ $dm^3 \cdot mol^{-1} \cdot s^{-1}$ [55], and thus yield amounts to 0.56 $\mu mol \cdot J^{-1}$.

$$e^-_{aq} + N_2O \rightarrow N_2 + O^{•-} (+ H_2O) \rightarrow N_2 + {}^•OH + {}^-OH \qquad (21)$$
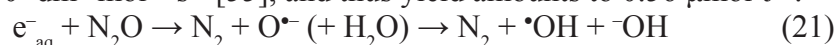
The •H atoms react slowly with N_2O ($k = 2.1 \times 10^6$ $dm^3 \cdot mol^{-1} \cdot s^{-1}$) [4], and therefore in these solutions their reactions are not eliminated. However, the yield of •H atoms represents $\cong 10\%$ of the total yield of radicals at neutral solutions.

A convenient way to study reactions of e^-_{aq} (without a contribution of •OH radicals) is irradiation of deaerated neutral aqueous solutions (with Ar/N_2) containing high concentration (> 0.1 M) of 2-methyl-2-propanol (*tert*-butanol). The •OH radicals are selectively scavenged by *tert*-butanol forming 2-hydroxy-2,2-dimethyl radical with $k = 6.0 \times 10^8$ $dm^3 \cdot mol^{-1} \cdot s^{-1}$ (Eq. (22)) [46]:

$$^•OH + (CH_3)_3C–OH \rightarrow H_2O + {}^•CH_2(CH_3)_2C–OH \qquad (22)$$
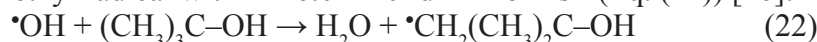
The yield of •H atoms is almost not affected since their rate constant with *tert*-butanol is low ($k = 1.7 \times 10^5$ $dm^3 \cdot mol^{-1} \cdot s^{-1}$) [46], and recently noted at 1.15×10^6 $dm^3 \cdot mol^{-1} \cdot s^{-1}$ [56]. The $^•CH_2(CH_3)_2C–OH$ formed is nearly unreactive due to steric hindrance, its optical absorption band is located < 270 nm and, in principle, does not interfere with other radicals. The irradiated system contains only e^-_{aq} and •H atoms with the respective radiation chemical yields 0.28 and 0.062 $\mu mol \cdot J^{-1}$.

The "cleanest" way to study •H-atoms reactions (without a contribution of •OH radicals and e^-_{aq}) is irradiation of highly acidic aqueous solutions saturated with H_2. The •OH radicals react with H_2 generating additional amount of •H atoms (Eq. (23)) with $k_{23} = 4.2 \times 10^7$ $dm^3 \cdot mol^{-1} \cdot s^{-1}$ [46]:

$$^•OH + H_2 \rightarrow H_2O + {}^•H \qquad (23)$$

This approach, due to the low solubility of H_2 under normal pressure conditions, has not found a practical use (a special pressure cell is needed). Therefore, •H-atoms reactions can be routinely studied by irradiations of highly acidic Ar/N_2-saturated aqueous solutions containing high concentration (> 0.1 M) of *tert*-butanol. The •OH radicals are removed in reaction (Eq. (22)) and e^-_{aq} are

converted to $^\bullet$H atoms *via* reaction with H_3O^+ (Eq. (12), Table 1), and thus their radiation chemical yield amounts to 0.34 $\mu mol \cdot J^{-1}$.

2.1.3. Generation of transients in aerated and O_2-saturated aqueous solutions: formation, acid-base equilibria, spectral, kinetic, and redox properties

In aerated and O_2-saturated aqueous solutions both $^\bullet$H atoms and e^-_{aq} react with molecular oxygen (O_2) according to reactions (Eqs. (24) and (25)) with $k_{24} = 2.1 \times 10^{10}$ $dm^3 \cdot mol^{-1} \cdot s^{-1}$ and $k_{25} = 1.9 \times 10^{10}$ $dm^3 \cdot mol^{-1} \cdot s^{-1}$ [46]:

$$^\bullet H + O_2 \rightarrow HO_2^\bullet \qquad (24)$$
$$e^-_{aq} + O_2 \rightarrow O_2^{\bullet-} \qquad (25)$$

Perhydroxyl radicals ($HO_2^\bullet$) and superoxide radical anions ($O_2^{\bullet-}$) exist in the acid-base equilibrium (Eq. (26)) with $pK_a = 4.88$ ($HO_2^\bullet$ radical is a conjugate acid of $O_2^{\bullet-}$ radical anion) [57].

$$HO_2^\bullet \leftrightarrows H^+ + O_2^{\bullet-} \qquad (26)$$

$HO_2^\bullet$ and $O_2^{\bullet-}$ radicals undergo disproportionation reaction *via* a pH-dependent mechanism that involves equilibrium (Eq. (26)) and reactions (Eqs. (27) and (28)):

$$HO_2^\bullet + HO_2^\bullet \rightarrow H_2O_2 + O_2 \qquad (27)$$

$$HO_2^\bullet + O_2^{\bullet-} \xrightarrow{\quad H^+ \quad} H_2O_2 + O_2 \qquad (28)$$

$$O_2^{\bullet-} + O_2^{\bullet-} \rightarrow \text{no reaction} \qquad (29)$$
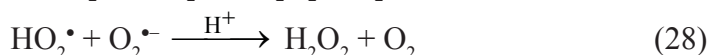
The values of k_{27} and k_{28} of 8.3×10^5 $dm^3 \cdot mol^{-1} \cdot s^{-1}$ and 9.7×10^7 $dm^3 \cdot mol^{-1} \cdot s^{-1}$ were calculated by fitting the experimental data of the observed rates of disproportionation at varying pH taking into account Eqs. (27)-(29) [57].

Radiolysis of water at pH > 6 in the presence of O_2 and formate ions (HCO_2^-) leads to the exclusive formation of $O_2^{\bullet-}$ *via* reactions depicted in Eqs. (24)-(26), (30) and (31):

$$^\bullet OH + HCO_2^- \rightarrow CO_2^{\bullet-} + H_2O \qquad (30)$$
$$CO_2^{\bullet-} + O_2 \rightarrow O_2^{\bullet-} + CO_2 \qquad (31)$$
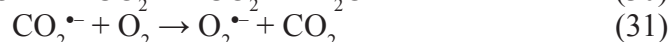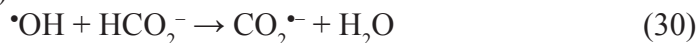
Interestingly, $^\bullet$OH radical is unreactive towards O_2, however, its conjugate base, the oxide radical anion ($O^{\bullet-}$) react with O_2 (Eq. (32)) forming ozonide radical anion ($O_3^{\bullet-}$):

$$O^{\bullet-} + O_2 \leftrightarrows O_3^{\bullet-} \qquad (32)$$

These two radicals exist in an equilibrium with $k_{32} = 3.0 \times 10^9$ $dm^3 \cdot mol^{-1} \cdot s^{-1}$ [46], and $k_{-32} = 3.3 \times 10^3$ s^{-1} [58].

The ozonide radical anion is characterized by its absorption at 430 nm which has been used for determination of its reaction rate constants with radicals [59, 60]. Both the $HO_2^\bullet$ and $O_2^{\bullet-}$ radicals absorb in the far UV region, which made their distinction and observation very difficult, if not impossible (Table 3). Their reaction rate constants with the variety of compounds were determined either by observation of the respective products or competition techniques.

Table 3. Spectral parameters and reduction potentials of transients formed during radiolysis of aerated and oxygenated water [49, 53].

Transient	λ_{max} [nm]	ε_{max} [dm^3·mol^{-1}·cm^{-1}] [49]	E^0 *vs.* NHE [V] [53]
HO$_2^\bullet$	225 (for pH 1.5)	1400 (for pH 1.5)	+1.48 (for the redox couple: HO$_2^\bullet$, H$^+$/H$_2$O$_2$) +0.79 (for the redox couple: HO$_2^\bullet$/HO$_2^-$)
O$_2^{\bullet-}$	245 (for pH 10.5)	2350 (for pH 10.5)	−0.33 (for the redox couple: O$_2$/O$_2^{\bullet-}$) +1.03 (for the redox couple O$_2^{\bullet-}$, H$^+$/HO$_2^-$)
O$_3^{\bullet-}$	430 (for pH 13.1)	1900 (for pH 13.1)	+1.01 (for pH 11-12; for the redox couple: O$_3$/O$_3^{\bullet-}$)

Redox properties of these transients can be summarized as follows: the HO$_2^\bullet$ and O$_2^{\bullet-}$ radicals are mild one-electron oxidants with a reduction potential varied with the pH (Table 3).

2.1.4. Radical reactions involving primary transients

$^\bullet$*OH radicals.* The $^\bullet$OH radical undergoes the following types of reactions: (i) electron transfer (ET); (ii) hydrogen atom abstraction; (iii) addition to C=C, C=N and C=S bonds; (iv) addition to aromatic rings; and (v) addition to electron-rich functional groups [45]. These reactions reflect *inter alia* its electrophilic character [61], and strong oxidizing properties. Rate constants for thousands of reactions of $^\bullet$OH radicals have been compiled, including reactions with molecules, ions, and radicals derived from inorganic and organic solutes [46].

In most ET reactions, formation of an $^\bullet$OH adduct precedes the actual ET reaction. Oxidation of metal ions (Eqs. (33a) and (33b)) and inorganic anions (Eq. (34)) illustrates this feature:

$$^\bullet OH + Me^+ \leftrightarrows MeOH^{\bullet+} \rightarrow Me^{2+} + {}^-OH \qquad (33a)$$
$$Me^+ = Tl^+, Ag^+$$
$$^\bullet OH + Me^{2+} \leftrightarrows MeOH^{\bullet 2+} \rightarrow Me^{2+} + {}^-OH \qquad (33b)$$
$$Me^{2+} = Cu^{2+}, Sn^{2+}, Fe^{2+}, Mn^{2+}$$
$$^\bullet OH + SCN^- \leftrightarrows HOSCN^{\bullet-} \rightarrow {}^\bullet SCN + {}^-OH \qquad (34)$$
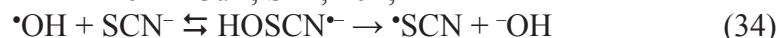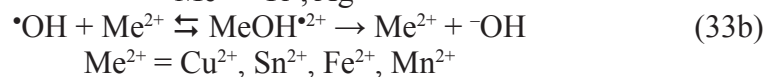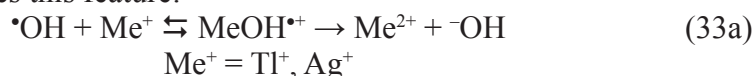
A driving force for H-abstraction reactions by $^\bullet$OH radicals is that the H–OH bond dissociation energy (BDE) is very high (111 kcal·mol^{-1}), while the BDEs

of the C–H and S–H bonds are usually much weaker. Reactions of $^\bullet$OH radicals with methanol (BDE H–CH$_2$ = 103 kcal·mol^{-1}) (Eq. (35)) and methanethiol (BDE S–H = 85 kcal·mol^{-1}) (Eq. (36)) confirm this:

$$^\bullet OH + CH_3OH \rightarrow H_2O + {}^\bullet CH_2OH \tag{35}$$

$$^\bullet OH + CH_3SH \rightarrow H_2O + CH_3S^\bullet \tag{36}$$

Since the BDE for primary hydrogens (H–CH$_2$) is higher than for the secondary (>CH–H) (98 kcal·mol^{-1}) and tertiary (>C–H) (95 kcal·mol^{-1}), a remarkable selectivity is observed for the H-abstraction reactions in ethanol (Eqs. (37a) and (37b)) and 2-propanol (Eqs. (38a) and (38b)):

$$^\bullet OH + CH_3CH_2OH \rightarrow H_2O + CH_3{}^\bullet CHOH \tag{37a}$$

$$^\bullet OH + CH_3CH_2OH \rightarrow H_2O + {}^\bullet CH_2CH_2OH \tag{37b}$$

$$^\bullet OH + (CH_3)_2CHOH \rightarrow H_2O + (CH_3)_2{}^\bullet COH \tag{38a}$$

$$^\bullet OH + (CH_3)_2CHOH \rightarrow H_2O + (CH_3)(CH_2{}^\bullet)CHOH \tag{38b}$$
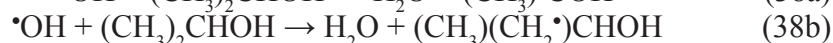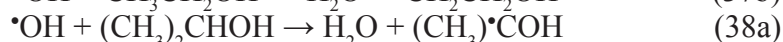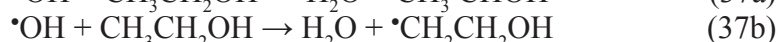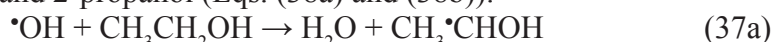
The yields (in %) of H-abstraction reactions (Eqs. (37a) and (38a)) are equal to 84.3 and 85.5%, respectively. The yields of H-abstraction reactions (Eqs. (37b) and (38b)) amounts only to 13.3% [62].

Addition of $^\bullet$OH radicals to C=C double bonds (Eq. (39)) is very fast and occurs close to diffusion-controlled rates (*e.g.* in ethylene k$_{39}$ = 4.4 × 10^9 dm^3·mol^{-1}·s^{-1}):

$$^\bullet OH + H_2C{=}CH_2 \rightarrow {}^\bullet CH_2{-}CH_2{-}OH \tag{39}$$

Addition will be the preferential way over H-abstraction, even in the molecules having weakly bound hydrogen atoms, such as pentadienylic in 1,3- and 1,4-cyclohexadienes and allylic ones in thymine.

Addition of $^\bullet$OH radicals to C=N double bonds was observed in purines (guanine and adenine, two of the bases in deoxyribonucleic acid, DNA). The C(8)–OH adducts are formed with the yield of 17 and 37%, respectively, and both radicals possess reducing properties [45].

Addition of $^\bullet$OH radicals to S=O double bonds occurs in sulfoxides and the resulting radical undergoes a very rapid β-fragmentation leading, in the case of dimethyl sulfoxide, to the methide radical (Eq. (40)) [63]:

$$^\bullet OH + (CH_3)_2S{=}O \rightarrow (CH_3)_2S(OH){-}O^\bullet \rightarrow {}^\bullet CH_3 + CH_3S({=}O){-}OH \tag{40}$$
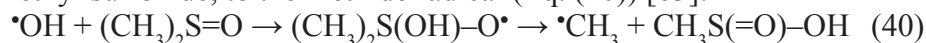
Addition of $^\bullet$OH radicals to aromatic rings leads to a short-lived π-complex (being in an equilibrium with substrates) prior to transformation into σ-complex, where the OH substituent bounds tightly to the carbon atoms (Eq. (41)):

$$\tag{41}$$
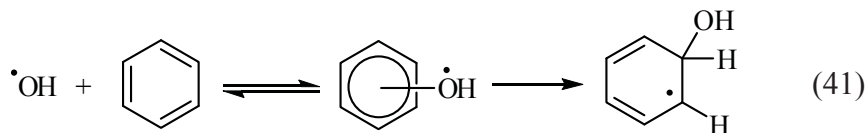
Electron-donating substituents (*e.g.* –OCH$_3$, –OH) in the aromatic ring direct $^\bullet$OH radicals into the *ortho*- and *para*-positions, while electron-withdrawing substituents (–NO$_2$) mostly into the *meta*-position. In the case of neutral substituents (–COOH), there is no preference for the site of addition, and an even distribution of isomers is observed [64].

Addition of $^{\bullet}$OH radicals to electron-rich functional groups was observed in sulfides and disulfides [65]. In the case of sulfides, the OH-adduct undergoes, depending on the pH, either proton-catalyzed hydroxide ion ($^{-}$OH) elimination (Eq. (42a)) or spontaneous dissociation (Eq. (42b)), both processes lead to formation of the monomeric sulfur radical cation:

$$^{\bullet}OH + R\text{–}S\text{–}R \rightarrow R\text{–}S^{\bullet}(\text{–}OH)\text{–}R \xrightarrow{\ H^{+}\ } R\text{–}S^{\bullet+}\text{–}R + H_2O \qquad (42a)$$

$$^{\bullet}OH + R\text{–}S\text{–}R \rightarrow R\text{–}S^{\bullet}(\text{–}OH)\text{–}R \rightarrow R\text{–}S^{\bullet+}\text{–}R + {}^{-}OH \qquad (42b)$$
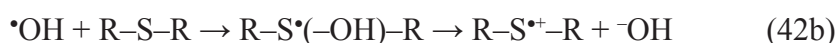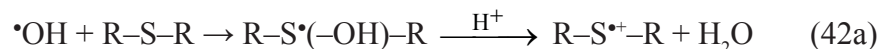
These radical cations undergo either deprotonation at neighboring carbon atoms forming α-(alkylthio)alkyl radicals or can be stabilized by 2c-3e bonding with other heteroatoms (*e.g.* S, N, and O).

Hydrated electrons (e^{-}_{aq}). The hydrated electron undergoes the following types of reactions: (i) reduction, (ii) dissociative electron attachment, (iii) addition to functional groups of high electron affinity, (iv) addition to aromatic rings containing electron-withdrawing substituents, and (v) addition to conjugated double bonds [45]. The hydrated electron acts as a nucleophile in its reaction with organic molecules. Similarly, as for $^{\bullet}$OH radicals, the rate constants for thousands of reactions of e^{-}_{aq} have been compiled, including reactions with molecules, ions, and radicals derived from inorganic and organic solutes [46].

Since the hydrated electron is the most powerful one-electron reductant, it is capable of reducing metal ions (Eqs. (43a)-(43c)) and inorganic anions (Eqs. (44a) and (44b)) [4, 53]:

$$e^{-}_{aq} + Me^{+} \rightarrow Me^{0} \qquad (43a)$$
$$Me^{+} = Ag^{+}, Cu^{+}, Tl^{+}$$

$$e^{-}_{aq} + Me^{2+} \rightarrow Me^{+} \qquad (43b)$$
$$Me^{2+} = Cu^{2+}, Co^{2+}, Cd^{2+}, Sn^{2+}, Mn^{2+}, Ni^{2+}, Pb^{2+}, Zn^{2+}$$

$$e^{-}_{aq} + Me^{3+} \rightarrow Me^{2+} \qquad (43c)$$
$$Me^{3+} = Fe^{3+}, Eu^{3+}$$

$$e^{-}_{aq} + MnO_4^{-} \rightarrow MnO_4^{2-} \qquad (44a)$$
$$e^{-}_{aq} + CrO_4^{2-} \rightarrow CrO_4^{3-} \qquad (44b)$$
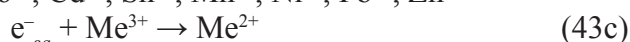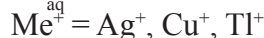
Hydrated electrons react with many organic compounds containing substituent halogen atoms by a dissociative electron attachment (Eqs. (45a) and (45b)):

$$e^{-}_{aq} + RX \rightarrow R^{\bullet} + X^{-} \qquad (45a)$$
$$X = Cl, Br, I$$

$$e^{-}_{aq} + \text{(5-bromouracil)} \rightarrow \text{(uracil-5-yl radical)} + Br^{-} \qquad (45b)$$
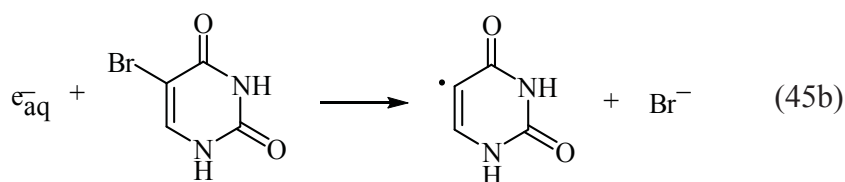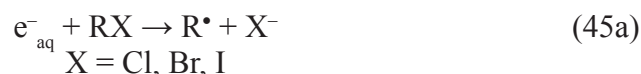
Hydrated electrons react at diffusion-controlled rates with a large number of compounds containing functional groups of high electron affinity like car-

bonyl, nitro and cyano groups (Eqs. (46a)-(46c)) by forming the corresponding radical anions [46]:

$$e^-_{aq} + {>}C{=}O \rightarrow {>}C^\bullet{-}O^- \tag{46a}$$

$$e^-_{aq} + {-}NO_2 \rightarrow {-}N^\bullet({=}O){-}O^- \tag{46b}$$

$$e^-_{aq} + {-}C{\equiv}N \rightarrow {-}C^\bullet{=}N^- \tag{46c}$$
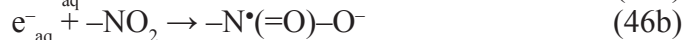
Hydrated electrons do not react with benzene with appreciable rate (k ~ 10^7 dm^3·mol^{-1}·s^{-1}). However, the rate constants with benzene containing electron-withdrawing substituents (–NO$_2$, –CN) are at a diffusion-controlled limit. The resulting radical anions undergo a very rapid protonation by water (Eq. (47)), yielding the same species as expected for the addition reaction of $^\bullet$H atoms (*vide infra*) (Eq. (52)):

$$\tag{47}$$
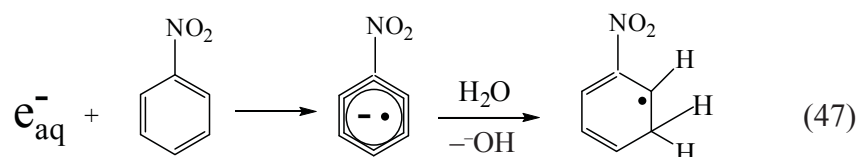
Hydrated electrons are not reactive with ethylene (k < 3 × 10^5 dm^3·mol^{-1}·s^{-1}). However, their reactivity substantially increase with the molecules containing conjugated double (Eq. (48)) amounts to 8 × 10^9 dm^3·mol^{-1}·s^{-1}.

$$e^-_{aq} + H_2C{=}CH{-}CH{=}CH_2 \rightarrow H_2C{=}CH{-}^\bullet CH{-}CH_2^- \xrightarrow{H_2O}$$
$$\xrightarrow{H_2O} H_2C{=}CH{-}^\bullet CH{-}CH_3 + {}^-OH \tag{48}$$
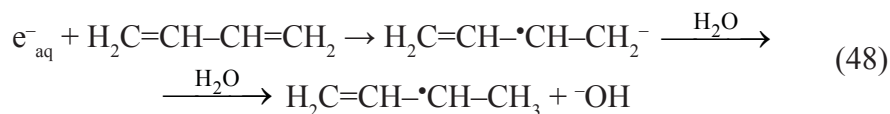
$^\bullet$*H atoms*. The $^\bullet$H atom undergoes the following types of reactions: (i) electron transfer (ET), (ii) hydrogen atom abstraction, (iii) addition to C=C bonds, (iv) addition to aromatic rings, (v) addition to electron-rich functional groups, and (vi) homolytic substitution [18, 45, 46]. These reactions reflect *inter alia* its weak nucleophilic [61], and strong reducing properties, however, less than e^-_{aq}. Interestingly, radical reactions of $^\bullet$H atoms resemble those involving $^\bullet$OH radicals.

In ET reactions $^\bullet$H atoms readily reduce metal ions having lower reduction potentials (Eqs. (49a) and (49b)) and inorganic anions (Eq. (50)) [46]:

$$H + Me^+ \rightarrow H^+ + Me^0 \tag{49a}$$
$$Me^+ = Ag^+, Tl^+$$
$$H + Me^{2+} \rightarrow H^+ + Me^+ \tag{49b}$$
$$Me^{2+} = Cu^{2+}, Hg^{2+}$$
$$H + Fe(CN)_6^{3-} \rightarrow H^+ + Fe(CN)_6^{4-} \tag{50}$$
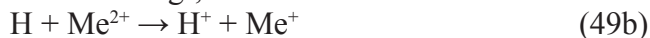
$^\bullet$H atoms also abstract hydrogen atoms, but with much lower rate constants than $^\bullet$OH radicals (Table 4). Since the H–H bond dissociation energy (104.3 kcal·mol^{-1}) is substantially lower than the BDE of H–OH bond (*vide supra*).

This phenomenon is particularly reflected in the reactions of $^\bullet$H atoms with methanol (Eq. (51)) and 2-methyl-2-propanol (*tert*-butanol) (Eq. (52))

Table 4. Comparison of the rate constants of the H-abstraction reactions involving $^\bullet$H atoms and $^\bullet$OH radicals with selected alkyl alcohols [46].

Alcohol	k ($^\bullet$H + ROH) [dm^3·mol^{-1}·s^{-1}]	k ($^\bullet$OH + ROH) [dm^3·mol^{-1}·s^{-1}]
CH_3OH	2.6×10^6	9.7×10^8
C_2H_5OH	1.7×10^7	1.9×10^9
C_3H_7OH	2.4×10^7	2.8×10^9
$(CH_3)_2CHOH$	7.4×10^7	1.9×10^9
$(CH_3)_3COH$	$(1.7\text{-}11.5) \times 10^5$	6.0×10^8

(Table 4) where the BDEs of primary hydrogens (H–CH$_2$) are only slightly lower than BDE of the H–H bond:

$$^\bullet H + CH_3OH \rightarrow H_2 + {^\bullet}CH_2OH \tag{51}$$
$$^\bullet H + (CH_3)_3C\text{–}OH \rightarrow H_2 + {^\bullet}CH_2(CH_3)_2C\text{–}OH \tag{52}$$

Addition of $^\bullet$H atoms to C=C double bonds (Eq. (53)) is very fast and occurs close to the diffusion-controlled rate (*e.g.* for ethylene $k_{53} = 3.0 \times 10^9$ dm^3·mol^{-1}·s^{-1}) [46]:

$$^\bullet H + H_2C{=}CH_2 \rightarrow {^\bullet}CH_2\text{–}CH_3 \tag{53}$$

Addition of $^\bullet$H atoms to aromatic rings leads directly (contrary to the $^\bullet$OH addition) to a σ-complex in which the $^\bullet$H atom bounds tightly to the carbon atoms (Eq. (54)).

$$\tag{54}$$
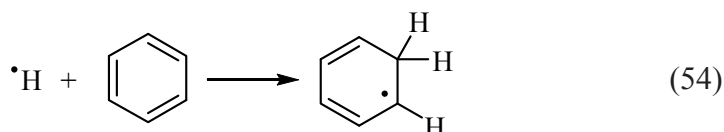
Because of the pronounced electrophilicity, $^\bullet$H atoms react readily by addition to the sulfur atoms in trithianes which contain three electron-rich thioether groups. However, the resulting adducts cannot be detected since they decompose by ring opening followed either by α- or β-scission [66].

$^\bullet$H atoms can also undergo bimolecular homolytic substitution (S$_H$2) with α-(alkylthio)carbonyl compounds (Eq. (55)) which is driven by the formation of the stronger S–H bond while simultaneously a relatively C–S bond is broken [67]:

$$^\bullet H + CH_3SCH_2C(=O)NH_2 \rightarrow CH_3SH + {^\bullet}CH_2C(=O)NH_2 \tag{55}$$

Radical reactions involving primary radicals from water radiolysis have been successfully used for the generation, identification and spectral and kinetic characterization of a large variety of radicals and radical ions derived from biological molecules, like amino acids, peptides, proteins, DNA and its constituents, and lipids. Numerous books and review articles addressing these topics have been published [11, 15, 45, 68-73].

2.1.5. Radical reactions involving $O_2^{\bullet-}$ and $HO_2^{\bullet}$ radicals

In principle, the reactivity of $O_2^{\bullet-}$ and $HO_2^{\bullet}$ radicals with organic compounds in aqueous solutions is rather low [57]. For instance, the reactions of $HO_2^{\bullet}/O_2^{\bullet-}$ with amino acids in their zwitterionic forms were found to be very slow with the rate constants in the range of 10^1-10^2 $dm^3 \cdot mol^{-1} \cdot s^{-1}$ [74]. The reactivity of $O_2^{\bullet-}$ and $HO_2^{\bullet}$ radicals with some biologically relevant compounds including metal ions and metal ion complexes have been studied extensively. Some selected rate constants are listed in Table 5.

Table 5. Comparison of the rate constants of $O_2^{\bullet-}$ and $HO_2^{\bullet}$ radicals with some selected metal ions, metal ion complexes, and organic compounds [74].

Compound (S)	k ($O_2^{\bullet-}$ + S) [$dm^3 \cdot mol^{-1} \cdot s^{-1}$]	k ($HO_2^{\bullet}$ + S) [$dm^3 \cdot mol^{-1} \cdot s^{-1}$]
Ascorbic acid (AH)	n.m.	1.6×10^4
Ascorbate anion (AH$^-$)	2.6×10^8	5.0×10^9
Nicotinamide-adenine dinucleotide – NADH	< 27	1.8×10^5
Fe^{II}	1.0×10^7	1.2×10^6
Fe^{III}	1.5×10^8	$< 10^3$
Cu^{II}	1.0×10^{10}	1.0×10^9
Cu^{I}	$(5\text{-}8) \times 10^9$	1.0×10^6
Mn^{II} porphyrins	5.6×10^8-9.0×10^9	–
Mn^{III} porphyrins	4.0×10^5-5.1×10^7	–
Fe^{II} porphyrins	3.1×10^6-3.7×10^8	–
Fe^{III} porphyrins	3.0×10^5-2.0×10^9	–

A majority of research has focused on iron, copper, manganese and their complexes. These metal ions are present in the active sites of superoxide dismutases.

2.1.6. Selective secondary radicals: generation, spectral, kinetic, and redox properties

Since the $^{\bullet}OH$ radical is a very strong oxidant and both e^-_{aq} and $^{\bullet}H$ atoms are very strong reductants, they do not react in a selective way. They react very fast with almost all compounds in various types of reactions. Moreover, in one-electron oxidation reactions $^{\bullet}OH$ radicals react with formation of a primary intermediate adduct which subsequently, in some cases, is transformed to one-electron oxidized products. Thus, there was a strong need for a generation of more selective radicals that are less reactive and/or can react mostly by a direct electron transfer [1, 4, 18].

Selective oxidizing radicals. A large variety of oxidizing inorganic radicals have been generated and their spectra, reaction rate constants with numerous substrates, and reduction potentials have been measured and compiled [48].

Selected examples of reactions leading to generation of the oxidizing selective inorganic radicals (using primary $^\bullet OH$ radicals) are presented below (Eqs. (56a)-(56d)):

$$^\bullet OH + X^- \rightarrow XOH^{\bullet-} \leftrightarrows {}^-OH + X^\bullet \xrightarrow{X^-} X_2^{\bullet-} \tag{56a}$$
$$X^- = Cl^-, Br^-, I^-, SCN^-$$

$$^\bullet OH + N_3^- \rightarrow {}^-OH + N_3^\bullet \xrightarrow{N_3^-} N_6^{\bullet-} \tag{56b}$$

$$^\bullet OH + X^- \rightarrow {}^-OH + X^\bullet \tag{56c}$$
$$X^- = ClO_2^-, NO_2^-$$
$$^\bullet OH + X^{2-} \rightarrow {}^-OH + X^{\bullet-} \tag{56d}$$
$$X^{2-} = CO_3^{2-}, SO_3^{2-}, SeO_3^{2-}$$
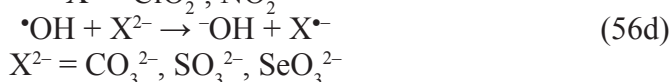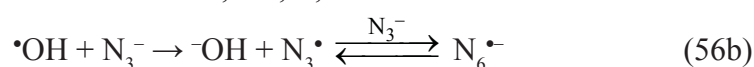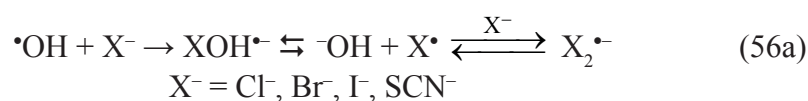
A compilation of some spectral parameters and reduction potentials of the most common oxidizing and reductive inorganic radicals is presented in Table 6.

Table 6. Spectral parameters and reduction potentials of some selective inorganic radicals [49, 53].

Radical	λ_{max} [nm] [49]	ε [dm$^3\cdot$mol$^1\cdot$cm^{-1}] [49]	Redox couple [53]	E^0 *vs.* NHE [V] [53]
$SO_4^{\bullet-}$	450	1100	$SO_4^{\bullet-}/SO_4^{2-}$	+2.47
$Cl_2^{\bullet-}$	340	8800	$Cl_2^{\bullet-}/2Cl^-$	+2.30
$NO_3^\bullet$	640	800-1000	$NO_3^\bullet/NO_3^-$	+2.3-2.5
$CO_3^{\bullet-}$	600	1860	$CO_3^{\bullet-}/CO_3^{2-}$	+1.78
$SeO_3^{\bullet-}$	420	1470	$SeO_3^{\bullet-}/SeO_3^{2-}$	+1.68
$Br_2^{\bullet-}$	360	9900	$Br_2^{\bullet-}/2Br^-$	+1.66
$(SCN)_2^{\bullet-}$	472	7580	$(SCN)_2^{\bullet-}/2SCN^{\bullet-}$	+1.33
$N_3^\bullet$	274	2025	$N_3^\bullet/N_3^-$	+1.33
$I_2^{\bullet-}$	380	9400	$I_2^{\bullet-}/2I^-$	+1.04
$NO_2^\bullet$	400	200	$NO_2^\bullet/NO_2^-$	+0.99
$ClO_2^\bullet$	360	1000	$ClO_2^\bullet/ClO_2^-$	+0.93
$SO_3^{\bullet-}$	250-255	1000-1380	$SO_3^{\bullet-}/SO_3^{2-}$	+0.63
$NO^\bullet$	–	–	$NO^\bullet/NO^-$	+0.39
$SO_2^{\bullet-}$	255	1770	$SO_2/SO_2^{\bullet-}$	−0.28
$CO_2^{\bullet-}$	235	3000	$CO_2/CO_2^{\bullet-}$	−1.90

Reactions involving hydrated electrons are also very useful for the generation of selective oxidizing radicals (Eqs. (57) and (58)):

$$e^-_{aq} + S_2O_8^{2-} \rightarrow SO_4^{\bullet-} + SO_4^{2-} \tag{57}$$

$$e^-_{aq} + NO_3^- \rightarrow NO_3^{2-} \xrightarrow{H_2O} NO_2^\bullet + 2HO^- \tag{58}$$
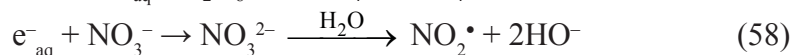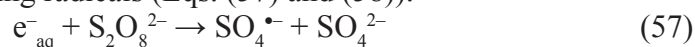
Selective reductive radicals. The number of selective reductive radicals is much lower in comparison to oxidizing radicals. The most common is the carbon dioxide radical anion ($CO_2^{\bullet-}$). Reactions leading to this radical and involving primary $^\bullet OH$ radicals and $^\bullet H$ atoms are presented below (Eqs. (59) and (60)):

$$^\bullet OH + HCO_2^- \rightarrow H_2O + CO_2^{\bullet-} \tag{59}$$

$$^\bullet H + HCO_2^- \rightarrow H_2 + CO_2^{\bullet-} \tag{60}$$
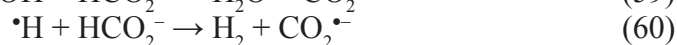
These secondary radicals exhibit sufficiently intense optical absorption in the visible and near UV range that permit kinetic spectrophotometric measurements of the rates of their formation and decay.

2.1.7. Radical reactions involving secondary radicals

Selective inorganic radicals react with other radicals and with inorganic and organic compounds mostly by one-electron oxidation or reduction without the formation of intermediate adducts (such as $^\bullet OH$ and $^\bullet H$ adducts). A comparison of the reactivities of some selected oxidizing radicals with inorganic and organic compounds is presented in Table 7.

Table 7. Rate constants k of some selected oxidizing radicals with inorganic and organic compounds [48].

Compound	k [dm³·mol⁻¹·s⁻¹]					
	$SO_4^{\bullet-}$	$Cl_2^{\bullet-}$	$CO_3^{\bullet-}$	$Br_2^{\bullet-}$	$N_3^\bullet$	$I_2^{\bullet-}$
N_3^-	3.0×10^9	1.2×10^9	–	4.0×10^8	–	$< 5 \times 10^6$
$Fe(CN)_6^{2-}$	–	–	2.7×10^8	2.8×10^7	4.0×10^9	–
Benzene	–	–	$< 5 \times 10^4$	–	$< 3 \times 10^6$	–
Anisole	4.9×10^9	–	2.8×10^5	–	$< 3 \times 10^6$	–
Phenol	–	4.0×10^8	2.0×10^7	6.0×10^6	5.0×10^7	–
Phenoxide	–	–	3.5×10^8	5.0×10^8	4.3×10^9	5.7×10^7
4-Methoxy-phenoxide	–	–	5.2×10^8	–	4.2×10^9	–
4-Methyl-phenoxide	–	–	4.8×10^8	4.7×10^8	–	9.8×10^7
Aniline	–	–	5.4×10^8	2.1×10^8	4.0×10^9	4.4×10^6
Tryptophan	2.0×10^9	2.6×10^9	4.4×10^8	7.0×10^8	4.1×10^9	$< 1 \times 10^6$
Tyrosine	3.0×10^9	2.7×10^8	2.1×10^8	2.0×10^8	1.0×10^8	$< 1 \times 10^6$
Methionine	1.1×10^9	4.0×10^9	3.0×10^7	1.7×10^9	$< 1 \times 10^6$	$< 1 \times 10^6$

For instance, the azide radical ($N_3^\bullet$) was found to oxidize aromatic systems such as aniline and phenoxide ions at a rate $\sim 4 \times 10^9$ dm$^3 \cdot$mol$^{-1} \cdot$s^{-1}, primarily *via* ET, whereas benzene and anisole are not observably oxidized by $N_3^\bullet$. Some of the presented radicals ($Cl_2^{\bullet-}$, $CO_3^{\bullet-}$, $N_3^\bullet$, and $Br_2^{\bullet-}$) show a great selectivity for tryptophan (Trp) residues in the presence of tyrosine (Tyr) residues. Moreover, these radicals react quite rapidly with amino acid residues (Trp, Tyr, Met, Cys, His) forming respective radicals located mostly on their side chains. These radicals are particularly useful for studying oxidative changes in amino acids, peptides and proteins that were very often coupled with long-range intramolecular electron transfer (LRET) [75-80].

2.1.8. Peroxyl radicals

Peroxyl radicals (ROO$^\bullet$) are important reactive intermediates formed during oxidation of organic and biological compounds which result from the reaction of free radical (R$^\bullet$) with molecular oxygen (Eq. (61)):

$$RX^\bullet + O_2 \rightarrow RXO_2^\bullet \tag{61}$$
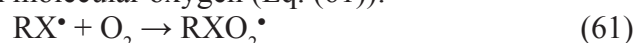
The radical site (-X$^\bullet$) is mostly located on non-metallic elements like carbon, oxygen, nitrogen and sulfur atoms. The most common peroxyl radicals are those involving carbon atom. These radicals are key intermediates in polymerization processes, either in a chain propagation step and/or termination step. Formation and reactions of ROO$^\bullet$ radicals have been extensively reviewed in numerous publications [81-84].

Carbon-atom peroxyl radicals. Most organic C-centered radicals react, in principle, irreversibly with O$_2$ with the rate constants typically $\sim 2 \times 10^9$ dm$^3 \cdot$mol$^{-1} \cdot$s^{-1} [85]. As far as the spectral properties are concerned the case frequently encountered is that the parent C-centered radical absorbs in the UV-Vis region while the corresponding peroxyl radical absorbs weakly only in the UV region with no specific spectral structure. The other case, where both the radical and its

Table 8. Absorption maxima and molar absorption coefficients of some selected vinyl peroxyl and aryl peroxyl radicals in aqueous solutions [81].

Peroxyl radical	λ_{max} [nm]	ε_{max} [dm$^3 \cdot$mol$^{-1} \cdot$cm^{-1}]
Vinyl	440	1100
Dichlorovinyl	540	1100
Phenyl	490	1600
4-Methoxyphenyl	600	2100
4-Methylphenyl	560	600
4-Aminophenyl	590	2000
3-Hydroxyphenyl	520	1400

corresponding peroxyl radical absorb in the UV region has been also observed. Usually, those peroxyl radicals are characterized by weak absorptions with λ_{max} < 250 nm and rather low molar absorption coefficients ~1000 $dm^3 \cdot mol^{-1} \cdot cm^{-1}$. Interestingly, the situation in the case of vinyl and aryl radicals is the inverse. The parent radicals exhibit no absorption in the accessible wavelength region while their respective peroxyl radicals absorb in the near UV or even in the visible region. Some selected examples are compiled in Table 8.

Peroxyl radicals can undergo a number of unimolecular and bimolecular processes. Unimolecular processes include following types of reactions: $HO_2^\bullet$ and $O_2^{\bullet-}$ elimination reactions, addition to the C=C double bonds, and, the most common, hydrogen abstraction and electron transfer reactions. Since the ROO–H bond energy in hydroperoxides derived from $ROO^\bullet$ radicals is rather weak (~360-370 $kJ \cdot mol^{-1}$), the H-abstraction reaction can occur at an appreciable rate, since the C–H bond energy of the H-donor is sufficiently low. Such conditions are fulfilled in abstraction of bis-allylic hydrogens present in polyunsaturated fatty acids where the C–H bond energy is equal to 320 $kJ \cdot mol^{-1}$ (Eq. (62)) [81, 86]:

$$ROO^\bullet + -CH_2=CH-CH_2-CH=CH- \rightarrow$$
$$\rightarrow ROOH + -CH_2=CH-^\bullet CH-CH=CH- \quad (62)$$
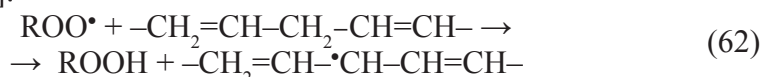
Peroxyl radicals can oxidize various organic compounds (phenothiazines, porphyrins, amines, sulfides) to the corresponding radical cations and various anions (ascorbate, phenolate, inorganic anions) to the corresponding radicals [85, 86]. N,N,N',N'-tetramethyl-*p*-phenylenediamine (TMPD) was used to probe the oxidizing properties of various peroxyl radicals. The rate constants of peroxyl radicals cover a broad range from 1.1×10^6 $dm^3 \cdot mol^{-1} \cdot s^{-1}$ to 1.9×10^9 $dm^3 \cdot mol^{-1} \cdot s^{-1}$ (Table 9).

Table 9. Rate constants k of some selected peroxyl radicals with ascorbate anions and TMPD [86].

	k [$dm^3 \cdot mol^{-1} \cdot s^{-1}$]				
	$CH_3O_2^\bullet$	$HOCH_2O_2^\bullet$	$ClCH_2O_2^\bullet$	$Cl_2CHO_2^\bullet$	$Cl_3CO_2^\bullet$
Ascorbate (AH⁻)	1.7×10^6	4.7×10^6	1.2×10^8	7.0×10^8	9.1×10^8
TMPD	4.3×10^7	7.2×10^7	4.2×10^8	7.4×10^8	1.7×10^9

It is worthy to note that the rate constants for oxidation reactions by peroxyl radicals increase with increasing number of chlorine atoms on the radicals. This trend was rationalized by the electron-withdrawing effect of these substituents which decrease the electron density on the radical site.

Peroxyl radicals, which do not decay in one of the unimolecular processes (*vide supra*), undergo bimolecular decay. In contrast to many other radicals,

they do not disproportionate but decay *via* a recombination process leading in the first step to a tetroxide (Eq. (63)):

$$ROO^\bullet + ROO^\bullet \rightarrow ROOOOR \qquad (63)$$

Depending on the properties of the peroxyl radicals, the tetroxide can decay *via* several channels (Eqs. (64) and (65)), which always involve the cleavage of the lateral O–O bond. Reactions depicted in Eqs. (64) and (65) are known as the Russell and the Bennett mechanisms, respectively:

$$ROOOOR \rightarrow R_2C{=}O + R_2CHOH + O_2 \qquad (64)$$
$$ROOOOR \rightarrow 2R_2C{=}O + H_2O_2 \qquad (65)$$

These reaction pathways require the existence of C–H bond α-positioned to the peroxyl function.

Hetero-atom peroxyl radicals. Oxygen-centered radicals react with O_2 very slowly, *e.g.* the tyrosyl radical (TyrO$^\bullet$) reacts with O_2 with the rate $< 1.3 \times 10^3$ $dm^3 \cdot mol^{-1} \cdot s^{-1}$. In principle, trioxyl radicals ROOO$^\bullet$ are unstable and decompose into alkoxyl radicals (RO$^\bullet$) and O_2.

Nitrogen-centered radicals react with O_2 more slowly than C-centered radicals. For instance, the rate constant for the reaction of aminyl radical ($^\bullet NH_2$) with oxygen was found to be equal to 3.4×10^7 $dm^3 \cdot mol^{-1} \cdot s^{-1}$.

Sulfur-centered radicals react with oxygen fast and the reverse reaction is also fast (Eq. (66)):

$$RS^\bullet + O_2 \leftrightharpoons RSOO^\bullet \qquad (66)$$

For the thiyl radical derived from mercaptoethanol (CH$_3$CH$_2$S$^\bullet$) the reaction with O_2 is diffusion controlled with $k_{66} = 2.2 \times 10^9$ $dm^3 \cdot mol^{-1} \cdot s^{-1}$ while the reverse reaction $k_{-66} = 6.2 \times 10^5$ s^{-1} implies the existence of equilibrium depicted in Eq. (66) [87, 88]. Thiyl peroxyl radicals can be monitored by UV-Vis spectroscopy due to their absorption band with λ_{max} located at 550 nm despite their low molar absorption coefficient $\varepsilon_{550} = (2\text{-}4) \times 10^2$ $dm^3 \cdot mol^{-1} \cdot cm^{-1}$. Thiyl peroxyl radicals undergo a thermal rearrangement to the thermodynamically more stable sulfonyl radicals (Eq. (67)), which can be further oxidized to sulfonyl peroxyl radicals (Eq. (68)):

$$RSOO^\bullet \rightarrow RS^\bullet({=}O)_2 \qquad (67)$$
$$RS^\bullet({=}O)_2 \rightarrow RS\,({=}O)_2{-}OO^\bullet \qquad (68)$$

These intermediates have attracted considerable interest because of their possible participation in radical processes occurring in biological systems.

2.2. RADIOLYSIS OF WATER AT AMBIENT TEMPERATURES WITH HIGH LET IRRADIATION

The earliest studies on radiolysis of water with high LET irradiation were performed just after discovery of radiation. However, only α-particles were available at that time. Later, the development of ion accelerators has enabled studies with ions (H$^+$, D$^+$, He^{2+}) of lower energies (10 MeV per ion-mass num-

ber). In the last two decades of twentieth century, ion beams of heavier ions with higher energies have become available. Facilities in France (GANIL), Japan (TIARA), Germany (FAIR), and in USA (NSRL) delivered C-Kr ions with 75-95 MeV/ion-mass number, H-Au ions with 2.5-27 MeV/ion-mass number, H-U ions with 2-10 GeV/ion-mass number, and Ne-Au with 0.3-1.5 GeV/ion-mass number, respectively [89].

2.2.1. Primary yields of $^{\bullet}$OH radicals, e^{-}_{aq}, and H_2O_2 as a function of LET [89-92]

The most intensively studied products of water radiolysis were hydrated electrons (e^{-}_{aq}), $^{\bullet}$OH radicals, and hydrogen peroxide (H_2O_2). Many of the results were obtained by a scavenging method [42]. Some of them were from the heavy-ion pulse radiolysis.

Hydrated electrons and $^{\bullet}$OH radicals. There are two important findings as far as the primary G-values are concerned: (i) the primary yields of e^{-}_{aq} and $^{\bullet}$OH radicals decrease with increasing LET (Table 10), and (ii) the lower primary yields of e^{-}_{aq} and $^{\bullet}$OH radicals are observed for lighter ions than for heavier ions with comparable LET.

Hydrogen peroxide. As compared to $^{\bullet}$OH radicals, e^{-}_{aq}, the radiation chemical yields are less sensitive to variation of LET (see Table 7).

Based on the dependency of G-values of the above products *vs.* LET (Table 10) the three reactions depicted by Eqs. (10), (11) and (15) of Table 1 seem to be the most significant among all intra-spur and intra-track reactions.

Table 10. Primary radiation chemical yields (per 100 eV) of e^{-}_{aq}, $^{\bullet}$OH radicals, and H_2O_2 as a function of LET.

	Species/ions				Species/ions		
	e^{-}_{aq}	$^{\bullet}$OH	H_2O_2		e^{-}_{aq}	$^{\bullet}$OH	H_2O_2
He ($\sim$2 eV·nm^{-1})	2.4	2.6	0.7	Si ($\sim$60 eV·nm^{-1})	1.2	1.3	0.75
C ($\sim$15 eV·nm^{-1})	1.9	1.9	0.8	Ar ($\sim$150 eV·nm^{-1})	1.1	1.1	0.9
Ne ($\sim$30 eV·nm^{-1})	1.6	1.6	0.8	Fe ($\sim$600 eV·nm^{-1})	0.8	1.0	1.1

2.2.2. Intra-track radical kinetics as a function of LET [93]

Information about the intra-track dynamics can be extracted by increasing scavenger concentration. With increasing scavenger concentration, the scavenging reactions become more efficient, and thus they can compete more significantly with intra-track reactions and diffusions.

The following chemical system was applied to the study the intra-track radical kinetics induced by different high LET irradiation: a deaerated aqueous

solutions containing methyl viologen (MV^{2+}) containing various concentration of formate ions ($HCOO^-$). The following reactions occur (Eqs. (18), (69)-(72)):

$$e^-_{aq} + MV^{2+} \rightarrow MV^{\bullet+} \tag{69}$$
$$^{\bullet}OH + HCOO^- \rightarrow H_2O + CO_2^{\bullet-} \tag{70}$$
$$^{\bullet}H + HCOO^- \rightarrow H_2 + CO_2^{\bullet-} \tag{71}$$
$$CO_2^{\bullet-} + MV^{2+} \rightarrow CO_2 + MV^{\bullet+} \tag{72}$$
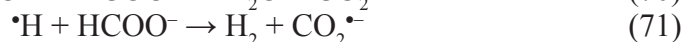
The G-values of $MV^{\bullet+}$ were measured in aqueous solutions after irradiation with He, C, Ne, Si, Ar, and Fe ions. The $G(MeV^{\bullet+})$ increased with increasing $HCOO^-$ concentration for all ions. This is due to the faster scavenging reactions in which more primary radicals are scavenged. With increasing LET, the $G(MeV^{\bullet+})$ decreased due to increased radical density in the track and as a consequence of increased efficiency of intra-track reactions. These experimental data were successfully reproduced by the Monte-Carlo simulation using the IONLYS-IRT code.

3. RADIOLYSIS OF ORGANIC SOLVENTS

There is a large variety of organic solvents that have been used for inducing radical reactions by means of high energy radiation [94]. The use of organic solvents has advantages over water. First, since a broad range of solvent polarities are available, compounds that are insoluble in water can be studied in a suitable solvent or mixture of solvents [4]. Second, depending on the solvent used, its radiolysis can offer a convenient method for the generation of radical ions and excited states and/or preferentially one of them. Some control over the type of ionic species and excited states formed can be achieved by choice of a suitable solvent and, in addition, of a saturating gas [5]. Thus, one may generate selectively radical cations, radical anions, and/or excited states derived from the solutes. The one disadvantage is the lack of a detailed knowledge of the mechanism of secondary processes occurring after primary ionization and/or excitation of some solvents. In contrast to water, there are still discrepancies as to the type and radiation chemical yields of primary radiolysis products. Product and free ion yields, rate constants, and spectroscopic parameters of transients in selected organic liquids have been collected [95-97].

Only the radiolysis of some most representative solvents (alcohols, acetonitrile, acetone, and halogenated hydrocarbons) for the generation of radical ions and excited states are covered here.

3.1. RADIOLYSIS OF ALCOHOLS

3.1.1. Formation of primary transients and their subsequent reactions

Radiolysis of neat alcohols leads to the formation of the alcohol positive ions and presolvated electrons ($e^-_{presolv}$) (Eq. (73)) [98, 99]:

$$RR'CH–OH \xrightarrow{\Large\sim\!\sim\!\sim\!\sim} RR'CH–OH^{\bullet+} + e^-_{presolv} \qquad (73)$$
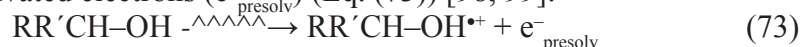
The alcohol derived radical cations disappear rapidly in ion-molecule reactions with another alcohol molecule producing either ketyl radicals (Eq. (74a)) or alkoxy radicals (Eq. (74b)):

$$\rightarrow RR'C^{\bullet}–OH + RR'CH–OH_2^+ \qquad (74a)$$

$$RR'CH–OH^{\bullet+} + RR'CH–OH \mid$$

$$\rightarrow RR'CH–O^{\bullet} + RR'CH–OH_2^+ \qquad (74b)$$

The reaction depicted in Eq. (74a) prevails substantially over the reaction depicted in Eq. (74b) since the >C–H bond dissociation energy (95 kcal·mol^{-1}) is lower than the BDE of the O–H bond (102 kcal·mol^{-1}). Similarly, as in water, the electron ejected in an ionization process (Eq. (73)), undergoing solvation on the picosecond time domain, after thermalization (Eq. (75)):

$$e^-_{presolv} + nRR'CH–OH \rightarrow e^-_{solv} \qquad (75)$$
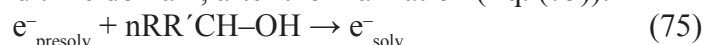
When the alcohol solutions are saturated with nitrous oxide (N$_2$O), the reduction reactions involving only ketyl radicals can be studied without a contribution of solvated electrons (e^-_{solv}). Solvated electrons can be rapidly scavenged by N$_2$O generating oxide radical ions (O$^{\bullet-}$) (Eq. (76)), which subsequently react with alcohol molecules forming ketyl radicals (Eq. (77)):

$$e^-_{solv} + N_2O \rightarrow N_2 + O^{\bullet-} \qquad (76)$$

$$O^{\bullet-} + RR'CH–OH \rightarrow {}^-OH + RR'C^{\bullet}–OH \qquad (77)$$
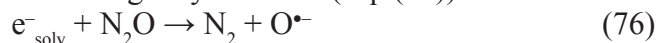
Since in alcohols mainly solvated electrons and reductive ketyl radicals (RR'C$^{\bullet}$–OH) are formed (Eqs. (73), (74a) and (77)), these solvents can be used to generate selectively radical anions derived from the solutes, as described below.

3.1.2. Selected radical reactions involving primary transients

A few systems will be presented to illustrate the generation of solute radical anions *via* reactions of e^-_{solv} and ketyl radicals with solute molecules and subsequent reactions of radical anions in alcohol solutions. Solute radical cations are not formed since the alcohol-derived radical cations disappear rapidly in reactions depicted in Eqs. (74a) and (74b).

Radical anions derived from retinyl polyene derivatives (Ret), retinal homologs (HomRet) and carotenes (Car) have been studied in methanol and 2-propanol [100, 101]:

$$Ret/HomRet/Car + e^-_{solv}/RR'C^{\bullet}–OH \rightarrow$$
$$\rightarrow Ret^{\bullet-}/HomRet^{\bullet-}/Car^{\bullet-} + RR'C=O + H^+ \qquad (78)$$

Radical anions derived from Ret and HomRet formed in reactions (Eq. (78)) undergo protonation by alcohol molecules (Eq. (79)) [102]:

$$Ret^{\bullet-}/HomRet^{\bullet-} + RR'CH–OH \rightarrow RetH^{\bullet}/HomRet^{\bullet} + RR'CH–O^- \quad (79)$$

The rate constants for protonation of radical anions in alcohols was found to decrease on increasing the polyene chain and the acidity of the hydroxyl group in alcohols.

Radical anions derived from fullerenes (C_{60}, C_{70}, C_{76}, C_{78}, and C_{84}) have been generated (in analogous reactions as depicted by Eq. (78)) and their spectral and kinetic properties have been characterized in 2-propanol [103].

Radical anions derived from naphthalene ($Nph^{\bullet-}$), phenanthrene ($Pha^{\bullet-}$), biphenyl ($Bph^{\bullet-}$), anthracene ($Anh^{\bullet-}$), *p-, o-, m-*terphenyls (t-$Phe^{\bullet-}$) undergo protonation in analogous reactions as depicted by Eq. (79).

3.2. RADIOLYSIS OF ACETONITRILE

3.2.1. Formation of primary transients and their subsequent reactions

Radiolysis of neat acetonitrile leads to the formation of acetonitrile positive radical ions and presolvated electrons (Eq. (80)):

$$CH_3CN \xrightarrow{\text{-}\wedge\wedge\wedge\wedge\wedge} CH_3CN^{\bullet+} + e^-_{presolv} \quad (80)$$
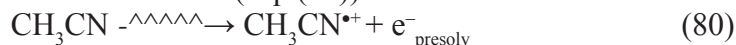
Presolvated electrons are mostly efficiently scavenged by the acetonitrile molecules leading to the formation of negative ions (Eq. (81)) or, to a lower extent, undergo solvation (Eq. (82)) and are subsequently trapped by the acetonitrile molecules (Eq. (83)):

$$e^-_{presolv} + CH_3CN^- \rightarrow CH_3CN^{\bullet-} \quad (81)$$
$$e^-_{presolv} + nCH_3CN \rightarrow e^-_{solv} \quad (82)$$
$$e^-_{solv} + CH_3CN \rightarrow CH_3CN^{\bullet-} \quad (83)$$

Recombination of positive radical ions with solvated electrons (Eq. (84)) and negative radical ions (Eq. (85)) leads to the excited triplet states:

$$CH_3CN^{\bullet+} + e^-_{solv} \rightarrow {}^3CH_3CN^* \quad (84)$$
$$CH_3CN^{\bullet+} + CH_3CN^{\bullet-} \rightarrow {}^3CH_3CN^* \quad (85)$$

The yields of reducing species was found in the range of G = 1.03-1.55. On the other hand, the low yields of G for the oxidizing species (~0.2) and for the triplets (~0.3) were measured [104, 105]. Contrary to alcohols, acetonitrile is an aprotic solvent which makes acetonitrile a convenient liquid system to study one-electron reduction of transition metal complexes that are not stable in aqueous and alcohol solutions and of the solute-derived radical anions which do not undergo a fast protonation by acetonitrile molecules.

3.2.2. Selected radical reactions involving primary transients

Taking into account the mechanism of radiolysis, Ar-saturated acetonitrile solutions were often used to generate of both radical cations and anions derived from the solutes (Eqs. (86)-(88)):

$$CH_3CN^{\bullet+} + S \rightarrow CH_3CN + S^{\bullet+} \quad (86)$$
$$CH_3CN^{\bullet-} + S \rightarrow CH_3CN + S^{\bullet-} \quad (87)$$

$$e^-_{solv} + S \rightarrow S^{\bullet-} \tag{88}$$
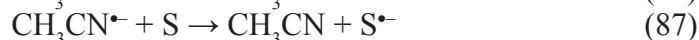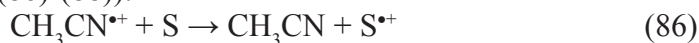
However, in O_2-saturated acetonitrile solutions, selective generation of radical cations of solute can be achieved (Eq. (86)). Oxygen serves as a strong quencher of solvated electrons, radical anions (Eq. (89)) and solvent triplets:

$$e^-_{solv}/CH_3CN^{\bullet-}/^3CH_3CN^* + O_2 \rightarrow O_2^{\bullet-} + CH_3CN \tag{89}$$
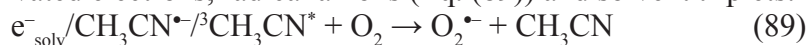
Radical ions derived from many aromatic compounds have been generated according to reactions depicted in Eqs. (86)-(88) [105-107].

3.3. RADIOLYSIS OF ACETONE

3.3.1. Formation of primary transients and their subsequent reactions

Radiolysis of neat acetone leads to the formation of the acetone positive ions and presolvated electrons (Eq. (90)):

$$(CH_3)_2 C=O \xrightarrow{\sim\sim\sim\sim} (CH_3)_2C=O^{\bullet+} + e^-_{presolv} \tag{90}$$
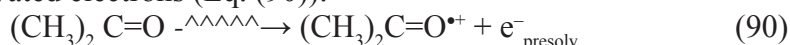
The subsequent reactions of the primarily formed species (Eq. (90)) are analogous to those occurring in acetonitrile and depicted in Eqs. (81)-(85). The total yield of excited states (G = 1.3) and of free ions (G = 1.2) were found [108].

3.3.2. Selected radical reactions involving primary transients

In Ar-saturated acetone solutions both radical ions (Eqs. (91)-(93)) and triplets (Eq. (94)) of solutes are formed, while in O_2-saturated solutions, only radical cations of a solute are formed (Eq. (93)):

$$(CH_3)_2C=O^{\bullet-} + S \rightarrow (CH_3)_2C=O + S^{\bullet-} \tag{91}$$
$$e^-_{solv} + S \rightarrow (CH_3)_2C=O + S^{\bullet-} \tag{92}$$
$$(CH_3)_2C=O^{\bullet+} + S \rightarrow (CH_3)_2C=O + S^{\bullet+} \tag{93}$$
$$^3(CH_3)_2C=O^* + S \rightarrow (CH_3)_2C=O + {}^3S^* \tag{94}$$
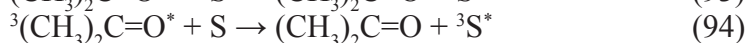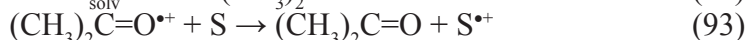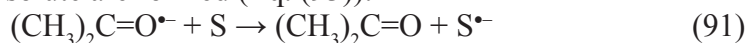
Radical ions and triplet excited states of naphthalene, anthracene, pyrene, biphenyl, *trans*-stilbene, nitromethane, retinyl polyenes derivatives, and retinal homologs have been generated *via* reactions depicted in Eqs. (90)-(94), and studied in acetone [108-110]. Radical cations of multiple methylated uracils and thymines were also generated, and were found to exist in a lactim-like form [110].

3.4. RADIOLYSIS OF HALOGENATED HYDROCARBONS

3.4.1. Formation of primary transients and their subsequent reactions

Radiolysis of neat halogenated hydrocarbons (RCl), leads to the formation of the positive radical ions and/or radicals and presolvated electrons (Eqs. (95a)-(95c)):

$$CH_2Cl_2 \xrightarrow{\sim\sim\sim\sim} CH_2Cl_2^{\bullet+} + e^-_{presolv} \tag{95a}$$
$$ClCH_2CH_2Cl \xrightarrow{\sim\sim\sim\sim} ClCH_2CH_2Cl^{\bullet+}/ClCHCH_2^{\bullet+}/CH_2ClCH_2^+ + e^-_{presolv} \tag{95b}$$

$$n\text{-}(C_4H_9)Cl \text{ -}^{\wedge\wedge\wedge\wedge\wedge}\!\to n\text{-}(C_4H_9)Cl^{\bullet+} + e^-_{presolv} \qquad (95c)$$
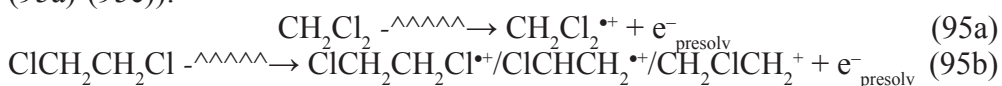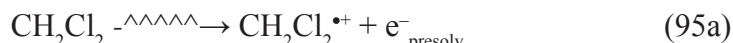
Presolvated electrons are mostly efficiently scavenged by the RCl molecules (dichloromethane, 1,2-dichloroetane, and *n*-butyl chloride) *via* a very fast dissociative attachment to the solvent molecules forming relatively unreactive radicals and chloride ions (Cl⁻) which do not react with the solute (Eq. (96)):

$$e^-_{presolv} + RCl \to R^\bullet + Cl^- \qquad (96)$$

or to lower extent undergo solvation and a subsequent trapping by the RCl molecules leading to the same products as in reaction depicted in Eq. (96) [111]. Thus, direct reactions of electrons with the solutes are eliminated and therefore these halogenated hydrocarbons are very convenient for the selective generation of solute radical cations.

3.4.2. Selected radical reactions involving primary transients

In the presence of solutes (S) of lower ionization potential as the above solvents, a rapid ET takes place (Eq. (97)):

$$CH_2Cl_2^{\bullet+}/ClCH_2CH_2Cl^{\bullet+}/n\text{-}(C_4H_9)Cl^{\bullet+} + S \to$$
$$\to CH_2Cl_2/ClCH_2CH_2Cl/n\text{-}(C_4H_9)Cl + S^{\bullet+} \qquad (97)$$
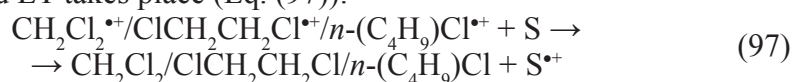
Radical cations derived from retinal and retinoic acid, fullerenes (C_{60}, C_{70}, C_{76}, C_{78}, and C_{84}) and chlorinated fullerenes ($C_{60}Cl_6$ and $C_{60}Cl_{12}$) have been generated *via* reactions depicted in Eq. (86) and their spectral properties have been characterized [103, 112, 113].

4. RADIOLYSIS OF IONIC LIQUIDS

Ionic liquids (ILs) constitute a bridge between molecular liquids and ionic solids. They are defined as molten salts with melting points below 100°C. These salts are a combination of organic and inorganic ions. The dynamic properties (*e.g.* relaxation) are distributed over a broader range of scales and diffusion is generally slower due to higher viscosities in comparison to molecular liquids. ILs are generally characterized by low volatility, good electric conductivity, and microheterogeneity producing different local environments that favors simultaneous solubility of polar and non-polar solutes [114]. Owing to their unique properties, ILs are an attractive media for the generation of radicals *via* high energy radiation. However, the knowledge about the radiation-induced primary reactive intermediates in ILs, and the approaches to convert them into specific radical intermediates is limited to only some investigated ILs. These comprise ILs composed of imidazolium ($BMIM^+$), quaternary ammonium (R_4N^+), pyrrolidinium, (Pyr), pyridinium (Py), phosphonium cations and bis(trifluoromethylsulfonyl)imide (NTf_2^-), dicyanamide, bis-(oxalate)-borate, tetrafluoroborate (BF_4^-), hexafluorophosphate (PF_6^-), chloride (Cl⁻), bromide

(Br$^-$), thiocyanate (SCN$^-$), and azide (N$_3^-$) anions. Different class of ILs can produce, upon irradiation, different reactive intermediates. Therefore, they can provide a new environment induced by radiation in which to test radical reactions including charge transfer processes [1, 115-117].

4.1. INITIAL EVENTS IN RADIOLYSIS

Ionization (Eq. (98)) and excitation (Eq. (99)) are the two major processes occurring in ILs:

$$IL \, \text{-}^{\wedge\wedge\wedge\wedge\wedge}\rightarrow IL^{\bullet+} \text{(holes)} + e^- \text{ (energetic electrons)} \qquad (98)$$
$$IL \, \text{-}^{\wedge\wedge\wedge\wedge\wedge}\rightarrow IL^* \qquad (99)$$

The energetic electrons start to lose their excess kinetic energy and become "thermalized". Since they are not equilibrated with the surrounding molecules they are called either "dry" or "presolvated". As the solvation process proceeds, the electrons become more and more localized and eventually solvated (Eq. (100)):

$$e^- \rightarrow e^-_{dry/presolv} \rightarrow e^-_{solv} \qquad (100)$$
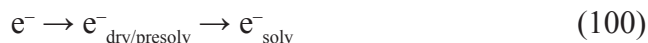
"Holes" resulting from ionization (Eq. (98)) can undergo either recombination with electrons (Eq. (101)) or fragmentation of any type (Eq. (102)) [116, 117]:

$$e^-_{dry/presolv} + IL^{\bullet+} \text{(holes)} \rightarrow IL^* \qquad (101)$$
$$IL^{\bullet+} \text{(holes)} \rightarrow Y + R^{\bullet} \qquad (102)$$
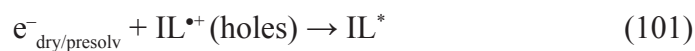
4.2. SELECTED RADICAL REACTIONS INVOLVING HOLES AND ELECTRONS

In the presence of electron scavengers, both types of electrons can form radical anions (Eq. (103)):

$$e^-_{presolv/solv} + S \rightarrow S^{\bullet-} \qquad (103)$$

where S designates different types of electron scavengers: those reacting with either presolvated or solvated electrons and those reacting with both of them. In the presence of "hole" scavengers the respective solute radical cations can be formed (Eq. (104)):

$$IL^{\bullet+} \text{(holes)} + S \rightarrow S^{\bullet+} \qquad (104)$$

Only a few examples of radiation-induced radical reactions in IL containing 1-butyl-3-methyl-imidazolium cation (BMI$^+$) will be presented.

The radical cations from 1-methyl-1,4-dihydronicotinamide (NADH), chlorpromazine (ClPz), and N,N,N',N'-tetramethyl-*p*-phenylenediamine (TMPD) (Eqs. (105)-(108)), and both the radical cations and anions from benzoquinone (BQ), duroquinone (DQ), methyl viologen (MV), chlorpromazine (ClPz), 6-hydroxy-2,5,7,8-tetramethylchroman-2-carboxylic acid (Trolox) and

thiophene and its derivatives were generated in this IL containing hexafluoro-phosphate (PF_6^-) or tetrafluoroborate (BF_4^-) anions [118, 119].

$$BMI^+ \text{-}^{\wedge\wedge\wedge\wedge\wedge}\rightarrow BMI^{\bullet 2+} + e^- \qquad (105)$$

$$e^- + PF_6^- \rightarrow PF_6^{\bullet -} \rightarrow PF_5^- + F^\bullet \qquad (106)$$

$$PF_6^{\bullet -}/F^\bullet + NADH/ClPz \rightarrow PF_6^-/F^- + NADH^{\bullet +}/ClPz^{\bullet +} \qquad (107)$$

$$BMI^{\bullet 2+} + TMPD \rightarrow BMI^+ + TMPD^{\bullet +} \qquad (108)$$
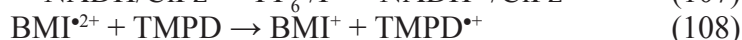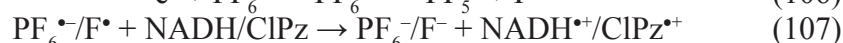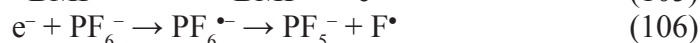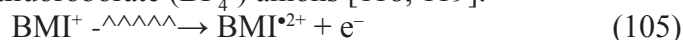
Dihalide ($Cl_2^{\bullet -}$ and $Br_2^{\bullet -}$) and pseudohalides (($SCN)_2^{\bullet -}$ and $N_6^{\bullet -}$) have been selectively generated in this IL with Cl^-, Br^-, SCN^-, and N_3^- anions (Eqs. (105), (109) and (110)) [120]:

$$BMI^{\bullet 2+} + Cl^-/Br^-/SCN^-/N_3^- \rightarrow BMI^+ + Cl^\bullet/Br^\bullet/{}^\bullet SCN/N_3^\bullet \qquad (109)$$

$$Cl^\bullet/Br^\bullet/{}^\bullet SCN/N_3^\bullet + Cl^-/Br^-/SCN^-/N_3^- \leftrightarrows Cl_2^{\bullet -}/Br_2^\bullet/(SCN)_2^{\bullet -}/N_6^{\bullet -} \qquad (110)$$
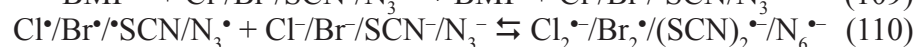
Providing a comprehensive review of radical reactions occurring in ILs in the absence and in the presence of various solutes is beyond the scope of this text.

REFERENCES

[1].   Bobrowski, K. (2012). Radiation induced radical reactions. In C. Chatgilialo-glu & A. Studer (Eds.), *Encyclopedia of radicals in chemistry, biology and materials* (pp. 395-432). John Wiley & Sons Ltd.

[2].   Buxton, G.V. (1987). Radiation chemistry of the liquid state: (1) Water and homogeneous aqueous solutions. In Farhataziz & M.A.J. Rodgers (Eds.), *Radiation chemistry. Principles and applications* (pp. 321-350). New York: VCH Publishers, Inc.

[3].   Buxton, G.V. (1999). Measurement of rate constants for radical reactions in the liquid phase. In Z.B. Alfassi (Ed.), *General aspects of the chemistry of radicals* (pp. 51-77). Chichester: John Wiley & Sons.

[4].   Buxton, G.V. (2008). An overview of the radiation chemistry of liquids. In M. Spotheim-Maurizot, M. Mostafavi, T. Douki & J. Belloni (Eds.), *Radiation chemistry: From basics to applications in material and life sciences* (pp. 3-16). Bonchamp-Les Laval: EDP Sciences.

[5].   Wojnarovits, L. (2003). Radiation chemistry. In A. Vertes, S. Nagy & Z. Klenc-sar (Eds.), *Handbook of nuclear chemistry* (pp. 1-55). Kluwer Academic Publishers.

[6].   Wishart, J.F., & Shkrob, I.A. (2009). The radiation chemistry of ionic liquids and its implications for their use in nuclear fuel processing. In R.D. Rogers, N.V. Plechkova & K.R. Seddon (Eds.), *Ionic liquids: From knowledge to application* (pp. 119-134). Washington, DC: American Chemical Society.

[7].   Mozumder, A. (1969). Charged particle tracks and their structures. In M. Burton & J.L. Magee (Eds.), *Advances in radiation chemistry* (pp. 1-102). New York: Wiley-Interscience.

[8].   Denaro, A.R., & Jayson, G.G. (1972). *Fundamentals of radiation chemistry*. London: Butterworths.

[9]. Freeman, G.R. (1982). Absorption of energy from ionizing radiation. In J.H. Baxendale & F. Busi (Eds.), *The study of fast processes and transient species by electron pulse radiolysis* (pp. 1-11). Dordrecht: Reidel Publishing Company.

[10]. Freeman, R.F. (1982). Basics of radiation chemistry. In J.H. Baxendale & F. Busi (Eds.), *The study of fast processes and transient species by electron pulse radiolysis* (pp. 19-34). Dordrecht: Reidel Publishing Company.

[11]. Bensasson, R.V., Land, E.J., & Truscott, T.G. (1993). *Excited states and free radicals in biology and medicine. Contributions from flash photolysis and pulse radiolysis*. New York: Oxford Univesity Press Inc.

[12]. Chatterjee, A. (1987). Interaction of ionizing radiation with matter. In Farhataziz & M.A.J. Rodgers (Eds.), *Radiation chemistry. Principles and applications* (pp. 1-27). New York: VCH Publishers, Inc.

[13]. Mozumder, A. (1999). *Fundamentals of radiation chemistry*. San Diego: Academic Press.

[14]. Spinks, J.W.T., & Woods, R.J. (1990). *Introduction to radiation chemistry* (3rd ed.). New York: Wiley.

[15]. Bensasson, R.V., Land, E.J., & Truscott, T.G. (1983). *Pulse radiolysis and flash photolysis. Contributions to the chemistry of biology and medicine*. Oxford: Pergamon.

[16]. Ziegler, J.F. (1999). The stopping of energetic light ions in elemental matter. *J. Appl. Phys./Rev. Appl. Phys.*, *85*, 1249-1272.

[17]. Meesungnoen, J., & Jay-Gerrin, J.-P. (2011). Radiation chemistry of liquid water with heavy ions: Monte Carlo simulation studies. In Y. Hatano, Y. Katsumura & A. Mozumder (Eds.), *Charged particle and photon interactions with matter* (pp. 355-400). Boca Raton: CRC Press.

[18]. Richter, H.W. (1998). Radiation chemistry: Principles and applications. In J.F. Wishart & D.G. Nocera (Eds.), *Photochemistry and radiation chemistry. Complementary methods for the study of electron transfer* (pp. 5-33). Washington, DC: American Chemical Society.

[19]. Wishart, J.F. (2008). Tools for radiolysis studies. In M. Spotheim-Maurizot, M. Mostafavi, T. Douki & J. Belloni (Eds.), *Radiation chemistry: From basics to applications in material and life sciences* (pp. 17-33). Bonchamp-Les Laval: EDP Sciences.

[20]. Ebert, M., Keene, J.P., Swallow, A.J., & Baxendale, J.H. (1965). *Pulse radiolysis*. New York: Academic Press.

[21]. Matheson, M.S., & Dorfman, L. (1969). *Pulse radiolysis*. Cambridge: MIT Press.

[22]. Karolczak, S. (1999). Pulse radiolysis – experimental features. In J. Mayer (Ed.), *Properties and reactions of radiation induced transients. Selected topics* (pp. 11-37). Warszawa: Polish Scientific Publishers PWN.

[23]. Janata, E. (2010). Instrumentation in pulse radiolysis. In J.F. Wishart & B.S.M. Rao (Eds.), *Recent trends in radiation chemistry* (pp. 97-119). Singapore: World Scientific.

[24]. Belloni, J., Crowell, R.A., Katsumura, Y., Lin, M., Marignier, J.-L., Mostafavi, M., Muroya, Y., Saeki, A., Tagawa, S., Yoshida, Y., De Waelle, V., & Wishart, J.F. (2010). Ultrafast pulse radiolysis method. In J.F. Wishart & B.S.M. Rao

(Eds.), *Recent trends in radiation chemistry* (pp. 121-160). Singapore: World Scientific.

[25].   Roffi, G. (1982). Optical monitoring techniques. In J.H. Baxendale & F. Busi (Eds.), *The study of fast processes and transient species by electron pulse radiolysis* (pp. 63-89). Dordrecht: Reidel Publishing Company.

[26].   Asmus, K.-D., & Janata, E. (1982). Conductivity monitoring techniques. In J.H. Baxendale & F. Busi (Eds.),. *The study of fast processes and transient species by electron pulse radiolysis* (pp. 91-113). Dordrecht: Reidel Publishing Company.

[27].   Madden, K.P., McManus, H.J.D., & Fessenden, R.W. (1994). Computer controlled in-situ radiolysis ESR spectrometer incorporating magnetic field-microwave frequency locking. *Rev. Sci. Instrum.*, *65*, 49-57.

[28].   Tripathi, G.N.R. (1989). Time-resolved Raman spectroscopy of chemical reaction intermediates in solution. In R.H.J. Clark & R.E. Hester (Eds.), *Time-resolved spectroscopy* (pp. 157-218). New York: John Wiley & Sons.

[29].   Warman, J.M., & De Haas, M.P. (2010). A history of pulse radiolysis time-resolved microwave conductivity (PR-TRMC) studies. In J.F. Wishart & B.S.M. Rao (Eds.), *Recent trends in radiation chemistry* (pp. 161-200). Singapore: World Scientific.

[30].   Asmus, K.-D., & Janata, E. (1982). Polarography monitoring techniques. In J.H. Baxendale & F. Busi (Eds.), *The study of fast processes and transient species by electron pulse radiolysis* (pp. 115-128). Dordrecht: Reidel Publishing Company.

[31].   Connor, D.B. (1994). Pulse radiolysis with circular dichroism. *Radiat. Phys. Chem.*, *44*, 371-376.

[32].   Le Caer, S., Pin, S., Renault, J.P., Vigneron, G., & Pommeret, S. (2010). Infrared spectroscopy and radiation chemistry. In J.F. Wishart & B.S.M. Rao (Eds.), *Recent trends in radiation chemistry* (pp. 201-209). Singapore: World Scientific.

[33].   Asmus, K.-D. (1984). Pulse radiolysis methodology. *Method. Enzymol.*, *105*, 167-178.

[34].   Magee, J.L., & Chatterjee, A. (1987). Theoretical aspects of radiation chemistry. In Farhataziz & M.A.J. Rodgers (Eds.), *Radiation chemistry. Principles and applications* (pp. 137-171). New York: VCH Publishers, Inc.

[35].   Chatterjee, A., & Magee, J.L. (1987). Track models and radiation chemical yields. In Farhataziz & M.A.J. Rodgers (Eds.), *Radiation chemistry. Principles and applications* (pp. 173-199). New York: VCH Publishers, Inc.

[36].   Mozumder, A., Hatano, Y., & Katsumura, Y. (2010). *Charged particle and photon interactions with matter: Recent advances, applications, and interfaces*. CRC Press.

[37].   Swallow, A.J. (1973). *Radiation chemistry: An introduction*. London: Longman.

[38].   Farhataziz, & Rodgers, M.A.J. (1987). *Radiation chemistry. Principles and applications*. New York: VCH Publishers, Inc.

[39].   Jonah, C.D., & Rao, B.S.M. (2001). *Radiation chemistry. Present status and future trends*. *Studies in physical and theoretical chemistry* (Vol. 87). Amsterdam: Elsevier Science B.V.

[40]. Wishart, J.F., & Rao, B.S.M. (2010). *Recent trends in radiation chemistry*. Singapore: World Scientific.

[41]. Thomas, J.K. (1969). Elementary processes and reactions in the radiolysis of water. In M. Burton & J.L. Magee (Eds.), *Advances in radiation chemistry* (pp. 103-198). New York: Wiley-Interscience.

[42]. Draganic, I.G., & Draganic, Z.D. (1971). *The radiation chemistry of water. Physical chemistry* (Vol. 26)*.* New York: Academic Press.

[43]. Buxton, G.V. (1982). Basic radiation chemistry of liquid water. In J.H. Baxendale & F. Busi (Eds.), *The study of fast processes and transient species by electron pulse radiolysis* (pp. 241-266). Dordrecht: Reidel Publishing Company.

[44]. von Sonntag, C. (1987). *The chemical basis of radiation biology*. New York: Taylor & Francis.

[45]. von Sonntag, C. (2006). *Free-radical-induced DNA damage and its repair*. Berlin, Heidelberg, New York: Springer-Verlag.

[46]. Buxton, G.V., Greenstock, C.L., Helman, W.P., & Ross, A.B. (1988). Critical review of rate constants for reactions of hydrated electrons, hydrogen atoms and hydroxyl radicals ($^\bullet OH/O^{\bullet-}$) in aqueous solution. *J. Phys. Chem. Ref. Data*, *17*, 513-886.

[47]. Ross, A.B., & Neta, P. (1979). *Rate constants for reactions of inorganic radicals in aqueous solution*. Gaithersburg: National Bureau of Standards.

[48]. Neta, P., Huie, R.E., & Ross, A.B. (1988). Rate constants for reactions of inorganic radicals in aqueous solution. *J. Phys. Chem. Ref. Data*, *17*, 1027-1284.

[49]. Hug, G.L. (1981). *Optical spectra of nonmetallic inorganic transient species in aqueous solutions*. Gaithersburg, MD: National Institute of Standards and Technology.

[50]. Li, J.L., Nie, Z.G., Zheng, Y.Y., Dong, S., & Loh, Z.H. (2013). Elementary electron and ion dynamics in ionized water. *J. Phys. Chem. Lett.*, 4, 3698-3703.

[51]. Ma, J., Schmidhammer, U., Pernot, P., & Mostafavi, M. (2014). Reactivity of the strongest oxidizing species in aqueous solutions: The short-lived radical cation $H_2O^{\bullet+}$. *J. Phys. Chem. Lett.*, 5, 258-261.

[52]. Weeks, J.L., & Rabani, J. (1966). The pulse radiolysis of deaerated aqueous carbonate solutions: I. Transient optical spectrum and mechanism. II pK for $^\bullet OH$ radicals. *J. Phys. Chem.*, *70*, 2100-2105.

[53]. Wardman, P. (1989). The reduction potentials of one-electron couples involving free radicals in aqueous solution. *J. Phys. Chem. Ref. Data*, *18*, 1637-1753.

[54]. Marsalek, E., Elles, C.G., Pieniazek, P.A., Pluharova, E., VandeVondele, J., Bradforth, S.E., & Jungwirth, P. (2011). Chasing charge localization and chemical reactivity following photoionization in liquid water. *J. Chem. Phys.*, *135*, 1-14.

[55]. Janata, E., & Schuler, R.H. (1982). Rate constant for scavenging e^-_{aq} in N_2O-saturated solutions. *J. Phys. Chem.*, *86*, 2078-2084.

[56]. Wojnárovits, L., Takacs, E., Dajka, K., Emmi, S.S., Russo, M., & D'Angelantonio, M. (2004). Re-evaluation of the rate coefficient for the H atom reaction with *tert*-butanol in aqueous solution. *Radiat. Phys. Chem.*, *69*, 217-219.

[57]. Bielski, B.H.J., Cabelli, D.E., Arudi, R.L., & Ross, A.B. (1985). Reactivity of $HO_2/O_2^{\bullet-}$ radicals in aqueous solution. *J. Phys. Chem. Ref. Data*, *14*, 1041-1100.

[58]. Gall, B.L., & Dorfman, L.M. (1969). Pulse radiolysis studies. XV. Reactivity of the oxide radical ion and of the ozonide ion in aqueous solution. *J. Am. Chem. Soc.*, *91*, 2199-2204.

[59]. Kläning, U.K., Sehested, K., & Holcman, J. (1989). Standard Gibbs energy of formation of the hydroxyl radical in aqueous solution. Rate constants for the reaction $ClO_2^{•-} + O_3 \rightarrow O_3^{•-} + ClO_2$. *J. Phys Chem.*, *89*, 760-763.

[60]. Holcman, J., Sehested, K., Bjergbakke, E., & Hart, E.J. (1982). Formation of ozone in the reaction between the ozonide radical ion, $O_3^{•-}$, and the carbonate radical ion, $CO_3^{•-}$, in aqueous alkaline solutions. *J. Phys. Chem.*, *86*, 2069-2072.

[61]. De Vleeschouver, F., Van Speybroeck, V., Waroquier, M., Geerlings, P., & De Proft, F. (2007). Electrophilicity and nucleophicility index for radicals. *Org. Lett.*, *9*, 2721-2724.

[62]. Asmus, K.-D., Möckel, H., & Henglein, A. (1973). Pulse radiolytic study of the site of •OH radical attack on aliphatic aalcohols in aqueous solution. *J. Phys. Chem.*, *77*, 1218-1221.

[63]. Veltwisch, D., Janata, E., & Asmus, K.-D. (1980). Primary processes in the reaction of •OH-radicals with sulphoxides. *J.C.S. Perkin II*, 146-153.

[64]. Rao, B.S.M. (2010). Radiation-induced oxidation of substituted benzenes: Structure-reactivity relationship. In J.F. Wishart & B.S.M. Rao (Eds.), *Recent trends in radiation chemistry* (pp. 385-410). Singapore: World Scientific.

[65]. Asmus, K.-D. (2001). Heteroatom-centered free radicals. Some selected contributions by radiation chemistry. In C. Jonah & B.S.M. Rao (Eds.), *Radiation chemistry: Present status and future prospects* (pp. 341-393). Amsterdam: Elsevier Science.

[66]. Asmus, K.-D., Hug, G.L., Bobrowski, K., Mulazzani, Q.G., & Marciniak, B. (2006). Transients in the oxidative and H-atom-induced degradation of 1,3.5-trithiane. Time-resolved studies in aqueous solution. *J. Phys. Chem. A*, *110*, 9292-9300.

[67]. Wisniowski, P.B., Bobrowski, K., Carmichael, I., & Hug, G.L. (2004). Bimolecular homolytic substitution (S_H2) reaction with hydrogen atoms. Time resolved ESR detection in the pulse radiolysis of α-(methylthio)acetamide). *J. Am. Chem. Soc.*, *126*, 14668-14677.

[68]. Davies, M.J., & Dean, R.T. (1997). *Radical-mediated protein oxidation. From chemistry to medicine*. Oxford, New York: Oxford University Press. (Oxford Science Publications).

[69]. Douki, T., & Cadet, J. (2008). Radiation-induced damage to DNA: From model compounds to cell. In M. Spotheim-Maurizot, M. Mostafavi, T. Douki & J. Belloni (Eds.), *Radiation chemistry: From basics to applications in material and life sciences* (pp. 177-189). Bonchamp-Les Laval: EDP Sciences.

[70]. Bobrowski, K., Houée-Levin, C., & Marciniak, B. (2008). Stabilization and reactions of sulfur radical cations: Relevance to one-electron oxidation of methionine in peptides and proteins. *Chimia*, *62*, 728-734.

[71]. Bobrowski, K. (2011). Radiation-induced radicals and radical ions in amino acids and peptides. In D.V. Staas & V.I. Feldman (Eds.), *Selectivity, control, and fine tuning in high energy chemistry* (pp. 41-67). Trivandrum, Kerala, India: Research Signpost.

[72].   Houée-Levin, C. (2011). One-electron redox processes in proteins. In D.V. Staas & V.I. Feldman (Eds.), *Selectivity, control, and fine tuning in high energy chemistry* (pp. 69-91). Trivandrum, Kerala, India: Research Signpost.

[73].   Houée-Levin, C., & Bobrowski, K. (2008). Pulse radiolysis studies of free radical processes in peptides and proteins. In M. Spotheim-Maurizot, M. Mostafavi, T. Douki & J. Belloni (Eds.), *Radiation chemistry: From basics to applications in material and life sciences* (pp. 233-247). Bonchamp-Les Laval: EDP Sciences.

[74].   Cabelli, D.E. (1997). The reactions of $HO_2^\bullet$ and $O_2^{\bullet-}$ radicals in aqueous solution. In Z.B. Alfassi (Ed.), *Peroxyl radicals* (pp. 407-437). New York: John Wiley & Sons.

[75].   Pecht, I., & Farver, O. (1998). Pulse radiolysis: A tool for investigating long-range electron transfer in proteins. In J.F. Wishart & D.G. Nocera (Eds.), *Photochemistry and radiation chemistry: Complementary methods for the study of electron transfer* (pp. 65-79). Washington, DC: American Chemical Society.

[76].   Bobrowski, K. (1999). Electron migration in peptides and proteins. In J. Mayer (Ed.), *Properties and reactions of radiation induced transients. Selected topics* (pp. 174-204). Warszawa: Polish Scientific Publishers PWN.

[77].   Houée-Levin, C., & Bobrowski, K. (2013). The use of methods of radiolysis to explore the mechanisms of free radical modifications in proteins. *J. Proteomics*, *92*, 51-62.

[78].   Bobrowski, K., Holcman, J., Poznanski, J., & Wierzchowski, K.L. (1997). Pulse radiolysis of intramolecular electron transfer in model peptides and proteins. 7. $Trp^\bullet \rightarrow TyrO^\bullet$ radical transformation in hen-egg white lysozyme. Effects of pH, temperature, Trp62 oxidation and inhibitor binding. *Biophys. Chem.*, *63*, 153-166.

[79].   Bobrowski, K., Poznanski, J., Holcman, J., & Wierzchowski, K.L. (1998). Long range electron transfer between proline-bridged aromatic amino acids. In J.F. Wishart & D.G. Nocera (Eds.), *Photochemistry and radiation chemistry: Complementary methods for the study of electron transfer* (pp. 131-143). Washington, DC: American Chemical Society.

[80].   Bobrowski, K., Wierzchowski, K.L., Holcman, J., & Ciurak, M. (1992). Pulse radiolysis, of intramolecular electron transfer in model peptides. IV. $Met/S \therefore Br \rightarrow Tyr/O^\bullet$ radical transformation in aqueous solution of $H\text{-}Tyr\text{-}(Pro)_n\text{-}Met\text{-}OH$ peptides. *Int. J. Radiat. Biol.*, *62*, 507-516.

[81].   von Sonntag, C., & Schuchmann, H.-P. (1997). Peroxyl radicals in aqueous solutions. In Z.B. Alfassi (Ed.), *Peroxyl radicals* (pp. 173-234). Chichester: John Wiley & Sons Ltd.

[82].   Schuchmann, H.-P., & von Sonntag, C. (1997). Heteroatom peroxyl radicals. In Z.B. Alfassi (Ed.), *Peroxyl radicals* (pp. 439-455). Chichester: John Wiley & Sons Ltd.

[83].   von Sonntag, C., & Schuchmann, H.-P. (1991). The elucidation of peroxyl radical reactions in aqueous solution with the help of radiation-chemical techniques. *Angew. Chem. Int. Ed.*, *30*, 1229-1253.

[84].   von Sonntag, C. (2006). Peroxyl radicals. In *Free-radical-induced DNA damage and its repair* (pp. 159-194). Berlin, Heidelberg: Springer.

[85]. Neta, P., Huie, R.E., & Ross, A.B. (1990). Rate constants for reactions of per-oxyl radicals in fluid solutions. *J. Phys. Chem. Ref. Data*, *19*, 431-513.

[86]. Alfassi, Z.B., & Neta, P. (1997). Kinetic studies of organic peroxyl radicals in aqueous solutions and mixed solvents. In Z.B. Alfassi (Ed.), *Peroxyl radicals* (pp. 235-281). Chichester: John Wiley & Sons Ltd.

[87]. Zhang, X., Zgang, N., Schuchmann, H.-P., & von Sonntag, C. (1994). Pulse radiolysis of 2-mercaptoethanol in oxygenated aqueous solution. Generation and reactions of the thiylperoxyl radical. *J. Phys. Chem.*, *98*, 6541-6547.

[88]. Tamba, M., Torregiani, A., & Tubertini, O. (1995). Thiyl- and thiyl-peroxyl radicals produced from the irradiation of antioxidant thiol compounds. *Radiat. Phys. Chem.*, *46*, 569-574.

[89]. Yamashita, S., Taguchi, M., Baldacchino, G., & Katsumura, Y. (2011). Radiation chemistry of liquid water with heavy ions: Steady-state and pulse radiolysis studies. In Y. Hatano, Y. Katsumura & A. Mozumder (Eds.), *Charged particle and photon interactions with matter: Recent advances, applications and inter-faces* (pp. 325-354). Boca Raton: CRC Press.

[90]. Baldacchino, G., & Katsumura, Y. (2010). Chemical processes in heavy ion track. In J.F. Wishart & B.S.M. Rao (Eds.), *Recent trends in radiation chem-istry* (pp. 231-253). New Jersey: World Scientific.

[91]. Yamashita, S., Katsumura, Y., Lin, M., Muroya, Y., Miyazakia, T., & Muraka-mi, T. (2008). Water radiolysis with heavy ions of energies up to 28 GeV. 1. Measurements of primary g values as track segment yields. *Radiat. Phys. Chem.*, *77*, 439-446.

[92]. Yamashita, S., Katsumura, Y., Lin, M., Muroya, Y., Maeyama, T., & Murakami, T. (2008). Water radiolysis with heavy ions of energies up to 28 GeV. 2. Ex-tension of primary yield measurements to very high LET values. *Radiat. Phys. Chem.*, *77*, 1224-1229.

[93]. Yamashita, S., Katsumura, Y., & Lin, M. (2008). Water radiolysis with heavy ions of energies up to 28 GeV. 3. Measurement of G(MV$^{\bullet+}$) in deaerated methyl viologen solutions containing various concentration of sodium formate and Monte Carlo simulation. *Radiat. Res*., *170*, 521-533.

[94]. Swallow, A.J. (1987). Radiation chemistry of the liquid state: (2) Organic liquids. In Farhataziz & M.A.J. Rodgers (Eds.), *Radiation chemistry. Principles and applications* (pp. 351-375). New York: VCH Publishers, Inc.

[95]. Allen, A.O. (1976). Y*ields of free ions formed in liquids by radiation*. Gaithers-burg: National Bureau of Standards.

[96]. Baxendale, J.H., & Wardman, P. (1975). *The radiolysis of methanol: product yields, rate constants, and spectroscopic parameters of intermediates*. Gaithers-burg: National Bureau of Standards.

[97]. Freeman, G.R. (1974). *Radiation chemistry of ethanol: A review of data on yields, reaction rate parameters, and spectral properties of transients*. Gaithers-burg: National Bureau of Standards.

[98]. Freeman, G.R. (1982). Labile species and fast processes in liquid alcohol ra-diolysis. In J.H. Baxendale & F. Busi (Eds), *The study of fast processes and transient species by electron pulse radiolysis* (pp. 399-416). Dordrecht: Reidel Publishing Company.

[99].   Dorfman, L.M. (1970). Electron and proton transfer reactions of aromatic molecule ions in solution. *Acc. Chem. Res*., *3*, 224-230.

[100]. Land, E.J., Lafferty, J., Sinclair, R.S., & Truscott, T.G. (1978). Absorption spectra of radical ions of polyenones of biological interest. *J. Chem. Soc. Faraday Trans. 1*, *74*, 538-545.

[101]. Bobrowski, K., & Das, P.K. (1987). Transient phenomena in the pulse radiolysis of retinyl polyenes. 6. Radical ions of retinal homologues. *J. Phys. Chem.*, *91*, 1210-1215.

[102]. Bobrowski, K., & Das, P.K. (1982). Transient phenomena in the pulse radiolysis of retinyl polyenes. 2. Protonation kinetics. *J. Am. Chem. Soc.*, *104*, 1704-1709.

[103]. Guldi, D.M., Hungerbuhler, H., & Asmus, K.D. (1993). Pulse radiolytic redox and alkylation studies on C_{60}. In H. Kuzmany, J. Fink, M. Mehring & S. Roth (Eds.), *Electronic properties of fullerenes* (pp. 64-68). Berlin, Heidelberg: Springer-Verlag.

[104]. Baptista, J.L., & Burrows, H.D. (1974). Solute ion and radical formation in the pulse radiolysis of acetonitrile solutions. *J. Chem. Soc., Faraday Trans. 1*, *70*, 2066-2079.

[105]. Bell, I.P., Rodgers, M.A.J., & Burrows, H.D. (1977). Kinetic and thermody-namic character of reducing species produced on pulse radiolysis of acetonitrile. *J. Chem. Soc., Faraday Trans. 1*, *73*, 315-326.

[106]. De la Fuente, J.R., Kciuk, G., Sobarzo-Sanchez, E., & Bobrowski, K. (2008). Transient phenomena in the pulse radiolysis of oxoisoaporphine derivatives in acetonitrile solutions. *J. Phys. Chem. A*, *112*, 10168-10177.

[107]. Hayon, E. (1970). Yield of ions and excited states produced in the radiolysis of polar organic liquids. *J. Chem. Phys.*, *53*, 2353-2358.

[108]. Rodgers, M.A.J. (1972). Nanosecond pulse radiolysis of acetone. *J. Chem. Soc., Faraday Trans. 1*, *68*, 1278-1286.

[109]. Rodgers, M.A.J. (1971). Pulse radiolysis studies of acetone solutions. *J. Chem. Soc., Faraday Trans. 1*, *67*, 1029-1040.

[110]. Lomoth, R., Naumov, S., & Brede, O. (1999). Genuine pyrimidine radical cations generated by radiation-induced electron transfer to butyl chloride or acetone parent ions. *J. Phys. Chem. A*, *103*, 2641-2648.

[111]. Wang, Y., Tria, J.J., & Dorfman, L.M. (1979). Identity and yield of positive charge centers in irradiated chloro-hydrocarbon liquids and the rates of their interaction with solute molecules. *J. Phys. Chem.*, *83*, 1946-1951.

[112]. Guldi, D.M., Liu, D., & Kamat, P.V. (1997). Excted states and reduced and oxidized forms of C_{76} (D_2) and C_{78} (C_{2v}'). *J. Phys. Chem. A*, *101*, 6195-6201.

[113]. Bobrowski, K., & Das, P.K. (1985). Transient phenomena in the pulse radiolysis of retinyl polyenes. 4. Environmental effects on absorption maximum of retinal radical anions. *J. Phys. Chem.*, *89*, 5733-5738.

[114]. Inman, D., & Lovering, D.G. (1981). *Ionic liquids*. New York: Plenum Press.

[115]. Shkrob, I.A., Marin, T.W., Bell, J.R., Luo, H., Dai, S., Hatcher, J.L., Rimmer, R.D., & Wishart, J.F. (2012). Radiation-induced fragmentation of diamide extraction agents in ionic liquid diluents. *J. Phys. Chem. B*, *116*, 2234-2243.

[116]. Takahashi, K., & Wishart, J.F. (2010). Radiation chemistry and photochemistry of ionic liquids. In Y. Hatano, Y. Katsumura & A. Mozumder (Eds.), *Charged*

particle and photon interactions with matter: Recent advances, applications, and interfaces (pp. 265-287). Boca Raton: CRC Press.

[117]. Wishart, J.F., Funston, A.M., & Szreder, T. (2006). Radiation chemistry of ionic liquids. In R.A. Mantz, P.C. Trulove, H.C. DeLong, G.R. Stafford, R. Hagiwara & D.A. Costa (Eds.), *Molten salts XIV* (pp. 802-813). Pennington: The Electrochemical Society.

[118]. Behar, D., Gonzalez, C., & Neta, P. (2001). Reaction kinetics in ionic liquids: Pulse radiolysis studies of 1-butyl-3-methylimidazolium salts. *J. Phys. Chem. A*, *105*, 7607-7614.

[119]. Michalski, R., Sikora, A., Adamus, J., & Marcinek, A. (2010). Mechanistic aspects of radiation-induced oligomerization of 3,4-ethylene-dioxythiophene in ionic liquids. *J. Phys. Chem. A*, *114*, 11552-11559.

[120]. Michalski, R., Sikora, A., Adamus, J., & Marcinek, A. (2010). Dihalide and pseudohalide radical anions as oxidizing agents in nonaqueous solvents. *J. Phys. Chem. A*, *114*, 861-866.

RADIATION CHEMISTRY
OF ORGANIC SOLIDS

Cornelia Vasile, Elena Butnaru
"Petru Poni" Institute of Macromolecular Chemistry, Romanian Academy,
41A Grigore Ghica Voda Alley, 700487 Iasi, Romania

1. INTRODUCTION

Radiation chemistry deals with chemical reactions produced by interactions of ionizing radiation with materials. The effects of radiation on matter depend on the type of the radiation and its energy level, as well as on the composition, physical state, temperature and the atmospheric environment of the absorbing material. The type and yield of the final products produced by exposure of an organic compound to ionizing radiation are often dependent on its physical state (gas, liquid or solid) and its molecular structure [1]. The effects of radiation on organic solids (polymers, lignocellulosic materials, *etc.*) are an area of increasing interest. Ionizing radiation can modify the physical, chemical, and biological properties of polymers; the changes occurring when polymer materials are in a solid state are different, as compared to chemical or thermal reactions carried out in melted polymers. After the interaction of ionizing radiation (gamma rays, X-rays, accelerated electrons, ion beams) with macromolecules, very reactive intermediates (primary entities, radicals and ions) are formed. These intermediates can follow several different reaction paths, that result in the formation of oxidized products, grafts, scissioning of main chains (degradation) or crosslinking. The type and degree of these transformations depend on the structure of the material (*e.g.* polymer) and the treatment applied before, during and after irradiation [2].

2. PRIMARY AND SECONDARY EFFECTS

Ionizing radiations can be classified in three categories:
- charged particles: electrons (e^-), positrons (e^+), and heavy ions;
- photons: gamma (γ), X-rays and light;
- neutrons (n).

   The term "ionizing radiation" in a wider sense also applies to photons or particles having sufficient energy to ionize a molecule of a material. This involves photons with energies ranging from the first ionization energy of the material (~10 eV) up to several million eV (MeV), as well as energetic charged particles, such as electrons, positrons, accelerated heavy ions, *etc*. The result of such energy absorption is the breaking or rearrangement of chemical bonds, *i.e.* decomposition of some of the initial material.

   Radiation principles explain how the gamma rays, electron beams (EB) and X-rays interact with matter. Independently from the type of radiation (electromagnetic or particle) most of the radiation effects are produced by secondary electrons. According to calculations by Bethe with primary electrons of $10^{3\text{-}15}$ eV more than 80% of the absorbed energy is transferred to secondary electrons.

   These interactions result in the formation of energetic electrons which are random throughout the materials and which cause the formation of energetic molecular ions. These ions may be subject to electron capture and dissociation, as well as to rapid rearrangement through ion-molecule reactions, or they may dissociate with time depending on the complexity of the molecular ion. The chemical changes in matter can occur *via* primary radiolysis effects, which occur as a result of the adsorption of the energy by the absorbing matter, or *via* secondary effects, which occur as a result of the high reactivity of the free radicals or electrons and the excited ions or molecules produced as a result of the primary effects. These highly reactive intermediates can undergo a variety of reactions leading to stable chemical products. In general, these chemical products can be detected and are referred to as radiolysis products. Understanding gamma-ray interaction with matter is important from the perspective of shielding against their effects on biological matter. These chemical changes can ultimately have biological consequences in the case where the target materials include living organisms.

   The main types of interactions of gamma and X-radiation with substances are the photoeffect both in its photoelectric and photonuclear forms, Compton effect and scattering and generation and/or annihilation (elastic collisions) of the pairs (electron positron pair production). To a minor extent, photofission, Rayleigh scattering and Thompson scattering also occur [3]. The photoelectric effect can displace atomic electrons, whereas the photonuclear reaction would displace elementary particles from the nucleus.

Gamma absorption by an atom
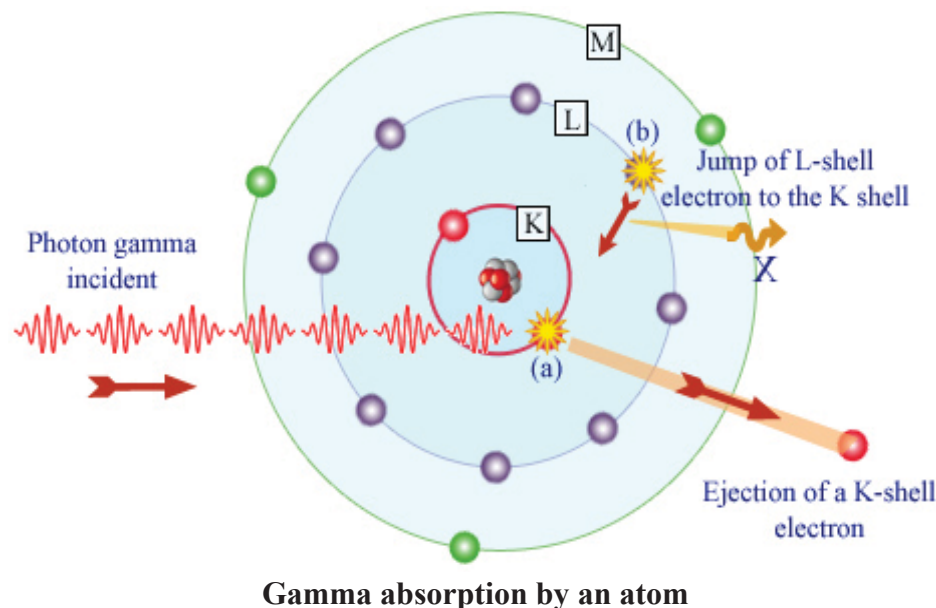
Fig.1. Schematic representation of photoelectric effect.

Photoelectric effect is the most effective mechanism of photon absorption, as shown in Fig.1.

The photoelectric effect occurs in two stages. First, a photon (a) removes a bound electron in one atom. In the case of gamma photons, it is usually an electron belonging to the innermost atomic shells, L or K (as shown in Fig.1). Then the atom that has lost one of its inner electrons is left in an excited state. An electron from an outer layer ((b) in Fig.1) moves to occupy the vacancy left by the ejected electron. If the ejected electron belonged to the K shell, an X-ray is emitted during this transition which is accompanied by the emission of a characteristic soft electromagnetic radiation in the X-ray, ultraviolet (UV) or visible region of the electromagnetic spectrum.

The photoelectric effect is the phenomenon that transforms light, infrared and ultraviolet rays into electricity in solar panels and photodiodes of cameras. It is also involved in the completely different field of radioprotection by transforming penetrating X- and gamma rays into electrons easy to stop and thus protects humans from the effects of these radiations.

The photoelectric process is always accompanied by a secondary emission since the atom cannot remain in an excited state indefinitely, thus:

• The atom emits X-rays and returns to the ground state.
• Auger electrons are emitted from the outer electronic shells carrying out the excitation energy. The secondary radiation is also later absorbed and occurs in scintillators used in gamma radiation detection.

The photoelectric effect is the most effective physical phenomenon in mitigating these radiations. The gamma-ray or X-ray photon absorbed by interact-

ing with a bound electron to form an atom radical (•) disappears. The photon simply vanishes. If the energy of the photon is greater than 0.339 MeV, an electron may be ejected from the atom producing an ion pair. The ejected electron will then produce secondary ionization events in its surrounding atoms in a similar manner to beta particles (electrons or positrons). The photoelectric effect has a high probability of occurring with lower energy photons and atoms having high atomic numbers. The shell structure of atoms plays a crucial role. The photon removes an electron only if its energy exceeds the binding energy of the electron on its shell. The probability (called cross section) of removing an electron from a shell becomes different from zero beyond this threshold. Where there is a certain small probability of a photoelectric effect type phenomenon, gamma rays tend to interact more with not only deeper, core-level energy states, but also with the nucleus of the material. In this case, a number of different phenomena go on such as nuclear excitation, different types of scattering, *etc*. [4]. Photonuclear reactions can be used to produce neutron sources which can be used in a variety of applications such as nuclear medicine and radiography.

In the Compton effect, the photon undergoes a collision with an atom thus being deviated from its trajectory and releasing part of its energy. This energy is usually enough to abstract an electron from the atom. Compton scattering is the inelastic scattering of a photon by a charged particle, usually an electron. It results in a decrease in energy (increase in wavelength) of the photon (which may be an X-ray or gamma-ray photon). This is called the Compton effect. The electrons in matter are neither free nor at rest. However, in some cases, one can approximate the state of an electron in a simple model as free and at rest. In this case a gamma rays can interact with a loosely bound electron by being scattered with an appropriate loss in energy, as illustrated in Fig.2.

The scattering of photons from charged particles is called Compton scattering after Arthur Compton, who was the first to measure photon-electron
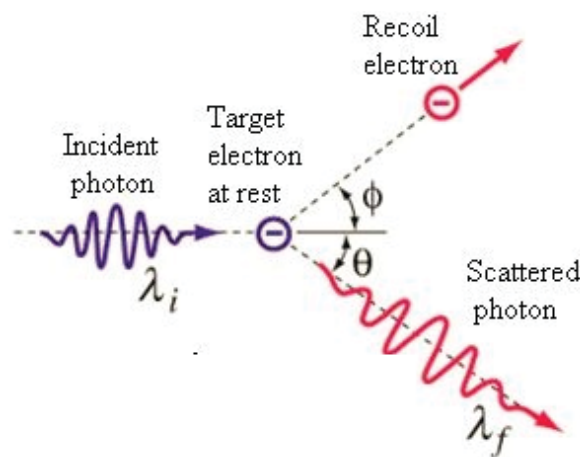
Fig.2. Compton scattering.

scattering in 1922. When the incoming photon gives part of its energy to an electron, then the scattered photon has lower energy and according to the Planck relationship has a lower frequency and longer wavelength. The wavelength change in such scattering depends only upon the scattering angle for a given target particle. The constant in the Compton formula (Eq. (1)) can be written as in Eq. (2) and is called the Compton wavelength for the electron:

$$\lambda_f - \lambda_i = \Delta\lambda = \frac{h}{m_o c}(1 - \cos\theta) \tag{1}$$

$$\frac{h}{m_e c} = \frac{hc}{m_e c^2} = \frac{1240 \text{ eV}\cdot\text{nm}}{0.511 \text{ MeV}} = 0.00243 \text{ nm} \left(2.43\times10^{-12} \text{ m}\right) \tag{2}$$

where: λ_i – the initial wavelength, λ_f – the wavelength after scattering, h – the Planck constant, m_o – the electron rest mass, c – the speed of light, and θ – the scattering angle.

Part of the energy of the photon is transferred to the recoiling electron. Inverse Compton scattering also exists, in which a charged particle transfers part of its energy to a photon. Compton scattering is of prime importance in radiobiology, as it is the most probable interaction of gamma rays and high energy X-rays with atoms in living cells and is applied in radiation therapy. In material physics, Compton scattering can be used to probe the wave function of the electrons in matter. The primary effect of the Compton interaction is ionization.

3. CHEMICAL EFFECTS OF RADIATIONS

The primary effect of high energy radiation is ionization and, to a minor extent, excitation of molecules and atoms. The radiation gradually releases its energy through the material giving rise to a track of reactive species (ions, excited molecules, radicals, electrons) whose reactions are responsible for the irreversible chemical transformations of the matter (radiolysis). Primary ionization generates electrons, whose energy is large enough to give rise to further ionizations and excitations. Thus, secondary electrons are responsible for a major part of radiation chemical effects. This explains the substantial analogy of the effects stemming from the different type of radiations either electromagnetic (gamma rays, X-rays) or charged particles (electrons, alpha, protons, deuterons, *etc*.). The probability that electrons with energy < 10 MeV and gamma radiations of 0.5-1 MeV (Compton effect) will interact with atoms and molecules is proportional to the electron density of the material and it is therefore relatively unselective and largely independent of chemical structures. A general radiolysis mechanism for a condensed phase is illustrated in Fig.3.
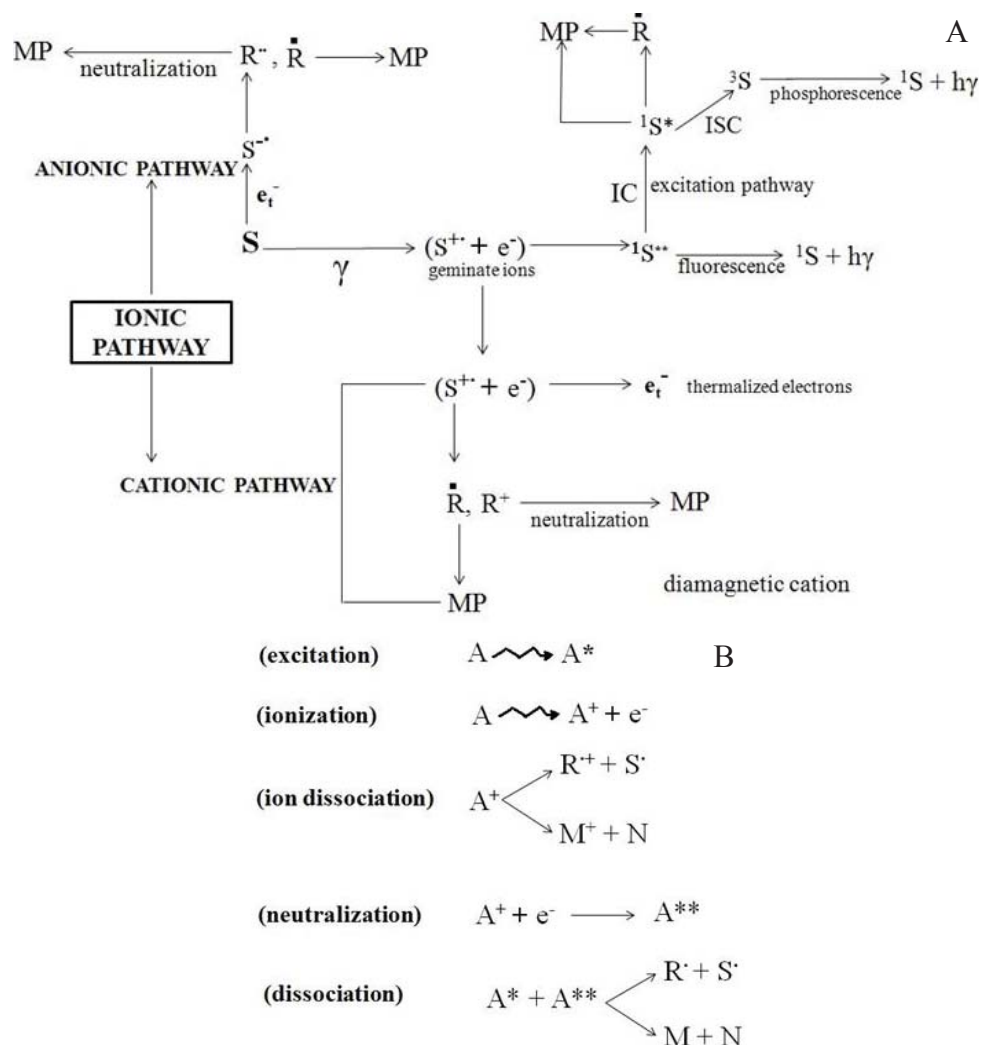
Fig.3. General radiolysis scheme (A) and primary processes in the radiolysis of organic compounds (B): $R^\bullet$ and $S^\bullet$ – free radicals; $S^{\bullet+}$ and $S^{\bullet-}$ – cation or anion radicals, respectively; ISC – intersystem crossing; IC – internal conversion; R^+ and R^- – diamagnetic cation or anion, respectively; MP, M and N – molecular products.

This consists of excitation radiolysis and ionic radiolysis pathways depending on the type of active species generated. The free radicals are the most important intermediates in all radiolysis processes. The excited species in condensed systems can undergo: (i) fast internal conversion (10^{-13} s) to the lowest excited levels with degradation to thermal energy of most of the electronic excitation energy, (ii) chemical reactions, (iii) return to the fundamental state of the same multiplicity with emission of radiation, (iv) fluorescence or (v) return to the fundamental state after intersystem crossing (ISC) with emission of phosphorescence radiation. The primary processes in the radiolysis of or-

ganic compounds can, in most cases, be represented by excitation, ionization, ion dissociation, neutralization and dissociation, as shown in Fig.3B.

Macromolecules are very sensitive to minute chemical changes at the appropiate places which have great influence on the morphology. A single bond altered may convert a free flowing polymer from a fluid to an elastic solid. An even smaller change may be lethal in biological systems.

The primary interactions of ionizing radiation with polymers include ionization, stabilization of electrons through generation of hot electrons, ion neutralization and free radicals formation. Free radicals are created either through chain scission or through the dissociation of the side chain (C–H(Cl)) bonds, as shown in Fig.4.

Ionization: $P \rightsquigarrow P^+ + e^-$

Excitation: $P \rightsquigarrow P^*$

Thermal stabilization of electron: $e \rightarrow e^-_{th}$

Neutralization: $P^+ + e^-_{th} \rightarrow P^*$

Free radicals formation: $P^* \rightarrow R_1^\bullet + R_2^\bullet$

Disproportionation: $\rightarrow R^\bullet + H^\bullet$
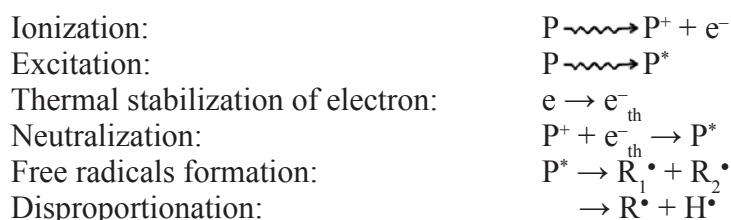
Fig.4. Primary processes occurring in polymer irradiation (P – polymer, R• – radical).

The irradiation of polymers, natural or synthetic, with ionizing radiation leads to the formation of reactive intermediates, free radicals, ions and atoms and molecules in excited states. These intermediates can undergo several reactions such as hydrogen abstraction, rearrangements and formation of new bonds, addition to the double bonds, chain scission, oxidation and grafting recombination (crosslinking and branching, to an extent which depends upon the polymer

Hydrogen abstraction: $R^\bullet + P \rightarrow RH + P^\bullet$

Addition to the double bonds: $RCH{=}CH_2 + H^\bullet \rightarrow RCH_2CH_2^\bullet$

Recombination
(branching or/and crosslinking): $R_m^\bullet + R_n^\bullet \rightarrow P_{m+n}$ or/and

and

Chain scission: $R_m^\bullet \rightarrow R_{m+n}^\bullet + R_n^\bullet$

Oxidation: $R^\bullet + O_2 \rightarrow ROO^\bullet$

$ROO^\bullet \rightarrow ROOH, -C{=}O, -OH, -COOH$

Grafting: $R^\bullet + M \rightarrow RM^\bullet$

$R^\bullet + nM \rightarrow RM_n^\bullet$
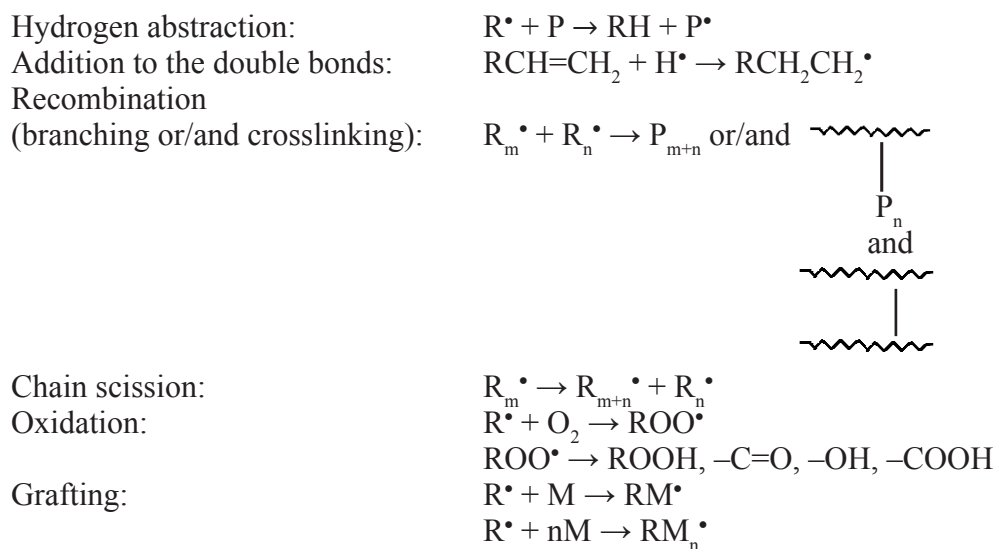
Fig.5. Secondary reactions in polymers occurring under irradiation (M – monomer).

structure), as shown in Fig.5. As a result both low molecular weight species and crosslinking occur with changes in molecular weight (decrease or increase, correspondingly). Both reactions can occur simultaneously, one of them being dominant depending on polymer structure, the presence of additives, the radiation dose and environmental conditions. Crosslinking dominates under vacuum, while chain scission may be a main reaction in presence of oxygen or air. As a consequence, radiolytic products from both a polymer and its additives are formed. As a rule, under the radiation effect on solid substances, the spatial distribution of radicals is non-uniform [5]. Sometimes it may present closely located radical pairs and/or agglomerations. Trapped radicals increase with irradiation dose.

The fundamental processes related to these reactions include:
- crosslinking – polymer chains are joined and a network is formed;
- chain scission – the molecular weight of the polymer is reduced through chain scission;
- oxidation – where the polymer molecules react with oxygen *via* peroxide radicals (oxidation and chain scission often occur simultaneously);
- long-chain branching – polymer chains are joined but a three-dimensional network is not yet formed;
- grafting – a new monomer is added onto the base polymer chain;
- polymerization – can also be initiated when monomers are irradiated;
- radiation curing (as in the case of coatings or composites) is a combination of polymerization and crosslinking.

Different polymers have different responses to radiation, especially crosslinking *vs.* chain scissioning. The same polymer such as poly(tetrafluoro-ethylene) can degrade by chain scission when $T < T_m$ (melting temperature of 315°C) or it crosslinks when $T > T_m$. Frequently different reactions occur simultaneously with predominance of some of them.

4. RADIATION YIELD

To quantify the radiation chemical effects of ionizing radiation, the number of molecules transformed or produced when a certain the quantity of radiation energy is absorbed should be known. The G(X) value is a measure of the radiation-chemical yield. It was originally defined as the number of molecules n(X), produced, destroyed or changed by radiation (consumed) to the irradiated matter by the mean energy imparted, E, usually of 100 eV of absorbed energy, as in Eq. (3):

$$G(X) = \frac{n(X)}{E} \tag{3}$$

Hence, the unit of the G-value of the International System of Units (SI) is mol/J. In the earlier literature the G-values were always given in units molecules/100 eV, but the new SI units will be used. (1 molecule/100 eV corresponds to 1.036×10^{-7} mol/J).

Table 1. G-values for crosslinking and chain scission for some common polymers.

Polymer	Crosslinking G(X)	Scission G(S)	G(S):G(X)
Low-density polyethylene	1.42	0.48	0.34
High-density polyethylene	0.96	0.19	0.20
Isotactic polypropylene	0.16-0.26	0.29-0.31	1.1-1.5
Atactic polypropylene	0.4-0.5	0.3-0.6	0.7-0.9
Poly(methyl methacrylate)	< 0.50	1.1-1.7	> 2
Poly(tetrafluoroethylene)	0.1-0.3	3.0-5.0	10
Natural rubber	1.3-3.5	0.1-0.2	0.14
Nylon-6	0.35-0.7	0.7	1.0
Nylon-6,6	0.5-0.9	0.7-2.4	1.4
Poly(vinyl acetate)	0.1-0.3	0.06	0.2
Poly(vinylidene fluoride)	0.6-1.00	0.30-0.6	0.3
Poly(methyl acrylate)	0.45-0.52	0.08	0.15
Polystyrene	0.019-0.051	0.0094-0.019	0.4
Polybutadiene	5.3	0.53	0.10
Polyisobutylene	0.05-0.5	5	> 10
Butyl rubber	< 0.5	2.9-3.7	> 6

In Table 1 lists the G-values for crosslinking, G(X), and chain scissioning, G(S), for some of the common polymeric materials irradiated at room temperature without oxygen. Materials with G(X) larger than G(S), the overall result is crosslinking, and whenever G(S) is larger than G(X), the overall result is degradation. Materials whose G(X) and G(S) values are both low are more resistant toward radiation.

Radiation effects are remarkably sensitive to molecular structure. G(S) and G(X) values vary from 0.1 to 10, as shown in Table 1. The ratio between them determines the changes in average molecular weight of polymers, as illustrated in Fig.6.

The G(X) of polyethylene (PE) is about one order of magnitude larger than that of polystyrene (PS) which demonstrates that aromatic rings exert a protective radiation effect.
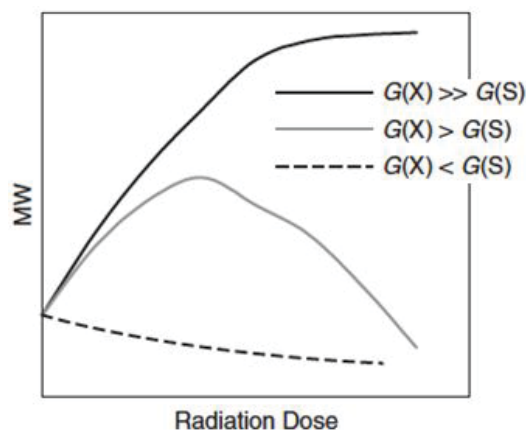
Fig.6. Relation between average molecular weight of polymers, G(X) and G(S) and radiation dose.

G(X) and G(S) also depend on irradiation conditions, such as temperature and atmosphere.

5. RADIOLYSIS PRODUCTS

Polymers used in medical devices and in primary packaging materials have been studied with respect to radiolysis products. Orthopedic implants and other medical devices that come into close contact with the human body are sterilized by either gas or high energy radiation. They are not free from the effect of ionizing radiation particularly if the process is performed in air. Food irradiation, sterilization of packaging materials for pharmaceutical or food products with ionizing irradiation can cause not only chemical and physical changes in polymer materials but also formation of some radiolysis products which can be solvent extractable or detectable by other techniques such as gas chromatography/mass spectroscopy (GC/MS), electron paramagnetic resonance (EPR), spectroscopic methods, in surrounding media [6]. Some examples are given in Table 2. The products and their concentrations are characteristic for each polymeric material. The polyolefin materials (polyethylene, PE, and polypropylene, PP) show an increase in low volatile compounds after irradiation due to an oxidative decomposition of the polymer and of additives. PE produces only traces of hydrocarbons, aldehydes, ketones, and carboxylic acids, which largely disappear within weeks. Other packaging materials, such as poly(ethylene terephthalate) (PET), polyamide (PA), and polystyrene (PS), did not significantly change their amount of solvent extractable compounds after irradiation with 25 to 44 kGy. PA-6 (nylon-6) yields pentanamide as the main

Table 2. Radiolysis products of polymers.

Name	Abbreviation	Radiolysis products	Observation	Ref.
Polyethylene	PE	Peroxy radicals on surface; chain scission, hydroperoxides, carbonyl mostly ketones, carboxylic acids, hydrocarbons (butane to nonane), acetic acid, 2-pentanone, pentanal, octane, propionic acid, 2-hexanone or 3-hexanone, hexanal, and heptanal, butanoic acid, 2-heptanone or 3-heptanone, alkyl benzenes	Gamma irradiation in air – 22 kGy	[7]
Polypropylene	PP	Hydrogen, hydroperoxides, ketones, aldehydes, alcohols and carboxylic acids. The ketones are very important in PP, but the carboxylic acids are the major products	Electron beam irradiation – 5, 10, 25 kGy	[8]
Poly(vinyl chloride)	PVC	2-ethyl-1-hexanol (100-1000 ppm), octane, 1-octene, 2-octene, 4-octene, acetic acid, 2-ethylhexyl ester; 1-octanol, heptane, 3-methylheptane, 3-heptanone, 2-ethylcyclohexanal, 4-octanone, undecane, pentylcyclopropane, 2-ethylhexanoic acid	Two months after irradiation with 22.5 kGy. Compounds results not only from polymers but also from additives	[7]
Poly(vinyl alcohol)	PVAL	Unsaturated bonds and carbonyl groups occur under irradiation; organic acids, alcohols	Gamma radiation at room temperature – 10 kGy	[9]
Poly(vinyl acetate)	PVA	Acetic acid, CO_2, CO, CH_4, H_2	Gamma radiation at room temperature under vacuum	[10]
Ethylene-vinyl acetate copolymers	EVA	102 radiolysis compounds, unsaturated hydrocarbons, ketones, methyl derivatives	Gamma radiation at room temperature and in air presence	
Ethylene-vinyl alcohol copolymer	EVOH	Alkyl aromatics such as tert-butyl benzene and isobutyl benzene, and oxygenated aromatics such as acetophenone and 2-phenyl isopropanol; propanal, methyl ethyl ketone, 2-butanol, tert-butyl benzene, and 2-methylpropylbenzene	Electron beam irradiation – 5-50 kGy	[11]
Polystyrene	PS	Acetophenone (30-50 ppm); benzaldehyde, phenol, 1-phenylethanol (< 10 ppm), and phenylacetaldehyde	Gamma radiation in air – 25-50 kGy	[12]

Table 2. Contd.

Name	Abbreviation	Radiolysis products	Observation	Ref.
Methyl methacrylate--acrylonitrile--butadiene-styrene	MABS	Benzaldehyde, acetophenone, phenol, 1-phenylethanol, 1-phenyl-1-propanone	Gamma radiation – 22.4 kGy	[7]
Polyamide	PA-6	Pentanamide ($\approx$ 75 ppm) and caprolactam; traces of some homologous amides	Gamma radiation in air – 25-50 kGy	[12]
Polyurethane	PU	ROOH, OH•, RO•, carboxylic acids, alcohols, esters, formats	25-1000 kGy, in air	[13]
Poly(dimethylsilox)ane	Silicone, PDMS	Crosslinking, chain scission to small extent, hydrogen methane, ethane	50 kGy – noncitotoxicity	[13]
Poly(ethylene terephthalate)	PET	Formic acid, acetic acid, 1,3-dioxalane, 2-methyl-1,3-dioxolane; acetaldehyde, 1,3-dioxolane, 2-methyl-1,3-dioxolane; terephthalic acid, bis-(2-hydroxyethyl) terephthalate, dimethyl terephthalate, monohydroxyethylene terephthalate	Gamma radiation – 5, 25 and 50 kGy, at ambient temperature or an electron beam accelerator	[14]
Polysaccharides		H_2, CH_4, CO, CO_2 or low molecular mass substances such as water, formaldehyde, methanol, aldehydes, ketones, formic acid, acetaldehyde, methanol, acetone, ethanol, methyl formate and sugars: glucose, maltose, erythrose, ribose, mannose		[15]
Proteins	Hen egg-white lysozyme	Sulphur and carbon-centred radicals RSS•, perthiyl radicals, sulphur-oxygen radicals (in presence of oxygen)	Gamma radiation – 0 to 20 kGy, in the solid state (lyophilized powder), at room temperature under three different atmospheres (air, nitrogen and oxygen)	[16]

product, plus traces of some homologous amides. The poly(vinyl chloride) (PVC) packaging material release of hydrochloric acid (HCl) during irradiation and large amounts of volatile substances were extracted from the PVC sheets. The main products of PVC and PP are fragments of additives, *i.e.* of stabilizers and phenol-type antioxidants, respectively. For consumer protection and also to meet general food packaging legislative requirements for irradiated packaging materials, it is necessary to evaluate the compositional changes in the polymers following irradiation, especially for irradiated polyolefins and PVC. Most attention should be paid to low volatile radiolysis products which are the most likely to migrate into a foodstuff or a pharmaceutical products. Under realistic polymer/food simulant contact conditions during irradiation, a large number of primary and secondary radiolysis products (hydrocarbons, aldehydes, ketones, alcohols, carboxylic acids) were produced. These compounds were detected in the food simulants after contact with all films tested, even at the lower absorbed doses of 5 and 10 kGy (approved doses for food preservation). The type and concentration of radiolysis products increases progressively with increasing dose. Volatile and non-volatile compounds produced during irradiation affected the sensory properties of potable water after contact with packaging films. Taste transfer to water was observed mainly at higher doses and was more noticeable for multilayer structures containing recycled low density polyethylene (LDPE) [17]. The main products of PS are acetophenone, benzaldehyde, phenol, 1-phenylethanol, and phenylacetaldehyde. Their concentrations are one order of magnitude below the residual styrene/styrene dimer levels [7, 18].

The radiolysis products formed during gamma-ray or electron beam radiation are generally later released. Due to rigid structure of these materials, the radiolysis products may be trapped inside the polymeric structure and be delivered later when the material enters into contact with environment that favours their release. The radiolysis products of some polyethylene irradiated at 20 kGy were evaluated 7.5 months after irradiation and it was found that the
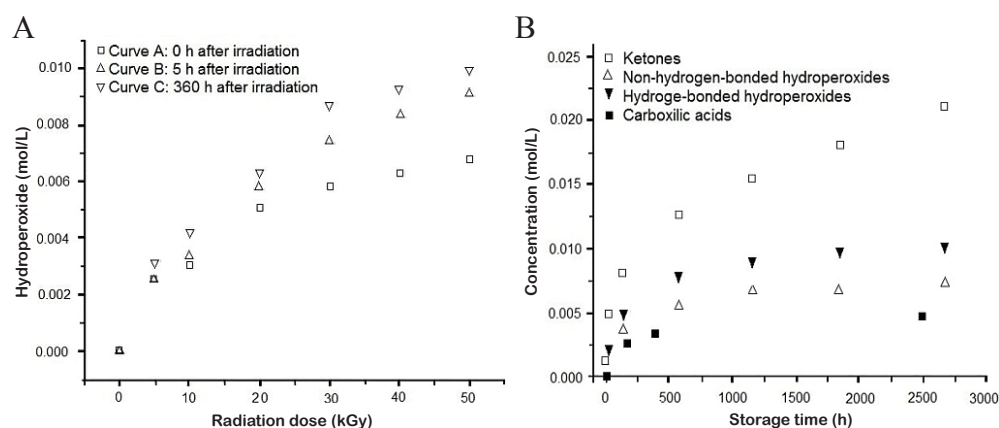
Fig.7. Variation of functional groups with radiation dose (A) and storage time of UHMWPE (B).

peroxy radicals continued to react, promoting chain scissioning, and the generation of carbonyl, of hydroperoxides and of ketones. In the radiation of ultra--high molecular weight polyethylene (UHMWPE), high concentrations and new radiolysis products were found, as shown in Fig.7.

When exposed to 25 or 50 kGy radiation doses, PS produces radiolysis products such as benzaldehyde, acetophenone (30-50 ppm), 1-phenylethanol (< 10 ppm) and phenol. Nylons evolved pentanamide (75 ppm) and caprolactam. PP generates alkyl radicals which can subsequently interact with molecular oxygen to form hydroxyl, carbonyl or carboxyl groups. These volatiles can have adverse flavour effects to irradiated food packaged in these polymers, in general in this order: LDPE > HDPE (high density polyethylene) > PS ~ PA and PET. The intensity of specific off-odors increases with the availability of oxygen in atmosphere.

The addition of the antioxidants reduces the formation of carboxylic acid derivatives in LDPE films. However, phenolic stabilizers, such as Irganox 1076, 1010 and 1330 and the arylphosphite antioxidant Irgafos 168 (in PVC, PE and PP) are susceptible to degradation under gamma irradiation. Low doses of irradiation (5 kGy) to HDPE trays can completely destruct phosphite antioxidants to their phosphate products with some covalently bonded on the polymer matrix so that they will not be found in simulants. At present, little is known about toxicity of radiolytic products from polymers and additives because of the variability of migration rates and because of the potential of polymeric entrapment of volatiles from the different polymers into food simulants [19].

6. CHANGES IN PHYSICAL AND CHEMICAL PROPERTIES

6.1. SYNTHETIC POLYMERS

Radiation is the unique source of energy which can initiate chemical reactions at any temperature, including ambient, under any pressure, in any phase (gas, liquid or solid), without use of catalysts [20]. Polymers are quite often irradiated for modification or sterilization (medical products). Therefore, the changes in their structure may be beneficial or undesirable. The application of radiation for modification of synthetic materials, mostly curing and crosslinking is a well-established technology [21].

The changes in the properties of the irradiated polymers in the solid state are:
• chemical changes:
    – crosslinking and chain scission,

- structural weakness,
- gas formation,
- double bond formation,
- oxidation,
- living radical effects after irradiation,
- effects on additives;
- physical changes:
  - changes in mechanical properties (mechanical strength, flexibility, Young's moduli, torsional resistance, *etc.*),
  - colour change,
  - changes in conductivity,
  - changes in crystallinity,
  - thermal stability and transitions.

Table 3. Linear polymers that predominantly undergo crosslinking or main-chain scissioning if irradiated with high energy radiation at room temperature in vacuum or in an oxygen-free atmosphere.

Predominant main-chain scission (average molar mass decreases)	Predominant crosslinking (average molar mass increases)
Polymethacrylates	Polyacrylates
Polymethacrylamide	Polyacrylamide
Poly(α-methacrylonitrile)	Polyacrylonitrile
Poly(α-methylstyrene)	Polystyrene
Polyisobutene	Polyethylene
Poly(tetrafluoroethylene)	Polypropylene
Poly(trifluorochloroethylene)	Polyisoprene
Poly(vinyl fluoride)	Polybutadiene
Poly(vinylidene chloride)	Polyamides
Poly(hexane-1-sulphone)	Poly(vinyl acetate)
Poly(propylene sulphide)	Poly(vinyl alcohol)
Poly(oxymethylene)	Polyvinylpyrrolidone
Polycarbonates	Polyurethanes
Poly(vinyl butyral)	Polychloroprene
Poly(phenyl vinyl ketone)	Natural rubber
Polysaccharides (cellulose, chitosan)	Polysiloxanes
Polysine, polyalanine	Copolymers of butadiene with styrene or acrylonitrile
Nucleic acids (DNA)	Copolymers of acrylonitrile with styrene

Radiation crosslinkable polymers

$$-CH_2-CH=CH-CH_2- \quad -CH_2-CH_2-$$

$$\begin{array}{c} -CH_2-CH- \\ | \\ C-O-CH_3 \\ \| \\ O \end{array} \quad -O-(CH_2)_5-\overset{\displaystyle O}{\overset{\|}{C}}-$$

Radiation degradable polymers

$$\begin{array}{c} CH_3 \\ | \\ -CH_2-CH- \end{array} \quad \begin{array}{c} CH_3 \\ | \\ -CH_2-C- \\ | \\ C-O-CH_3 \\ \| \\ O \end{array} \quad \begin{array}{c} O \\ \| \\ -O-CH-C- \\ | \\ CH_3 \end{array} \quad -CF_2-CF_2-$$

Radiation resistant polymers

$$-CH_2-CH-$$

$$-O-\!\!\!\bigcirc\!\!\!-\overset{\displaystyle R_1}{\underset{\displaystyle R_2}{C}}-\!\!\!\bigcirc\!\!\!-O-\overset{\displaystyle O}{\overset{\|}{C}}-$$
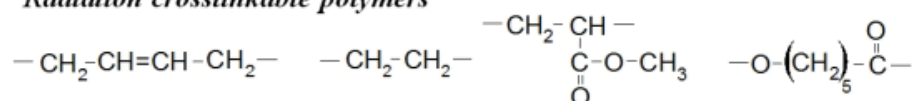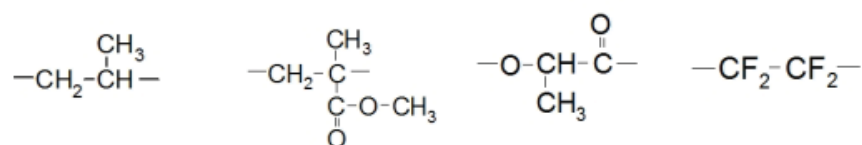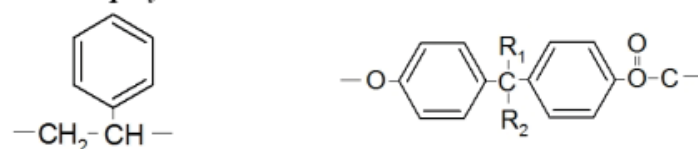
Fig.8. Examples of chemical structures of polymers with different responses to radiation.

The different responses to radiation for different polymers are related to the chemical structures of the polymers. Some examples of chemical structures that correspond to crosslinking types, degrading or scissioning types, and radiation-resistant polymers are given below. A classification of common polymers is summarized in Table 3 and the structure of some are depicted in Fig.8.

The formation of reactive oxygen species can result in the oxidation of polymer with the formation of peroxide, alcohol and carbonyl compounds. The most stable polymers are vinyl derivatives, PS and the PET with polyamides (nylons) having intermediary stability while polyolefins as the least stable polymers.

In solid state, the radicals can be found for months after irradiation. Commercial polymers often contain some additives. The effect of the additives on radiolysis is important. Radiation protecting additives have aromatic cyclic structures and reduce degradation by radiation. Plasticizers can have a similar protective role.

Mechanical properties of irradiated polymers depend on the ratio of chain scission and crosslinking and are related to molecular weight.
The mechanical properties of polymers of the crosslinking type are improved upon irradiation with low absorbed doses (up to 0.1 MGy). The elastic modulus, tensile strength and hardness are increased, whereas the solubility is decreased with increasing absorbed dose. At very high absorbed doses, these polymers become hard and brittle. The polymers of the degradation type undergo deterioration of their mechanical properties even at low absorbed doses. Low doses of 5 and 10 kGy had no effect on mechanical properties such as tensile strength, elongation at break and Young's modulus. However, at 30 kGy, there was a decrease in tensile strength in HDPE, PP and a decrease in elongation at break of LDPE and a polyethylene ionomer. The mechanical properties of

neither an ethylene-vinyl acetate (EVA) nor polystyrene were affected by ir-radiation.

Important aromatic polymers such as polyimides and polyarylsulphones, as shown in Fig.9, are resistant to high energy radiation compared to nonaromatic polymers.

Poly(aryl ether sulfone)
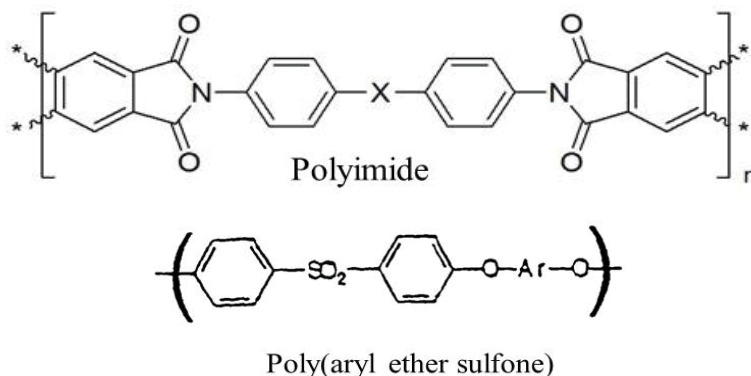
Fig.9. General chemical structure of polyimide and polysulphone.

The mechanical and electrical properties of a poly(pyromellitimide) remain satisfactory in the presence of air up to absorbed dose of 100 MGy. Most aromatic polymers proved to be radiation resistant only in the absence of oxygen. For example, the mechanical properties of polystyrene were not appreciable deteriorated when exposed in the absence of oxygen to the absorbed doses up to 10 MGy, but these properties decreased to 50% of their initial values at an absorbed dose of only 0.8 MGy in the presence of oxygen. Irradiation of pre-packaged meat and poultry should alter neither physicochemical properties of a packaging film nor result in the transfer of components or residues from packaging material to contaminate the food in contact with the plastic film. The irradiation of plastic film results in a combination of chemical crosslinking and a consequent increase of tensile strength of the film, or a fragmentation leading to a decreased strength and increased permeability of packaging films. In addition to these events, the formation of volatile radiolysis products (hydrogen, methane, HCl, *etc.*) is influenced by presence of oxygen in the irradiated products. It was reported that irradiation at 5, 10 and 30 kGy had no effect on the O_2, CO_2 permeability or water vapour transmission rates of a variety of polymers including LDPE, HDPE, PS, EVA, biaxially oriented PP and an ionomer.

Colour change can appear when the double bonds formed on irradiated polymers such as poly(methyl methacrylate) (PMMA) and PVC.

Conductivity change can increase when the double bond increased in irradiated polymers.

The overall migration into food simulants as distilled water was not affected by low irradiation doses; at 30 kGy, migration into 3% acetic acid was decreased for PP and an ionomer.

6.2. NATURAL POLYMERS

Studies of the radiolysis of biopolymers [22] serve the dual purposes of giving information on: (1) the chemical mechanisms by which radiation modifies life processes and (2) the structure-properties-application relationships in macromolecules. Irradiation effects on biopolymers result in the cleavage of chemical bonds. Because of the very complex composition of most biopolymers, many different chemical reactions are initiated and in each case a host of products are formed under the influence of high energy radiation. A variety of biopolymers composed of linear strands, including certain polysaccharides, proteins and nucleic acids undergo predominantly main-chain scission, and this is of outstanding importance in the case of deoxyribonucleic acids (DNA), because the killing of living cells correlates well with double-strand breaks.

6.2.1. Amino acids, proteins and DNA

Amino acids and proteins exist as zwitterions. Under irradiation amino acids undergo by the electron capture deamination, as indicated in Fig.10A. With proteins both deamination and decarboxylation take place. For those molecules containing sulphur groups, they are cleaved by a radiolytic mechanism and hydrogen sulphide is produced as a by-product, as shown in Fig.10B.

In living cells, both direct and indirect depositions of energy are possible. Direct effects in chromatin components result in the formation of specific radical products, many of which are highly reactive. Secondary reactions of the cationic radicals are largely unknown. Indirect effects occur when energy is deposited in water or other components in a solution, and radiolysis products such as e^-_{aq} and •OH react with the biopolymer have been investigated, as shown in Fig.11.

Commonly DNA molecules are tightly associated with 8 to 12 water molecules per nucleotide forming a primary solvation shell which increases the radiation-induced damage to DNA by ~50%. When the water molecules are ionized, an entire transfer to DNA can occur and electrons ejected from water molecules can be scavenged by DNA molecules. The events due to the direct effect are single- and double-strand breaks, crosslinking, base release, and lesions in bases and sugar moieties. Hydrogen bonds between the two strands of the double helix are broken. A large number of radiolysis products results. From base damage the following products have been identified: 5-hydroxy-5,6-dihydrothymine, 5,6-dihydrothymine, 5-hydroxyuracil, 5,6-dihydroxyuracil, 5-hydroxycytosine, 2-hydroxyadenine, 8-hydroxyadenine, 7-hydro-8-oxo--guanine, 2,6-diamino-4-oxo-5-formamidopyrimidine, 4,6-diamino-5-formamidopyrimidine.

Studies carried out half a century ago showed that this process is effective in inactivating enzymes. Replacing •OH to the less reactive inorganic radical anion $•Br_2^-$ has been done. It is then possible to determine the role of tyrosine

AMINOACIDS
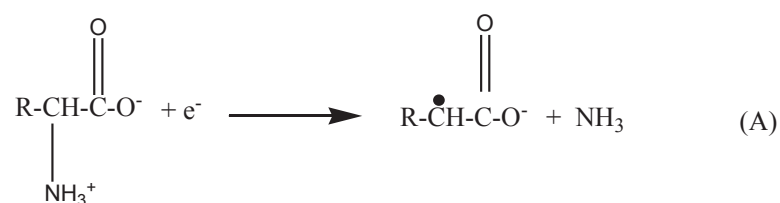
PROTEINS
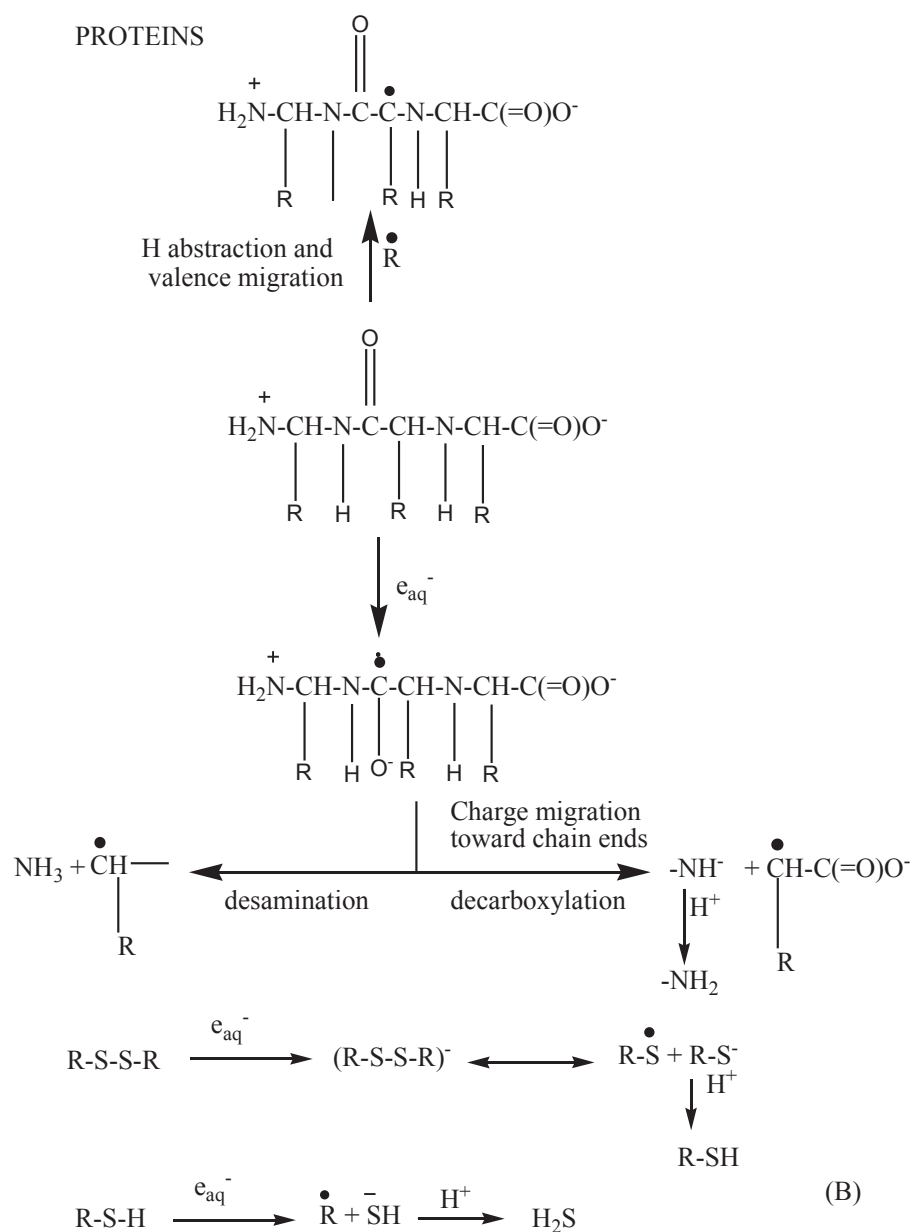
Fig.10. Radiolytic mechanism of amino acids (A) and proteins (B).

Direct effect: DNA $\xrightarrow{\text{radiation}}$ $DNA^+ + e^- + DNA^*$

Indirect effect: $H_2O \xrightarrow{\text{radiation}}$ $H_2O^+ + e^-$

$H_2O + DNA \rightarrow H_2O + DNA^+$

$e^- + DNA \rightarrow DNA^-$
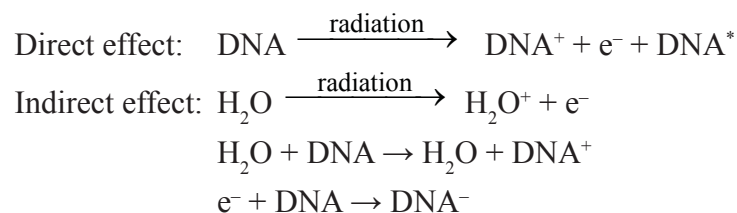
Fig.11. Radiolytic mechanism of DNA.

in functional and structural integrity of several proteinase inhibitors. Both e^-_{aq} and –OR react rapidly with DNA, but only •OH initiates reactions which damage DNA. Radiolysis of double-stranded DNA leads to an increase in optical absorption. The •OH is believed to attack the deoxyribose moiety, causing strand
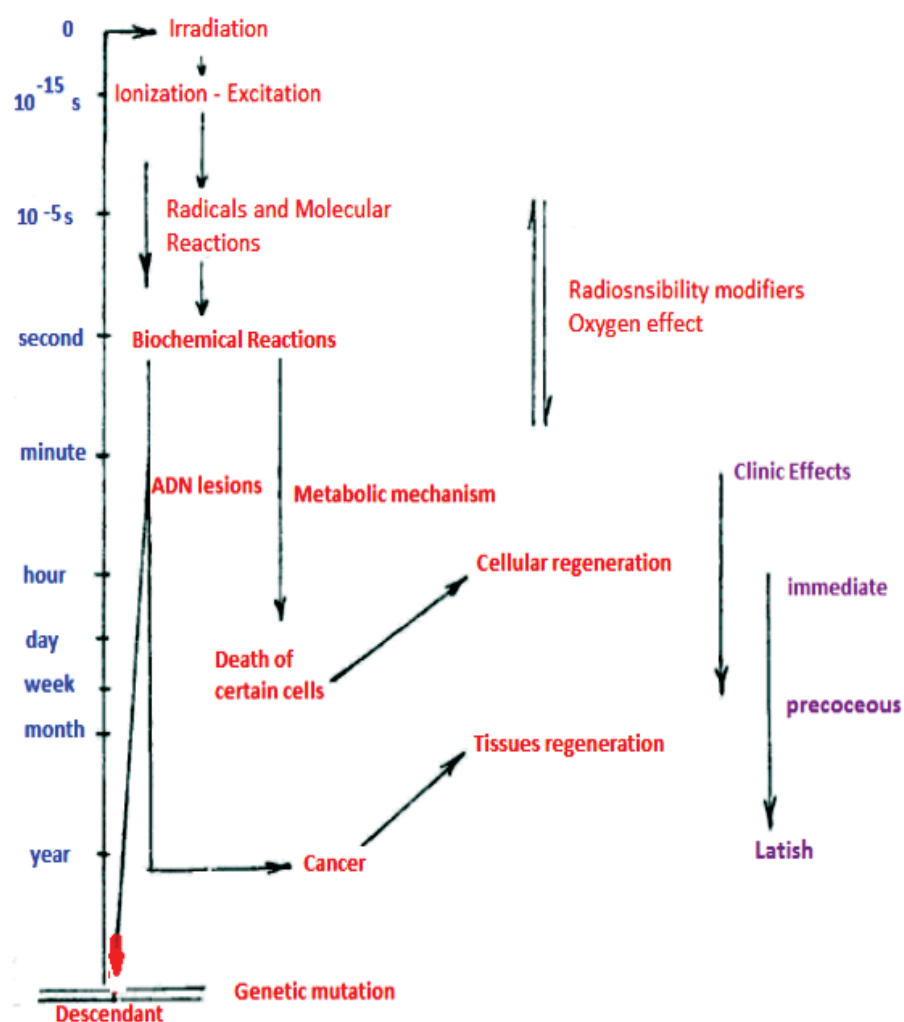
Fig.12. Schematic representation of phenomena launched by ionizing radiations in biological molecules/organisms.

breaks and partial denaturation, thus reducing the hypochromic effect. After the DNA is partially denatured, or single-stranded, •OH attacks the bases also. Three kinds of strand breaks have been observed: (i) immediate, (ii) those appearing post irradiation, and (iii) those appearing on post-irradiation treatment with alkali. Radiolysis of chromatin results in DNA strand breaks, base damage, and protein-DNA crosslinks. Yields for strand breaks and base damage are lower in chromatin than in purified DNA, and lower still in intact cells [23].

In living organisms, this denaturation of the biological molecules without adequate protection over a long period of exposure could have deleterious effects on health, as illustrated in Fig.12.

6.2.2. Polysaccharides

Irradiation of polysaccharides in the solid state induces the radical formation in molecular chains as a result of the direct action of radiation [24]. Here mainly two events take place: (1) direct energy transfers to the macromolecule to produce macroradicals and (2) the generation of primary radicals due to the presence of water (moisture). The course of the degradation of carbohydrates in the solid state is illustrated in Fig.13. The main effects are fragmentation, hydrolysis and rearrangement leading to low molecular weight products. When polysaccharides such as starch, cellulose, chitosan, amylose and dextran are subjected to high energy radiation, a vast number of products is formed, such
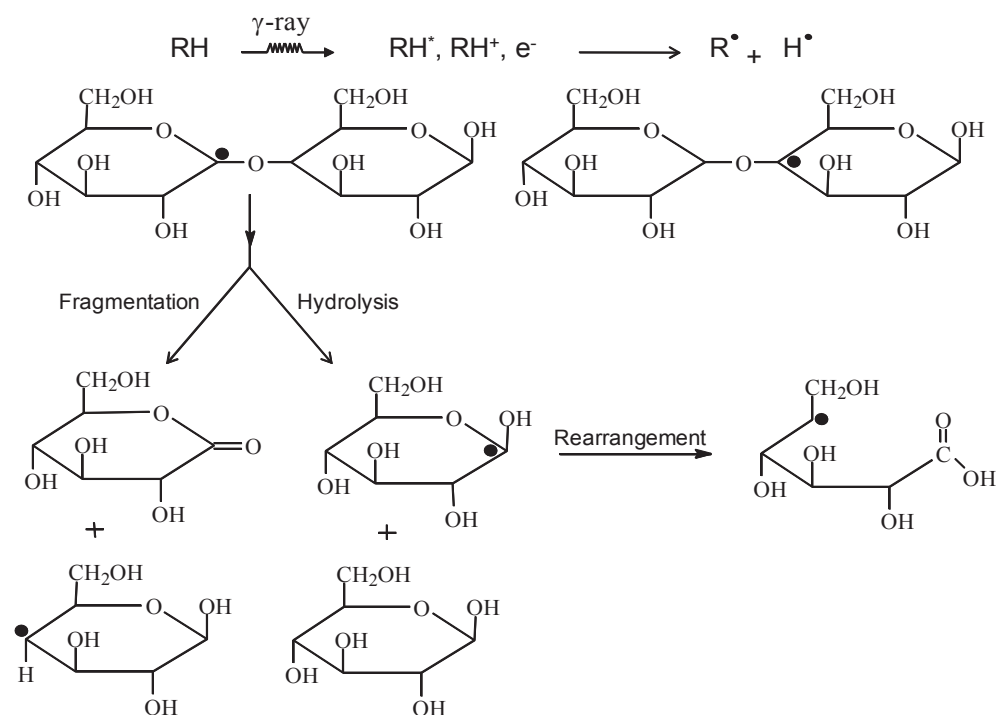
Fig.13. Events in solid state radiation of carbohydrates.

as gaseous H_2, CH_4, CO, CO_2 and low molecular mass substances such as water, formaldehyde, methanol, aldehydes, ketones and sugars. The remaining polymer contains carbonyl, carboxyl, and aldehyde groups. The average molecular molar mass is reduced because of the predominant main-chain scissioning through cleavage of the C–O–C glycoside bond between base units. When high energy radiation is directly absorbed by polysaccharides, electronically excited moieties, radical cations and electron are generated. Free radical processes play an important role, while the radical cations generated are rapidly transformed to free radicals by deprotonation.

During the solid state radiolysis of polysaccharides, scissioning of the glycosidic bond, analogous to the reactions shown in Fig.13, is the dominant process which eventually leads to a decrease in the molecular weight of the macromolecules. Degradation and the resulting changes in average molecular weight products are often quantified as radiation yields of degradation G(s). Moisture content strongly influences the reaction pathways and yields. The radiolysis of water contributes to this. The yields of radicals are significantly higher than in dry polysaccharide so the contribution of indirect effect may be greater than based on percent of moisture, and also due to the effect of water molecules on the dry matrix structure and polymer chain mobility [25].

6.3. COMPLEX MATERIALS

Complex materials, including multilayer laminated and coextruded ones, are very useful because they combine a number of desirable properties which no single of material possesses. Most are based on polyolefin, PS, PET, PA, EVA, and other synthetic or natural polymers. The effect of gamma irradiation
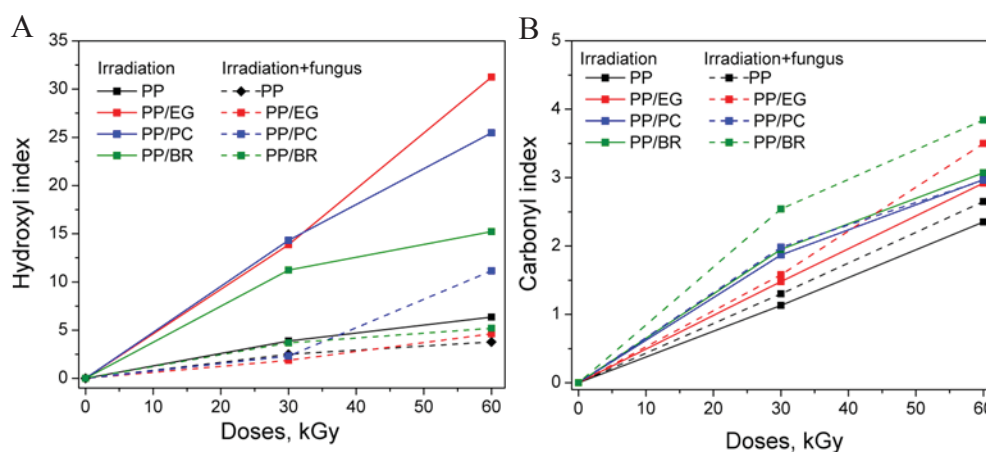
Fig.14. Variation of (A) hydroxyl and (B) carbonyl indexes of gamma-irradiated PP and PP/biomass composites compared with those of 7 weeks fungal degradation of the PP/biomass samples. (Adapted from Ref. [26]).

on PP biocomposites (*Eucalyptus globulus*, pine cones, and *Brassica rapa*) has been studied by Parparita *et al.* [26]. The biomass lignin content acts as an antioxidant and has a stabilization effect against gamma irradiation degradation. For the materials studied, gamma irradiation promoted the biodegradability under the action of the *Bjerkandera adusta* fungus [27]. Removing a protective layer of relatively inert polyolefin, increased the effects of absorbed dose which leads to increase of oxygen containing functional groups, as illustrated in Fig.14. In this manner, an eco-friendly method for improving integration of some "undegradable" materials in natural cycles could be improved.

7. RADIATION PROTECTION

Measures to fully protect polymers against radiation exposure do not exist. The stabilization of polymeric materials against high energy radiation may be achieved through the use of antioxidants, ultraviolet and heat stabilizers, which, in turn, also undergo degradation. Radiolysis products could originate more from additive decomposition than from the originating polymers themselves.

Protective agents added to the polymers in small amounts are effective only to a limited extent and function *via* different mechanisms. They can act mainly as antioxidants by preventing radiation-induced oxidative chain reactions or more generally as free radicals scavengers. Other additives may act as energy absorbers in accepting electronic excitation energy transferred from a polymer. In this manner, agents that operate protectively are aromatic compounds, including polymers with aromatic constituents or fillers (inorganic materials or carbon black). Electronic excitation energy transported to or directly absorbed by aromatic rings is delocalized due to the π-electron-based resonant structure of the aromatic ring, and thus converted to heat by collision with neighbouring groups or molecules. Hence, bond rupture is much less likely in the case on nonaromatic compounds.

8. CONCLUSIONS

Study of the radiation chemistry of solid organic materials is important for many applications, as in the medical, pharmaceutical, and food preservation fields because the effects of radiation exposure can be beneficial or deleterious. Limits should be based on known effects. Much greater effort is needed in this direction.

Acknowledgements

REFERENCES

[1].   Willard, J.E. (1987). Radiation chemistry of organic solids. In Farhataziz & M.A.J. Rogers (Eds.), *Radiation chemistry. Principles and applications* (pp. 395-434). New York: VCH Publishers.

[2].   Kempner, E.S. (2011). Direct effects of ionizing radiation on macromolecules. *J. Polym. Sci. Part B. Polym. Phys.*, *49*(12), 827-831. DOI: 10.1002/polb.22250.

[3].   Nelson, G., & Reilly, D. (1991). Gamma-ray interactions with matter. In D. Reilly, N. Ensslin, H. Smith, Jr. & S. Kreiner (Eds.), *Passive nondestructive analysis of nuclear materials* (pp. 27-42). U.S. Nuclear Regulatory Commission. (NUREG/CR-5550, LA-UR-90-732).

[4].   Willett, E. (2005). *The basics of quantum physics: Understanding the photoelectric effect and line spectra*. New York: The Rosen Publishing Group.

[5].   Grigoriev, E.I., & Trakhtenber, L.I. (1996). Primary chemical processes in the irradiated solid. In E.I. Grigoriev & L.I. Trakhtenberg (Eds.), *Radiation-chemical processes in solid phase: Theory and application* (pp. 37-48). CRC Press.

[6].   Demertzis, P.G., Franz, R., & Welle, F. (1999). The effects of γ-irradiation on compositional changes in plastic packaging films. *Packag. Technol. Sci.*, *12*(3), 119-130. DOI: 10.1002/(SICI)1099-1522(199905/06)12:3<119::AID-PTS460> 3.0.CO;2-G.

[7].   Buchalla, R., Boess, C., & Bögl, K.W. (1999). Characterization of volatile radiolysis products in radiation-sterilized plastics by thermal desorption-gas chromatography-mass spectrometry: screening of six medical polymers. *Radiat. Phys. Chem.*, *56*, 353-367. DOI: 10.1016/S0969-806X(99)00311-4.

[8].   De Rojas Gante, C., & Pascat, B. (1990). Effects of B-ionizing radiation on the properties of flexible packaging materials. *Packag. Technol. Sci.*, *3*, 97-115. DOI: 10.1002/pts.2770030207.

[9].   Lü, G., Chen, H., & Liu, D. (1993). The degradation in solid state of polyvinyl alcohol by gamma-irradiation. *Radiat. Phys. Chem.*, *42*(1-3), 229-232. DOI: 10.1016/0969-806X(93)90240-U.

[10]. Geuskens, G., Borsu, M., & David, C. (1972). Photolysis and radiolysis of polyvinylacetate-II: Volatile products and absorption spectra. *Eur. Polym. J.*, *8*(7), 883-892. DOI: 10.1016/0014-3057(72)90048-1.

[11]. Komolprasert, V. (2007). Packaging for foods treated by ionizing radiation. Chapter 6. In J.H. Han (Ed.), *Packaging for nonthermal processing of food* (pp. 87-116). Oxford, UK: Blackwell Publishing Ltd. DOI: 10.1002/9780470277720.ch6.

[12]. Buchalla, R., Begley, T.H., & Morehouse, K.M. (2002). Analysis of low-molecular weight radiolysis products in extracts of gamma-irradiated polymers by

gas chromatography and high-performance liquid chromatography. *Radiat. Phys. Chem.*, *63*, 837-840. DOI: 10.1016/S0969-806X(01)00642-9.

[13]. Bohrer, D. (2012). Contamination from sterilization procedures. In D. Bohrer (Ed.), *Sources of contamination in medicinal products and medical devices* (pp. 433-511). Wiley.

[14]. Komolprasert, V., McNeal, T.P., & Begley, T.H. (2003). Effects of gamma- and electron-beam irradiation on semi-rigid amorphous polyethylene terephthalate co-polymers. *Food. Addit. Contam.*, *20*(5), 505-517. DOI: 10.1080/0265203031000070119.

[15]. Sokhey, A.S., & Hanna, M.A. (1993). Properties of irradiated starches. *Food Struct.*, *12*(4), 397-410. Retrieved March 30, 2016, from http://digitalcommons.usu.edu/cgi/viewcontent.cgi?article=1329&context=foodmicrostructure.

[16]. Baumeister, W., Fringeli, U.P., Hahn, M., & Seredynski, J. (1976). Radiation damage of proteins in the solid state: Changes of β-lactoglobulin secondary structure. *BBA – Protein Struct.*, *453*(1), 289-292. DOI: 10.1016/0005-2795(76)90276-2.

[17]. Chytiri, S., Goulas, A.E., Badeka, A., Riganakos, K.A., & Kontominas, M.G. (2005). Volatile and non-volatile radiolysis products in irradiated multilayer coextruded food-packaging films containing a buried layer of recycled low-density polyethylene. *Food. Addit. Contam.*, *22*(12), 1264-1273. DOI: 10.1080/02652030500241645.

[18]. Bohrer, D. (2013). *Sources of contamination in medicinal products and medical devices*. New Jersey: Wiley.

[19]. Hui, Y.H. (2006). *Handbook of food science, technology, and engineering*. Boca Raton: CRC Taylor and Francis.

[20]. Rao, V. (2012). Radiation processing of polymer. In S. Thomas & W. Yang (Eds.), *Advances in polymer processing: From macro- to nano- scales* (pp. 402-437). Woodhead Publishing Limited and CRC Press.

[21]. Drobny, J.G. (2003). *Radiation technology for polymers*. Boca Raton: CRC Press.

[22]. Schnabel, W. (2014). *Polymers and electromagnetic radiation: Fundamentals and practical applications*. Weinheim: Wiley-VCH.

[23]. Myers Jr., L.S., & Kay, E. (1979). Radiolysis of DNA and other biopolymers. *Int. J. Radiat. Oncol. Biol. Phys.*, *5*(7), 1055-1060. DOI: 10.1016/0360-3016(79)90619-9.

[24]. IAEA. (2004). *Radiation modification of polysaccharides*. Vienna: IAEA. (IAEA-TECDOC-1422). Retrieved November 6, 2015, from http://www-pub.iaea.org/MTCD/publications/PDF/te_1422_web.pdf.

[25]. IAEA. (2010). *Report of the 2nd RCM on "Development of radiation-processed products of natural polymers for application in agriculture, healthcare, industry and environment", Reims, France, 12-16 October 2009. Working material*. Vienna: IAEA. Retrieved March 16, 2016, from http://www-naweb.iaea.org/napc/iachem/meetings/RCMs/RC-1091-2_report_complete.pdf.

[26]. Parparita, E., Zaharescu, T., Darie, R.N., & Vasile, C. (2015). Biomass effect on γ-irradiation behavior of some polypropylene biocomposites. *Ind. Eng. Chem. Res.*, *54*(8), 2404-2413. DOI: 10.1021/ie5043984.

[27]. Butnaru, E., Darie-Niţă, R.N., Zaharescu, T., Balaeş, T., Tănase, C., Hitruc, G., Doroftei, F., & Vasile, C. (2016). Gamma irradiation assisted fungal degradation of the polypropylene/biomass composites. *Radiat. Phys. Chem.*, *125*, 134-144. DOI: 10.1016/j.radphyschem.2016.04.003.

RADIATION-INDUCED POLYMERIZATION

Xavier Coqueret
Université de Reims Champagne-Ardenne, CNRS UMR 7312, Institut de Chimie Moléculaire de Reims, BP 1039, 51687 Reims Cedex 2, France

1. INTRODUCTION

Polymers can be synthesized into a variety of topological structures (linear, branched and three-dimensional networks) by two types of polymerization, either of which involves a chain addition process or a step-growth mechanism. Radiation-induced polymerization, for the most part, proceeds by a chain addition mechanism [1].

In principle, step-growth processes can be triggered by the generation of catalysts resulting from the interaction between radiation and the precursors of some acidic or basic species, or between some radiolytic products with acid or base generators. However, this step-growth process has received little attention and is currently limited to few applications of technical relevance. For example, the step-growth addition of the thiol groups on a multifunctional mercaptan derivative to diisocyanates is effectively catalyzed by photobases under ultraviolet (UV) radiation. This results in the formation of hard, flexible materials with interesting uses in microelectronics and as binders for industrial paints and coatings [2].

High energy radiation interacts with organic matter by various physical and chemical mechanisms resulting in the formation of short-lived excited species, and of chemical entities such as thermalized electrons and neutral or ionic free radicals exhibiting longer lifetimes allowing them to undergo bimolecular reactions with various molecular compounds by translational diffusion [3]. The *in-situ* generation of such longer-lived reactive species can be exploited to initiate chain polymerization mechanisms. The resulting process is called radiation-initiated polymerization, the propagation being, in principle, not directly affected by radiolytic events. Propagation essentially proceeds with the same mechanistic and kinetic features of conventional, thermally initiated chain polymerizations. The radiation-induced initiation process makes it possible to trigger polymerization under reaction conditions (temperature, initiation rate, type, location and spatial distribution of the initiating species) that are

unusual, if not specific, compared to the activation with thermally cleavable initiators (such as peroxides) or with redox systems (such as a reductive metal associated with a peroxide). A number of advantages can be found from these peculiarities of radiation-initiated polymerization that benefit processing efficiency or which produce final materials with unique properties [4].

The basic aspects of chain polymerization are discussed in the next section. Then, the specific features of radiation-initiated polymerization carried out by free radical or by cationic propagation will be addressed [5].

2. BASIC ASPECTS OF CHAIN POLYMERIZATION

Chain polymerization is defined as "a chain reaction in which the growth of a polymer chain proceeds exclusively by reaction(s) between monomer(s), (M), and reactive site(s), represented by an asterisk in Eq. (1), on the polymer chain with regeneration of the reactive site(s), at the end of each growth step".

$$\sim\!\sim\!\sim (M)_n \sim\!\sim\!\sim M^* + M \longrightarrow \sim\!\sim\!\sim (M)_{n+1} \sim\!\sim\!\sim M^* \qquad (1)$$
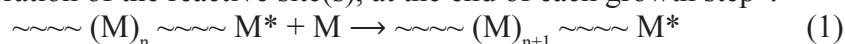
The chain reaction mechanism includes a sequence of steps forming a chain mechanism, that is a complex reaction path in which one or more reactive intermediates (frequently radicals) are continuously regenerated. This usually happens through a repetitive cycle of steps which propagate the reaction. When the propagation step involves a monomer that is repeatedly bound to an active center, such a process results in the formation of an oligomeric, higher molecular weight entity, which eventually grows further to form a polymeric chain that has an active end group. The most common polymerization processes involve carbon centered free radicals. However, ionic mechanisms, covalent group-transfer and organometallic complexes involved in coordination polymerization have specific features that may offer advantages of technical interest.

Propagation in chain polymerization usually occurs without the formation of small molecules. However, in very specific cases, low-molar-mass molecular by-products are formed, that are not included in the chain undergoing the propagation step. When such molecular extension process occurs, the chain process is a condensation chain polymerization. More commonly, the type of chemical reactions involved in this growth step is specified by using the terms free radical chain polymerization, ring-opening chain polymerization, cationic chain polymerization, *etc*.

The four main steps of the chain mechanism are presented in the following sections for the free radical polymerization of unsaturated compounds such as vinyl, acrylic and styrenic monomers.

2.1. KEY STAGES OF THE CHAIN POLYMERIZATION MECHANISM

Step 1 – Chain initiation

Chain initiation can take place as soon as the properly selected initiator starts to decompose into free radicals (In°). Initiation is completed when the initiator radical has added to the first monomer unit, M, to produce the chain initiating species, $M_1°$. From a kinetic standpoint, the rate of initiation, R_i, is controlled by the initiator decomposition, which is a slower reaction than the subsequent addition of an electron-deficient radical onto the electron rich π bond of the ethylenic monomer. Though directly related to the decomposition rate of the initiator, R_d, the effective initiation rate, R_i, depends on an efficiency factor that takes into account the actual fraction of generated free radicals that effectively add to the monomer for producing $M_1°$, the chain initiating species. The quenching efficiency of dioxygen for carbon-centered free radicals is extremely high, and, as a result, peroxy radicals are unable to initiate the propagation process. Consequently, free radical polymerizations are preferably conducted with the exclusion of oxygen (*in vacuo* or by deaeration with an inert gas). When a low residual amount of dioxygen is present in the polymerization medium, polymerization starts after an induction period corresponding to the consumption of O_2 *via* the quenching reaction. In some cases, particularly when a photochemical or a radiochemical activation process is used for the initiation, the rate of formation of new free radicals is high enough to overcome the quenching of O_2 that is initially present in the medium and of the amount of O_2 that constantly diffuses from the ambient atmosphere into the reaction medium. This favorable situation can be achieved under intense ultraviolet or light irradiation of properly photosensitized compositions or by processing the radically polymerizable monomers under high dose rate electron beams (EB).
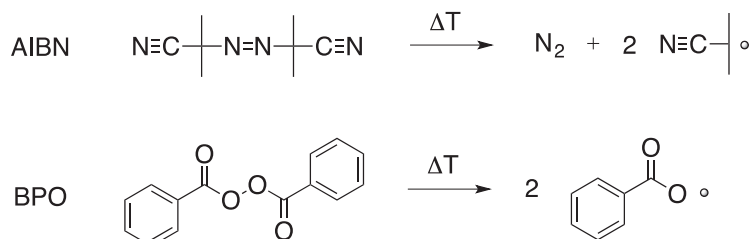
Scheme 1. Examples of thermal initiators with their decomposition products: azo-bis--isobutyronitrile (AIBN) and benzoyl peroxide (BPO).

Typical initiators that are activated by heat include various types of organic compounds with a scissile functional group that is decomposed at reasonable operating temperatures, such as aromatic azo derivatives (–N=N–), disulfides (–S–S–), or peroxides (–O–O–) (Scheme 1). Inorganic and organic redox systems (such as Fenton reagent (FR), peroxide-dimethyl aniline shown
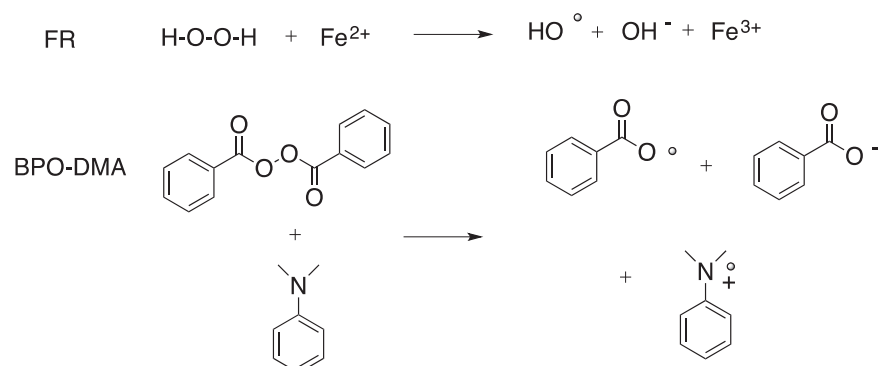
Scheme 2. Examples of redox initiators: Fenton reagent (FR) and benzoyl peroxide–N,N--dimethylaniline system (BPO-DMA).

in Scheme 2) offer the advantage of generating free radicals efficiently at temperatures between 0 and 50°C, without needing to heat the reaction medium in order to induce thermal initiator decomposition.

Step 2 – Chain propagation

Propagation consists of the iterative growth of the initiating radical, $M_1°$, that forms, after a sufficient number of additions, a macroradical, as shown in Eq. (2).

$$\sim\!\sim\!\sim (M)_n \sim\!\sim\!\sim M° + M \longrightarrow \sim\!\sim\!\sim (M)_{n+1} \sim\!\sim\!\sim M° \text{ (rate constant } k_p) \quad (2)$$
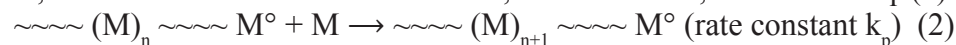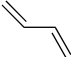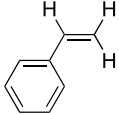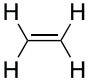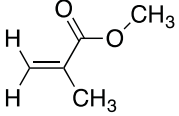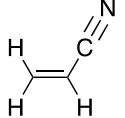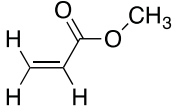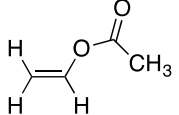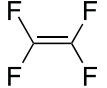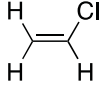
Both for kinetic and thermodynamic reasons, the head-to-tail placement is overwhelmingly predominant for free radical addition of monosubstituted unsaturated monomers (CH_2=CHR) that yield polymer chains where tertiary carbon atoms and methylene groups alternate. Monomers suitable for free radical chain polymerization show varying degrees of reactivity depending on the affinity of the free radical for its monomer. The rate constants for propagation of common unsaturated monomers range between 10^2 and 10^4 $L \cdot mol^{-1} \cdot s^{-1}$ (as shown in Table 1). By comparing the effects of substituents on the stability of the free radical, higher propagation rate constants are observed for less stabilized active centers. However, for achieving the formation of chains with a high degree of polymerization, the reactivity of free radicals has to be mainly directed towards propagation, limiting competing reactions of charge transfer.

Step 3 – Chain termination

Active free radicals in the polymerization of unsaturated monomers are unstable and tend to undergo self-annihilation when on occasion randomly encountering another free radical. This bimolecular process results in the termination of the molecular chains propagated by two encountering macroradicals. Termination occurs either by combination or by disproportionation, which yields a single macromolecule or saturated and unsaturated polymer chains. Combination is the simplest mechanism where the two macroradicals overlap their singly occupied molecular orbital to form a stable σ bond, resulting in the

Table 1. Propagation rate constants k_p for common monomers undergoing free radical polymerization.

Monomer	Structure	k_p [L·mol^{-1}·s^{-1})] at T = 60°C[a]
Butadiene		100
Styrene		165
Ethylene		242
Methyl methacrylate		515
Acrylonitrile		1 960
Methyl acrylate		2 090
Vinyl acetate		2 300
Tetrafluorethylene		9 100 (83°C)
Vinyl chloride		11 000 (50°C)

[a] At T = 60°C, unless otherwise specified. Data were collected from Ref. [5].

formation of a polymer which is the sum of monomer units added by each one of the participating chains (Eq. (3)). Disproportionation is a redox process yielding a hydrogen saturated macromolecule together with its omega unsatu-

rated counterpart (Eq. (4)). This takes place *via* the abstraction of a hydrogen atom at the saturated carbon next to the active center by the other macroradical. The activation energy required for the abstraction process is generally much higher than the straightforward combination of the two macroradicals. As a consequence, for a number of polymers (*e.g.* poly(methyl acrylate), polyacrylonitrile, polystyrene), disproportionation takes place as a minor mechanistic pathway compared to combination. Disproportionation competes significantly and may become the predominant termination process when the propagating radical is sterically hindered, as in methyl methacrylate polymerization.

$$\sim\sim\sim M_n \sim\sim\sim CH_2{-}HRC° + °CHR{-}CH_2 \sim\sim\sim M_p \sim\sim\sim \rightarrow \sim\sim\sim M_{n+p+2} \sim\sim\sim \quad (3)$$

$$\sim\sim\sim M_{nv} \sim\sim\sim CH_2{-}HRC° + °CHR{-}CH_2 \sim\sim\sim M_p \sim\sim\sim \rightarrow$$
$$\sim\sim\sim M_n \sim\sim\sim CH_2{-}CH_2R + RHC{=}CH \sim\sim\sim M_p \sim\sim\sim \quad (4)$$
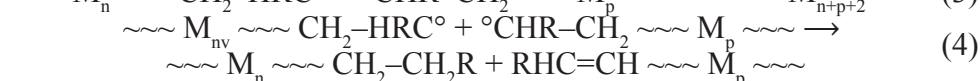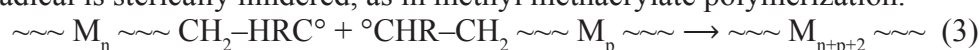
Step 4 – Chain transfer
Chain transfer can be considered as a competing process to propagation. Instead of adding to a monomer, the growing macroradical can react with various types of molecular compounds present in the reaction medium: the initiator, solvent, dead polymer, impurities, or any transfer agent, introduced purposely in the reaction medium to obtain a desired effect on the resulting molecular weight (MW) or on end group functionalization.

The transfer reaction can be depicted by an exchange of an atom by a free radical mechanism, the macroradical abstracting an atom, A, to form a stable polymer molecule fitted with A as an end group, generating the free radical B° (Eq. (5)).

$$\sim\sim\sim M_n \sim\sim\sim CH_2{-}HRC° + A{-}B \rightarrow \sim\sim\sim M_n \sim\sim\sim CH_2{-}HRC{-}A + B° \quad (5)$$

$$B° + n\,M \rightarrow B{-}M_n° \quad (6)$$
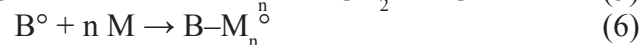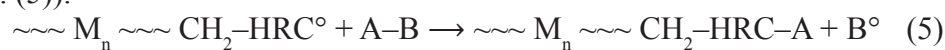
Chain transfer can compete with propagation in a process where the active center of a growing polymer chain is transferred to various components in the polymerization medium, such as solvent, monomer, initiator, polymer or to a purposely selected additive (a transfer agent). Transfer reactions occur easily with the use of a chlorinated solvent ($CHCl_3$) or with a solvent having an easily abstractable H atom (isopropanol), a monomer, or a polymer. When the molecule subject to the transfer process is a macromolecule formed earlier in the reaction medium, the chain growing from the main polymer backbone will create a side chain. The repetition of this phenomenon leads to multi-branched polymers.

The occurrence of this event terminates the chain involved with the macroradical, but the active site is transferred to another radical, B°, which can restart a new chain polymerization (Eq. (6)). In such a case, the instantaneous number of growing chains is kept constant, with little or no effect on the polymerization rate. The impact of transfer on the average length of the formed polymer chain is discussed below.

2.2. KINETIC ASPECTS OF FREE RADICAL CHAIN POLYMERIZATION

Because of the fast bimolecular combination of free radicals in fluid media, the chain reaction kinetics of free radical polymerization is governed by a steady state that results from the balance between the formation of new growing chains yielded by initiator decomposition and by the addition to the first monomer unit M (Eqs. (7a) and (7b)) and the radical disappearance by termination (Eq. (8)).

$$\text{Initiator decomposition} \quad I \longrightarrow 2\,R° \quad \text{(rate determining)} \qquad (7a)$$
$$\text{Formation of chain initiating radical} \quad R° + M \longrightarrow R\text{–}M_1° \qquad (7b)$$
$$\text{Termination} \quad \sim\sim M_i° + \sim\sim M_j° \longrightarrow \sim\sim M_{i+j} \sim\sim \text{ or } \sim\sim M_i' + \sim\sim M_1' \qquad (8)$$
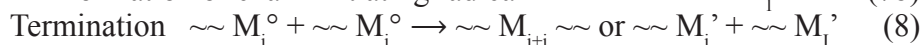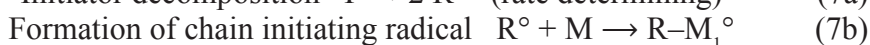
The dynamic balance is expressed by equal rates for initiation and for termination yielding

$$2\,f\,k_d\,[I] = 2\,k_t\,[M°]^2 \qquad (9)$$

where: f – the efficiency factor of free radicals involved in the chain initiation, k_d – the rate constant for initiator decomposition, k_t – the rate constant for the termination reaction, $[M°]$ – the concentration in propagating free radicals.

Considering typical values for the rate of reaction (7b) ($R_i \approx 10^{-4}\text{-}10^{-6}$ mol·L^{-1}·s^{-1}) and for the bimolecular termination rate constant for Eq. (8) ($k_t \approx 10^6\text{-}10^8$ L·mol^{-1}·s^{-1}), a steady state for free radical concentration is reached within a fraction of a second. The steady-state value of a propagating free radical concentration can be introduced in the expression of the polymerization rate, R_p, defined as the rate of monomer consumption in the propagation step,

$$R_p = k_p\,[M]\,[M°] \qquad (10)$$

yields

$$R_p = k_p\,(f\,k_d/k_t)^{0.5}\,[M]\,[I]^{0.5} \qquad (11)$$

where k_p is the rate constant for propagation. Rate constants k_p are in the range $10^2\text{-}10^4$ L·mol^{-1}·s^{-1}, depending on the structure of the unsaturated monomer. A much higher value of k_t compared to k_p does not prevent propagation because the radical species are present in very low concentrations (typically 10^{-8} mol·L^{-1}) and because R_p is inversely proportional to the square root of k_t.

Besides the polymerization rate, of importance in free radical chain polymerization is the kinetic chain length, λ. In a chain process unaffected by transfer reactions, the kinetic chain length is defined as the average number of propagation steps for each initiation. This quantity corresponds to the ratio of the polymerization rate, R_p, to the initiation rate, R_i, or to the termination rate, R_t, since the latter two quantities are equal. In chain polymerization, it is worth noting that λ represents the average number of monomer molecules added to a growing chain at the moment it is deactivated by termination. Depending on the relative contribution of disproportionation and combination to the overall termination process, the terminated polymer chain will exhibit a number-aver-

age degree of polymerization ($\overline{DP}_n$) between 1 (only disproportionation) and 2 (only combination) times the λ value.

The kinetic data derived from the chain kinetic model are instantaneous values subject to changes in the physical parameters for the reaction, such as temperature and viscosity. Autoacceleration occurs in radical chain polymerization and normally in bulk polymerization. As monomer conversion increases, the gradual formation of polymer in the reaction medium increases the viscosity, essentially reducing the efficiency of chain termination by reducing the diffusion of the macroradicals. This change in viscosity has little effect on initiation and propagation, but it results in a strong increase of the free radical concentration. Autoacceleration, called the Trommsdorff-Norrish effect, is particularly effective when multifunctional monomers are involved in the polymerization.

Chain transfer reactions reduce the average molecular weight of the final polymer while keeping constant the total number of free radicals. Therefore, transfer reactions have no direct effect on polymerization rate, but can be used to control the average degree of polymerization to form chains, acting on the kinetic chain length $\lambda = R_p/(R_i + R_{tr})$, where $R_{tr} = k_{tr}[M_i°][TA]$ is the rate of the transfer reaction to the transfer agent TA. Thiols are particularly efficient in this.

2.3. POLYMERIZATION THERMODYNAMICS

As polymerization reactions convert a large number of monomer molecules into a few macromolecular chains, they are generally associated with a strong decrease of entropy ($\Delta S_p < 0$). This situation impacts the free energy state function $\Delta G_p = \Delta H_p - T\Delta S_p$ that governs what happens to the chemical transformations. Polymerization can proceed if the enthalpy variation is exothermal enough ($\Delta H \ll 0$), so that the net balance appearing in ΔG_p is negative. Monosubstituted unsaturated monomers typically exhibit polymerization enthalpies ranging from 70 to 90 kJ·mol⁻¹. This generally allows for an efficient polymerization to proceed if the monomer concentration is high enough. Taking into account the reversibility of the propagation step of free radical polymerization, the growth of chains is stopped when the free energy $\Delta G_p = \Delta H_p° - T\Delta S_p° - RT \ln[M]$ approaches 0. At a given monomer concentration, the temperature increases to a critical value $T_c = \Delta H_p°/(\Delta S_p° + R \ln([M]_c)$, called the ceiling temperature. The polymerization of vinyl acetate, methyl acrylate and styrene is not significantly affected by thermodynamic constrains under normal polymerization conditions, but for methyl methacrylate, a monomer exhibiting a lower enthalpy of polymerization due to the presence of a methyl substituent on the double bond, the ceiling temperature is 220°C for pure monomer.

2.4. MICROSTRUCTURE OF POLYMER CHAINS

Chain polymerization of vinyl monomers ($CH_2=CHR$) yields polymers having stereocenters ($-CH_2-C^*HR-$) which can exhibit either of two different configurations. Free radical propagation is weakly sensitive to the influence of the stereocenter located at the penultimate unit on the macroradical. This results in a weak preference for the formation of a syndiotactic dyad with respect to an isotactic one at each propagation step. The final polymers are therefore essentially atactic in terms of microstructure and are amorphous materials.

2.5. CONTROLLED FREE RADICAL POLYMERIZATION

The limitations due to the termination reactions taking place during conventional free radical polymerization have been overcome by using various molecules, metal complexes or stable free radicals that convert the growing

- Nitroxide-mediated polymerization

$$P_n\text{-}T \underset{k_{deact}}{\overset{k_{act}}{\rightleftharpoons}} P_n° + T° \qquad k_t \qquad T° = \underset{R \quad R}{\overset{O°}{N}}$$

with propagation k_p, $+ M$

- Atom transfer radical polymerization

$$P_n\text{-}X + Mt^n/L \underset{k_{deact}}{\overset{k_{act}}{\rightleftharpoons}} P_n° + X\text{-}Mt^{n+1}/L \qquad Mt^n/L = Cu(I)Cl/ligand$$

with k_t, propagation k_p, $+ M$

- Reversible addition fragmentation chain transfer

$$P_m° + P_n\text{-}X \overset{k_{exchange}}{\rightleftharpoons} P_m\text{-}X + P_n° \qquad Y\text{-} = \underset{Z \quad Y\text{-}}{\overset{Y}{C}}$$

with k_t, k_p, $+ M$ on each side

Scheme 3. Principles of the three main methods for achieving controlled free radical polymerization.

free radicals into a dormant species, thus dramatically reducing the occurrence of termination [6]. Controlled free radical polymerization (CRP) can be achieved by using stable free radicals as nitroxides (nitroxide-mediated polymerization, NMP), by reversible addition-fragmentation chain transfer (RAFT) to various thiocarbonyl compounds, or by halogen atom transfer from a transition-metal--catalyst subject to a redox exchange (atom transfer radical polymerization, ATRP), as shown in Scheme 3. The active center is capable of reactivation, functionalization, and chain extension to form block copolymers and even more complex polymer architectures. The potential of CRP differs from ionic living polymerization processes because of the tolerance of the selected reversible chemistries to a variety of functional monomers and to unconventional polymerization media.

2.6. FREE RADICAL COPOLYMERIZATION

Chain polymerizations can be carried out with mixtures of two or more monomers to form polymeric products with an almost unlimited composition and structure, hence with new properties. The monomers enter into the copolymer in amounts determined by their relative concentrations and reactivity. Whereas alternating, statistical and random copolymers are produced by simultaneous and competing polymerization of monomer mixtures, graft and block copolymers result from a sequence of separate polymerizations. The instantaneous composition of a copolymer produced by a chain process cannot be determined simply from knowledge of the homopolymerization rates of the two monomers. The relative contribution of cross-propagation with respect to the homopolymerization is described by using the reactivity ratios of each monomer. For a mixture of two monomers, the first order Markov model for copolymerization assumes that the reactivity of the propagating species is dependent only on the monomer unit at the end of the chain, with there being four possible propagation reactions (Scheme 4).

Initiation

$$I \rightarrow 2\,R°$$
$$R° + A \rightarrow RA° \qquad\qquad R° + B \rightarrow RB°$$

Propagation

$$\sim\sim\sim\sim A° + A \rightarrow \sim\sim\sim\sim A°\ k_{aa} \qquad \sim\sim\sim\sim A° + B \rightarrow \sim\sim\sim B°\ k_{ab}$$
$$\sim\sim\sim B° + B \rightarrow \sim\sim\sim\sim B°\ k_{bb} \qquad \sim\sim\sim\sim B° + A \rightarrow \sim\sim\sim\sim A°\ k_{ba}$$

Termination

$$\sim\sim\sim\sim A° + °A \sim\sim\sim\sim \rightarrow \sim\sim\sim\sim A\text{-}A \sim\sim\sim\sim\ k_{t,aa}$$
$$\sim\sim\sim\sim A° + °B \sim\sim\sim\sim \rightarrow \sim\sim\sim\sim A\text{-}B \sim\sim\sim\sim\ k_{t,ab}$$
$$\sim\sim\sim B° + °B \sim\sim\sim\sim \rightarrow \sim\sim\sim\sim B\text{-}B \sim\sim\sim\sim\ k_{t,bb}$$
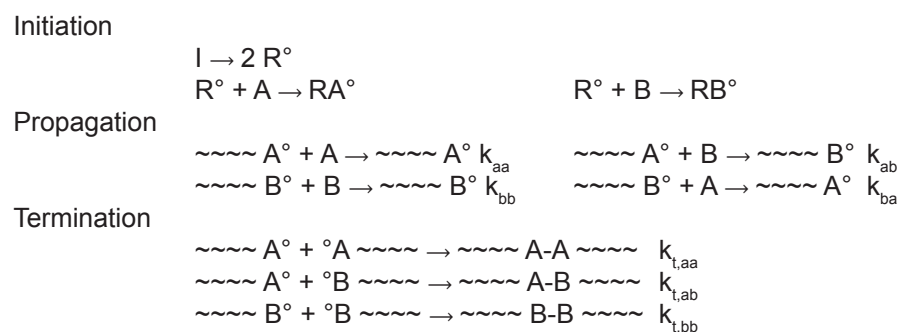
Scheme 4. First order Markov model for the free radical copolymerization of monomers A and B.

The reactivity ratios of both monomers with respect to the macroradicals fitted with A° and B° as the propagating end groups, $r_a = k_{aa}/k_{ab}$ and $r_b = k_{bb}/k_{ba}$, respectively, are the main parameters that govern the instantaneous rate of incorporation of both monomers in the growing chains, for a given monomer composition in the reaction medium $f_a = [A]_t/([A]_t + [B]_t)$. The Mayo-Lewis relation (Eq. (10)), derived from the kinetic scheme of the terminal model, states how the instantaneous composition of the formed copolymer, $F_a = d[A]_t/(d[A]_t + d[B]_t)$, is dependent on the variable f_a and on the parameters r_a and r_b.

$$F_a = (r_a f_a^2 + f_a(1 - f_a))/(r_a f_a^2 + 2 f_a(1 - f_a) + r_b(1 - f_a^2)) \qquad (12)$$

An important feature of free radical copolymerization is the composition drift that is expected to take place during a batch process, and the distribution of monomer units along the chain that may ideally take place at random if $r_a \cdot r_b = 1$, or form alternating –A–B– sequences, or eventually produce isolated units of one monomer between blocks of the other.

3. RADIATION-INITIATED POLYMERIZATION

Compared to thermal and redox initiation processes, activation methods using radiation exhibit unique features that allow for a time and spatial control of polymerization. Several applications take advantage of these properties: the ultraviolet radiation or electron beam (UV/EB) curing of solvent-free coatings and inks in industry and in graphic arts, the synthesis of vinyl acetate or acrylate latices by emulsion polymerization initiated by using gamma rays, the out-of-autoclave curing of performance composites using EB and/or X-rays, laser or EB micropatterning and nanolithography for microfluidic and electronic devices [7].

Ultraviolet radiation and high energy electron beam radiation can trigger chain polymerization either by direct interaction with monomers or through the intermediacy of some other constituents present in the reaction medium.

3.1. PHOTOINITIATED POLYMERIZATION

Unsaturated monomers can be activated by short wavelength photons, by specific additives called photoinitiators that generate active centers (free radical or cationic species) upon exposure to an ultraviolet source. Radical initiation mechanisms either involve the direct homolysis of a C–C of the photoexcited initiator (Type I initiation with aromatic carbonyl compounds) or a cascade of reactions (Type II initiation by electron transfer and hydrogen abstraction), as shown in Scheme 5.
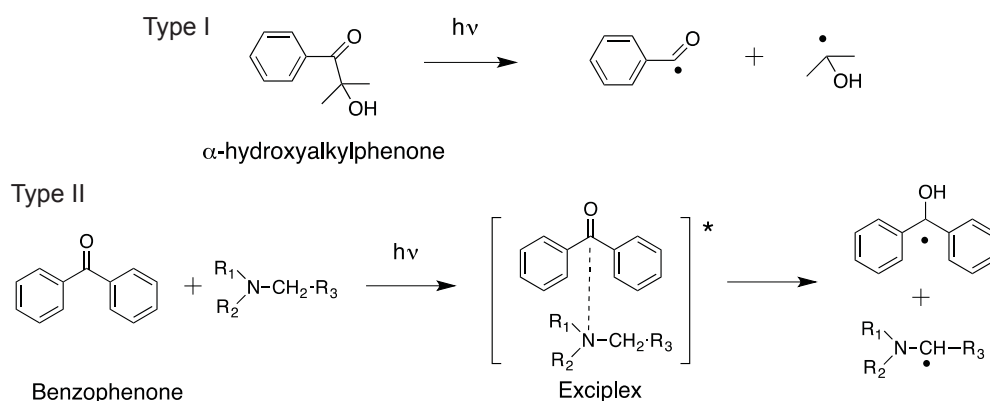
Scheme 5. Examples of Type I and Type II photoinitiators for free radical polymerization.

Aromatic onium salts can generate cationic active centers (Brønsted acids or carbenium ions) upon absorption of ultraviolet radiation [8]. There are two basic classes of cationic initiators grouped by dependence on the mechanisms of photolysis. The first group includes diaryliodonium and triarylsulfonium salts, which undergo fragmentation to yield aryl radicals and/or arylionium cation radicals. Dialkylphenacylsulfonium and dialkyl-4-hydroxyphenylsulfonium salts form the second group that generates yields and Brønsted acids by a reversible photolysis (Scheme 6).

$Y = BF_4, PF_6, AsF_6, SbF_6, B(C_6F_5)_4$
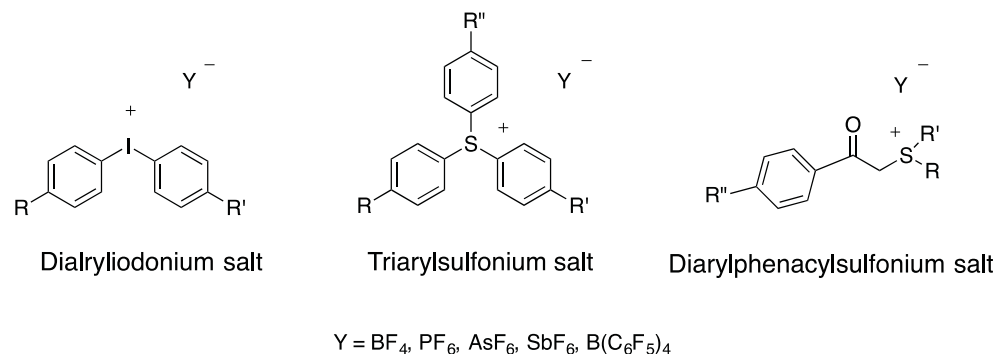
Scheme 6. Examples of onium salts used for radiation-initiated cationic polymerization.

Both classes of onium salts can be photosensitized in order to extend their response to long wavelength ultraviolet and to light. This can be achieved by energy transfer, electron transfer or through the intermediary of free radicals. A simplified description of the direct and sensitized pathways for the generation of cationic species from a diaryliodonium salt is represented in Scheme 7. Structural variations within the cations of onium salts have a marked influence on the photolytic efficiency, whereas the nature of anion mainly affects the course of the resulting cationic polymerization.
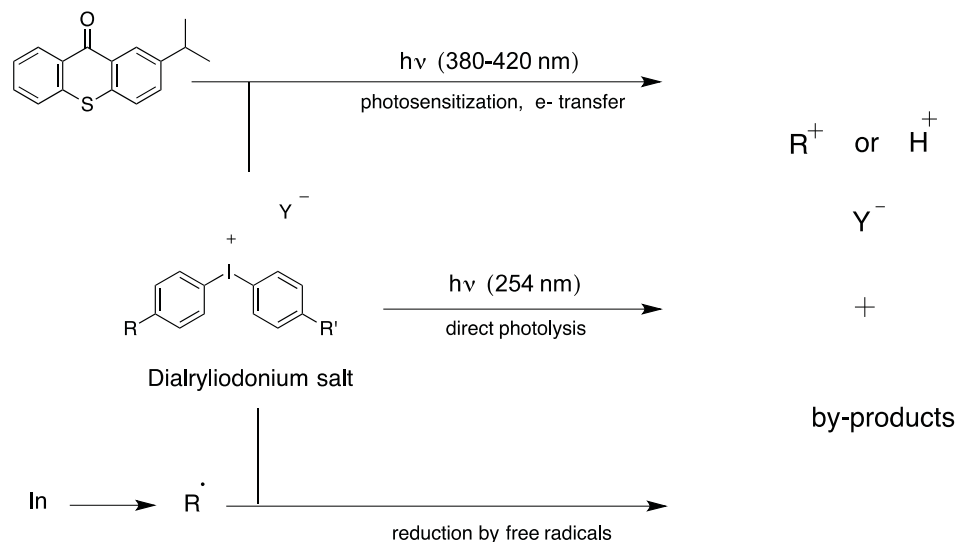
Scheme 7. Examples of onium salts used for radiation-initiated cationic polymerization ("In" is a source of free radicals generated by any type of mechanism).

3.2. POLYMERIZATION INDUCED BY HIGH ENERGY RADIATION

Despite the high intrinsic efficiency of commercial photoinitiators for free radical or for cationic polymerization, the effectiveness of photochemically triggered initiation is limited by the low penetration depth of ultraviolet radiation into opaque compositions. This is why accelerated electrons as well as photonic ionizing radiations (gamma and X-rays) have a significant advantage over ultraviolet radiation and light. Light is the visible range of the electromagnetic spectrum. The depth of penetration is much greater with less attenuation for ionizing radiation than for ultraviolet radiation and light. Pigmented coatings, printing inks but also adhesives and sealants sandwiched between non--transparent materials as well as fiber-reinforced composites can be cured by crosslinking polymerization of multifunctional monomer compositions.

The radiolysis of olefinic monomers produces cations, anions, and free radicals. Such species are capable of initiating chain polymerization. The cationic polymerization of isobutylene, of vinyl ethers, of epoxies, and of styrene and the anionic polymerization of acrylonitrile have been observed in the absence of additional initiators under controlled laboratory conditions. Long-lived cationic chain reactions involving carbenium or oxonium intermediates are unlikely because of the high reactivity of active centers that make transfers and deactivation reactions very fast unless special conditions (purity of involved chemicals, low temperature) are maintained throughout the process. For that reason, onium salts are used in the monomer composition.

From a practical perspective, most radiation polymerizations are mediated by free radicals, since at temperatures of technical relevance ionic species are not stable and dissociate to yield radicals.

Pulse radiolysis experiments on various mono- or multiacrylate monomers monitored by time-resolved spectroscopy have permitted a better understanding of the various pathways that lead to initiation. The mechanism [9] involves the attachment of a thermalized electron to an acrylate carbonyl group, and the subsequent formation of a radical anion dimer under the form of a charge transfer complex, or of a covalent adduct (Scheme 8). Protonation of the radical-anions yields the effective initiators for propagation. On the basis of experimental data, this model considers the direct formation of free radicals by homolytic dissociation of electronically excited molecular segments as a minor pathway, based on acrylates that were studied.
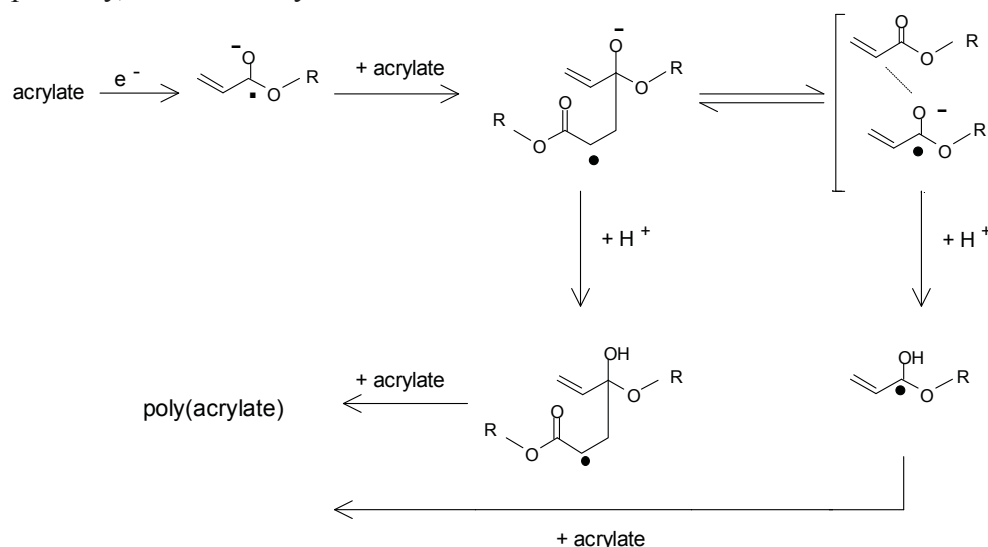
Scheme 8. Initiation mechanism for acrylate polymerization under high energy radiation [9].

The subsequent steps of the free radical polymerization follow the same pathway as that of conventional crosslinking polymerization initiated by thermal or redox processes. The specific aspects of the cationic polymerization of epoxies are discussed below. Contrary to the mechanism of onium salt photolysis upon selective absorption of ultraviolet radiation, the dominant pathway under ionizing radiation in a medium rich in monomers is the production of free radicals which can reduce the onium salt, and generate in a second stage carbenium cations (Scheme 9). Reduction of the onium salt can also occur from its interaction with solvated electrons (reduction pathway). This mechanism was confirmed by pulse radiolysis experiments on diglycidyl ether of bisphenol A (DGEBA) in the presence of an iodonium salt [7].
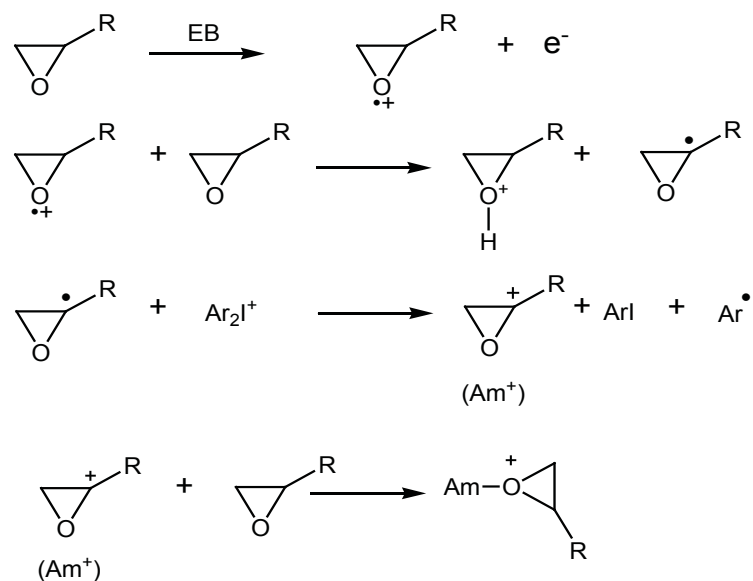
Scheme 9. Initiation mechanism for epoxy polymerization under high energy radiation.

Initiation
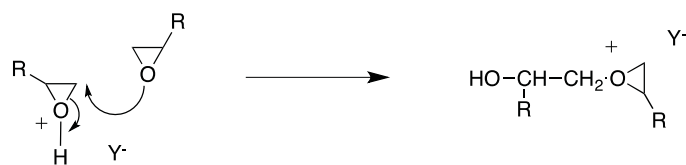
ACE propagation
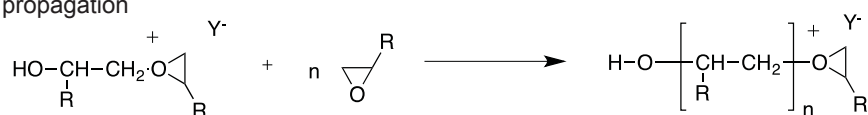
AM propagation
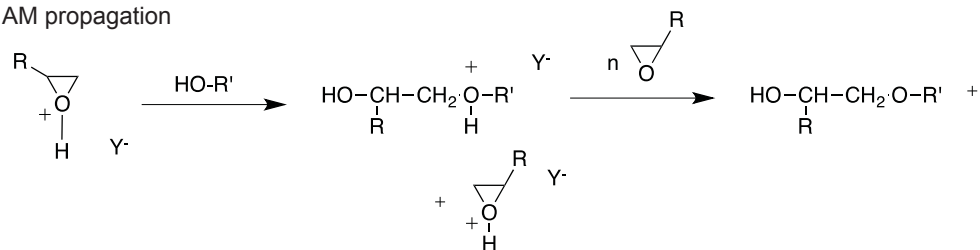
Transfer reaction
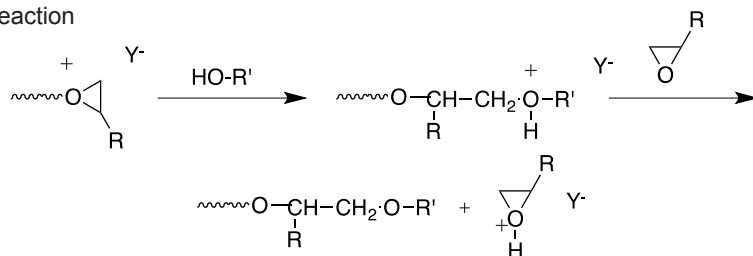
Scheme 10. Propagation and transfer reactions during the cationic polymerization of epoxides.

Cationic chain propagation results from the reaction of oxonium ions with epoxy monomers by activated chain end (ACE) or activated monomer (AM) mechanisms. The ACE mechanism consists of the repeated addition of the monomer on the growing chain by the nucleophilic attack of the oxygen from the epoxy monomer on the carbon atom adjacent to the oxonium ion (Scheme 10). The AM mechanism takes place in presence of hydroxyl containing species and involves their addition to the protonated monomer followed by a charge transfer. The activated monomer is then regenerated and can react again with a hydroxylic compound. As the epoxy ring opens, hydroxyl groups are formed which favor the AM mechanism. Other transfer reactions can take place between an active chain and nucleophilic species such as water, alcohol or any other hydroxylic compounds resulting in the liberation of a proton and an inactive oligomer.

Two cationic species cannot react together. Thus, no termination reaction occurs by self-quenching of the active centers, as in the case of free radical processes. Once irradiation has ceased, cationic polymerization will continue to propagate without new initiation, by the so-called dark cure phenomenon, until the active centers are trapped in a glassy network or quenched by some inhibitor entering the material. This behavior enables further thermal activation giving rise to some benefits of post-curing.

3.3. GENERAL AND SPECIFIC FEATURES
OF RADIATION-INDUCED POLYMERIZATION

One of the attributes of radiation as an alternative mode for activating chemical reactions is the immediacy and the control of the spatial distribution for generating active centres. The ability to trigger polymerization reactions independent of temperature is of interest for decoupling the influence of thermal activation on the various steps of the chain polymerization mechanism that follow initiation. This last feature can be exploited both from a fundamental perspective (mechanistic studies, determination of activation energies, pulse laser polymerization) and for technical reasons (design of low cost molding equipment, use of temperature sensitive substrates, design of thermal post--treatments).

The crosslinking polymerization of multifunctional monomers and pre--polymers is by far the largest use of this technology. Various analytic methods can be used for monitoring the kinetic behavior of polymerizable compositions exposed to ultraviolet radiation, to light and to ionizing radiation [7] and for studying the influence of the processing conditions on the properties of the materials produced. A selection of results illustrates some of the important aspects of polymerization kinetics and of network formation.
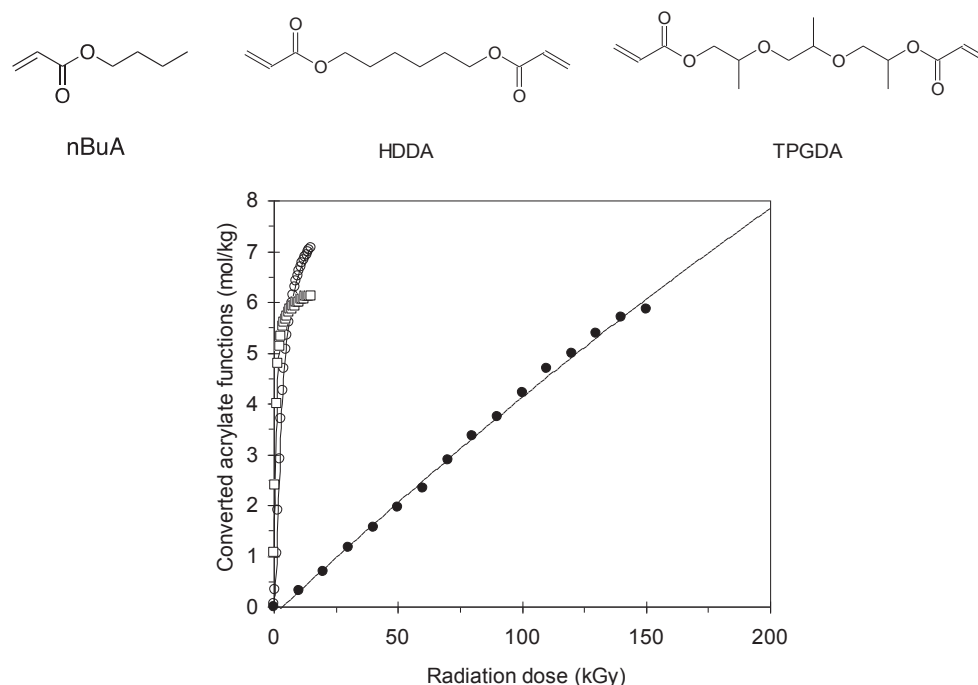
Fig.1. Kinetic profiles of acrylate consumption in monomer films as a function of EB radiation dose: nBuA (●), TPGDA (□) and HDDA (○).

The gel effect associated with crosslinking polymerization is shown by comparing the kinetic profiles under exposure to increasing EB doses of a monoacrylate (n-butylacrylate, nBuA) with those of diacrylates (hexanediol diacrylate, HDDA and tripropyleneglycol diacrylate, TPGDA). All three monomers exhibit similar initial acrylate functionality content (7-8 mol·kg^{-1}). The plots of Fig.1 clearly show that diacrylates polymerize much faster than nBuA, as a result of the Trommsdorff effect. The extremely fast polymerization of compositions including multiacrylates is used in ink formulations for graphic arts and for coatings for optical fibers, with curing speeds under high energy radiation as high as 1000 m·min^{-1} on high-performance industrial lines.

The viscosity of solvent-free radiation-curable compositions typically ranges from 0.5 to 5 Pa·s at application temperatures which facilitates the spreading of the composition onto a substrate or the impregnation of the composition as the matrix in a composite material. Since polymerization is aimed at converting the monomer and prepolymer blend into a hard material, curing proceeds with a dramatic evolution of the mobility of monomer functions in the medium, from the initially fluid state, to a gel, and eventually to a vitreous network. The viscosity gradually increases by several orders of magnitude until solidification, being influenced by polymerization kinetics.

An instructive result was obtained by comparing the polymerization profile of an aliphatic polyurethane triacrylate (APU3), which has an initial acrylate

A

B
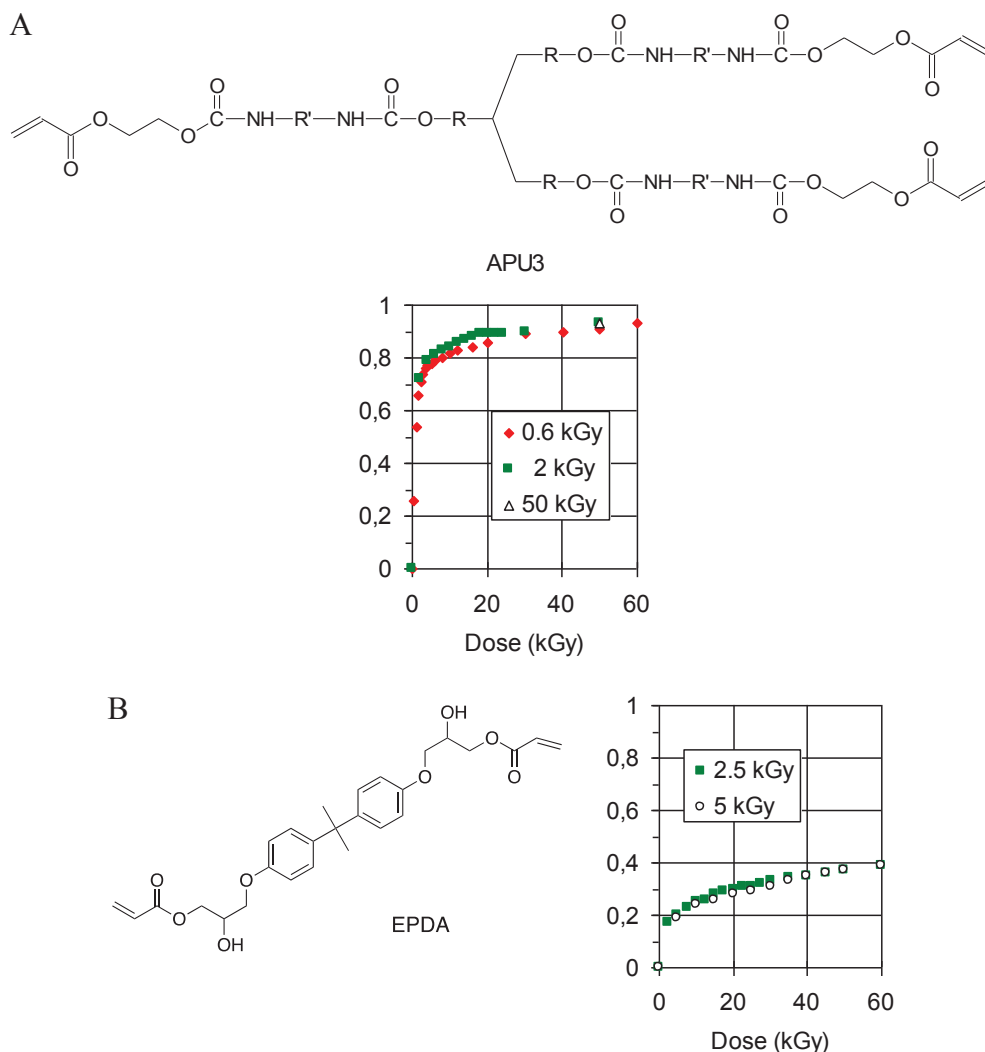
Fig.2. Kinetic profiles of acrylate consumption in pre-polymer films as a function of EB radiation dose: APU3 (A) and EPDA (B).

content of 3.5 mol·kg^{-1}, with those observed for an aromatic epoxydiacrylate (bisphenol A epoxy diacrylate, EPDA) with an initial acrylate content of about 6 mol·kg^{-1}, being subjected to various EB dose increments (as shown in Fig.2). The polyurethane pre-polymer possesses a flexible backbone that forms a soft material upon curing. Its kinetic profile shows a steep increase in acrylate fractional conversion, up to 0.75 for a dose lower than 10 kGy, regardless of the dose increment (Fig.2A). The profile then gently levels off to reach a conversion level higher than 0.9. The corresponding plot recorded for the aromatic epoxy diacrylate shows an initial fast polymerization to a conversion level of 0.2 for a dose of 2.5 kGy, followed by a weak reactivity with a rather small increase of conversion up to 0.4 at 60 kGy (Fig.2B). At this point, the concen-
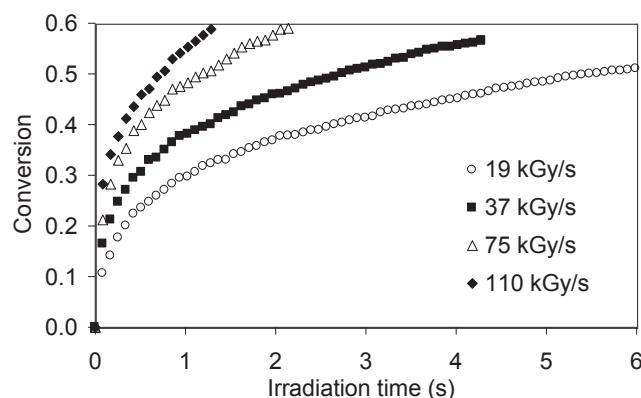
Fig.3. Kinetic profiles of acrylate consumption in EPAD pre-polymer as a function of EB radiation dose rate.

tration of unreacted acrylate functionality is about 3.6 mol·kg^{-1}, a value that is even higher than the acrylate concentration in the unreacted APU3 sample. This shows the influence of incipient vitrification that limits the propagation step, in spite of there being a still large concentration of monomer in the partially cured EPAD samples. These experiments were conducted at room temperature with small increments of dose using thin films of the curable compositions which limited any increase in temperature. Under these quasi-isothermal conditions, vitrification took place in the PUA3 material at conversion levels slightly above 0.7, the critical value at which the kinetics started to level off. The vitrification phenomenon took place at much lower conversion levels (typically 0.2) in the more rigid EPAD pre-polymer when cured at room temperature. These observations stress the importance of the relation between the effective curing temperature and the conversion dependence of the glass transition on the material networks.

The influence of dose rate on polymerization kinetics can be examined, provided that isothermal conditions are maintained within the sample. The results of a series of EB curing experiments conducted with EPAD at different dose rates ranging from 19 to 110 kGy·s^{-1} are plotted in Fig.3.

The rate of polymerization measured in the initial regime (steep increase) was shown to be proportional to the square root of the dose rate $\dot{D}$, as would be expected from the bimolecular termination kinetics in a fluid medium (Eq. (13)).

$$R_p = \frac{k_p R_{init}}{2\sqrt{k_t}} [C = C] \propto \frac{k_p}{2\sqrt{k_t}} [C = C] \left(\dot{D}\right)^{0.5} \qquad (13)$$

Deviations from this law were observed as soon as the initial slope weakened as a consequence of mobility being restricted. From the lines drawn in the final regime, a first order dependence of the polymerization rate on $\dot{D}$ was observed. This situation corresponds to a chain process with monomolecular termination by occlusion of the growing free radicals in a vitrified matrix.

From a practical viewpoint, careful attention must be paid to the thermal effects within a sample subjected to radiation-induced polymerization. There should be a finely-tuned interplay between the control of the polymerization exotherm (typically 80 and 100 kJ·mol^{-1}, for acrylates and epoxy functionality, respectively), the energy conversion from the deposited radiation dose, the heat and radiative exchanges with the surrounding environment and the conversion dependence of vitrification.

3.4. APPLICATIONS OF RADIATION-INDUCED POLYMERIZATION

High energy radiation can be used to synthetize linear polymers by emulsion free radical polymerization, but is rarely done. The process consists of irradiating an oil-in-water dispersion of one or several hydrophobic monomers in the presence of a surfactant. Hydroxyl radicals are produced by water radiolysis and are the main species responsible for the polymerization initiation after entering the monomer micelles. This process results in the formation of latex particles with the typical dimension of about 100 nm. The particles grow in size during the reaction since monomers continue to diffuse from reservoir droplets and to swell the polymer particle. Since initiation occurs at a slow rate in the aqueous phase, the kinetic chain length inside a single particle is extremely long producing polymer chains of high molecular weight. Emulsion polymerization is used to manufacture several commercially important polymers that find use in adhesives, coatings, paper coatings and textile coatings. Low dose rate ^{60}Co gamma radiation can be used as an efficient initiating process which can be used as alternative to thermal initiation of peroxides under modest heating conditions. The radiation process makes it possible to decouple the thermal activation of the polymerization from the initiation step and thus avoids affecting the chain length of the formed polymers. This is likely to receive increasing interest for commercial developments in the coming years.

Solvent-free formulations of adhesives, inks and coatings can be cured by radiation-induced crosslinking polymerization. This important use is expanding as a an alternative to solvent-based and/or heat-curing processes which are being restricted because of their detrimental impact on the environment. Radiation processing brings several important benefits in terms of ecoconception (energy saving, limitation of volatile organic compound (VOC) emission). *In-situ* polymerization of restorative resins infused into damaged archeological objects made of wood or into weak artistic pieces of porous structure is another illustration of the unique in-depth chemical effects that can be created using the mild ambient conditions of high energy radiation processing.

Compared to ultraviolet-initiated polymerization, a well-established technology for the curing of various coatings and inks, high energy radiation processing proves to be more efficient than intense ultraviolet for initiating in depth

the crosslinking polymerization of solvent-free compositions, including unsaturated monomers and reactive pre-polymers to yield mechanically functional and chemically resistant materials. Printed labels and materials produced by the packaging industry are fully cured using high energy EB and do not need initiators for free radical polymerization. This results in lower amounts of unreacted monomers and other extractable compounds. Adhesion to substrates can also be improved by grafting reactions that take place at the substrate-coating interface. Advances in improved formulations and in process control spur on developments in food packaging and in industrial coatings (flooring, building parts with long resistance to long outdoor environment).

Fiber-reinforced polymer composites can also be efficiently cured by high energy electron beams and offer significant advantages for the manufacture of a variety of aerospace, ship and ground vehicle components. The EB curing process is shorter than for conventional thermosets and yields materials with reduced residual internal stress. Innovative formulation concepts based on polymerization-induced phase separation achieve higher mechanical performance than state-of-the-art thermally cured materials. Advanced studies on network formation provide an understanding of structure-properties relationships.

Finally, the spatial control of radiation-induced polymerization is used in making photomasks. These are used in the microelectronics industry for producing opaque plates with holes or transparencies for patterning a photopolymerizable composition in the domains that are exposed to the frontal beam of ultraviolet radiation. After development in an appropriate solvent a negative
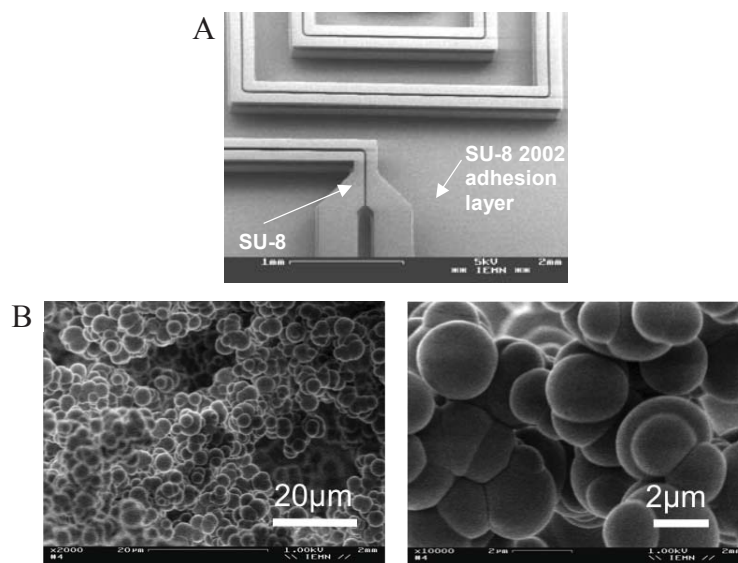
Fig.4. Scanning electron micrographs of a microchannel made by cationic photolithography (A), and porous polymer monoliths synthetized within a closed microsystem by EB-initiated polymerization (B).

photoresist is obtained. Micro- and nanowriting with a laser and/or an electron beam scanned across the radiation sensitive composition avoids using an optical mask and produces much finer patterns and lower resolutions.

Figure 4A shows the scanning electron micrograph of a channel fabricated on a chip by the photomasking process using the cationic photopolymerization of an aromatic epoxide. In a subsequent step, the channels were covered by a lid and a porous polymer monolith was polymerized *in situ* using EB radiation using an acrylate composition dissolved in a mixture of porogenic and precipitating solvents (Fig. 4B). The interconnected polymer-sphere morphology obtained by this technique can be used for producing microreactors and separation microcolumns for lab-on-a-chip applications [10].

4. CONCLUSIONS

Ultraviolet radiation and high energy electron beam radiation efficiently initiate free radical or ionic polymerization depending on the experimental conditions, on the type monomer being used and on the presence of initiators that may be needed. Besides the specific features of radiation-triggered initiation, the basic mechanisms and kinetic models of conventional chain polymerization presented above can be used. However, the specific conditions of radiation processing, dose deposition, dose rate effects as well as thermal effects should be carefully considered. Many end uses can benefit from the numerous advantages offered by radiation processing. Some areas of considerable technical relevance are addressed in specific chapters, such as the radiation synthesis of nanoparticles, radiation grafting, and composite materials.

REFERENCES

[1]. Chapiro, A. (2004). Radiation effects in polymers. In *Encyclopedia of materials: Science and technology* (2nd ed.). Amsterdam: Elsevier.
[2]. Smith, B.W., & Suzuki, K. (2007). *Microlithography: science and technology* (2nd ed.). Boca Raton: CRC Press.
[3]. Ferry, M., Ngono-Ravache, Y., Aymes-Chodur, C., Clochard, M.C., Coqueret, X., Cortella, L., Pellizzi, E., Rouif, S., & Esnouf, S. (2016). Ionizing radiation effects in polymers. In *Reference module in materials science and materials engineering*. Amsterdam: Elsevier. http://dx.doi.org/10.1016/B0-08-043152-6/01918-5.
[4]. Matyjaszewski, K., & Davis, T.P. (2003). *Handbook of free radical polymerization*. New York: John Wiley & Sons.

[5]. Odian, G. (2004). *Principles of polymerization* (4th ed.). New York: John Wiley & Sons.

[6]. Matyjaszewski, K., & Davis, T.P. (2003). *Handbook of free radical polymerization*. New York: John Wiley & Sons.

[7]. Fouassier, J.P., & Lalevée, J. (2012). *Photoinitiators for polymer synthesis: scope, reactivity, and efficiency*. Weinheim: Wiley VCH.

[8]. Crivello, J.V., Walton, T.C., & Malik, R. (1997). Fabrication of epoxy matrix composites by electron beam induced cationic polymerization. *Chem. Mater., 9*, 1273-1284.

[9]. Knolle, W., & Mehnert, R. (1995). On the mechanism of the electron-initiated curing of acrylates. *Radiat. Phys. Chem.*, *46*, 963-974.

[10]. Chuda, K., Jasik, J., Carlier, J., Tabourier, P., Druon, C., & Coqueret, X. (2006). Characteristics and fluidic properties of porous monoliths prepared by radiation--induced polymerization for Lab-on-a-Chip applications. *Radiat. Phys. Chem.*, *75*, 26-33.

IONIZING RADIATION-INDUCED CROSSLINKING AND DEGRADATION OF POLYMERS

Giuseppe Spadaro, Sabina Alessi, Clelia Dispenza
Università degli Studi di Palermo, Dipartimento di Ingegneria Chimica, Gestionale, Informatica, Meccanica, Edificio 6, Viale delle Scienze, 90128 Palermo, Italy

1. INTRODUCTION

The interaction of ionizing radiation with matter results in the formation of very reactive species (free neutral radicals, cationic and anionic ions, excited molecules). These can significantly modify the molecular structure of the irradiated material. In particular, irradiation of organic polymers induces molecular chain branching, crosslinking and molecular degradation or scissioning. Chain branching and crosslinking increase the molecular weight of the polymer. Crosslinking forms an insoluble three-dimensional polymer network; while degradation or scissioning causes a reduction of the initial molecular weight [1, 2].

During irradiation, all these phenomena coexist and their prevalence depends on several factors, such as the initial molecular structure and morphology of the polymer and the irradiation environment. If the polymer is irradiated in presence of air, the molecular modifications are different with respect to the effects of irradiation in vacuum or in presence of an inert gas. During irradiation in air, the free radicals, produced by interaction of ionizing radiation and polymers, can also react with oxygen, giving rise to oxidative degradation, which competes with other reactions that occur in absence of oxygen.
All these molecular modifications can modify the properties of the material.

Studies have been devoted to understanding the mechanisms of the modification of the molecular structures and of the properties of polymers resulting from exposure to ionizing radiation.

Such studies are of importance for using polymeric materials in radiative environments, such as in nuclear power plants, in space or in the sterilization of polymeric medical disposables or of food plastic packaging [3-8].

The irradiation of polymers is a very useful industrial process, an alternative to the more traditional chemical processes, which induce or modify some

material properties. Some industrial applications are the crosslinking of wire and cable insulation, the formation of heat recoverable films and tubings, foams, and the degradation of some polymers to help produce powders used in non- -stick or release applications [9-11].

Regardless of the different kinds of molecular modifications induced by irradiation, it is possible to divide the polymers in three categories, related to their resistance to ionizing radiation.

Highly radiation-resistant polymers are characterized by an almost un- modified molecular structure up to the absorbance of doses in the range of 250-1000 kGy in air. These polymers contain aromatic groups in their molecular structure, such as polyimides, polyphenyl ethers, polyphenyl ketones, aromatic polyamides, polysulphones, polyetherimides, epoxy resins, polyphenylene sul- phide, polyethylene terephthalate, polyethersulphones, polyphenylene oxides.

Aliphatic polyethers, aliphatic polysulphones and polymers containing C–Cl bonds in the macromolecular structure are highly sensitive to irradiation; their molecular structures undergo dramatic changes after the absorption of only a few tenths of a kGy in air.

Polymers such as polyolefines, polyamides and aliphatic polyesters present an intermediate resistance.

2. MOLECULAR MODIFICATIONS OF IRRADIATED POLYMERS

2.1. IRRADIATION UNDER VACUUM

When polymers are irradiated under vacuum or in presence of an inert gas, their molecular modifications depend only on their initial molecular structure and morphology. Ionizing radiation of polymers causes chain branching, cross- linking or scissioning (degradation).
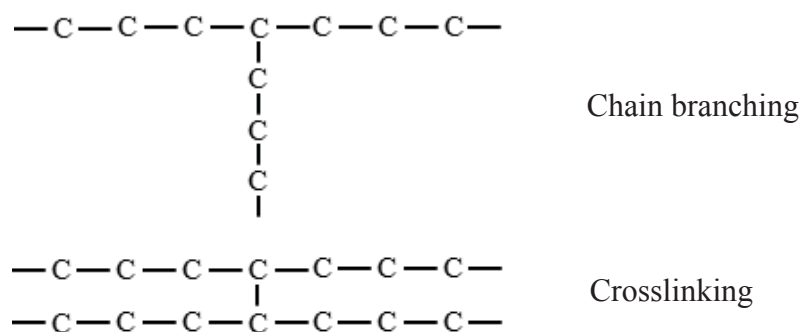
Fig.1. Scheme of chain branching and crosslinking.

Chain branching and crosslinking are the predominant effects for polymers having relatively unhindered main chains, according to the scheme shown in Fig.1.

When the polymers have highly substituted quaternary atoms, molecular degradation or scissioning is the main effect.

The molecular modifications are essentially due to the reactions of free radicals, produced by both the direct action of ionizing radiation on the macro-molecular structure and the further evolution of ionic and exited species initially produced by irradiation.

Several mechanisms dealing with the molecular modifications induced by irradiation have been reported in the literature [1, 2, 12].

For example, in the case of polyethylene (PE), the free radicals formed by dissociation of C–H and C–C bonds (alkyl, allyl, polyenyl) and the double bonds formed with H_2 evolution give rise to either crosslinking or chain branching reactions:

$$-CH_2\overset{\bullet}{C}HCH_2- \ + \ -CH_2\overset{\bullet}{C}HCH_2- \ \longrightarrow \ \begin{array}{c} -CH_2CHCH_2- \\ | \\ -CH_2CHCH_2- \end{array}$$

$$-CH_2\overset{\bullet}{C}HCH_2- \ + \ -CH_2CH{=}CH_2- \ \longrightarrow \ \begin{array}{c} -CH_2CHCH_2- \\ | \\ \overset{\bullet}{C}H_2CHCH_2- \end{array}$$
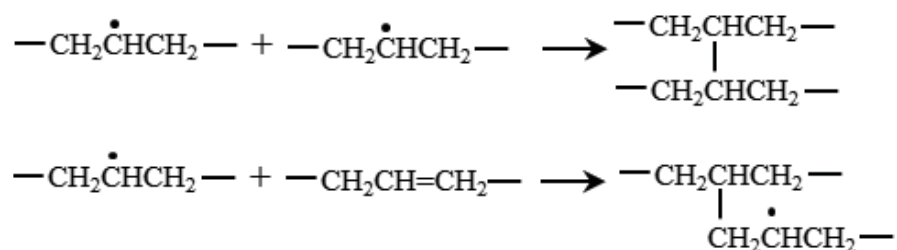
When degradation occurs, the stable free radicals formed by the dissociation of quaternary carbon bonds do not migrate along the polymer chains and the steric hindrance favours their further evolution toward disproportionation and chain scission reactions, according to the scheme reported for poly(methyl methacrylate) (Fig.2).

The quantitative determination of molecular modifications induced by ionizing radiation has been made through the measurement of the G-value, which represents the number of molecules formed or changed for 100 eV of absorbed energy. G(X) is the number of crosslinks formed per 100 eV of absorbed energy,

$$\begin{array}{ccc} & CH_3 \quad\quad CH_3 & CH_3 \quad\quad CH_3 \\ & | \quad\quad | & | \quad\quad | \\ -CH_2- CH- CH_2-C- & \longrightarrow & -CH_2-C\bullet \ + \ \bullet CH_2-C- \\ & | \quad\quad | & | \quad\quad | \\ & CO_2CH_3 \quad CO_2CH_3 & CO_2CH_3 \quad CO_2CH_3 \end{array}$$

$$\begin{array}{ccc} & CH_3 & CH_3 \quad\quad CH_2 \\ & | & | \quad\quad \| \\ 2 \ -CH_2- C\bullet & \longrightarrow & -CH_2- CH \ + \ -CH_2- C \\ & | & | \quad\quad | \\ & CO_2CH_3 & CO_2CH_3 \quad CO_2CH_3 \end{array}$$
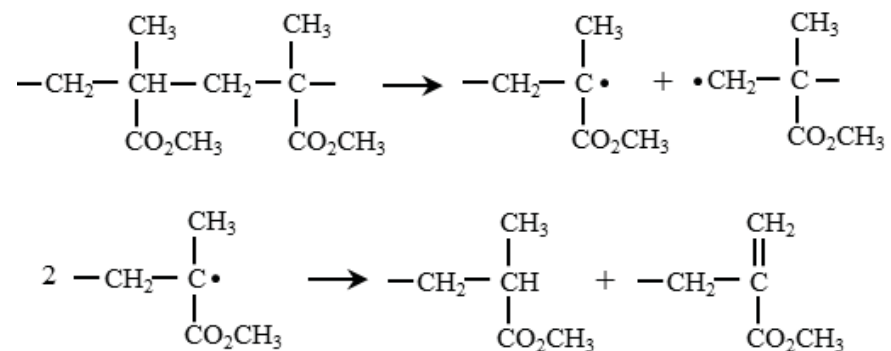
Fig.2. Example of chain scission reaction in the case of poly(methyl methacrylate).

while G(S) is the number of chain scissions formed by 100 eV of absorbed energy.

As two polymer chains are joined when a crosslink is formed, G(chains linked) = 2 G(X).

The most common methods used to measure G(X) and G(S) are based on solubility tests. Crosslinking causes the formation of three-dimensional insoluble networks (gel). The "gel fraction" is the ratio of the weight of the insoluble part divided by the initial weight of the polymer, while the remaining part is the "soluble fraction".

Solubility data are used in the Charlesby-Pinner equation:

$$s + s^{0.5} = \frac{p}{q} + \frac{1}{q\,P_n D} \tag{1}$$

where: s – the soluble fraction, p – the chain scission probability per unit dose per monomer unit, q – the crosslinking probability per unit dose per monomer unit, P_n – the number average degree of polymerization for the polymer of the most probable distribution of molecular weight, D – the absorbed dose.
The Eq. (1) can be expressed in terms of G(S) and G(X):

$$s + s^{0.5} = \frac{G(S)}{2G(X)} + \frac{4.82 \times 10^6}{G(X)\,M_n D} \tag{2}$$

where M_n is the number average molecular weight.

Plotting Eq. (2) as function of 1/D allows one to determine G(S) and G(X). The extrapolation of the curve until 1/D = 0 gives the ratio G(S)/2G(X), while G(X) is calculated from Eq. (2) the slope of the curve.

In Ref. [9], the values of G(X) and G(S) for the most common polymers are reported.

Many authors have found deviations in their experimental results from the Charlesby-Pinner equation which have been attributed to the non-random distribution of the initial molecular weight.

Other experimental techniques, such as elastic modulus, swelling values or light scattering and ^{13}C NMR measurements can be also used to calculate G(X).

The extent of chain branching and crosslinking depends on the amorphous phase content of a polymer, which occurs along molecular chains in the solid state, where there are amorphous and crystalline regions. Polymers with similar molecular structure but different degrees of crystallinity give different values of G(X) and G(S) for the same irradiation conditions. For example, in Ref. [9], isotactic polypropylene G(X) varies in the range 0.3-0.5, while for atactic polypropylene G(X) is higher, 0.4-1.1. Similar results are shown in Ref. [9] for polyethylenes with different degrees of crystallinity.

2.2. IRRADIATION IN AIR

When polymers are irradiated in air, the free radicals produced by ionizing radiation can yield oxidized functional groups (carbonyl, peroxides, hydroperoxides, hydroxyl, carboxyl). Oxidized macromolecules can undergo chain scission with molecular weight decrease.

The oxidative degradation induced by irradiation in air can be studied by different techniques.

The most common is infrared analysis, which allows one to monitor the formation of the oxidized groups and other molecular modifications (double bonds,
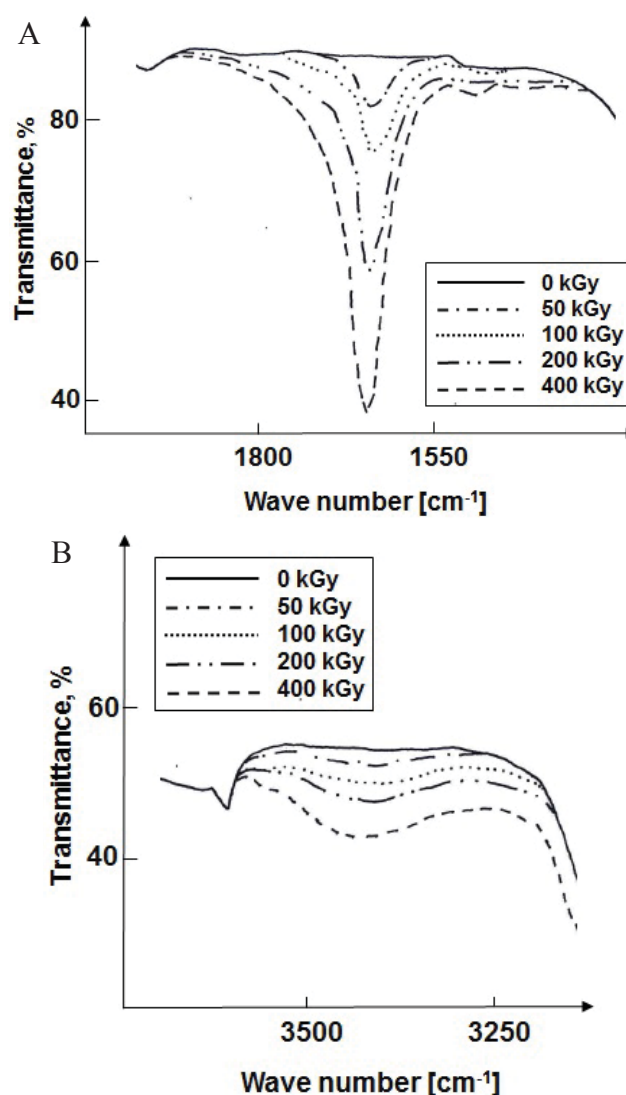

Fig.3. IR analysis of LDPE, irradiated at various doses and at constant dose rate: (A) wavenumber range of 1720 cm^{-1}, (B) wavenumber range of 3500 cm^{-1}.

terminal methyl group formation, *etc.*) resulting from molecular degradation. The decrease of molecular weight can also be determined by gel permeation chromatography (GPC) and by the measurement of intrinsic viscosity.

Figure 3 shows the infrared analyses of a low density polyethylene (LDPE) irradiated in air at different doses, in the wavenumber range of 1720 cm^{-1} (A), the typical absorption range of carbonyl groups, and in the wavenumber range of 3500 cm^{-1} (B), the typical absorption range of hydroxyl groups.

Irradiation in air causes the formation of both carbonyl and hydroxyl groups, and their amounts increase with increasing dose. A useful relative quantitative determination of the extent of oxidation reactions can be done by measuring the height of the peaks corresponding to the oxidation functional groups. If the thickness of the analysed sample is constant, this value can be related to the oxidized functional group concentration in the irradiated sample and to the extent of oxidative degradation reactions. The peak generally used for the evaluation of the oxidation reactions is the carbonyl one at 1720 cm^{-1} wavenumber.

Other indirect techniques can measure the modifications of the physico-chemical (glass and other molecular transitions), mechanical and electrical properties due to irradiation.

The formation of oxidized physicochemical groups and the molecular modifications due to irradiation of a solid polymer in air are not uniform within the material. The extent of the oxidative degradation phenomena is higher in the external layers of the polymers and a concentration gradient of oxidized groups, moving from the external surfaces toward the bulk, has been observed. A similar trend can be also observed for the molecular weight modifications. This non-uniformity can be more or less marked, depending on the molecular structure and morphology of the polymer and on the irradiation conditions.

During irradiation in air, a polymer undergoes different reactions depending on its molecular structure and morphology (chain branching, crosslinking and degradation or scissioning). These also occur during irradiation under vacuum or in presence of inert gases. The oxidative reactions due to interaction of free radicals with atmospheric oxygen dissolved in the solid polymer. For a given polymer, the prevalence of one or the other depends on the reaction kinetics.

The reactions of free radicals with oxygen are very fast and the free radicals produced by irradiation react immediately with oxygen dissolved in the solid polymer. The kinetics of the further oxidative reactions is controlled by the oxygen diffusion rate through the polymer. Those molecular structures, morphologies and irradiation conditions which favour the oxygen diffusion in the polymer cause a more uniform oxidation within the material, while a marked gradient of these phenomena is observed when oxygen diffusion is hindered. In the first case the material mainly undergoes oxidative degradation, while, in the second case, a prevalence of the reactions usually occurring during the irradiation under vacuum or under inert atmosphere occurs.

The study of non-uniform oxidation of polymers during their irradiation in air can be carried out by microtome cutting very thin polymer sheets moving from the external surfaces toward the interior bulk. These sheets can be then analysed by experimental techniques apt to measure the molecular modifications due to irradiation, and in particular by IR analysis. Also other techniques such as GPC, solubility, density measurements, calorimetric analysis and mechanical property determinations can be used.

In Fig.4, the IR analysis and solubility tests results for a linear low density polyethylene (LLDPE) irradiated in air are shown. Sheets of the same thickness were cut by a microtome and the extent of the oxidation reactions was measured through the carbonyl group absorption peak, while the corresponding molecular weight modifications were measured by gel extraction tests. The carbonyl concentration and the gel fraction profiles, *i.e.* measured as a function of the distance from the external surface of the irradiated polymer, are shown.
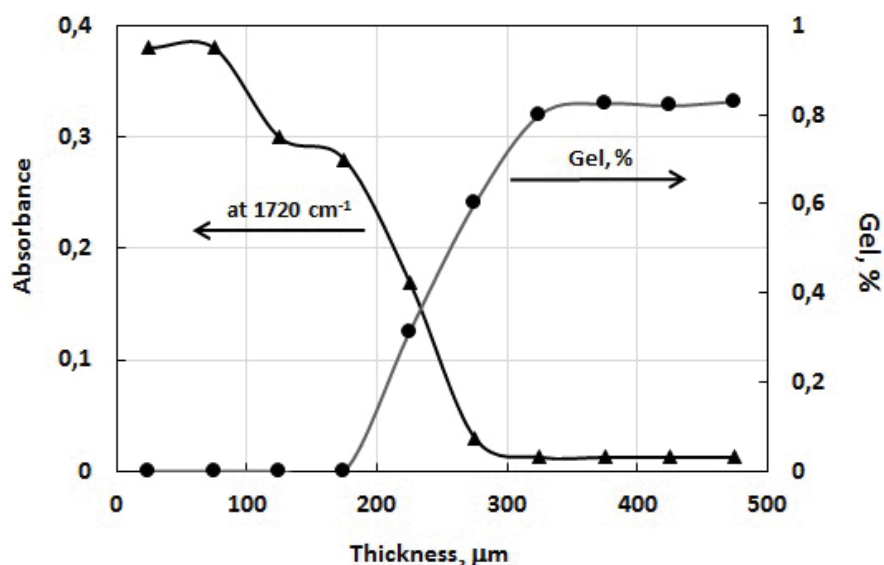
Fig.4. Carbonyl concentration and gel fractions profiles for a LLDPE sample irradiated in air at the dose of 170 kGy and the dose rate of 1 kGy/h.

In the outer layers the oxygen penetration favours oxidative degradation while crosslinking occurs in the bulk, as evidenced by the decrease of carbonyl group concentration, accompanied by the increase of gel fraction.

In Fig.5, the IR analysis results for two linear low density polyethylenes, irradiated in air at the same total dose and dose rate, are shown. The carbonyl concentration profiles are noted.

Before irradiation the two polymers have different crosslinked densities, as determined by gel extraction tests performed in xylene (a typical solvent for polyethylene), which indicate a total solubility of the uncrosslinked sample and
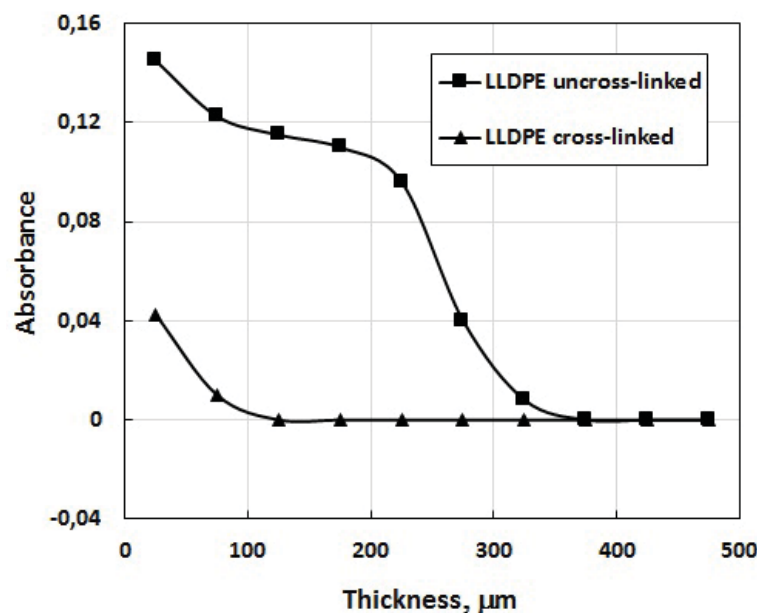
Fig.5. Carbonyl concentration profiles for two LLDPE. Irradiation conditions: dose rate – 1 kGy/h, dose – 100 kGy.

a gel fraction of about 80% for crosslinked one. A marked and deeper oxidation is observed for the first one with respect the crosslinked polyethylene. This can be attributed to the higher diffusivity of oxygen in the uncrosslinked polymer.

In Fig.6 the effects of irradiation in air on three different types of polyethylene, low density polyethylene, linear low density polyethylene, and high
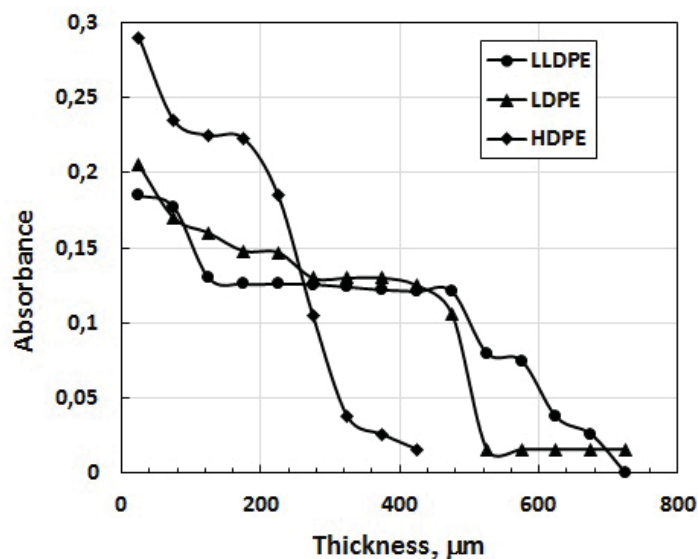
Fig.6. Carbonyl concentration profiles for LLDPE, LDPE and HDPE. Irradiation conditions: dose rate – 0.1 kGy/h, dose – 10 kGy.

density polyethylene (HDPE), irradiated at the same total absorbed dose and dose rate, are shown. The difference in the carbonyl concentration profiles can be attributed to the different oxygen diffusivity in the three polymers. LDPE and LLDPE have almost the same crystallinity degree and almost the same oxygen diffusivity, while HDPE has higher crystallinity and a lower oxygen diffusivity. The thickness of the oxidized layers is almost the same for LLDPE and LDPE while less interior oxidation is observed for the more crystalline HDPE.

Processing parameters, the dose rate and the total absorbed dose, play an important role in determining the extent of crosslinking and oxidative degradation phenomena.

In Fig.7, the carbonyl concentration profiles for LLDPE samples irradiated in air at the same total dose but at different dose rates are reported.

At high dose rates, the instant concentration of free radicals in the polymer is so high that the oxygen, diffusing in the polymer from ambient conditions, is immediately consumed close to the surfaces. At lower dose rate the lower instant concentration of free radicals allows for diffusion of the oxygen into the bulk of the irradiated sample with an increase of the thickness of the oxidized layer.
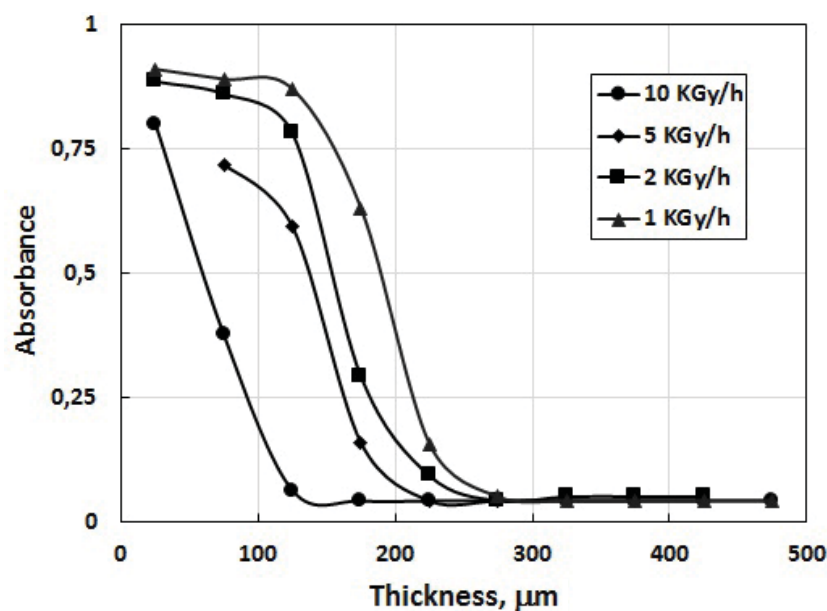
Fig.7. Carbonyl concentration profiles for samples of LLDPE irradiated in air at the total absorbed dose of 675 kGy and different dose rates.

Consequently, the whole effect of irradiation on the same polymer and at the same dose is different because of changing the dose rate.

At high dose rates the oxidative degradation phenomena are essentially concentrated in the external layers. As already described, the bulk of the material undergoes the same reactions occurring during irradiation under vacuum

or under inert atmosphere and in particular for polyethylene the main effect is crosslinking.

At low dose rates the degradation phenomena involve larger parts of the irradiated material.

These considerations are confirmed by the results shown in Fig.8, where the carbonyl concentration profiles for samples of LLDPE irradiated in air at the same dose rate and different total doses are reported.
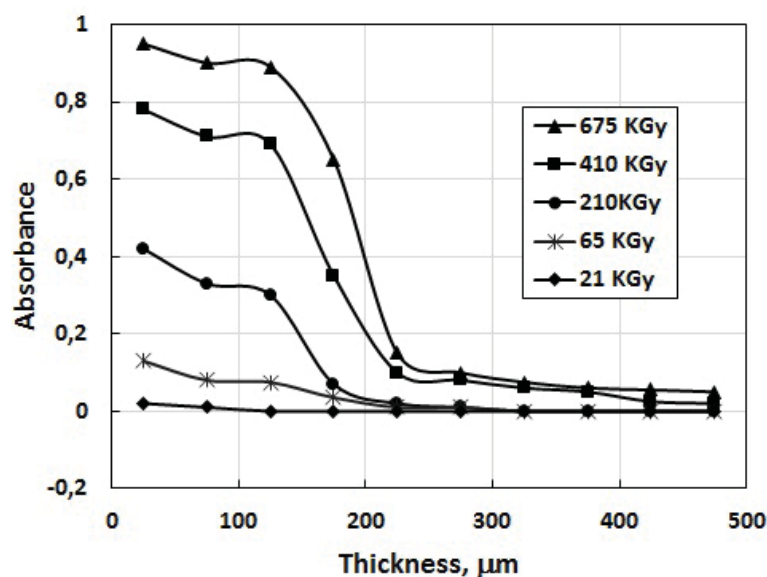
Fig.8. Carbonyl concentration profiles for samples of LLDPE irradiated in air at the constant dose rate of 1 kGy/h and different total absorbed doses.

Since the polymer is always irradiated at the same dose rate, the thickness of the oxidized layer is always the same, while the concentration of carbonyl groups increases with the absorbed dose.

Other examples based on the measurement of other properties can be found in the literature.

In Ref. [13], the density profiles for a non-irradiated LDPE and for LDPE irradiated in air at different doses and different dose rates are shown. The increase in density is related to oxidation reactions. It is possible to observe, by decreasing the irradiation dose rate, a generalized increase of density with respect to the non-irradiated starting material. The density profiles show that this effect is confined to external surfaces at high dose rates and involves deeper penetration at low dose rates.

In Ref. [14], the molecular weight of nylon-6 wire jacketing irradiated in air at different dose rates and to different total doses had been measured. Decreasing the dose rate, increased the extent of the oxidative degradation and decreased the average molecular weight of the irradiated polymer.

All these results have very important practical consequences.

For instance, polymer samples with different thicknesses, irradiated in air with the same dose and dose rate conditions, present a different ratio between oxidative degradation and crosslinking extent. This effect will affect the properties of the polymeric material, as it will be discussed in the following sections.

For the polymeric materials used in radiative environments for long periods of time at very low dose rates, as in nuclear power plants or in space, the influence of the dose rate in the study of the reliability of a material has to be taken into account. Careful consideration of the dose rate effects is needed for the extrapolation to the effective working conditions from laboratory results obtained both in short timeframes and at high dose rates [13].

The molecular modifications induced by the action of ionizing radiation can also occur after irradiation. This is very significant for semi-crystalline polymers, such as polyethylene and polypropylene. The macroradicals formed in the amorphous regions rapidly react with each other or with the oxygen diffused into the polymer, while those formed in the crystalline regions in order to react, need to diffuse to the surface of the crystallites or to the amorphous phases. The radical diffusion rate can be very low and the irradiated materials can undergo chemical modifications for long periods of time after irradiation (up to several days). In Ref. [14], the post-irradiation oxidation of polypropylene was studied by IR analysis. The results showed that the carbonyl group concentration increases during storage in air.

2.3. IONIZING RADIATION EFFECTS ON POLYMER PROPERTIES

The molecular modifications induced by irradiation modify polymer properties, such as the thermal behaviour and the mechanical and electrical characteristics.

2.3.1. Thermal behaviour

The most common technique used to study the thermal behaviour of polymers is the differential thermal calorimetry (DSC) which determines the melting temperature and the melting enthalpy for semi-crystalline polymers, and for all polymers, the glass and other secondary transitions occurring in the amorphous phases. Other experimental methods are dynamic mechanical thermal analysis (DMTA) and dielectric tests, performed at different temperatures and frequencies.

The melting behaviour depends on the crystalline properties of the polymer. The melting enthalpy indicates the amount of the crystalline phase with respect to the total mass of the polymer (crystallinity degree), while the melting temperature can be affected by the crystallite regularity.

Since molecular modifications induced by ionizing radiation occur mostly in the amorphous regions, at low doses irradiation does not appreciably

modify the crystallinity of the polymer. A modification can occur at higher ir-radiation doses with introduction of irregularities in the crystallites due to both crosslinking and degradation which is enhanced by oxidation. In these cases, the DSC curves show a decrease of both in the melting temperature and in the enthalpy with the formation of additional small melting peaks at low tempera-tures, due to the presence of low molecular weight molecules [15, 16].

The glass transition is related to the free movement of the main chains of the polymers, while the other secondary transitions are related to similar phe-nomena involving smaller molecular segments. Chain scission and degradation favour molecular mobility and a decrease of the temperatures of all the transi-tions, while an opposite effect is caused by chain branching and crosslinking [17, 18].

2.3.2. Mechanical properties

The mechanical properties of polymers can be studied through different tests: tensile, compression, flexural, *etc.* Among all, tensile tests are the most sensitive to the molecular modifications induced by irradiation. Here tensile mechanical tests are considered, even if similar consideration can be made on other experimental techniques.
The most significant tensile parameters are the Young's elastic modulus, the elongation at break and the breaking strength.

The mechanical behaviour essentially depends on the molecular weight and on the degree of crystallinity. The increase of the crystallinity and of the molecular weight due to crosslinking causes an increase in the mechanical strength, with an increase of the Young's elastic modulus. For the elongation at break, which is related to the ductile or brittle behaviour of the material, two effects can be observed: an increase in the molecular weight increase and a reduction, up to the start of brittleness, caused by crosslinking and crystallin-ity. The chemical bonding of polymer chains, in the case of crosslinking, and the crystallinity act as links which hinder their free movement. All these prop-erties affect the breaking or ultimate strength, *i.e.* the stress corresponding to the breaking of the polymer chains. High elastic modulus values correspond to a high stress levels and tend to increase the ultimate strength, which decreases the elongation at break and starting brittleness.

Ionizing radiation mainly affects the molecular behaviour of polymers and does not modify appreciably the crystallinity, at least up to the absorption of moderate doses. The mechanical behaviour of irradiated polymers essentially depends on the relative extent of chain scission, chain branching and crosslink-ing [13, 19].

As for degradation or scissioning phenomena, a great interest has been devoted to the worsening of the mechanical properties, which can become dramatic in the case of oxidative degradation. Defects induced in the molecu-lar structure can strongly reduce the elongation at break, changing the poly-

meric properties from ductile to brittle. This is very important when the materials are used in the presence of ionizing radiation and good mechanical performance is required.

It has been shown above how the different molecular, morphological and processing parameters involved in ionizing radiation effect the molecular structure of the materials. In Ref. [14], the effect of the dose rate on the elastic modulus of a Viton rubber irradiated in air had been studied. Sheets of the same thickness were cut, starting from the surface and going toward the bulk, and the tensile elastic modulus was determined. The non-irradiated sample had a uniform modulus value for all of the tested sheets. For the irradiated samples a non-uniform profile was observed. Compared to the non-irradiated material, modulus decreases in the outside layers, while it increases in the bulk. This is explained by non-uniform molecular modifications induced by irradiation in air: oxidative degradation in the external layers and chain branching and crosslinking in the bulk. Decreasing the dose rate, the modulus profile along the thickness becomes more uniform, with lower modulus values.

According to what has already observed for the ratio between external oxidized and internal non-oxidized layers of polymer irradiated in air, the mechanical strength also depends on the thickness. Under irradiation, thicker samples present a higher mechanical strength.

Since the elongation at break is very sensitive to degradation phenomena, its reduction has been used as a reliable parameter for polymers used in radiation environment. For example, in Ref. [14], data corresponding to the reduction of 50% of the elongation at break of the non-irradiated material was reported for the most common polymers.

In evaluating the effect of ionizing radiation on the mechanical properties of polymers, also post-irradiation effects have to be considered, which can cause further worsening of the properties [14].

The improvement of mechanical properties by irradiation has been important in applications of radiation processing of polymers, such as the irradiation of ultra-high molecular weight polyethylene for medical prosthesis devices.

2.3.3. Electrical properties

The modifications induced by ionizing radiation effect both the conductivity and the dielectric properties of polymers.

The most common polymers are insulating materials characterized by the presence of a completely full valence band and of a conductive band separated by a prohibited energy interval. In general, their conductivity is strongly affected by the presence of impurities which cause the formation of additional bands, which decrease the insulating properties.

The electrical conductivity is increased by irradiation. This is due to the formation of mobile charge carriers: electrons, holes, ions, which create additional energy intervals [9-20].

There are two different kinds of irradiation-induced conductivity: pulse and stationary conductivity.

The pulse conductivity is induced by pulse irradiation and is proportional to the dose rate. It is subdivided into the instant and the delayed conductivity.

The instant conductivity is characterized by a very short lifetime of about 10^{-10} s.

The delayed conductivity continues also after irradiation. It relaxes down to a dark value which, for doses causing significant structural modifications of a polymer, can be appreciably different from the initial value before irradiation.

The stationary conductivity is induced by continuous irradiation and depends on dose rate according to the Eq. (3):

$$\sigma = k\, D^{\alpha} \tag{3}$$

where $0 < \alpha < 1$, until a saturation value.

The dielectric properties of polymers can be described by a model based on a set of capacitors and resistance elements.

If an alternating field is applied, the material is crossed by a current out of phase, in advance, with respect to the applied voltage, of an angle ϕ.

The dielectric behaviour of a polymer is described by two properties: ε' and ε''; ε' is the permittivity (or dielectric constant) and it is related to the capacity and to the stored energy, while ε'' is the loss factor and it is related to the resistance and to the dissipated energy. The ratio $\varepsilon''/\varepsilon' = \tan\delta$ is the tangent of the loss angle, complementary of the phase angle ϕ, which is also related to the dissipative phenomena. All of these properties are essentially due to the presence and mobility of charges and polar groups in the polymer backbone and depend on polarization phenomena of different types, occurring in different times: 10^{-15} s for electronic polarization, 10^{-14}-10^{-12} s for atomic polarization, from 10^{-10} s to seconds or minutes for dipolar polarization due to the presence of polar groups, and longer times for interfacial polarization effects.

Irradiation mainly affects the dipolar polarization and the effects can be both transitory and permanent. The transitory effects derive from the short-lived irradiation products (trapped electrons, peroxide and hydroperoxide groups during irradiation in air), while the permanent effects derive from the permanent induced changes in the molecular structure.

Molecular degradation causes an increase in the molecular mobility and consequently in the permittivity. This effect is enhanced by oxidative degradation phenomena, which also causes an increase in the oxidized groups.

An opposite effect is observed in the case of crosslinking which reduces the molecular mobility.

Tan δ and ε'' are increased by degradation and decreased by crosslinking.

Related to these phenomena is the dielectric strength, *i.e.* the maximum applied electrical field before the occurrence of dielectric breakdown. The dielectric strength can be dramatically decreased by both localized defects due

to molecular degradation and localized heating due to the increase of conductivity and of polarization.

As with the mechanical effects, the knowledge of radiation effects on the electrical properties of polymers is very important for several applications.

This is the case of polymers used as insulating materials in radiative environments, where the preservation of their electrical properties is required.

On the other hand, the positive effect of crosslinking on both the dielectric properties and dielectric strength values is the basis of the electron beam irradiation-induced crosslinking of polymer insulating materials, which is one of the most successful industrial applications of radiation processing.

3. CONCLUSIONS

This chapter dealt with the modifications induced by ionizing radiation on the molecular structure and on the properties of polymers.

Under ionizing radiation polymers undergo chain scission, chain branching and crosslinking reactions and their relative extent depends on the initial molecular structure and morphology of the polymer and on the irradiation conditions.

In particular the effect of irradiation in air has been illustrated with particular emphasis on the conditions which cause more or less uniform distribution of oxidation effects on irradiated samples.

The molecular modifications effect the polymer properties, such as the physicochemical, the mechanical and the electrical behaviour.

These results are very important for both the knowledge of the reliability of polymers used in radiative environments and the improvement of the applicative properties of polymeric materials by radiation processing.

REFERENCES

[1]. Chapiro, A. (1962). *Radiation chemistry of polymeric systems*. New York: Interscience Publishers.
[2]. Spinks, J.W.T., & Woods, R.J. (1990). *An introduction to radiation chemistry*. Wiley-Interscience.
[3]. Schonbacher, H., & Stolarz-Lzicka, A. (1979). *Compilation of radiation damage test data. Part I: Cable insulating materials*. Geneva: CERN.
[4]. Tavlet, M., Fontaine, A., & Schonbacher, H. (1998). *Compilation of radiation damage test data. Part II: Thermoset and thermoplastic resins, composite materials* (2nd ed.). Geneva: CERN.

[5].   Beynel, P., Mayer, P., & Schonbacher, H. (1982). *Compilation of radiation damage test data. Part III: Materials used around high energy accelerators*. Geneva: CERN.

[6].   Guarino, F., Hauviller C., & Tavlet, M. (2001). *Compilation of radiation damage test data. Part IV: Adhesives for use in radiation areas*. Geneva: CERN.

[7].   IAEA. (1990). *Guidelines for industrial radiation sterilization of disposable medical products*. Vienna: IAEA. (IAEA-TECDOC-539).

[8].   Komolprasert, V., & Morehouse, K.M. (2004). *Irradiation of food and packaging*. American Chemical Society.

[9].   Woods, R.J., & Pikaev, A.K. (1994). *Applied radiation chemistry*. Wiley-Interscience.

[10].   IAEA. (2009). *Controlling of degradation effects in radiation processing of polymers*. Vienna: IAEA. (IAEA-TECDOC-1617).

[11].   Makuuchi, K., & Cheng, S. (2012). *Radiation processing of polymeric materials and its applications*. Wiley.

[12].   Kabanov, V.Ya., Feldman, V.I., Ershov, B.G., Polikarpov, A.I., Kiryukhin, D.P., & Apel, P.Yu. (2009). Radiation chemistry of polymers. *High Energ. Chem.*, *43*, 1, 1-18. DOI: 10.1134/s0018143909010019.

[13].   Gillen, K.T., & Clough, R.L. (1991). Accelerated aging methods for predicting long-therm mechanical performance of polymers. In D.W. Clegg & A.A. Collyer (Eds.), *Irradiation effects on polymers* (pp. 157-223). London & New York: Elsevier Applied Science.

[14].   Clough, R.L., Gillen, K.T., & Dole, M. (1991). Radiation resistance of polymers and composites. In D.W. Clegg & A.A. Collyer (Eds.), *Irradiation effects on polymers* (pp. 79-156). London & New York: Elsevier Applied Science.

[15].   Spadaro, G. (1993). Gamma-radiation ageing of a low density polyethylene. *Radiat. Phys. Chem.*, *6*, 851-854.

[16].   Spadaro, G., & Valenza, A. (2000). Calorimetric analysis of an isotactic polypropylene gamma-irradiated in vacuum. *J. Therm. Anal. Calorim.*, *61*, 589-596.

[17].   Spadaro, G., Calderaro, E., Schifani, R., Tutone, R., & Rizzo, G. (1984). Ageing of organic electrical insulating materials due to radiation. Physical properties of a cycloaliphatic epoxy resin irradiated under vacuum. *Radiat. Phys. Chem.*, *23*, 613-618.

[18].   Spadaro, G., Calderaro, E., & Rizzo, G. (1984). Ageing of organic electrical insulating materials due to radiation. II. Physical properties of a cycloaliphatic epoxy resin irradiated in moisture saturated air. *Radiat. Phys. Chem.*, *24*, 257-261.

[19].   Lyons, B.J., & Weir, F.E. (1973). The effect of radiation on the mechanical properties of polymers. In M. Dole (Ed.), *The radiation chemistry of macromolecules* (Vol. II, pp. 281-306). New York: Academic Press.

[20].   Hedvig, P. (1972). Electrical conductivity of irradiated polymers. In M. Dole (Ed.), *The radiation chemistry of macromolecules* (Vol. I, pp. 127-144). New York: Academic Press.

RADIATION-INDUCED OXIDATION OF POLYMERS

Ewa M. Kornacka

Institute of Nuclear Chemistry and Technology, Dorodna 16, 03-195 Warszawa, Poland

1. INTRODUCTION

A polymer is a macromolecule formed by the combination of simple molecules, monomers, of low molecular weight. A polymer molecule usually has at least 2000 atoms linked by covalent bonds.

In general, polymers can be divided into inorganic and organic, and also into naturally occurring and synthetically produced. Polymers may contain additives such as dyes, fillers, antioxidants, flame retardant materials and other components needed to carry out their use in many application areas. The properties of polymers largely depend on both their microstructure and macrostructure.

Ionizing radiation excites active species, like radicals. In the radiation processing of polymers, usually two kinds of radiation are used: (i) high energy electrons from accelerators, which give continuous and homogeneous radiation, but have limited penetration depth, and are a source of high doses of radiation per unit of time, and (ii) gamma rays from radionuclides of cobalt-60 and cesium-137, which more deeply penetrate materials and give relatively small doses of radiation per unit of time.

2. THE INFLUENCE OF IONIZING RADIATION ON THE MOLEULAR STRUCTURE OF POLYMERS

For macromolecules, degradation indicates changes in physical properties caused by chemical reactions resulting in the breaking of macromolecular chains. As a result, polymers have shorter chain molecules and a reduced molar mass.

Polymer degradation can be induced by thermal, mechanical, photochemical, biological, or chemical treatments or by ionizing radiation:

- Thermal degradation is caused by exposure to elevated temperatures and takes place without chemical agents.
- Mechanical degradation is caused by the application of external factors, *e.g.* external stress on moisture diffusion, oxygen, temperature.
- Photochemical degradation is caused upon the absorption of light wherein triplet oxygen converts to singlet oxygen, a highly reactive form of the gas, which effects spin-allowed oxidations. In the atmosphere, the organic compounds are degraded by hydroxyl radicals, which are produced from water and ozone.
- Biological degradation is caused by the action of enzymes on polymers. Microorganisms produce a variety of enzymes capable of reacting with both natural and synthetic polymers.
- Chemical degradation is caused by solvolysis and mainly by hydrolysis to give lower molecular weight molecules. Hydrolysis takes place in the presence of water containing an acid or a base. Polymers are susceptible to attack by atmospheric oxygen, especially at elevated temperatures encountered during processing.
- Ionizing radiation causes some chemical degradation in polymers such as the breaking of the main chains of the macromolecule, changes in the number and nature of double bonds, and the emission of low molecular weight gaseous products, as well as oxidation of the polymer.

The interaction between the incident radiation and the irradiated material is characterized by linear energy transfer (LET). Electrons or gamma rays have a relatively small value in contrast to the alpha particles [1]. Ionizing radiation
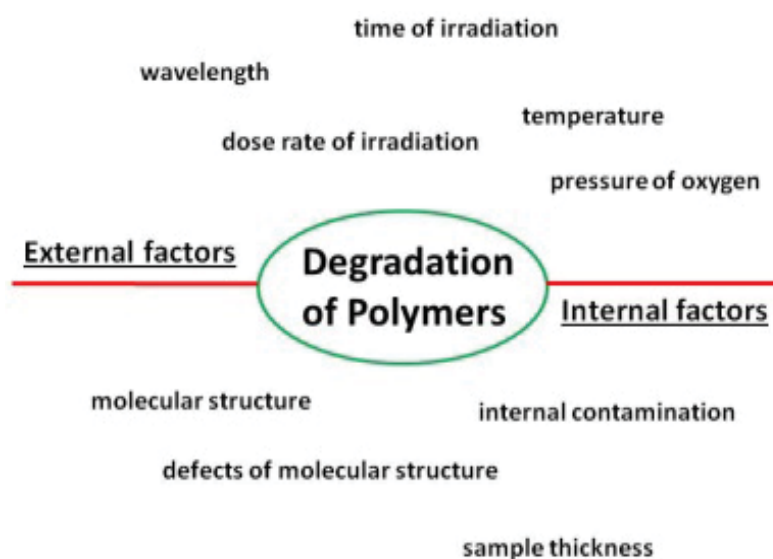
Fig.1. Scheme of the impacts of the main factors leading to polymer degradation.

transfers a large quantity of energy towards the irradiated material. The transfer of the energy is not selective and represents a principal difference with the photochemical processes. Degradation of polymers is a consequence of radical processes which are generated in a material upon irradiation. The extent of free radical degradation increases as the dose increases.

There are strong connections between different types of degradation [2]. Usually there is simultaneous and overlapping of several types of degradation. A typical example of this is the simultaneous action of light, oxygen and other atmospheric agents, or the simultaneous influence of heat, mechanical stresses and oxygen. Figure 1 is a diagram of the impact of the most important factors leading to polymer degradation.

The molecular modifications induced by ionizing radiation are shown in Fig.2:

- crosslinking reaction forming new C–C covalent bonds between adjacent molecular chains, increasing the polymer molecular weight up to the formation of a three-dimensional network;
- chain scission of a backbone resulting in a decrease of the molecular weight of the polymer;
- changes in the nature and number of double bonds;
- oxidation degradation of the polymer during irradiation in the presence of oxygen.
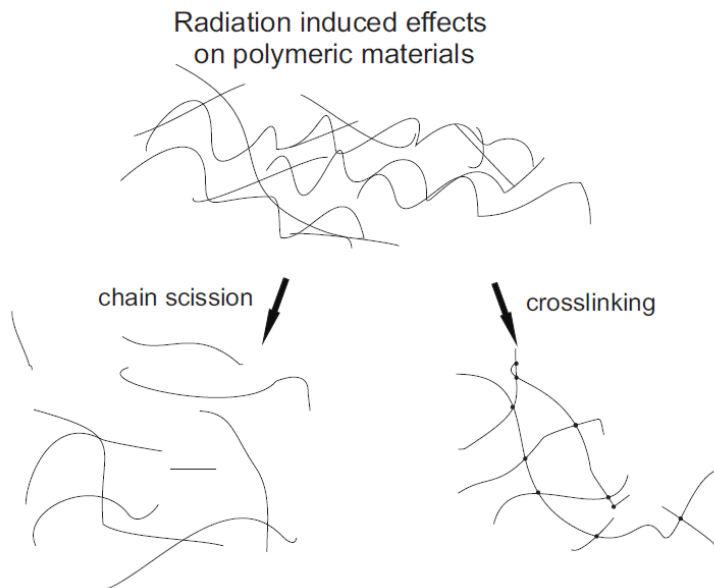
Fig.2. Ionizing radiation-induced crosslinking and chain scissioning of polymeric materials.

Polymers in which ionizing radiation causes crosslinking often have better mechanical properties. If chain scissioning dominates, *e.g.* polypropylene, then

CHAIN SCISSION ⟶ **CROSSLINKING**
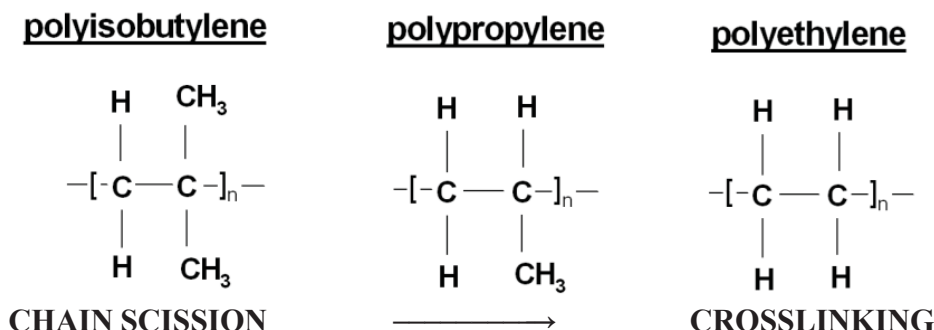
Fig.3. The pathway of the influence of ionizing radiation on different chain structure polymers.

low molecular weight fragments, gas evolution (odor) and unsaturated bonds (color) may appear.

Free radicals determine the initiating centers for scissioning and/or crosslinking, hence for the induced modifications within the macromolecular chain (Fig.3). In polymers containing mainly $-[CH_2-CH_2]_n-$ units, crosslinking predominates; if a polymers has a tetra-substituted carbon, as of the type $-[CH_2-CR_1R_2]_n-$, chain scissioning (degradation) predominates [3].

The mechanism occurring during irradiation has three distinct stages: initiation, propagation and termination. The chemical reactions induced by ionizing radiation on polypropylene are as follows:

• Initiation

$$R–H \xrightarrow{\gamma} R^\bullet + H^\bullet \qquad (1)$$
$$R–H + H^\bullet \to R^\bullet + H_2 \qquad (2)$$

• Propagation

β-scission

$$–CH_2–C^\bullet(–CH_3)–CH_2–CH–(CH_3)– \leftrightarrows –CH_2–C(–CH_3)=CH_2 + H–C^\bullet(–CH_3) \quad (3)$$
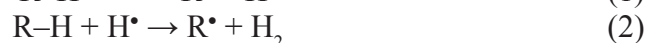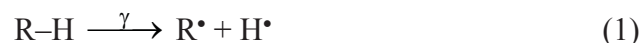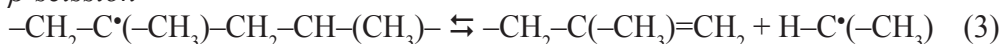
Addition of free radicals to double bonds

$$R^\bullet + –CH_2=CH_2– \to R–CH_2–H–C^\bullet \qquad (4)$$

• Termination

$$R^\bullet + R^\bullet \to R–R \qquad (5)$$
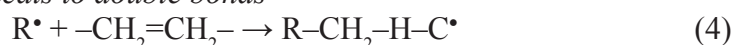
3. RADIATION-INDUCED OXIDATION OF POLYMERS

By definition, the term "oxidation" occurs when a polymer molecule reacts with oxygen *via* peroxide radicals. The irradiation of polymers in the presence of oxygen gives different results with respect to irradiation under vacuum. The presence of oxygen affects the quantitative and qualitative degradation processes, and increases the rate of degradation and possibly the crosslinking of

a polymer. The oxidation of aliphatic and aromatic polymers leads to the emergence of alcohols, ketones, carboxylic acids as stable by-products of radiolysis [4]. The gamma oxidative degradation of a polymer in air, for example, is described by the following chain reaction scheme:

- Initiation

$$RH \rightarrow R^\bullet + H^\bullet \tag{6}$$

- Propagation

$$R^\bullet + O_2 \rightarrow ROO^\bullet \qquad\qquad \text{radical conversion} \tag{7}$$
$$ROO^\bullet + RH \rightarrow ROOH + R^\bullet \tag{8}$$
$$ROOH \rightarrow RO^\bullet + {}^\bullet OH \tag{9}$$
$$\left.\begin{array}{l}{}^\bullet OH + RH \rightarrow H_2O + R^\bullet \\ RO^\bullet + RH \rightarrow ROH + R^\bullet\end{array}\right\} \quad \text{chain branching} \tag{10}$$
$$\tag{11}$$
$$RO^\bullet \rightarrow \text{chain scission reactions} \tag{12}$$

- Termination

$$\left.\begin{array}{l}2R^\bullet \rightarrow R\text{–}R \\ ROO^\bullet + R \rightarrow ROOR \\ ROOH \rightarrow RO + H_2O\end{array}\right\} \quad \begin{array}{l}\text{crosslinking reactions} \\ \text{to non-radical products}\end{array} \quad \begin{array}{l}(13) \\ (14) \\ (15)\end{array}$$

It should be noted that the free radicals $R^\bullet$ react with molecular oxygen and/or hydroperoxides thus initiating new chain reaction.

If two carbon-centered radicals recombine with each other, the polymer can form a three-dimensional network, crosslinking. Crosslinking is effective in the amorphous phase of polymers since their chains are highly mobile; whereas radicals in crystalline regions are localized in the ordered crystalline lamellae and their transfer is very limited.

During irradiation in the presence of oxygen (reaction (7)), radicals react with oxygen to form highly active peroxy radicals. The resulting peroxides are thermally stable. Oxidation initiates chain reactions predominantly in the amorphous regions, because oxygen is unable to penetrate into the ordered crystalline regions. Therefore, in presence of oxygen, with some polymers, chain scissioning predominates over crosslinking. The rate at which peroxy radicals of alkyls are produced is very high. Hydroperoxide is a precursor of many oxygen containing groups, but is not stable and over time leads to oxidation degradation products which are mainly ketones, esters, and carboxilic acids. The formation of oxidation by-products is accompanied by chain scissioning and a deterioration of mechanical properties. The reactions leading to the formation of stable by-products, such as carboxylic acid groups or carbonyl structures, are slow.

Sometimes, the effect of oxidation is preferred, and even desirable, as in the process of grafting polymers through peroxide groups to modify surfaces and some chemical and physical properties. Active superoxide radicals bind other functional groups of polymers when used for grafting [5].

The study of the oxidative degradation of polymers is frequently conducted through the use of complementary analytical techniques, such as EPR
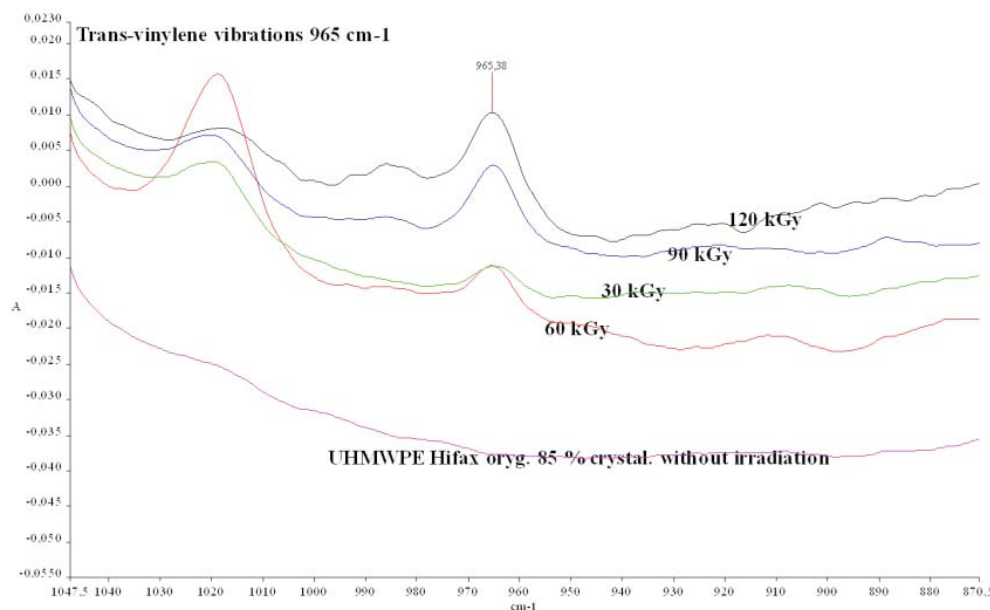
Fig.4. FTIR spectra of UHMWPE irradiated to 0 (—), 30 (—), 60 (—), 90 (—) and 120 (—) kGy.

(electron paramagnetic resonance) and FTIR (Fourier transform infrared) spectroscopy. EPR spectroscopy explores the radicals produced in polymers upon irradiation and assesses their decay as a function of time. FTIR spectroscopy estimates the presence and the amount of double bonds and of oxidation products in a polymer.

For example, the use of ionizing radiation with ultra-high molecular weight polyethylene (UHMWPE) shows both the formation of radicals and of stable products. The primary effect is the random scissioning of C–C and C–H bonds. The scissioning of a C–H bond gives vinylene double bonds, trans-vinylene double bonds, H• radicals, and secondary alkyl macroradicals in both the crystalline and in the amorphous phase of the polymer.

The trans-vinylene yield can be quantified using infrared spectroscopy by monitoring the absorbance band at 965 cm^{-1}. Figure 4 shows the absorbance spectra of the trans-vinylene unsaturation bond after the irradiation of UHMWPE at different doses. The increase of the irradiation dose results in an increased concentration of trans-vinylene groups, which shows that the radicals were incorporated into the polymer chain. The increase in trans-vinylene groups is used as an internal dosimeter for crosslinked UHMWPE, when radiation is used for improving UHMWPE's wear resistance or sterilizing medical device made thereof [6]. The content of carbonyl and carboxyl groups and of unsaturated compounds also increases.

In the presence of oxygen, radicals are oxidized. Such radical processes compete with crosslinking. Figure 5 shows the mutual quantitative relationship
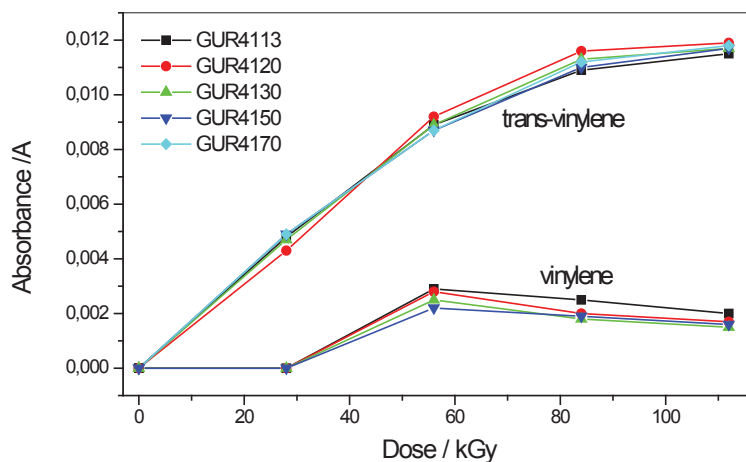
Fig.5. FTIR spectra of UHMWPE irradiated to 0 (—), 30 (—), 60 (—), 90 (—) and 120 (—) kGy.

of both types of unsaturated bonds present in UHMWPE after irradiation at different doses. These are precursors which are attacked by oxygen radicals.

The formation of double bonds in the polymer shown in the FTIR tests is compatible with EPR results when there are alkyl radicals produced by allyl radicals resulting converted from alkyl ones [7]. Both of these radicals oxidize and convert to the radicals as indicated in Fig.6.

The FTIR spectra, reported in Fig.7, contain important information on the reaction of the peroxyl radical population. One of stable products of this process are ketons which spectra are detected at 1718 cm^{-1}, as shown in Fig.7. The dominant ketonic species probably result from β-scissioning reaction of alkoxyl radicals.
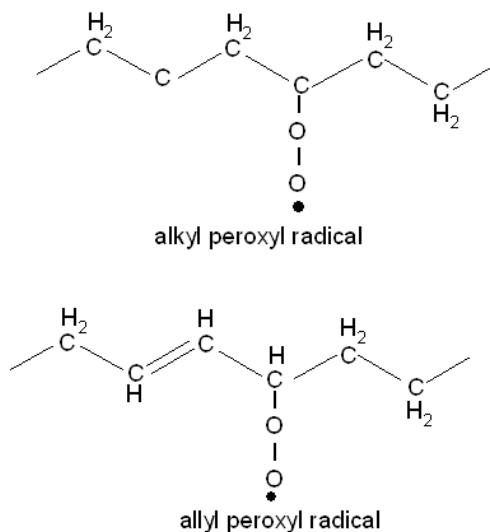
Fig.6. Structure of the alkyl peroxyl radical and allyl peroxyl radical.
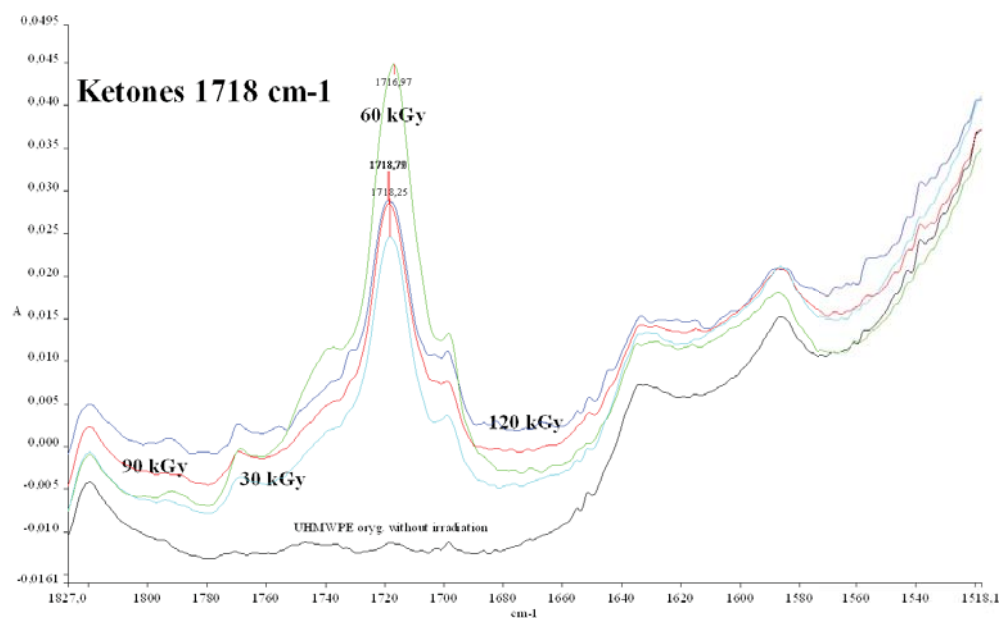
Fig.7. FTIR spectra of UHMWPE irradiated to 0 (—), 30 (—), 60 (—), 90 (—) and 120 (—) kGy.

4. POST-IRRADIATION OXIDATION

The effect of radiation on polymers can be seen in two ways. First is the direct action and the second is a delayed action as in the post-irradiation effects observed during storage. The degradation of polymers due to post-irradiation effects results from the reactions of residual radicals with oxygen in the air [8]. Free radicals trapped in the crystalline regions move toward the boundary regions and to the amorphous phases where they undergo oxidative degradation reactions with oxygen dissolved in the polymer. In order to avoid this, free radicals can be removed by thermal annealing. Oxidation can also be inhibited by suitable additives which act as radical scavengers.

Removing impurities is also a response to the benefits of the oxidation of polymers. This method, which has been used in environmental protection, reduces the molecular weight allowing for biodegradation. Oxygen-biodegradation is a two-step process:
- oxidized polymers are converted into water wettable fragments,
- bioxidative degradation produces CO_2, H_2O and biomass.

5. ANTIOXIDANTS

The post-irradiation oxidation of polymers can also be avoided by using anti-oxidants, such as hindered-amine light stabilizers (HALS) resins. The electronic structure of piperidyl type molecules acts as radical traps. The effect of substituents on the antiradical activity is important and determines their properties. Differences in radioprotection effects are attributed to a variety of reactivity of nitroxides with radiation-induced secondary free radicals. Amine stabilizers can efficiently scavenge radicals responsible for the oxidative chain [9]. This efficiency results from the cyclical regeneration of the scavenging piperidyl species.

For example, the protection of polymers by HALS is as follows:

- Amines are oxidized by superoxide
  $>NH + ROO^\bullet \rightarrow >NO^\bullet + ROH$
- Aminoethers nitroxyl radicals are formed by reaction of alkyl radicals
  $>NO^\bullet + R^\bullet \rightarrow >NOR$
- Regeneration of nitroxyl radicals
  $>NOR + ROO^\bullet \rightarrow >NO^\bullet + ROOR$

The addition of antioxidant additives not only causes the faster decay of radicals in the amorphous phase, with inhibition of radiation damage, but also can increase the apparent viscosity in the molten state by increasing crystallization temperatures due to influence of the stabilizers on nucleation, which can be followed by degradation and exhaustion of the additives.

Another way to achieve resistance to ionizing radiation in polymers could be to mix them with elastomers. Some elastomers may be more radiation tolerant than polyolefins. Elastomers with phenyl rings can increase the stability to radiation since the ring structure dissipates the energy. A styrene-butadiene-styrene (SBS) triblock copolymer in a blend with polypropylene should have such an effect. Protective role of the elastomer towards polypropylene needs insight into radiation chemistry of the materials.

Compounds playing the role antioxidants often occur in nature. The use of natural antioxidants in polymers is encouraging because of their stabilization effects as well as their non-toxic character. The bioactive form of vitamin E, α-tocopherol, is a compound with very low toxicity and extremely effective antioxidant properties for plastics and rubbers, *e.g.* as used in the melt processing of polyolefins [10]. The recommended concentration of α-tocopherol in UHMWPE at 0.3 mass% gives comparable results to the addition of synthetic antioxidants (as BHT and Irganox 1076) used at higher concentrations [11]. Such small additions of vitamin E are effective to protect polymers from exposure to environmental factors after the irradiation treatment.

The use of antioxidants makes possible the radiation sterilization of polymers.

REFERENCES

[1]. Kudoh, H., Sasuga, T., & Seguchi, T. (1996). High-energy ion irradiation effects on polymer materials. In R.L. Clough & Sh.W. Shalaby (Eds.), *Irradiation of polymers. Fundamentals and technological applications* (pp. 2-10). Washington, DC: American Chemical Society.

[2]. Grigoriev, E.I., & Trakhtenberg, L.I. (1996). *Radiation-chemical processes in solid phase. Theory and application.* Boca Raton: CRC Press.

[3]. Makuuchi, K., & Cheng, S. (2012). *Radiation processing of polymer materials and its industrial applications.* Hoboken: A John Wiley & Sons, Inc., Publication.

[4]. Wagner, C.D. (1969). Chemical synthesis by ionizing radiation. In M. Burton & J.L. Magee (Eds.), *Advances in radiation chemistry* (Vol.1, pp. 199-244). New York: Wiley-Interscience.

[5]. Camara, S., Gilbert, B.C., Meier, R.J., Van Duin, M., & Whitwood, A.C. (2006). EPR studies of peroxide decomposition, radical formation and reactions relevant to cross-linking and grafting in polyolefines. *Polymer*, *47*, 4683-4693. DOI: 10.1016/j.polymer.2006.04.015.

[6]. ASTM. (2004). *Standard test method for evaluating trans-vinylene yield in irradiated ultra-high-molecular-weight polyethylene fabricated forms intended for surgical implants by infrared spectroscopy*. F 2381-04.

[7]. Kornacka, E.M., Przybytniak, G., & Święszkowski, W. (2013). The influence of crystallinity on radiation stability of UHMWPE. *Radiat. Phys. Chem.*, *84*, 151-156. DOI: 10.1016/j.radphyschem.2012.06.027.

[8]. O'Neil, P., Birkinshaw, C., Leahy, J.J., & Barklie, R. (1999). The role of long lived free radicals in the ageing of irradiated ultra high molecular weight polyethylene. *Polym. Degrad. Stabil.*, *63*, 31-39. PII: S0141-3910(98)00058-5.

[9]. Przybytniak, G., Mirkowski, K., Rafalski, A., Nowicki, A., & Kornacka, E. (2007). Radiation degradation of blends polypropylene/poly(ethylene-co-vinyl acetate). *Radiat. Phys. Chem.*, *76*, 1312-1317. DOI: 10.1016/j.radphyschem.2007.02.022.

[10]. Al-Malaika, S., Ashley, H., & Issenhuth, S. (1994). The antioxidant role of α-tocopherol in polymers. I. The nature of transformation products of α-tocopherol formed during melt processing of LDPE. *J. Polym. Sci. Part A: Polym. Chem.*, *32*, 3099-3114. DOI: 10.1002/pola.1994.080321610.

[11]. Ridley, M.D., & Jahan, M.S. (2007). Measurements of free radical in vitamin E-doped ultra-high molecular weight polyethylene: Dependence on materials processing and irradiation environments. *Nucl. Instrum. Meth. Phys. Res. B*, *265*, 62-66. DOI: 10.1016/j.nimb.2007.08.026.

RADIATION-INDUCED GRAFTING

Marta Walo

Institute of Nuclear Chemistry and Technology, Dorodna 16, 03-195 Warszawa, Poland

1. INTRODUCTION

For many decades, radiation-induced grafting has been a way to functionalize the surfaces of existing polymer forms [1] so that they can be used in a variety of applications, such as biomedical, environmental and industrial uses [2]. Radiation grafting changes the surface of polymeric materials by chemically bonding polar or non-polar monomers having functional groups, such as –COOH, –OR, –OH, $-NH_2$, $-SO_3H$, –R and their derivatives, to affect surface properties without influence on the bulk material.

Ultraviolet radiation (UV), gamma rays and electron beam (EB) radiation can be used to generate active sites (free radicals) on a polymeric surface which can then react with vinyl monomers to form a graft copolymer.

A graft copolymer can be defined as branched copolymer composed of a main chain of a polymer backbone onto which side chain grafts (branches) are covalently attached. The polymer backbone may be a homopolymer or copolymer and differs in chemical structure and composition from the graft material [3].

A simplified structure of a graft copolymer composed of a backbone and graft side chains is presented in Fig.1.
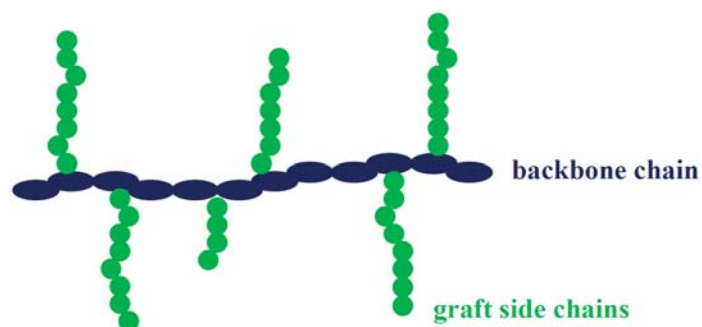
Fig.1. Simplified structure of graft copolymer.

The modification of polymer surfaces can be achieved by conventional grafting or by reversible addition-fragmentation chain transfer (RAFT)-mediated grafting methods. With conventional grafting methods, the molecular weight and polydispersity of grafted chains cannot be controlled. As a result the surface is covered with grafted chains of different lengths, as shown in Fig.2A. To obtain graft copolymers with predetermined graft molecular weight and very narrow chain length distribution, a novel method using a controlled radical polymerization (CRP) of reversible addition-fragmentation chain transfer polymerization grafting has been used [4, 5], as shown in Fig.2B.
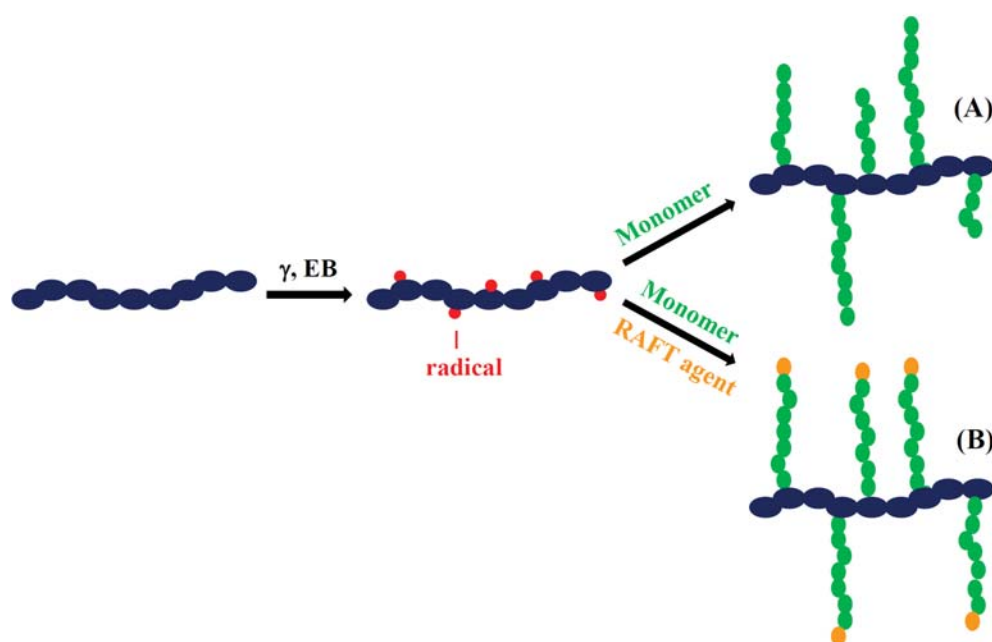
Fig.2. Radiation-induced grafting using (A) conventional and (B) RAFT-mediated polymerization initiated by ionizing radiation.

Surface modification by the conventional grafting method has several general advantages such as [6, 7]:
- It is a simple, relatively clean and repeatable process.
- Any polymer can be the modified surface which can be in the form of film, membrane, fiber, fabric, or powder and most free radical polymerizable monomers such as styrene, methacrylamides, acrylamides, methacrylates, acrylates, acrylonitrile, vinyl acetates, vinyl chlorides, acrylic acid, *N*-vinyl-pyrrolidone, can be grafted.
- The graft copolymer is very pure, with no initiator or related impurities remaining on the modified surface.
- The degree of grafting may be controlled by changes the reaction conditions (*e.g.* monomer concentration, reaction temperature, atmosphere, type of solvent, addition of suppressor of homopolymerization, addition of acid)

and the radiation exposure parameters (type of radiation, dose rate, irradiation time, dose).

- In comparison with chemical methods, radiation-induced grafting does not require heating of the system to initiate the graft polymerization reaction so that the polymer structure of the substrate is not changed and temperature sensitive monomers can be grafted.

Key strengths of RAFT-mediated grafting are [8-10]:

- The ability to control the molecular weight of grafted chains to have a narrow molecular weight distribution.
- Grafting can be done with a wide range of functional monomers: methacrylates, acrylates, acrylamides, acrylonitrile, styrene, dienes and vinyl monomers.
- Well-defined polymers with different topologies and molecular architecture can be synthesized (*e.g.* gradient, block, star, comb, or hyperbranched co-polymers).
- Macromolecule chain extension through the addition of other monomers is possible which can lead to the formation of block copolymers.

From an application perspective, graft surface modification of polymeric materials has many uses [2, 11, 12]:

- to improve or reduce polymer hydrophicility and/or hydrophobicity;
- to modify blood compatability of medical devices;
- to influence cell adhesion and growth on scaffolds used in tissue engineering;
- to improve the lubricity of implants;
- to facilitate the design of membranes used in batteries, fuel cells, chromatography;
- to prepare metal ion adsorbents.

2. METHODS OF RADIATION-INDUCED GRAFTING

Radiation-induced grafting can be performed by two major methods: a mutual or simultaneous technique or a pre-irradiation technique [13]. Typically grafting is performed in solution or emulsion where the reaction medium is usually water with a small amount of surfactant (*e.g.* Tween 20) [2, 14].

The selection of either method depends on the polymer to be modified, the reactivity of monomer and the radiation source.

The pre-irradiation technique is particularly useful if access to a gamma source or an accelerator is limited. A polymer surface may be pre-irradiated (in air or in vacuum) and then even after some storage time can be used to initiate the graft polymerization.

2.1. MUTUAL OR SIMULTANEOUS METHOD

In this method, the polymeric material is immersed in the monomer solution (or in pure monomer) and exposed to ionizing radiation. Irradiation can be performed in air or in inert atmosphere (*e.g.* nitrogen) usually using gamma sources. This is the simplest and a common method chosen for polymeric material surface modification and is suitable for substrates that are sensitive to radiation.

The mechanism for this process is given in the following sequence of equations:

$$PH \xrightarrow{\gamma} P^\bullet + H^\bullet \tag{1}$$

$$P^\bullet + M \rightarrow PM^\bullet \tag{2}$$

$$PM^\bullet + nM \rightarrow PM_{n+1}^\bullet \tag{3}$$

Ionizing radiation forms in the polymeric substrate active sites, PH (Eq. (1)). The primary radicals of polymer backbone, $P^\bullet$, react with a molecule of the monomer, M, initiating the graft polymerization (Eq. (2)). After the initiation step, the propagation step takes place and the graft chain grows onto the polymer backbone and continues to occur after successive joining of the monomer to the macroradical centers (Eq. (3)).

Since the grafting mixture is exposed to ionizing radiation, active sites can be formed in polymer backbone, in the monomer and in the solvent. Side reactions can also take place which limit the degree of grafting due to the consumption of monomer by radicals other than in the polymeric backbone. In the mutual method, there is, in parallel with the grafting reaction, homopolymerization of monomers leading to the formation of a homopolymer (Eqs. (4)-(6)) [13].

$$M \xrightarrow{\gamma} M^\bullet \tag{4}$$

$$M^\bullet + nM \rightarrow M_{n+1}^\bullet \tag{5}$$

$$M_{n+1}^\bullet + M_m^\bullet \rightarrow M_{n+m+1}^\bullet \tag{6}$$

Homopolymerization suppresses the degree of grafting by increasing the viscosity when the homopolymer formed is soluble in the monomer or solvent used in grafting. The diffusion of monomer to the reactive sites on the polymer backbone becomes difficult. Moreover, due to the consumption of monomer in homopolymer formation, less monomer is available for the grafting reaction [15].

To reduce the formation of homopolymer, inorganic salts can be added to the grafting system when water or other media are the solvents.

2.2. PRE-IRRADIATION METHOD

The pre-irradiation method involves a sequence of the following steps:
- The polymer substrate is irradiated in air or in an inert atmosphere to generate active radical sites.
- Monomer reaction is initiated with the irradiated polymeric substrate.

- Heating is applied to support the propagation of the reaction when peroxides are involved.

$$PH \xrightarrow{\gamma} P^\bullet + H^\bullet \qquad (7)$$
$$P^\bullet + O_2 \rightarrow POO^\bullet \qquad (8)$$
$$POO^\bullet + PH \rightarrow POOH + P^\bullet \qquad (9)$$
$$POOH \xrightarrow{\Delta} PO^\bullet + {}^\bullet OH \qquad (10)$$
$$PO^\bullet + M \rightarrow POM^\bullet \qquad (11)$$
$$POM^\bullet + nM \rightarrow POM_{n+1}{}^\bullet \qquad (12)$$

With polymeric substrates exposed to ionizing radiation in air, peroxide radicals are generated due to oxidation of alkyl radicals (Eqs. (7)-(8)). These products when in contact with the polymeric substrate convert into the hydroperoxides (Eq. (9)). The hydroperoxides decompose under heating to alkoxy radicals (Eq. (10)). Radicals obtained this way are capable of initiating the graft polymerization in the presence of monomers (Eqs. (11)-(12)).

In the case of this pre-irradiation method in the presence of oxygen, it is possible to carry out the graft modification of a substrate for some time after irradiation, due to the stability of the hydroperoxides, especially when the irradiated substrate is stored at 0°C or lower.

Another variation of the pre-irradiation method is to use non-oxidized reactive radical species generated by radiation. In this case, in order to obtain a high concentration of radicals, the polymer should be irradiated at high dose rates, *e.g.* by high energy electrons, under an inert atmosphere or in vacuum and the grafting carried out immediately after the irradiation exposure.

An important advantage of the pre-irradiation method is that less homopolymer is formed. However, hydroperoxide species can be formed by thermal decomposition to produce ${}^\bullet OH$ radicals which can be involved in homopolymerization [16].

An important parameter that should be taken into account before planning a grafting process using the mutual or simultaneous method is to compare the radiation chemical yield G-value of polymeric substrate and of the monomer. (The G-value is defined as the number of product molecules formed or initial molecules changed for every 100 eV of energy absorbed; the SI unit of radiation-chemical yield is μmol/J, 1 molecule/100 eV = 1.036×10^{-7} mol/J = 0.1036 μmol/J). The reaction proceeds in the favor of graft polymerization when $G(R_p{}^\bullet)$ of the irradiated polymer is much greater than for the monomer. In contrast to homopolymerization which is prevailed when $G(R_M{}^\bullet)$ of the monomer is higher than for the polymeric substrate [13]. G-values for various polymers may be found in the literature [14, 17].

In pre-irradiation technique, monomer is not exposed to radiation. Radicals are generated only on the polymeric substrate. Therefore, this method is relatively free from homopolymer formation.

The most significant differences between the mutual and the pre-irradiation methods are summarized in Table 1 [13, 14].

Table 1. Comparison of mutual and pre-irradiation methods of radiation-induced grafting [13, 14].

Parameter	Mutual method	Pre-irradiation method
Type of radiation	Gamma, EB	EB, gamma
Absorbed dose	Low (10 kGy or less)	High (100 kGy and more)
Dose rate	Low [kGy/h]	High [kGy/s]
Irradiation time	Long [h]	Short [min] or [s]
Atmosphere	Inert gas	Air/inert gas/vacuum
Side reactions: homopolymerization	High	Low
Temperature	Ambient	Irradiation: ambient/low temperature, graft polymerization: high (peroxide decomposition)

2.3. RAFT-MEDIATED GRAFTING

Research has been carried out in the field of controlled radical polymerization, *i.e.* atom transfer radical polymerization (ATRP) [18, 19], nitroxide mediated polymerization (NMP) [20, 21] and reversible addition-fragmentation chain transfer (RAFT) polymerization [22, 23]. Each of these methods enables the synthesis of well-defined graft copolymers with narrow molecular weight distribution (polydispersity) of the grafted chains. However, only the RAFT polymerization process can be initiated by gamma or electron beam radiation. Radiation generates active sites (free radicals) in polymeric substrate which can further react with monomers in the presence of a RAFT agent to form grafted coatings. In other methods, heat or a photoinitiator must be used to generate a free radical on an initiator and then the active center is transferred to the monomer/polymer backbone.

RAFT-mediated grafting initiated by ionizing radiation can be performed by the mutual and the pre-irradiation methods as well. The difference compared to conventional method of grafting lies in the presence of the RAFT agent in the grafting system. RAFT agents are commercially available thiocarbonylthio compounds [ZC(=S)SR] such as dithioesters, dithiocarbamates, trithiocarbonates, xanthates [24]. The general structure of a RAFT agent is presented in Fig.3.

Z group modifies addition and fragmentation rates in polymerization whereas R group can be detached easily to form R$^{\bullet}$ (must also be able to reinitiate polymerization) [24]. The success of RAFT-mediated grafting depends on appropriate selection of RAFT agent for monomer. In literature, data on diverse RAFT agents working appropriately with various monomers is available (*e.g.* [24-27]).
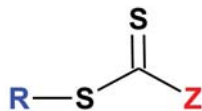
Fig.3. The general structure of RAFT agent [24].

The key step in RAFT polymerization is chain equilibrium reaction between the active radicals and dormant propagating polymer chains (Eq. (13)). A rapid equilibrium between the active propagating radicals ($P_n^\bullet$ and $P_m^\bullet$) and the dormant thiocarbonyl thio-capped chains provides equal probability for all chains grow and allows the synthesis of low polydispersity polymers [9, 10, 28, 29].
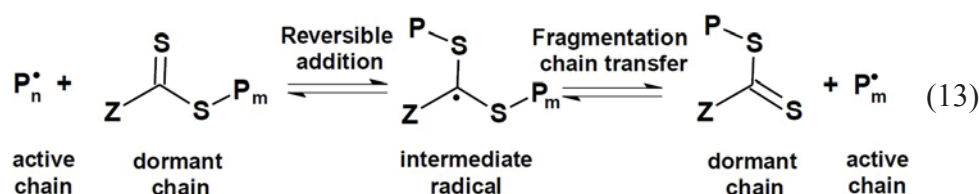
To obtain graft copolymer with predetermined molecular weight, M_n, preparation of a solution with appropriate RAFT agent and monomer concentration is necessary.

The theoretical number average molecular weight, M_n, of grafted polymer chains can be calculated according to the Eq. (14) [30]:

$$M_n = M_{RAFT} + \frac{n\,M}{n_{RAFT}}k \qquad (14)$$

where: M_{RAFT} – molecular weight of the RAFT agent, n – number of moles of the monomer initially present in the system, n_{RAFT} – number of moles of RAFT agent, M – molecular weight of monomer, k – conversion.

In RAFT-mediated grafting, the determination of the molecular weight of grafted chains onto a polymer surface is done by size exclusion chromatography (SEC). The assumption is made that in the RAFT polymerization process, the graft chain growth is in a dynamic equilibrium with the free polymer chains in solution. Therefore, analysis of the free polymer precipitated from the solution provides information on the molecular weight and polydispersity of grafted polymer [31].

3. PARAMETERS AFFECTING THE RADIATION-INDUCED GRAFTING

The degree of grafting depends on many factors, such as the type of polymer and monomer, monomer concentration, type of radiation, temperature, reaction

atmosphere, concentration of homopolymerization suppressor and type of solvent [13, 32, 33]. Therefore, the efficiency of the process can be controlled by the selection of these reaction parameters.

The following discusses the factors that control the radiation-induced grafting.

3.1. TYPE OF POLYMER

Radiation-induced grafting can be used for surface modification of all commercially available synthetic and natural polymers. Materials for grafting have to meet certain requirements since the chemical structure and morphology significantly affect the degree of grafting and the final properties of grafted materials. For radiation degradable polymers, high irradiation dose used usually in the pre-irradiation method is not recommended. In contrast, radiation resistant materials may be modified by both grafting methods.

The degree of grafting strongly depends on the amount of radicals in the irradiated polymeric substrate. Electron paramagnetic resonance (EPR) spectroscopy can be used to monitor the radicals in the sample and to identify and track the conversion of radiation generated paramagnetic species to their subsequent products. This method allows for the comparison of radical amounts in polymers and is helpful in predicting their behavior in radiation-induced grafting. For example, for polystyrene (PS), polypropylene (PP) and polyethylene (PE) irradiated at the same dose by ionizing radiation, the concentration of radicals stable at room temperature and the radiation yields of radicals $(G(R_p^\bullet))$ is in following order: PS < PP < PE. Under comparable conditions, the same relationship was found for the degree of radiation-induced grafting of acrylic acid on these polymers using the mutual method [34].

Among many polymers, whose surfaces were modified by radiation grafting, the largest group are polyolefins: polyethylene and polypropylene, often in the form of filters, films, brushes or powders (*e.g.* [35-40]). However, there are many examples of surface modification which were successfully carried out onto polyamide (PA) (*e.g.* [41, 42]), poly(ethylene terephthalate) (PET) (*e.g.* [43, 44]), polyurethane (PUR) (*e.g.* [45, 46]), silicon (*e.g.* [47, 48]), cellulose (*e.g.* [49, 50]), poly(tertafluoroethylene) (PTFE) (*e.g.* [51, 52]) or poly(vinylidene fluoride) (PVDF) (*e.g.* [53, 54]).

3.2. TYPE OF MONOMER

The degree of radiation grafting (gravimetrically determined by the percentage of mass increase) is a function of the reactivity of the consumed monomer. Monomer reactivity depends on the polarity, the energy of bonds,

and the chemical structure, *etc*. The degree of grafting is also influenced by the monomer concentration and the type of solvent used for grafting. The reactivity of a monomer depends not only on the kinetics of the process but also on the diffusion of the reactant to the polymer surface, which affects the rate and efficiency of grafting [13]. Generally, with increasing monomer concentration, the degree of grafting increases. However, using too high concentration of monomer may enhance homopolymerization and decrease the degree of grafting [55]. For every grafting system, the monomer concentration should be adjusted to avoid this undesired homopolymerization of the monomer.
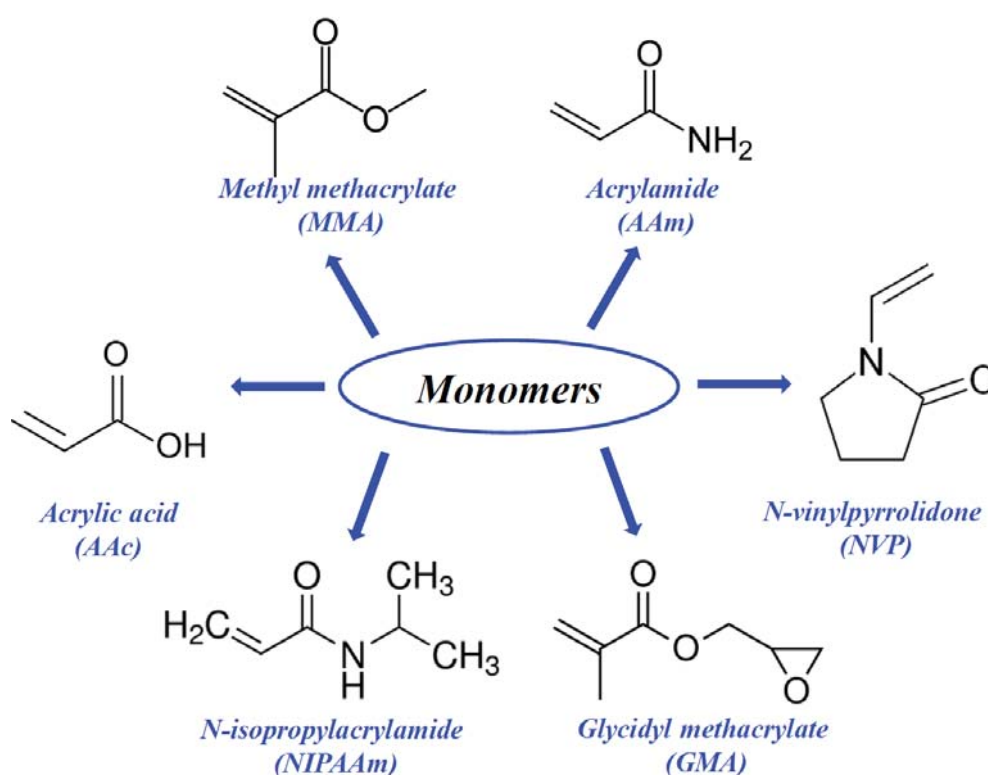
Fig.4. Chemical structure of the most frequently used monomers in radiation-induced grafting.

The most frequently used monomers in graft polymerization are vinyl monomers such as: methyl methacrylate (MMA), glycidyl methacrylate (GMA), acrylamide (AAm), acrylic acid (AAc), *N*-vinylpyrrolidone (NVP), *N*-isopropylacrylamide (NIPAAm).

The chemical structure of some of the monomers used in radiation-induced grafting is presented in Fig.4.

3.3. TYPE OF SOLVENT

Depending on the solvent, its properties and behavior during the grafting process, the degree of grafting for the same monomer, dose, atmosphere reaction, temperature, *etc.* can differ significantly. The type of solvent affects not only the grafting efficiency but also the homogeneity of the grafted chains, which can be obtained using good swelling solvents [13]. Water and alcohols are widely used for grafting of hydrophilic monomers. However for every grafting system, the solvent should be selected experimentally, especially for the RAFT-mediated grafting processes.

3.4. TYPE OF RADIATION (DOSE, DOSE RATE)

Radiation-induced grafting may be carried out using gamma radiation (^{60}Co, ^{137}Cs) and EB radiation as well. Grafting by the mutual method is usually performed using a gamma source, as compared to the pre-irradiation method, where the preferred radiation is an electron beam [13, 56]. The main difference in these two types of radiation is the dose rate defined as dose delivered in a specific unit of time. In the case of isotope sources, the dose rate is relatively low (kGy/h), while for electron beams it is high (kGy/s). Consequently, the irradiation time in a gamma source is much longer (h) than when using a high energy electron beam (min or s). This factor significantly affects the degree of grafting. The higher the dose, the greater the amount of radicals are generated in the polymeric material, which has a direct impact on the degree of grafting. The dose rate effects the concentration and lifetime of radicals, the oxidation and time after that the termination of the growth graft chains occurs. In mutual or simultaneous grafting, for the same dose, increase in the dose rate results in lower efficiency of grafting, because the high concentration of radicals increases their recombination leading to a rapid termination process and to more homopolymerization.

3.5. TEMPERATURE

Irradiation temperature and grafting temperature are important parameters influencing the process of radiation-induced grafting.

3.5.1. Irradiation temperature

In the pre-irradiation method, the polymeric substrate might be irradiated at sub-ambient temperatures (0°C and lower) in order to restrain the combination of radicals generated during irradiation. Then, even after storage, the trapped radicals may be used to initiate graft polymerization.

During mutual grafting, irradiation temperature also affects the degree of grafting. If irradiation is performed above the glass transition temperature of polymer, T_g, due to enhanced mobility of chain segments, the active sites can migrate to the surface increasing population of the radicals involved in grafting. On the other hand, below the T_g irradiated polymers are rigid and thus monomers have access to the active centers produced *via* irradiation on the external layer of material. Thus, selection of irradiation temperature determines the final effect of the grafting process. Thermal conditions influence also diffusion of monomers in solution.

3.5.2. Grafting temperature

In general, the rate of grafting increases with the increase of the reaction temperature. The grafting process is also controlled by diffusion, so this effect could be significant. In the solution there are many competing reactions which reduce the concentration of radicals and accelerate their termination. Typically, increasing the temperature is to (i) enhance the process of grafting by changing the kinetics of the reaction or (ii) decompose peroxides leading to the formation of active centers that initiate monomers and chain propagation polymerization in the process.

3.6. ATMOSPHERE OF RADIATION GRAFTING

Radiation-induced grafting may be carried out under an inert atmosphere (*e.g.* nitrogen), in vacuum or in the presence of air. The use of an anaerobic atmosphere prevents reactions of alkyl radicals with oxygen and the formation of peroxide radicals, which in consecutive reactions convert to the stable oxidation products. The absence of oxygen reduces the radicals involved in the grafting process. The presence of oxygen can lead to oxidative degradation of the irradiated polymeric material, which impairs its physicochemical properties. Moreover, oxygenated degradation products can be toxic and can affect the biological tolerance, which is particularly undesirable in materials to be used in biomedical applications [57]. In pre-irradiation method, the irradiation can be carried out in the presence of oxygen, to form peroxides and hydroperoxides which, after thermal decomposition, initiate graft polymerization.

3.7. SUPRESSION OF HOMOPOLYMER FORMATION

The use of homopolymerization suppressors is an important element in the process of radiation grafting in aqueous systems. During exposure to ionizing radiation, active centers can be formed in polymeric materials and in the monomer. If the monomer concentration is high and the reactivity of the radicals is

high as well, the dominant reaction is homopolymer formation. This is undesirable since surface modification will not be achieved. Research in this field has showed reduction and, in some cases, elimination of the homopolymerization process by adding to the irradiation system a small amount of a suppressor (usually of a few millimoles). 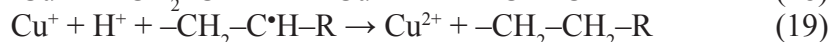For this purpose, inorganic metal salts are used, *e.g.* iron (II) chloride ($FeCl_2$), copper (II) chloride ($CuCl_2$), copper (II) sulfate ($CuSO_4$), ammonium iron (II) sulfate ($Fe(NH_4)_2(SO_4)_2(6H_2O)$) (Mohr's salt) [13, 14]. These additives are used in aqueous solutions of monomers and after dissolving they become hydroxyl radical scavengers, reducing homopolymerization. There is a threshold concentration of these salts to prevent homopolymerization, above which there is no formation of a homopolymer. Further increasing the concentration of such an inhibitor affects very little of the degree of grafting. There are a few studies which confirm that the copper and iron salts not only inhibit the homopolymerization process, but also help to increase the efficiency of grafting. Such an effect was observed by Dworjanyn *et al.* [58] when grafting styrene onto cellulose or polyolefin substrates.

To understand the mechanism of the action of metal ions in aqueous systems, water radiolysis products are formed during irradiation (Eq. (15)). In the mutual or simultaneous grafting method, among radical products of water radiolysis there are some uncontrolled effects resulting from hydroxyl radicals that are capable of initiating homopolymer chain growth. Also, in the case of the mutual method in the presence of oxygen, hydroperoxides are formed in the polymeric substrate, and their degradation at elevated temperatures leads to the formation of active radicals $^\bullet OH$ (Eq. (16)). Therefore, the metal ions are added to the system to deactivate hydroxyl radicals to inactive OH^- anions (Eq. (17)) [59, 60]. Metal ions play a role as hydroxyl radical scavengers.

$$H_2O \xrightarrow{\gamma, e^-} {}^\bullet OH, H^\bullet, e^-_{aq}, O_2, H_2O_2 \qquad (15)$$

$$POOH \rightarrow PO^\bullet + {}^\bullet OH \qquad (16)$$

$$Fe^{2+} + {}^\bullet OH \rightarrow Fe^{3+} + OH^- \qquad (17)$$
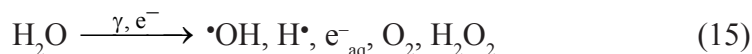
In the literature [61], it was noted that in aqueous systems in which grafting process is carried out by the mutual method in the presence of Cu^{2+} ions, the mechanism of suppression of the homopolymerization process can be illustrated by the following equations:

$$Cu^{2+} + -CH_2-C^\bullet H-R \rightarrow Cu^+ + H^+ + -CH=CH-R \qquad (18)$$

$$Cu^+ + H^+ + -CH_2-C^\bullet H-R \rightarrow Cu^{2+} + -CH_2-CH_2-R \qquad (19)$$

$$Cu^+ + {}^\bullet OH \rightarrow Cu^{2+} + OH^- \qquad (20)$$

Cu^{2+} ions are involved directly in the deactivation of homopolymer radicals according to (Eq. (18)). Cu^+ ions in solution are then oxidized to Cu^{2+} ions and again participate in the process of inhibiting the homopolymer chain growth (Eq. (19)). Cu^+ ions can also deactivate $^\bullet OH$ radicals as expressed by (Eq. (20)).

3.8. ROLE OF ADDITIVES

The addition of mineral acid (*e.g.* hydrochloric acid, sulfuric acid) to the aqueoues solution of a monomer enhances the degree of grafting [13, 62]. Under such conditions (low pH), hydrated electrons generated during water radiolysis are trapped by protons and converted into hydrogen atoms. The ability of the species to abstract hydrogen from polymeric material is higher than their pecursors, *i.e.* electrons. Therefore, the yield of radicals formed in polymeric chains incerases, which results in the enhancement of active sites initiating grafting. Also, the addition of polyfunctional monomers (*e.g.* divinyl benzene, multifunctional acrylates in amount of about 1% v/v) can accelerate the grafting process and such action is recommended when improved properties of the finished product is desired, especially in radiation-grafted fuel cell membranes [63].

4. CHARACTERIZATION OF RADIATION-GRAFTED COPOLYMERS

Upon completion of the graft polymerization process, prior to the characterization of grafted substrate, samples should be extracted by suitable solvents in order to remove unreacted monomers, free polymer, and additives. Then the product can be dried to a constant weight. The degree of grafting, DG (wt%) can be determined gravimetrically using the following equation:

$$DG = (W - W_0)/W_0 \times 100\% \qquad (21)$$

where W and W_0 are the weights of the grafted and non-grafted polymer, respectively.

There are a number of analytical techniques which can be used to provide information about the polymer surface, ranging from the micron to the nanometer scale. A comparative analysis of non-grafted and grafted samples can confirm the effects of the grafting process by using several methods: attenuated total reflection Fourier transform infrared (ATR-FTIR) spectroscopy, Raman spectroscopy, X-ray photoelectron spectroscopy (XPS), atomic force microscopy (AFM), scanning electron microscopy (SEM), contact angle (CA) measurements.

Monitoring structural and morphological changes induced by radiation grafting can be performed as well as by: differential scanning calorimetry (DSC), thermogravimetry (TGA), dynamic mechanical analysis (DMA), X-ray diffraction (XRD) and others.

In case of RAFT-mediated grafting, size exclusion chromatography (SEC) is a key method to evaluate the molecular weight of grafted chains.

REFERENCES

[1]. Chapiro, A. (1962). *Radiation chemistry of polymeric systems*. New York: John Wiley & Sons.

[2]. Nasef, M.M., & Güven, O. (2012). Radiation-grafted copolymers for separation and purification purposes: Status, challenges and future directions. *Prog. Polym. Sci.*, *37*(12), 1597-1656. DOI: 10.1016/j.progpolymsci.2012.07.004.

[3]. Herman, F.M. (2007). Graft copolymers. In *Encyclopedia of polymer science and technology. Concise* (3rd ed., p. 526). New Jersey: Wiley.

[4]. Moad, G., Chong, Y.K., Postma, A., Rizzardo, E., & Thang, S.H. (2005). Advances in RAFT polymerization: The synthesis of polymers with defined end-groups. *Polymer*, *46*(19), 8458-8468. DOI: 10.1016/j.polymer.2004.12.061.

[5]. Moad, G., & Thang, S.H. (2008). Radical addition–fragmentation chemistry in polymer synthesis. *Polymer*, *49*(5), 1079-1131. DOI: 10.1016/j.polymer.2007.11.020.

[6]. Choi, J.H., Jung, C.H , Kim, D.K., & Ganesan, R. (2008). Radiation-induced grafting of inorganic particles onto polymer backbone: A new method to design polymer-based nanocomposite. *Nucl. Instrum. Meth. B*, *266*(1), 203-206. DOI: 10.1016/j.nimb.2007.11.012.

[7]. Güven, O., & Sen, M. (1991). Preparation and characterization of poly(N-vinyl 2-pyrrolidone) hydrogels. *Polymer*, *32*(13), 2491-2495. DOI: 10.1016/0032-3861 (91)90093-X.

[8]. Moad, G., Chiefari, J., Chong, Y.K., Krstina, J., Mayadunne, R.T.A., Postma, A., Rizzardo, E., & Thang, S.H. (2000). Living free radical polymerization with reversible addition – fragmentation chain transfer (the life of RAFT). *Polym. Int.*, *49*, 993-1001. DOI: 10.1002/1097-0126(200009)49:9<993::AID-PI506>3.0.CO;2-6.

[9]. Moad, G., Rizzardo, E., & Thang, S.H. (2006). Living radical polymerization by the RAFT process – A first update. *Aust. J. Chem.*, *59*(10), 669-692. DOI: 10.1071/CH06250.

[10]. Barner-Kowollik, C., Blinco, J.P., Destarac, M., Thurecht, K.J., & Perrier, S. (2012). Reversible addition fragmentation chain transfer (RAFT) polymerization: Mechanism, process and applications. In *Encyclopedia of radicals in chemistry, biology and materials* (Vol. 4, pp.1895-1929). Chichester: John Wiley & Sons, Ltd.

[11]. Ratner, B.D., & Hoffman, A.S. (2004). Physicochemical surface modification of materials used in medicine. In B.D. Ratner, A.S. Hoffman, F.J. Schoen & J.E. Lemons (Eds.), *Biomaterials science: An introduction to materials in medicine* (2nd ed., pp. 201-218). USA: Elsevier Academic Press.

[12]. Hoffman, A.S. (1995). Surface modification of polymers. *Chinese J. Polym. Sci.*, *13*(3), 195-203.

[13]. Nasef, M.M., & Hegazy, E.S.A. (2004). Preparation and applications of ion exchange membranes by radiation-induced graft copolymerization of polar monomers onto non-polar films. *Prog. Polym. Sci.*, *29*(6), 499-561. DOI: 10.1016/j.progpolymsci.2004.01.003.

[14]. Makuuchi, K., & Cheng, S. (2012). *Radiation processing of polymer materials and its industrial applications* (1st ed.). USA: John Wiley & Sons, Inc.

[15]. Kumar, V., Bhardwaj, Y.K., Rawat, K.P., & Sabharwal, S. (2005). Radiation-induced grafting of vinylbenzyltrimethylammonium chloride (VBT) onto cotton

fabric and study of its anti-bacterial activities. *Radiat. Phys. Chem.*, *73*(3), 175-182. DOI: 10.1016/j.radphyschem.2004.08.011.

[16]. Choi, S.H., & Nho, Y.C. (2000). Radiation-induced graft copolymerization of binary monomer mixture containing acrylonitrile onto polyethylene films. *Radiat. Phys. Chem.*, *58*(2), 157-168. DOI: 10.1016/S0969-806X(99)00367-9.

[17]. Charlesby, A. (1960). *Atomic radiation and polymers*. England: Pergamon Press Limited.

[18]. Kato, M., Kamigaito, M., Sawamoto, M., & Higashimura, T. (1995). Polymerization of methyl methacrylate with the carbon tetrachloride/dichlorotris-(triphenylphosphine)ruthenium(II)/methylaluminum bis(2,6-di-tert-butylphe-noxide) initiating system: Possibility of living radical polymerization. *Macromolecules*, *28*(5), 1721-1723. DOI: 10.1021/ma00109a056.

[19]. Wang, J.S., & Matyjaszewski, K. (1995). Controlled/"living" radical polymerization. Atom transfer radical polymerization in the presence of transition-metal complexes. *J. Am. Chem. Soc.*, *117*(20), 5614-5615. DOI: 10.1021/ja00125a035.

[20]. Georges, M.K., Veregin, R.P.N., Kazmaier, P.M., & Hamer, G.K. (1993). Narrow molecular weight resins by a free-radical polymerization process. *Macromolecules*, *26*(11), 2987-2988. DOI: 10.1021/ma00063a054.

[21]. Hawker, C.J, Bosman, A.W., & Harth, E. (2001). New polymer synthesis by nitroxide mediated living radical polymerizations. *Chem. Rev.*, *101*(12), 3661-3688. DOI: 10.1021/cr990119u.

[22]. Chiefari, J., Chong, Y.K., Ercole, F., Krstina, J., Jeffery, J., Le, T.P.T., Mayadunne, R.T.A., Meijs, G.F., Moad, C.L., Moad, G., Rizzardo, E., & Thang, S.H. (1998). Living free-radical polymerization by reversible addition-fragmentation chain transfer: The RAFT process. *Macromolecules*, *31*(16), 5559-5562. DOI: 10.1021/ma9804951.

[23]. Destarac, M., Charmot, D., Franck, X., & Zard, S.Z. (2000). Dithiocarbamates as universal reversible addition-fragmentation chain transfer agents. *Macromol. Rapid Commun.*, *21(15)*, 1035-1039. DOI: 10.1002/15213927(20001001)21:15<1035::AID-MARC1035>3.0.CO;2-5.

[24]. Moad, G., Rizzardo, E., & Thang, S.H. (2005). Living radical polymerization by the RAFT process. *Aust. J. Chem.*, *58*(6), 379-410. DOI: 10.1071/CH05072.

[25]. Barsbay, M., & Güven, O. (2013). RAFT mediated grafting of poly(acrylic acid) (PAA) from polyethylene/polypropylene (PE/PP) nonwoven fabric via preirradiation. *Polymer*, *54*(18), 4838-4848. DOI: 10.1016/j.polymer.2013.06.059.

[26]. Kodama, Y., Barsbay, M., & Güven, O. (2014). Poly(2-hydroxyethyl methacrylate) (PHEMA) grafted polyethylene/polypropylene (PE/PP) nonwoven fabric by γ-initiation: Synthesis, characterization and benefits of RAFT mediation. *Radiat. Phys. Chem.*, *105*, 31-38. DOI: 10.1016/j.radphyschem.2014.05.023.

[27]. Walo, M., Przybytniak, G., Męczyńska-Wielgosz, S., & Kruszewski, M. (2015). Improvement of poly(ester-urethane) surface properties by RAFT mediated grafting initiated by gamma radiation. *Eur. Polym. J.*, *68*, 398-408. DOI: 10.1016/j.eurpolymj.2015.05.019.

[28]. Barsbay, M., & Güven, O. (2009). A short review of radiation-induced raft-mediated graft copolymerization: A powerful combination for modifying the surface

properties of polymers in a controlled manner. *Radiat. Phys. Chem.*, *78*(12), 1054-1059. DOI: 10.1016/j.radphyschem.2009.06.022.

[29]. Chong, Y.K., Le, T.P.T., Moad, G., Rizzardo, E., & Thang, S.H. (1999). A more versatile route to block copolymers and other polymers of complex architecture by living radical polymerization: The RAFT process. *Macromolecules*, *32*, 2071-2074. DOI: 10.1021/ma981472p.

[30]. Barsbay, M., Guven, O., Davis, T.P., Barner-Kowollik, C., & Barner, L. (2009). RAFT-mediated polymerization and grafting of sodium 4-styrenesulfonate from cellulose initiated via γ-radiation. *Polymer*, *50*(4), 973-982. DOI: 10.1016/j.polymer.2008.12.027.

[31]. Barsbay, M., Guven, G., Stenzel, M.H., Davis, T.P., Barner-Kowollik, C., & Barner, L. (2007). Verification of controlled grafting of styrene from cellulose via radiation-induced RAFT polymerization. *Macromolecules*, *40*(20), 7140-7147. DOI: 10.1021/ma070825u.

[32]. Gupta, B., Jain, R., Anjum, N., & Singh, H. (2006). Preirradiation grafting of acrylonitrile onto polypropylene monofilament for biomedical applications: I. Influence of synthesis conditions. *Radiat. Phys. Chem.*, *75*(1), 161-167. DOI: 10.1016/j.radphyschem.2005.04.003.

[33]. Binh, D., & Huy, H.T. (1998). The effect of concentration of acrylic acid, dose rates and temperature on preirradiated graft of natural rubber-based thermoplastic elastomer. *Radiat. Phys. Chem.*, *53*(2), 177-180. DOI: 10.1016/S0969-806X(98)00009-7.

[34]. Przybytniak, G., Kornacka, E.M., Mirkowski, K., Walo, M., & Zimek, Z. (2008). Functionalization of polymer surfaces by radiation-induced grafting. *Nukleonika*, *53(*3), 89-95.

[35]. Catarí, E., Albano, C., Karam, A., Perera, R., Silva, P., & González, J. (2005). Grafting of a LLDPE using gamma irradiation. *Nucl. Instrum. Meth. B*, *236*(1-4), 338-342. DOI: 10.1016/j.nimb.2005.03.273.

[36]. Bucio, E., & Burillo, G. (1996). Radiation-grafting of 2-bromoethylacrylate onto polyethylene film by preirradiation metod. *Radiat. Phys. Chem.*, *48* (6), 805-810. DOI: 10.1016/S0969-806X(96)00066-7.

[37]. Hegazy, E.-S.A., AbdEl-Rehim, H.A., Kamal, H., & Kandeel, K.A. (2001). Advances in radiation grafting. *Nucl. Instrum. Meth. B*, *185*(1-4), 235-240. DOI: 10.1016/S0168-583X(01)00834-5.

[38]. Barsbay, M., Kavaklı, P.A., & Güven, O. (2010). Removal of phosphate using copper-loaded polymeric ligand exchanger prepared by radiation grafting of polypropylene/polyethylene (PP/PE) nonwoven fabric. *Radiat. Phys. Chem.*, *79*(3), 227-232. DOI: 10.1016/j.radphyschem.2009.09.003.

[39]. Desai, S.M. Solanky, S.S., Mandale, A.B., Rathore, K. & Singh, R.P. (2003). Controlled grafting of *N*-isoproply acrylamide brushes onto self-standing isotactic polypropylene thin films: surface initiated atom transfer radical polymerization. *Polymer*, *44*(25), 7645-7649. DOI: 10.1016/j.polymer.2003.09.060.

[40]. Sherazi, T., Ahmad, S., Kashmiri, M., Kim, D., & Guiver, M.D. (2009). Radiation-induced grafting of styrene onto ultra-high molecular weight polyethylene powder for polymer electrolyte fuel cell application: II. Sulfonation and characterization. *J. Membrane Sci.*, *333*(1-2), 59-67. DOI: 10.1016/j.memsci.2009.01.052.

[41]. Makhlouf, C., Marais, S., & Roudesli, S. (2007). Graft copolymerization of acrylic acid onto polyamide fibers. *Appl. Surf. Sci.*, *253*(12), 5521-5528. DOI: 10.1016/j.apsusc.2006.12.086.

[42]. Nasr, H.I., Haggag, K.M., & El Kharadly, E.A. (1980). Polyamides with improved moisture regain via γ-rays. *Radiat. Phys. Chem.*, *16*(6), 447-449. DOI: 10.1016/0146-5724(80)90190-9.

[43]. Chumakov, M.K., Shahamat, L., Weaver, A., LeBlanc, J., Chaychian, M., Silverman, J., Richter, J.K., Weiss, D., & Al-Sheikhly, M. (2011). Electron beam induced grafting of N-isopropylacrylamide to a poly(ethylene-terephthalate) membrane for rapid cell sheet detachment. *Radiat. Phys. Chem.*, *80*(2), 182-189. DOI: 10.1016/j.radphyschem.2010.07.030.

[44]. Zhitariuk, N.I., & Shtanko, N.I. (1990). Influence of some factors on radiation grafting of styrene on poly(ethylene terephthalate) nuclear membranes. *Eur. Polym. J.*, *26*(8), 847-851. DOI: 10.1016/0014-3057(90)90156-X.

[45]. Walo, M., Przybytniak, G., Kavaklı, P.A., & Güven, O. (2013). Radiation-induced graft polymerization of N-vinylpyrrolidone onto segmented polyurethane based on isophorone diisocyanate. *Radiat. Phys. Chem.*, *84*, 85-90. DOI: 10.1016/j.radphyschem.2012.06.039.

[46]. Alves, P., Coelho, J.F.J., Haack, J., Rota, A., Bruinink, A., & Gil, M.H. (2009). Surface modification and characterization of thermoplastic polyurethane. *Eur. Polym. J.*, *45*(5), 1412-1419. DOI: 10.1016/j.eurpolymj.2009.02.011.

[47]. Meléndez-Ortiz, H.I., Alvarez-Lorenzo, C., Burillo, G., Magariños, B., Concheiro, A., & Bucio, E. (2015). Radiation-grafting of N-vinylimidazole onto silicone rubber for antimicrobial properties. *Radiat. Phys. Chem.*, *110*, 59-66. DOI: 10.1016/j.radphyschem.2015.01.025.

[48]. Gonzalez-Perez, G., Burillo, G., Ogawa, T., & Avalos-Borja, M. (2012). Grafting of styrene and 2-vinylnaphthalene onto silicone rubber to improve radiation resistance. *Polym. Degrad. Stabil.*, *97*(8), 1495-1503. DOI: 10.1016/j.polymdegradstab.2012.05.003.

[49]. Madrid, J.F., & Abad, L.V. (2015). Modification of microcrystalline cellulose by gamma radiation-induced grafting. *Radiat. Phys. Chem.*, *115*, 143-147. DOI: 10.1016/j.radphyschem.2015.06.025.

[50]. Wojnárovits, L., Földváry, Cs.M., & Takács, E. (2010). Radiation-induced grafting of cellulose for adsorption of hazardous water pollutants: A review. *Radiat. Phys. Chem.*, *79*(8), 848-862. DOI: 10.1016/j.radphyschem.2010.02.006.

[51]. Gubler, L., Gürsel, S.A., & Scherer, G.G. (2005). Radiation grafted membranes for polymer electrolyte fuel cells. *Fuel Cells*, *5*(3), 317-335. DOI: 10.1002/fuce.200400078.

[52]. Qiu, J., Ni, J., Maolin, Z., & Wei, G. (2007). Radiation grafting of styrene and maleic anhydride onto PTFE membranes and sequent sulfonation for applications of vanadium redox battery. *Radiat. Phys. Chem.*, *76*(11-12), 1703-1707. DOI: 10.1016/j.radphyschem.2007.01.012.

[53]. Estrada-Villegas, G.M., & Bucio, E. (2013).Comparative study of grafting a polyampholyte in a fluoropolymer membrane by gamma radiation in one or two-steps. *Radiat. Phys. Chem.*, *92*, 61-65. DOI: 10.1016/j.radphyschem.2013.07.015.

[54]. Ferreira, H.P., Parra, D.F., & Lugao, A.B. (2012). Radiation-induced grafting of styrene into poly(vinylidene fluoride) film by simultaneous method with two different solvents. *Radiat. Phys. Chem.*, *81*(9), 1341-1344, DOI: 10.1016/j.radphyschem.2012.01.047.

[55]. Taher, N.H., Dessouki, A.M., & El-Arnaouty, M.B. (1998). Radiation initiated graft copolymerization of N-vinylpyrrolidone and acrylamide onto low density polyethylene films by individual and binary system. *Radiat. Phys. Chem.*, *53*(4), 437-444. DOI: 10.1016/S0969-806X(98)00008-5.

[56]. Gupta, B., Büchi, F.N., & Scherer, G.G. (1994). Cation-exchange membranes by preirradation grafting of styrene into FEP films. 1. Influence of synthesis conditions. *J. Polym. Sci. Pol. Chem.*, *32*(10), 1931-1938. DOI: 10.1002/pola.1994.080321016.

[57]. Chapiro, A. (1995). Radiation chemistry in the field of biomaterials. *Radiat. Phys. Chem.*, *46*(2), 159-160. DOI: 10.1016/0969-806X(95)00006-J.

[58]. Dworjanyn, P.A., Garnett, J.L., Long, M.A., Nho, Y.C., & Khan, M.A. (1993). Role of homopolymer suppressors in UV and radiation grafting in the presence of novel additives – Significance of processes in analogous curing reactions. In E. Reichmanis, C.W. Curtis & J.H. O'Donnell (Eds.), *Irradiation of polymeric materials: processes, mechanisms, and applications* (pp. 103-117). American Chemical Society. (ACS Symposium Series, Vol. 527).

[59]. Gargan, K., & Lovell, K.V. (1990). Preirradation grafting of hydrophilic monomers onto polyethylene.1. The influence of homopolymerization inhibitors. *Int. J. Radiat. Appl. Instrum. C: Radiat. Phys. Chem.*, *36*(6), 757-761. DOI: 10.1016/1359-0197(90)90174-G.

[60]. Goel, N.K., Rao, M.S., Kumar, V., Bhardwaj, Y.K., Chaudhari, C.V., Dubey, K.A., & Sabharwal, S. (2009). Synthesis of antibacterial cotton fabric by radiation-induced grafting of [2-(Methacryloyloxy)ethyl]trimethylammonium chloride (MAETC) onto cotton. *Radiat. Phys. Chem.*, *78*(6), 399-406. DOI: 10.1016/j.radphyschem.2009.03.011.

[61]. Lin, Z., Tongwen, X., & Zhang, L. (2006). Radiation-induced grafting of N-isopropylacrylamide onto the brominated poly(2,6-dimethyl-1,4-phenylene oxide) membranes. *Radiat. Phys. Chem.*, *75*(4), 532-540. DOI: 10.1016/j.radphyschem. 2005.10.018.

[62]. Viengkhou, V., Ng, L.-T., & Garnett, J.L. (1997). The effect of additives on the enhancement of methyl methacrylate grafting to cellulose in the presence of UV and ionising radiation. *Radiat. Phys. Chem.*, *49*(5), 595-602. DOI: 10.1016/ S0969-806X(97)00001-7.

[63]. Dworjanyn, P.A., & Garnett, J.L. (1989). Role of multifunctional acrylates in radiation grafting and curing reactions. *Int. J. Radiat. Appl. Instrum. C: Radiat. Phys. Chem.*, *33*(5), 429-436. DOI: 10.1016/1359-0197(89)90107-0.

RELEVANT METHODOLOGIES FOR THE CHARACTERIZATION OF IRRADIATED MATERIALS

Cornelia Vasile[1], Elena Stoleru[1], Sossio Cimmino[2], Clara Silvestre[2]

[1] *"Petru Poni" Institute of Macromolecular Chemistry, Physical Chemistry of Polymers Department, Romanian Academy, 41A Grigore Ghica Voda Alley, 700487 Iasi, Romania*
[2] *Istituto per i Polimeri, Compositi e Biomateriali, Consiglio Nazionale delle Ricerche, IPCB/CNR, Via Campi Flegrei 34, 80078 Pozzuoli, Naples, Italy*

1. INTRODUCTION

Irradiation dose and dose rate affect either the surface properties only and/or the bulk properties of a material as well. Dose and dose rate should be established according to the final end use of the material being irradiated. The bulk and surface properties of polymers differ in terms of the chemical structure, the morphology and the surface energy because of the oxidation of surfaces and the orientation of macromolecules in a way that can enhance their interactions [1].

2. METHODOLOGIES FOR THE CHARACTERIZATION OF SURFACE PROPERTIES

Surface properties play an important role in a number of applications where polymeric materials are used. A property, such as surface wetting, is important in printing and in adhesive bonding and in the manufacture of membranes and biomedical devices [2, 3]. The covalent bonds of polymers and the mobility of polymeric chains lead to the unique effects on the surface properties of polymers. Surface layers display compositions and properties that are time-dependent and can vary with the conditions to which a polymer is exposed. When a polymer is in contact with a solid substrate, the polymer molecular mobility leads to important differences. The number of chemical elements found in

Table 1. Summary of surface analysis techniques. (Adapted from Ref. [4]).

Incident excitation by	Direct surface analysis methods		
	Emitted analyzed response		
	Electrons	Ions	Photons
Electrons	- Auger electron spectroscopy (AES)[a] - Scanning Auger microscopy (SAM)[a] - Scanning electron microscopy (SEM)[a] - Transmission electron microscopy (TEM)[a,b] - Low energy electron diffraction (LEED)[a] - Reflection high energy electron diffraction (RHEED)[a] - Spin polarized electron spectroscopy (SPE)[a,b]		- Energy dispersive analysis of X-rays (EDAX)[b]
Ions		- Secondary ion mass spectrometry (SIMS)[a] - Low energy ion scattering spectroscopy (LEIS)[a] - Rutherford backscattering spectroscopy (RBS)[b]	- Nuclear reaction analysis (NRA)[b]
Photons	- X-ray photoelectron spectroscopy/electron spectroscopy for chemical analysis (XPS/ESCA)[a] - Ultraviolet photoelectron spectroscopy (UPS)[a] - Auger emission extended X-ray absorption fine structure ((AE)XAFS)[a]		- Fourier transform infrared spectroscopy (FTIR)[b] - Raman vibrational spectroscopy (Raman)[b] - X-ray absorption fine structure analysis (XAFS)[b]
Electric/ magnetic field	- Scanning tunneling microscopy (STM)[a] - Atomic force microscopy (AFM)[a]		- Glow discharge optical emission spectroscopy (GDOES)[a]

[a] Surface < 10 nm.
[b] Near surface ~1 μm.

polymers is quite limited, with C, H, N, O and Si and sometimes F, Cl, Br, and S, but the way in which these elements can be assembled into polymeric materials is unlimited.

The important properties of polymer surfaces are: surface composition, free surface energy, wettability, roughness, zeta potential, polymer surface dynamics, aging behavior, wetting transition, adhesion, barrier properties, friction and wear, biocompatibility, bioadhesion, *etc*. Methods to determine these properties are listed in Table 1. The properties of polymers depend on the average molecular weight, crosslinked density and processing conditions.
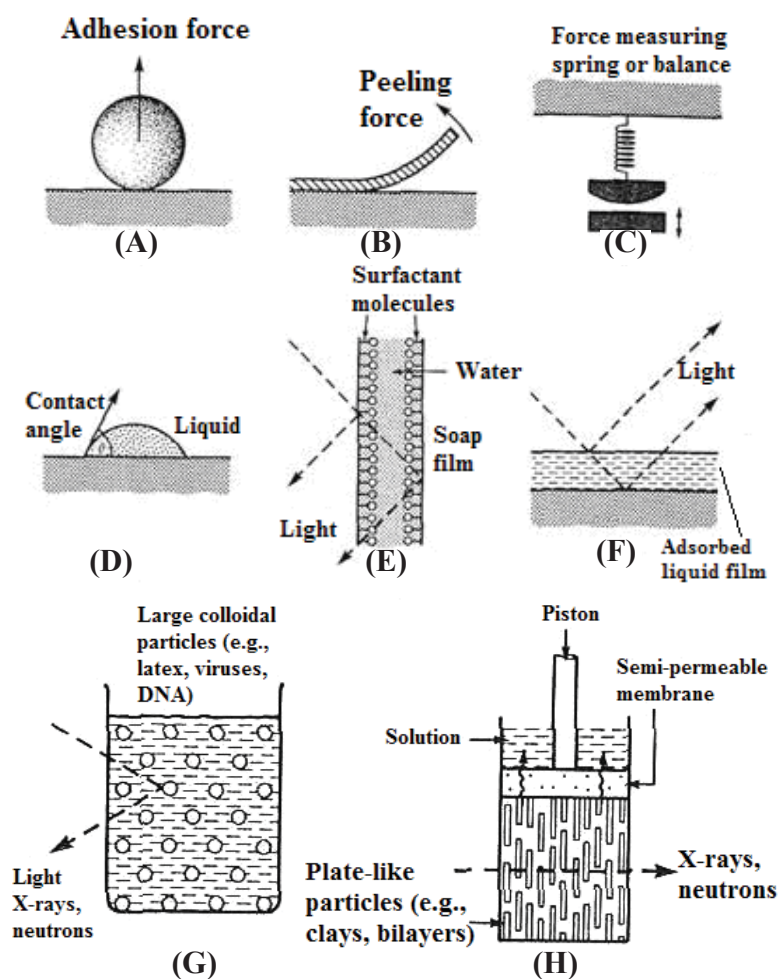
Fig.1. Schematic representation of the measurement of forces between particles and surfaces: (A) adhesion measurements, (B) peeling measurements, (C) direct measurement of a force as a function of surface separation, (D) contact angle measurement, (E) equilibrium thickness of thin free films (soap films, foams), (F) equilibrium thickness of thin adsorbed film, (G) interparticle spacing in liquids (colloidal suspensions, paints, pharmaceutical dispersions), (H) sheet-like particle spacing in liquids. (Adapted from Ref. [5]).

Table 2. Comparison between the possibilities offered by the analysis techniques in the study of polymer surfaces [6, 7].

Technique	Depth resolution	Lateral resolution	Depth profiling	Imaging & mapping	Quantitative accuracy	Detection limits/ sensitivity	Sample considerations
XPS/ESCA	5 to 30 nm	> 250 µm	Ion-etching, angle-resolved	None	5%	0.1 monolayer 0.1 at% $Z > 2/10^{-2}$-10^{-3}	Ultra-high vacuum
AES/SAM	2 to 30 nm	> 30 nm	Ion-etching, angle-resolved	SEM elemental & chemical	20%	0.1 monolayer 0.1 at% $Z > 2$	Ultra-high vacuum, electron beam (EB), damage, charging
FTIR	ZnSE-ATR: 2-4 µm, GE-ATR: 0.4-1 µm	10 µm	See ATR	No	Low % (solution)	ng·µg/10^{-2}	Yes
Raman	5 µm	1 µm	Limited	Yes	No	µg/10^{-1}-10^{-2}	Yes
EDS	~1 µm	~1 µm	No	SEM elemental line-scans	5%	10 ppm $Z > 5$	High vacuum, electron beam damage

Topographic probes

Technique	Lateral		Vertical		Sample considerations	Additional capabilities
	Resolution	Range	Resolution	Range		
SEM	3 nm	N/A	N/A	N/A	High vacuum, electron beam damage	Backscatter mode
AFM/STM	< 0.1 nm	100 µm	< 0.1 nm	7 µm	Air or liquid, < 25 mm diameter, < 10 mm high	Lateral force, nanoindentation
Nanoindentation	< 100 nm	300 µm	< 100 nm	500 µm	Samples with a homogeneous microstructure	

Indirect methods for surface investigation are the following: contact angle methods, atomic force microscopy (AFM), differential thermal analysis (DTA), differential scanning calorimetry (DSC), molecular mass distribution, nanoindentation, *etc*.

The methods used to determine specific surface properties are:
- composition: AES/SAM, XPS (X-ray photoelectron spectroscopy), SEM/EDS (scanning electron microscopy/energy-dispersive), SIMS (secondary ion mass spectrometry);
- chemistry: XPS, FTIR/Raman, SIMS;
- morphology/topography: SEM, AFM/STM, nanoindentation.

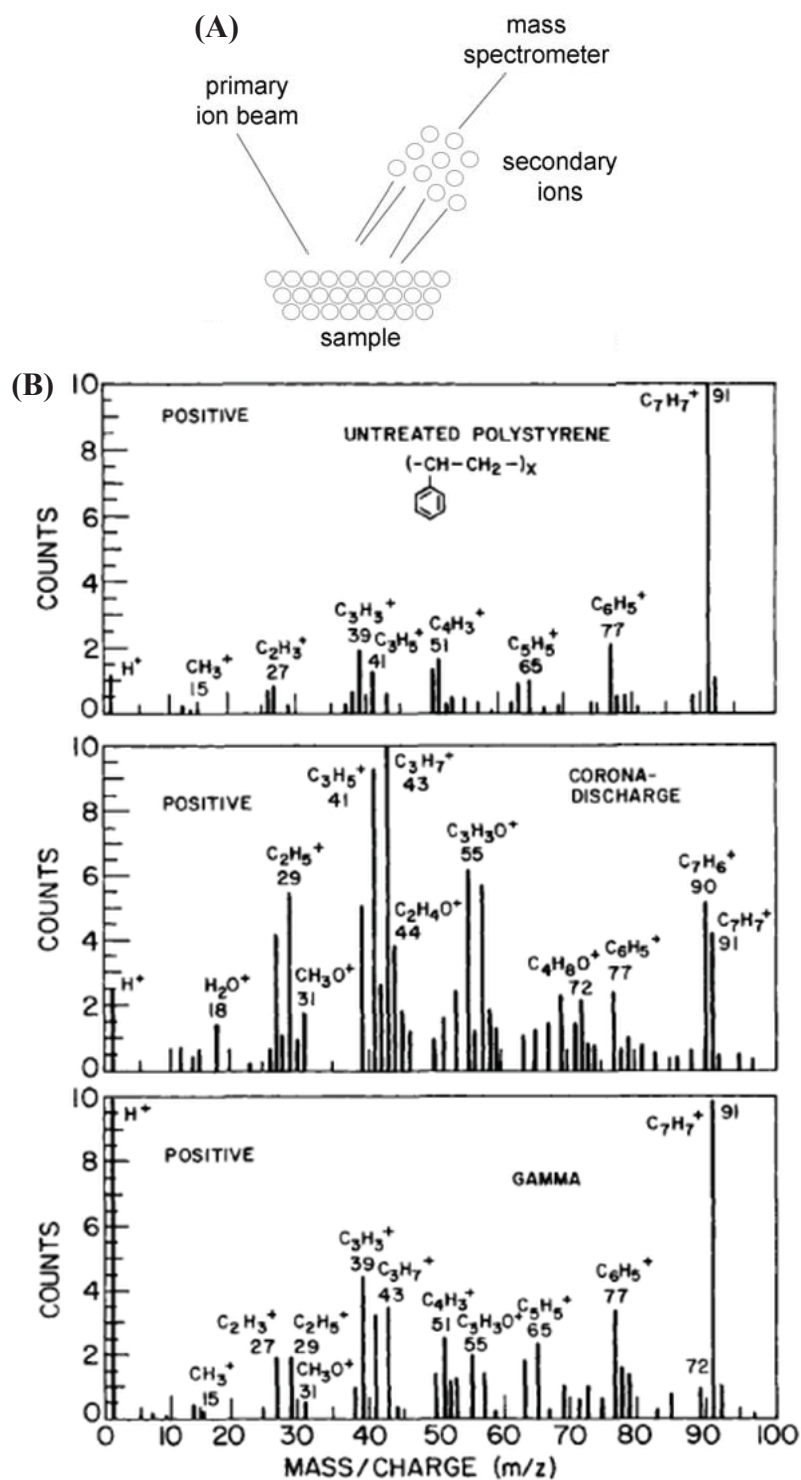The principles of several types of measurements are schematically represented in Fig.1.

Particle detachment (Fig.1A) and peeling forces (Fig.1B) provide information on adhesion forces that are attractive forces when solid surfaces are in contact. Figure 1B is a peel test, which has practical use when evaluating adhesive tapes, material fracture and crack propagation. A spring or a balance can be used to measure the separation force between two macroscopic surfaces as a function of the separation distance (Fig.1C). Surface tension and contact angle measurements give information on liquid-liquid or liquid-solid surface contact (Fig.1D). This is used for testing wettability and the stability of surface films, and detergency. The thickness of free soap films and liquid films adsorbed on surfaces (Figs.1E and F) can be measured and this gives information on the repulsive forces that stabilize wetting films. Optical techniques, as internal reflection spectroscopy or ellipsometry, are used to measure film thickness of about 0.1 nm. Dynamic interparticles separation and motions in liquids can be measured by nuclear magnetic resonance (NMR), light scattering, X-ray scattering and neutron scattering (Fig.1G). Sheet-like (lipid bilayers) or rod-like particles are examined applying methods, as illustrated in Figs.1G and H. This last method is useful in studying the microstructure of soaps and of biological membranes.

Depending on the measurement principle, each method has some limits wherein it can be used (Table 2).

2.1. DEPTH PROFILING TECHNIQUES

Depth profiling is used to determine the composition of one or more components of a film as a function of depth.

Secondary ion mass spectroscopy (SIMS) (Fig.2) operates on the principle that bombardment of a material with a high energy ion beam (primary ions) results in the ejection or sputtering of atoms from the material [10, 11]. In SIMS analyses, material is removed from the sample by sputtering, and is, therefore, a locally destructive technique.

Fig.2. The principle of SIMS (A), positive static SIMS spectra for unirradiated and irradiated polystyrene (B) [8, 9].

In static SIMS, the primary ion fluence must be kept low enough ($< 10^{13}$ ions·cm^{-2}) to prevent a surface area from being hit more than once. For this reason, this technique is considered as non-destructive.

Dynamic SIMS is widely used to analyze thin films, layer structures and dopant profiles.

Time of flight-secondary ion mass spectrometry (ToF-SIMS) uses principles very similar to SIMS, but removes a very small amount of material from the sample as compared to the relatively large amount removed by SIMS analysis. ToF-SIMS identifies elements and bonding states of atoms present on the very surface of a sample, the outer one or two monolayers. It is used for depth profiling of various organic and inorganic films, including polymer films and multilayer films and film fragments. The emitted ions are related to the chemical structure of the materials and usually consist of molecular and quasi-molecular ions that occur from fragmentation, rearrangement, decomposition and reaction of the constituent molecules of the material.

SIMS is an excellent tool for surface analysis because of its many advantages, such as: (i) the detection of large organic molecules up to several thousands of mass units, (ii) fast data acquisition with a time of flight (ToF) analyzer; and (iii) chemical information on the top few angstroms layers of material is obtained. SIMS imaging is one of the exciting developments in this field.

Monitoring secondary ion emission in relation to sputtering time allows for depth profiling of the sample composition. Layers of up to 10 000 Å thick can be depth-profiled using SIMS. SIMS can provide an accuracy of about 6% and a precision of less than 0.5%.

Analytical information obtained using SIMS are the following:
• Mass spectrum – identifies the elemental and ion composition of the uppermost 10 to 20 Å of the analyzed surface.
• Depth profile – under typical static SIMS conditions (2 keV < ion energy < 4 keV), the primary ions penetrate to a depth of ~3 nm below the surface. A depth resolution of a few angstroms is possible.
• Secondary ion mapping – measures the lateral distribution of elements and molecules on the surface. Lateral resolution is less than 100 nm for elements and about 500 nm for large molecules.

Libraries of static SIMS spectra [12] provide a guide for the interpretation of results. Careful spectral interpretation combined with fragmentation pathways (*e.g.* on pyrolysis/electron impact mass spectrometry) allows different classes of polymers to be distinguished as well as individual members of one class to be identified. The complementary combination of XPS and static SIMS is a powerful tool in the surface analysis of modified polymers [8].

Gamma irradiation of polystyrene (PS) to 150 kGy leads to surface oxidation of the polymer to depths greater than 10 nm as opposed to ≈3 nm depth attained by either plasma or corona-discharge treatment. Peaks indicative of the presence of aliphatic oxygen containing molecular ions were also observed.

The data suggests that oxidation by corona discharge is restricted to the top monolayers of the surface within the SIMS sampling depth (~3 nm). With gamma irradiation, the oxidized layer is considerably deeper into the bulk of the polymer [9].

ATR-FTIR and Raman spectroscopy non-destructively identify molecular species through their vibration states, chemical bond information and molecular orientation. Very little sample preparation is necessary. An attenuated total reflection (ATR) accessory operates by measuring the changes that occur in a totally internally reflected infrared beam when the beam comes into contact with a sample (Fig.3A). ATR-FTIR spectroscopy reflects more than just the outermost atomic layers, generally from 1000 Å up to 1 μm; but generally, penetration depth ranges from 40 Å to 3 μm.

For ATR-FTIR to be successful, the following two requirements must be met: (i) the sample must be in direct contact with the ATR crystal, because the evanescent wave or bubble only extends beyond the crystal from 0.5 to 5 μm; (ii) the refractive index of the crystal must be significantly greater than that of the sample, if not, internal reflectance will not occur. The most popular ATR crystal materials are zinc selenide (ZnSe), germanium and diamond which, because of its robustness, is often preferred.

Using the ATR-FTIR method, Gupta *et al.* had studied the effect of gamma irradiation on CR-39 polymer $(C_{12}H_{18}O_7)_n$ (which is a nuclear track detector and is used in optical devices) [14]. Parparita *et al.* had studied gamma irradiation induced changes on polypropylene (PP) biocomposites containing different bio-additives (Fig.3C) [13]. The results of Gupta *et al.* [14] study clearly indicated the lowering of the thermal stability of CR-39 as an effect of gamma irradiation, as shown in Fig.3B.

The gamma irradiation of PP and PP/biomass composites resulted in the formation of hydroxyl (mainly hydroperoxides and alcohols) (3350 cm^{-1}) and carbonyl groups (mainly ketones, esters and acids) (1740 cm^{-1}) which were detected by infrared spectroscopy [13] in the 3200-3600 and $1900\text{-}1500 \text{ cm}^{-1}$ region, respectively. The carbonyl and hydroxyl indices increased with the absorbed dose (Fig.3C). It was stated that these changes could be related either to polymer oxidation or to a higher content of biomass found at composite surfaces after irradiation.

X-ray photoelectron spectroscopy (XPS) is perhaps the most widely used surface spectroscopy and one of the more popular spectroscopic techniques available for the surface characterization of polymers [15, 16]. Samples irradiated with X-rays emit photoelectrons which characterize the binding energies (BE) of the elements in the sample and the chemical bonding of those elements. The photoemission peaks in the XPS spectra allow identification of all elements except hydrogen and helium. Monoenergetic soft X-rays (usually AlK_α or MgK_α) are used to irradiate a sample material in high vacuum (typically $\leq 10^{-9}$ torr). The emitted photoelectrons are collected with an electron lens assembly and
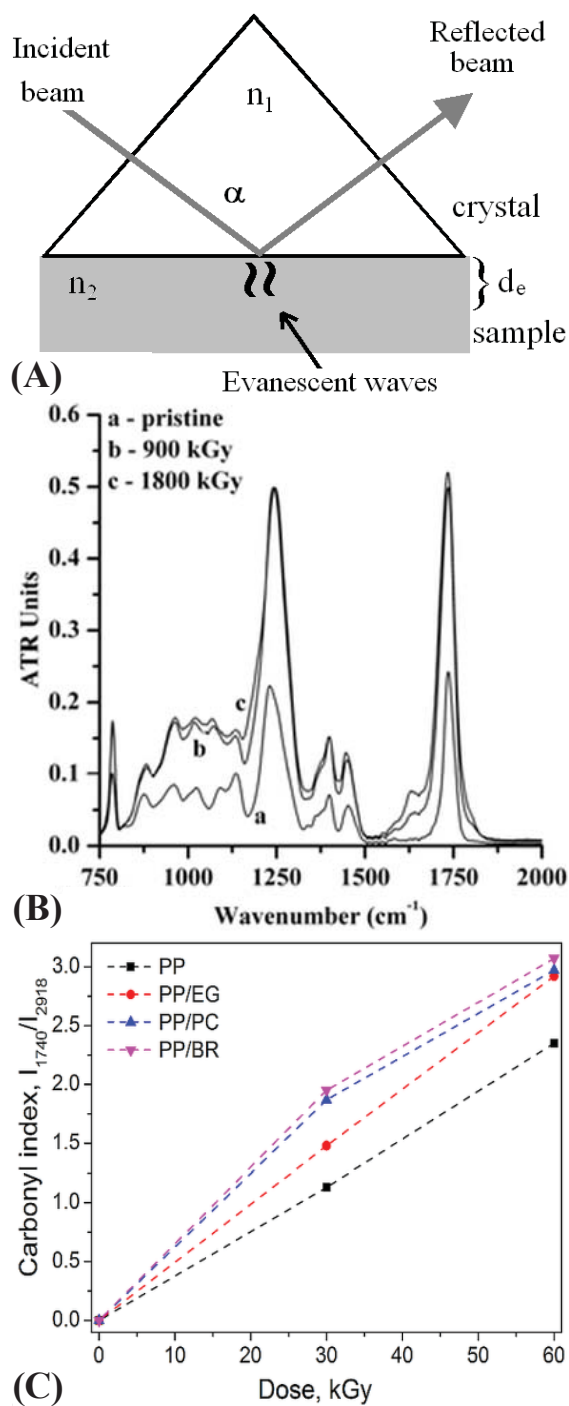
Fig.3. (A) Scheme of ATR-FTIR principle; (B) ATR-FTIR spectra of pristine CR-39 polymer unirradiated and gamma-irradiated to different doses; (C) dose-dependent variations of carbonyl index in irradiated PP and in different PP/biomass composites: PP/*Eucalyptus globulus* (EG), PP/*pine cones* (PC), PP/*Brassica Rapa* (BR) [13].

their energy is analyzed and counted. Since the energy levels in materials are quantified, the resulting energy spectrum consists of discrete peaks associated to the electronic energy states in the sample. The peaks of a photoelectron spectrum are grouped in three categories: (i) peaks due to photoemission from the core levels of the atom, (ii) those due to photoemission from the valence level and (iii) those due to Auger emission.

Analysis of the core level binding energies (*i.e.* measurement of chemical electron shifts) and of core level intensities, use of shake-up satellites, depth profiles and spatially resolved studies, and finally valence band spectra, are shown to produce many different but complementary keys to obtain information about the atomic, chemical and structural composition of macromolecular surfaces. The XPS emission process is represented schematically in Fig.4. Absolute binding energies (BE) of an emitted photoelectron are the energy difference between (n − 1)-electron final state (E_f) and the n-electron initial state (E_i) in the atom:
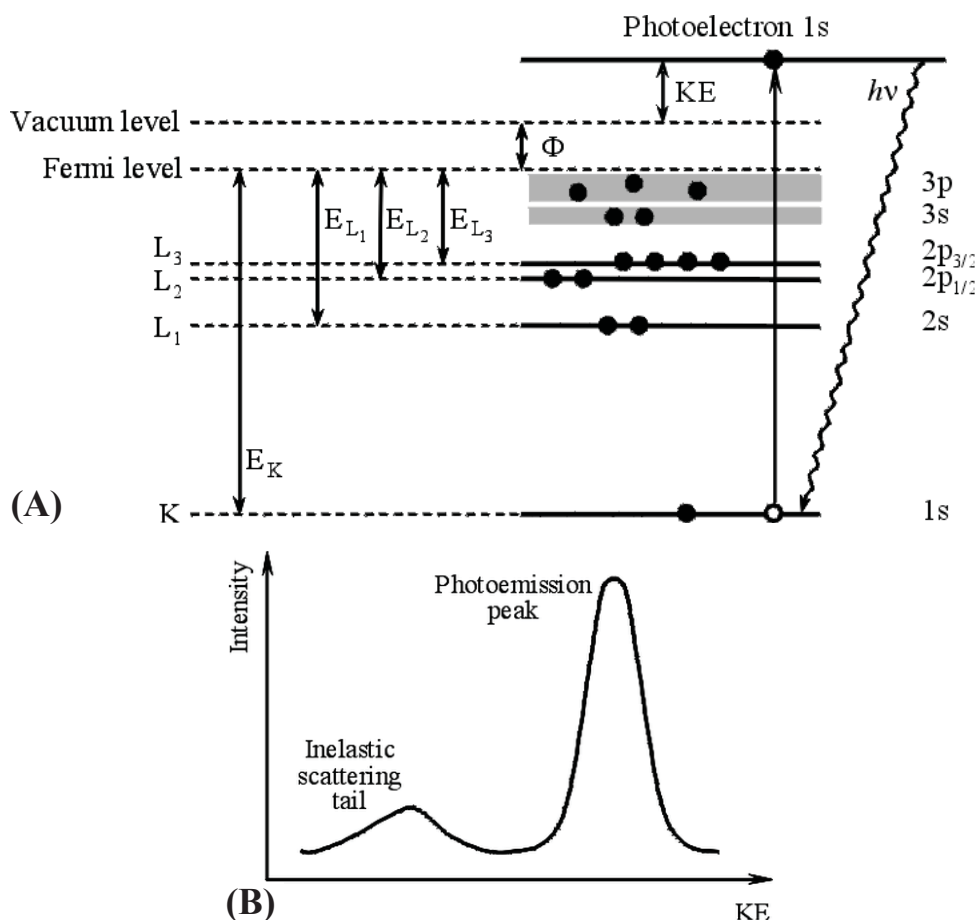

Fig.4. XPS photoemission process (A) and characteristic shape of a photoelectron peak, with contribution from the inelastic scattering background (B).

$$BE = E_f(n - 1) - E_i(n) \tag{1}$$

BE can be obtained by measuring the kinetic energy of the photoelectrons. The identification of the elements present on the surface is done directly by determining the binding energies of the core photoelectrons.

For energetic (950-1200 eV) electrons, XPS spectrometry (AlK$_\alpha$ X-ray source) provides an evaluation of the C1s, N1s, and O1s levels (most common core levels encountered in polymers) by varying the take-off measurement angle from ~10-90°, which corresponds to the analysis in depth from ~1 to 10 nm. The change in binding energy is known as the chemical shift. The chemical shift is closely related to the electronegativity of the species to which the atom of interest is bonded, which makes possible the chemical analysis of a given sample. Chemical shifts can range from a few tenths of an eV up to ~8 eV. The C1s BE increases monotonically with the number of oxygen atoms bonded to carbon, that is C–C < C–O < C=O < O–C=O < O–(C=O) O–. Consistent with this, the carbon becomes more positive. The reference photoemission peak in polymer XPS spectra is the C1s line (285.0 eV) from a hydrocarbon chain (C–C, C–H). Typical C1s, O1s, *etc.* binding energies for covalent bonds are tabulated and provided in Ref. [17].

The XPS intensity (the integrated area under the photoelectron peak) is proportional to the atom quantity. Therefore quantitative elemental analysis of the material can be made. In most cases, the deconvolution of complex experimental peaks is necessary. Standard samples are poly(tetrafluorethylene) (C and F) and polyethylene glycol (C and O).

Core level information are as follows:

- Shake-up peaks (also called loss peaks because intensity is lost from the primary photoemission peak) are most apparent for systems with aromatic structures, unsaturated bonds or transition metal ions.
- Surface derivatization technique has been developed, as a complementary method, to determine the density of specific species on treated surfaces. This method allows for precise identification of chemical groups, using a chemical reaction specific to only the functional group of interest. For example, examining substances containing functional groups like those below:

$$-\underset{|}{\overset{|}{C}} - OH \qquad -\underset{|}{\overset{|}{C}} - O - C \qquad -\underset{|}{\overset{|}{C}} - O - \overset{\overset{O}{\|}}{C} -$$
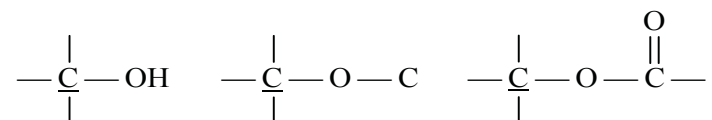
Peaks due to these groups in C1s spectra exhibit almost equal binding energies (about 286.5 eV) and, hence, cannot be separated using mathematical procedures, making the derivatization technique absolutely necessary. After treatment of a surface of non-polar polymers such as polyethylene (PE) and polypropylene by flame or plasma, with the objective to incorporate oxygen at the surface in order to improve adhesive properties, it is not possible to discriminate an ether from an epoxide or an alcohol structure,
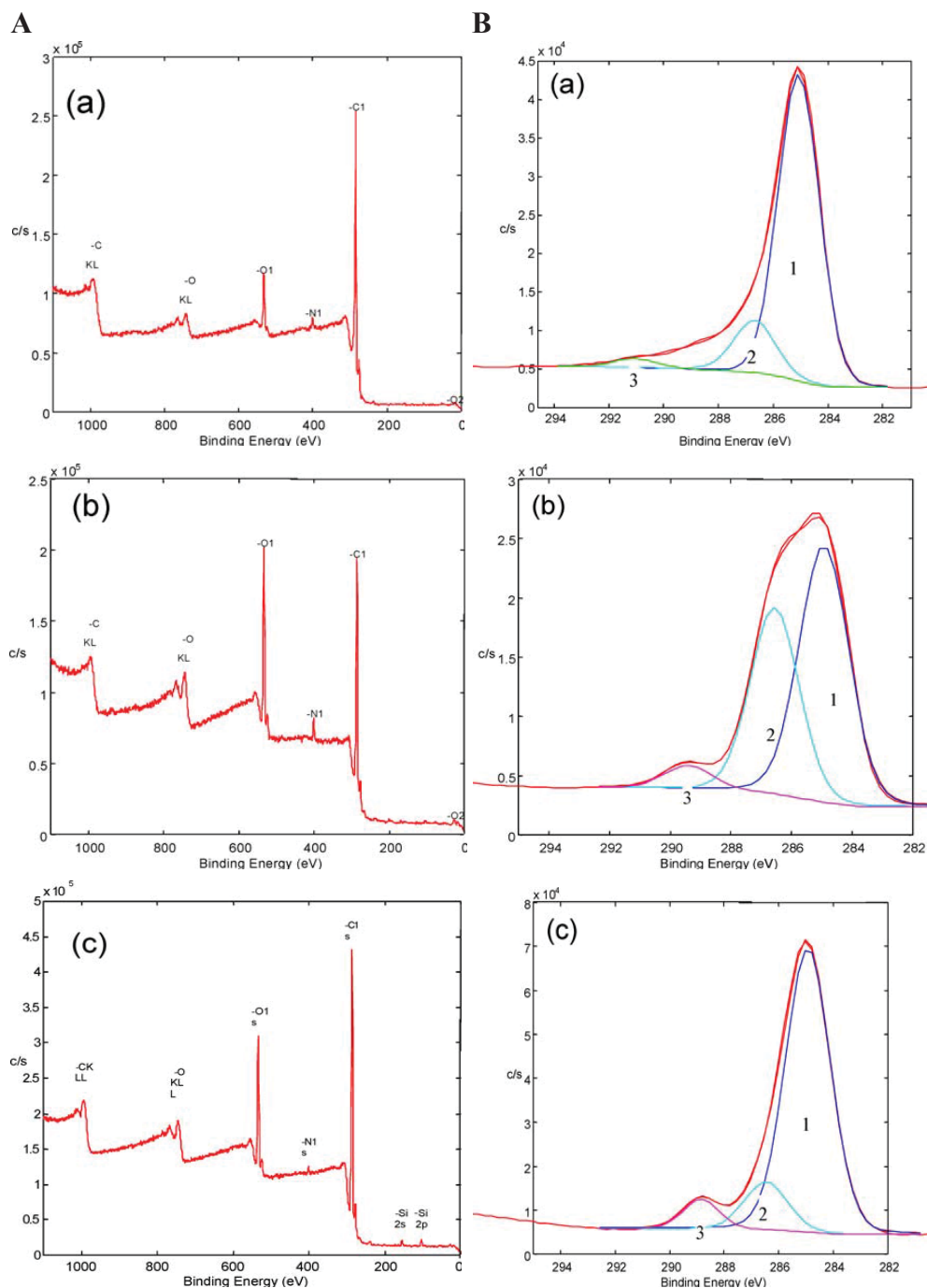
A

B

Fig.5. A – XPS wide scan spectra of carbon fibers: (a) untreated, (b) air-oxidation treated, and (c) gamma-irradiated; B – XPS core level spectra of C1s region of carbon fibers: (a) untreated, (b) air-oxidation treated, and (c) gamma-irradiated (graphitic carbon (C–C, peak 1), hydroxyl group (OH, peak 2), and the carboxyl group (COOH, peak 3) were found) [18].

since all carbons and oxygens present in C–O bonds exhibit very minor differences in core level BE. To detect a carboxylic group –(COOH), the reaction under precise conditions with 2,2,2-trifluoroethanol will produce $CO(OCH_2CF_3)$ groups on the polymer surface. Thus, the carboxylic function is directly titrated by recording the XPS F1s peak, with distinctive advantages, due to the three fluorine atoms replacing one carboxylic group, the F1s cross-section being larger than the C1s one and the peak area of F1s unambiguously attributed to the specific reaction. The detection limit in this case is well below 0.2% groups per carbon atom.

- Surface modification of polymers. XPS is conducted without special preparation of samples, but is carried out in an ultra-high vacuum environment (10^{-9} Torr). Thus, biomaterial samples must be in a dry state. Some instruments using a liquid nitrogen-cooled stage permit the analysis of frozen hydrated samples. Although X-rays can penetrate materials to depths of 1 μm or more, XPS provides information about the outermost 5-75 Å layer, because photoelectrons originating deeper in the sample lose energy in inelastic collision and/or do not have sufficient energy to be emitted from the sample. The depth of analysis is typically 3 to 10 nm, with a lateral resolution of 150 μm. This is used in applications which include: liquid/solid interfaces, impurity segregation, polymer coatings, transfer films, thin film chemistry. Using the XPS technique, it was observed [18] that the composites reinforced with the gamma-irradiated carbon fibers showed higher interfacial adhesion and thus better flexural and shear properties than the composites reinforced with air-treated fibers (Fig.5). It was suggested that the higher content of carboxyl groups observed on the surface of the gamma-irradiated carbon fibers was most likely responsible for the stronger fiber-matrix bonding.

- Neutron reflectivity is ideally suited for determining the structure of the interface between immiscible polymers. It is also used for solving of other polymer problems, such as: surface separation in polymer blends, polymer adsorption from solution, the study of grafted polymer layers, and surface-driven lamellar ordering in block copolymers [19]. Neutron reflectometry coupled with ellipsometry shows details of the thin film morphology and structure at solid/liquid interfaces and is used in the study of biocompatible thin films.

Optical and scanning force microscopies (SFM) covers atomic force microscopy (AFM), scanning tunneling microscopy (STM) and near-field scanning optical microscopy (NSOM). Polymer science has benefited from the continuous development of scanning probe microscopy (SPM) techniques, which allow full characterization of polymer films at the nanoscale: such as film morphology, mechanical properties (*i.e.* stiffness, deformability, adhesion, and friction), electrical and thermal properties (*i.e.* glass-transition, melting and crystallization temperatures), and so forth. The capability of studying surface reorganizations in real time through *in situ* experiments makes SPM a valuable and ver-

satile tool, able to give insight on the physicochemical properties of polymer films with unprecedented detail.

Topographical features of polymer surfaces are easily revealed and material contrasts can be established either by differences in the mechanical properties of the materials or by selective removal of one of the two phases using a selective solvent. A comparison of different optical and SPM surface analysis techniques is provided in Figs.6A and B.

One of the most common techniques used for measurement of the surface morphology and other mechanical properties is atomic force microscopy. Using this technique, an oscillating small spring-like cantilever with a sharp tip fixed on its free end examines the sample surface. Tip radius of curvature can be as small as a size of one atom and ranges up to 1 μm. The deflections of the cantilever are determined by the detector and the forces between tip and surface are estimated. These forces can be as small as 10^{-9}-10^{-10} N.
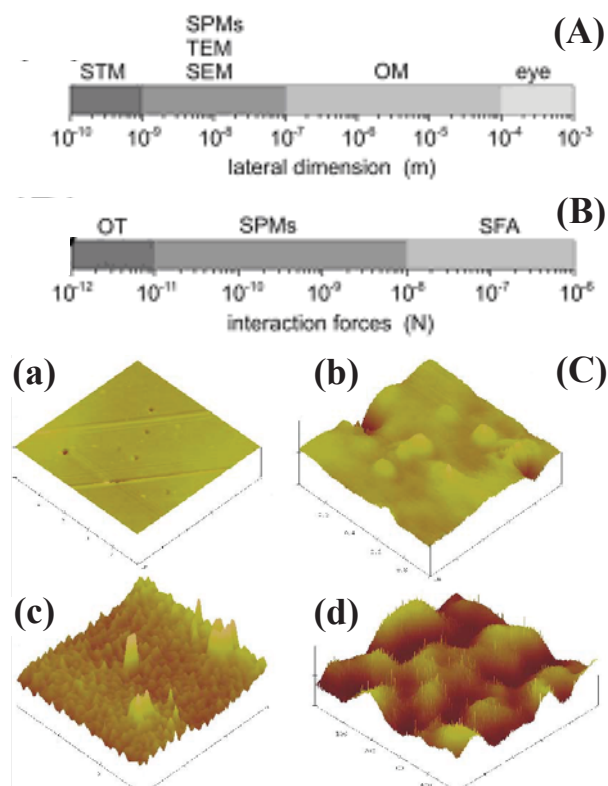
Fig.6. (A) Comparison of different SPMs with surface imaging techniques classified according to measurable size (STM – scanning tunneling microscopy, SPMs – scanning probe microscopies, TEM – transmission electron spectroscopy, SEM – scanning electron microscopy, and OM – optical microscopy). (B) Surface force techniques are classified according to the strength of interactions. (C) AFM images of (a) pristine poly(methyl methacrylate) (PMMA), irradiated with fluencies of (b) 4×10^{14}, (c) 4×10^{15} and (d) 1×10^{16} e/cm^2 [20].

Changes in surface morphology of pristine PMMA samples after irradiation are shown in Fig.6C. The tapping mode of the AFM (TM-AFM) showed the hills of the nano size surrounded by crater type features in all irradiated samples. It was found that the root-mean-square (RMS) surface roughness of the samples increased from 2.7 to 5.6 nm when the electron fluency correspondingly increased from 2×10^{14} to 1×10^{16} e/cm^2 [20].

Care must be taken when topographical features are imaged by tapping mode AFM in that different phases have very different mechanical properties.
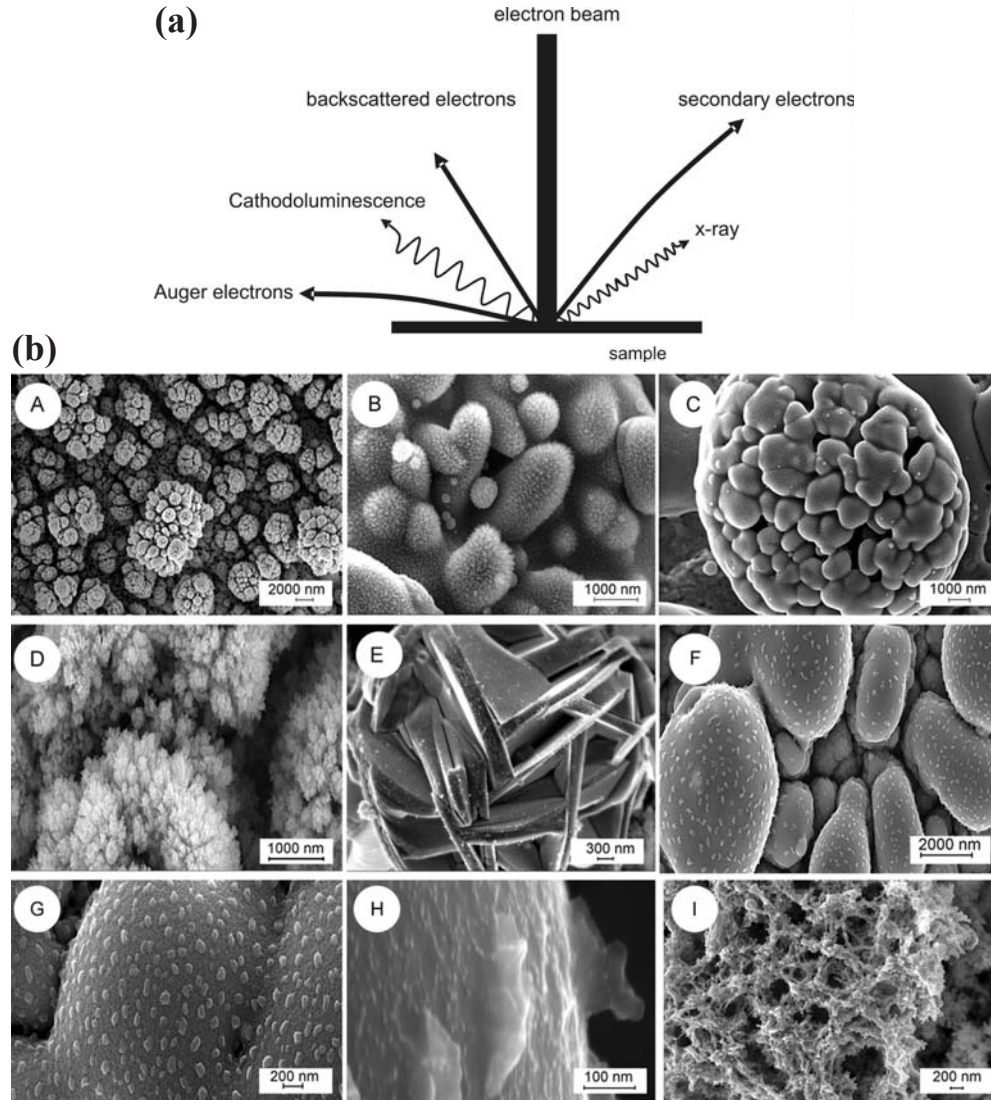
(a)

(b)

Fig.7. (a) Emissions produced in a performing SEM analysis. (b) SEM images of MoO$_3$ nanostructures: (A-E) deposited in the pin-to-pin electrode configuration, (F-H) deposited in the pin-to-plate electrode configuration, (I) porous networks of MoO$_3$ deposited in the pin-to-plate configuration [23].

Differences in tip indentation into the surface may interfere with the real topographical features and the interpretation of the apparent surface topography becomes difficult [21].

Biodegradable polycaprolactone (PCL)/poly-l-lactide (PLLA)/coconut fiber composites were irradiated using an electron beam accelerator to an absorbed dose of 100 kGy [22]. Regions with different elasticity indicated the presence of fibers on the surface of the composites. The spherical structure sizes decreased on the surface of the composites.

The different kinds of signals and images that are produced using a scanning electron microscope are shown in Fig.7 and described in Table 3. For the successful examination of a specimen by SEM, the sample must be carefully prepared. Embedded liquids and gases in the sample must be removed by appropriate treatment (*e.g.* storage at elevated temperatures or in vacuum). Surfaces of non-conductive samples should be sputtered with a thin conductive layer. For these reasons noble metals like gold, palladium and platinum serve as the typical coating materials. In the case of X-ray analysis, the sample is analyzed according to its composition and should not be coated with the above-mentioned metals but with carbon. Many thin polymer films, though non-conductive in bulk, can be imaged without coverage by a conducting material (metals, carbon, *etc.*).

Table 3. Emissions related to SEM operation and features to examine/obtained information.

Emission/signal	Features to examine/obtained information
Secondary electrons	Topographical observation of surface, potential contrast, crystalline structure, magnetic contrast
Backscattered electrons	Compositional observation of surface, magnetic contrast
X-ray	Element analysis of specimen
Transmitted electrons	Internal structure
Cathodoluminescence	Internal characteristics

Scanning can also be done in the transmission mode to circumvent problems associated with transmission electron microscopy (TEM), such as poor contrast [24]. X-rays produce an energy dispersive X-ray (EDX) spectrum that can identify the elements in the imaged area. Some SEM capabilities are: large depth of field, 3 nm resolution (100 000x), digital imaging and archiving, electron channeling, *etc*. Spatial resolution of a few nanometers along all three spatial axes has been demonstrated. Element analysis using the EDX spectrum and the wavelength dispersive X-ray (WDX) spectrum is mainly applied to inorganic materials. These methods are only rarely used in the field of polymer science, but find applications such as the characterization of inorganic-organic hybrid surfaces.

Standard SEM is conducted in a high vacuum environment, which prevents biological samples from being investigated in their native state. Newer instruments, called environmental scanning electron microscopes (ESEM), allow visualization of at least partially hydrated samples.

Contact angle measurement is the most common method for determining the free surface energy of solid surfaces. This provides data on surface energetics, roughness, heterogeneity, as well as on surface dynamics, allowing one to monitor the behavior at solid-liquid interfaces. There are two main methods of solid surface tension measurements: (i) the contact angle (the most frequently used and most accessible technique) and (ii) the inverse gas chromatography method.

The contact angle method is sensitive to the topmost few angstroms, due to the forces involved in the wetting process. A liquid drop deposed on a solid surface will modify its shape under the pressure of different surface/interfacial tensions until equilibrium is reached. In the thermodynamics of wetting, the minimization of the free energy of the system imposes one and only one value for the contact angle. A liquid drop on a solid surface can have many different stable angles, continuously varying between two relatively well reproducible values, the maximum being usually called the advancing angle and the minimum – the receding angle. The difference between these two values is known as the contact angle hysteresis. From the contact angle hysteresis, the fraction of polar and non-polar surface segments can be estimated. One of the main disadvantages of the contact angle method is that only ideal surfaces (rigid, homogeneous, and smooth) can be used to measure the true equilibrium contact angle for a liquid-solid interface.

Young's equation describes a state of stable equilibrium, being valuable for an ideal surface:

$$\gamma_{sv} - \gamma_{sl} = \gamma_{lv} \cos \theta \qquad (2)$$

where: γ_{sv} – the surface tension of the solid (s) in equilibrium with the saturated vapor (v) of the liquid (l), γ_{sl} – the interfacial tension between the solid and the liquid, and γ_{lv} – the surface tension of the liquid in equilibrium with its saturated vapor, θ – the equilibrium contact angle between a drop of liquid deposited on a solid and the respective surface, as shown in Fig.8.

Surface tension has the dimension of force per unit length or of energy per unit area. The two are equivalent, but when referring to energy per unit of area, it is common to use the term surface energy, which is the more general term in that it applies also to solids.

The wetting liquid must be a neutral one, so that neither physical nor chemical interactions with the solid occur.

The surface tension may be considered as a sum of independent terms. The geometrical mean could describe polar and dispersion interactions, by the following equation:
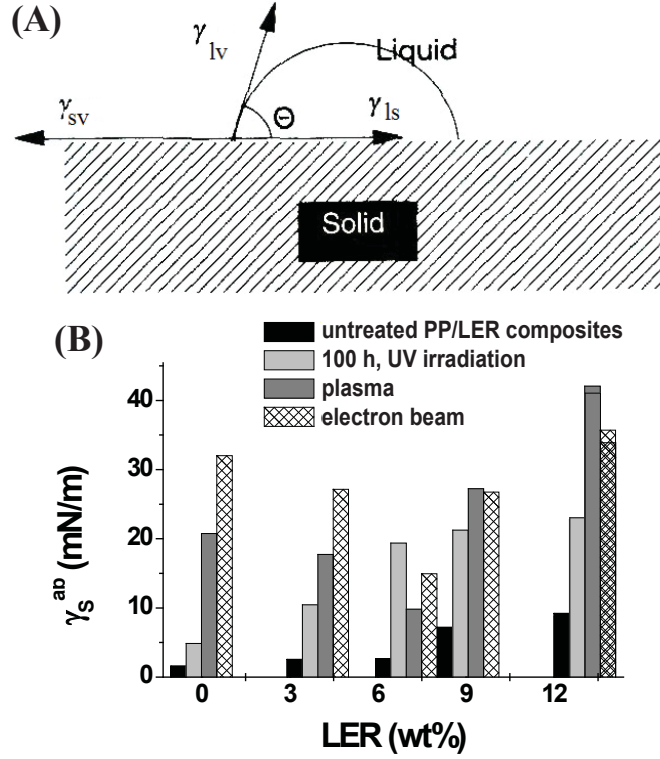
Fig.8. (A) Interfacial tensions at the contact between three media and (B) acid-base component of the free surface energy *vs.* epoxidized lignin (LER) content for isotactic polypropylene (IPP)-based composites, exposed to different irradiation sources [25].

$$\gamma_{sl} = \gamma_s + \gamma_l - 2\left(\gamma_s^d \gamma_l^d\right)^{1/2} - 2\left(\gamma_s^p \gamma_l^p\right)^{1/2} \tag{3}$$

where: γ_s and γ_l – the total surface tension of the solid (s) and of liquid (l), respectively; γ_s^d (or γ_s^{LW}) and γ_l^d (or γ_l^{LW}) – dispersive components of surface tension of solid and liquid, respectively; γ_s^p and γ_l^p – polar components of surface tension of solid and liquid, respectively.

Also the harmonic mean method [26] may be used where the dispersion (I_d noted also with γ_s^{LW}, γ_l^{LW}, respectively – Eq. (5)) and the polar (I_p) terms are substituted by:

$$I_d = 2\left(\gamma_l^d \gamma_s^d\right) / \left(\gamma_l^d + \gamma_s^d\right) \text{ and } I_p = 2\left(\gamma_l^p \gamma_s^p\right) / \left(\gamma_l^p + \gamma_s^p\right) \tag{4}$$

In both cases the two components of the free surface energy of solid can be determined using at least two liquids of having known surface tensions and of different polarities (generally, water and methylene iodide).

The asymmetric acid-base parts of a bipolar system can be split into separate surface energy components: the acid (γ^+) and the basic (γ^-) components of the surface energy. γ^+ is the contribution of the proton donor (electron acceptor), while γ^- that of the proton acceptor (electron donor).

With these considerations, the Young-Good-Girifalco-Fowkes equation becomes:

$$\gamma_1 \left(1 + \cos\theta\right) = 2\left[\left(\gamma_s^{LW}\gamma_1^{LW}\right)^{1/2} + \left(\gamma_s^+\gamma_1^-\right)^{1/2} + \left(\gamma_s^-\gamma_1^+\right)^{1/2}\right] \qquad (5)$$

The interfacial tension γ_{ij}^{ab} between the i and j phases can be expressed as:

$$\gamma_{ij}^{ab} = 2\left[\left(\gamma_i^+\gamma_i^-\right)^{1/2} + \left(\gamma_j^+\gamma_j^-\right)^{1/2} - \left(\gamma_i^-\gamma_j^+\right)^{1/2} - \left(\gamma_i^+\gamma_j^-\right)^{1/2}\right]$$

or

$$\gamma_{ij}^{ab} = 2\left[\left(\gamma_i^+\right)^{1/2} - \left(\gamma_j^+\right)^{1/2}\right]\left[\left(\gamma_i^-\right)^{1/2} - \left(\gamma_j^-\right)^{1/2}\right] \qquad (6)$$

where $\gamma_{i(\text{or } j)}^-$ and $\gamma_{i(\text{or } j)}^+$ are the contributions of the proton acceptor (electron donor) and proton donor (electron acceptor) to the polar component of the free surface energy, respectively.

Two methods may be applied for evaluation of the different components of the free surface energy of a system using Eq. (5). The first one requires three polar liquids having known surface tension components to be deposited on the respective surface in order to obtain the corresponding contact angles. The second method requires one non-polar liquid for finding γ^{LW} and two other polar liquids. The acid-base component of free surface energy increased due to any treatment of IPP/LER blends whether by ultraviolet (UV) irradiation, plasma exposure or electron beam bombardment (Fig.8B). This acid-base component increases regardless of the treatment applied [25].

Four commonly used methods for contact angle (surface tension) measurement are: (i) the sessile drop, (ii) the tilting plate, (iii) the captive bubble, and (iv) the Wilhelmy plate technique.

Work of adhesion (W_a) is defined as the work required when separating liquid and solid phases, or the negative free energy associated with the adhesion of the solid and liquid phases. It is used to express the strength of the interaction between the two phases and it is given by the Young-Dupré equation as:

$$W_a = \gamma\left(1 + \cos\theta\right) \qquad (7)$$

Wetting tension, (τ) a measure of the force/length or strength of the wetting interaction, is defined as:

$$\tau = \gamma_{lv}\cos\theta \qquad (8)$$

It is also referred to as adhesion tension or work of wetting.

Chemiluminescence (CL) is the emission of light (luminescence) as the result of a chemical reaction. Such chemical reactions produce energy in sufficient amount to induce the transition of an electron from its ground state to an excited electronic state. This electronic transition is often accompanied by vibrational and rotational changes in the molecule. Given reactants **A** and **B**, with an excited intermediate, the following describes such reactions:

$$[\mathbf{A}] + [\mathbf{B}] \rightarrow [\lozenge] \rightarrow [\text{Products}] + \text{light} \qquad (9)$$

Chemiluminescence is defined as the emission of ultraviolet, visible or infrared radiation from a molecule or atom as the result of the transition of an

electronically excited state. When the reaction occurs in a living system or it is derived from one, the process is called bioluminescence (BL).

Sometimes, the excited product [◊] is an ineffective emitter, but it can transfer the excitation energy to an efficient fluorophore (F) added to the system:

[◊] + F → C + F*
$$\downarrow$$
F + Light
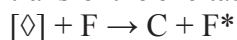
The emission is then identical with the fluorescence of the fluorophore F. Analytically, the CL reactions are attractive since they: (i) have excellent sensibility and wide detection limits due to the absence of source noise and scatter; (ii) are sometimes highly selective due to the limited number of available reactions; (iii) are simple, robust and rely on inexpensive instrumentation suitable to both batch or flow analytical techniques. CL methods have been used in drug analysis, in sea water analysis or in determining antioxidant activity in natural and synthetic products [27]. They have been widely used for sensitive detection and measurement of reactive oxygen species involved in the oxidative processes. Oxidative changes in food are important in terms of nutritional quality, flavor, odor, spoilage, and potential toxicity resulting from ingestion of oxidation reaction products. Oxidative stress is an important hypothesis in explaining the genesis of several pathologies, including cancer, atherosclerosis, aging or Alzheimer's disease. Several components of food and natural products (phenolic compounds, vitamins, *etc.*) have protective functions in the aforementioned pathologies. This seems to be due to their ability to scavenge reactive oxygen.

The radiation degradation of polypropylene was studied by measuring the chemiluminescence from gamma-irradiated samples. The chemiluminescence emitted by recombination of peroxy radicals was found to increase with the increasing dose, thus reflecting the degree of oxidation of the polymer. The degradation of PP is attributed mainly to oxidation, since the degradation of PP irradiated in air was markedly greater than that in vacuum. The degree of oxidation was found to be very high at the surface of the films where oxygen can diffuse during irradiation and was decreased sharply with increasing depth from the surface. The degradation during PP storage after irradiation was estimated by the decay curves of the chemiluminescence [28].

Chemiluminescence analysis was used to determine the oxidation layer formed by electron beam irradiation of polypropylene for medical devices. Oxidation was found to occur near the surface of the film where the diffusion of oxygen was greater [29].

Ethylene-vinyl acetate (EVA) copolymers undergo thermal degradation by the macromolecular breakdown after irradiation to a dose of 12 kGy, as shown in Fig.9 [30]. The oxidation induction period, *i.e.* time until the CL intensity reached its maximum value, decreased with increasing treatment temperature.
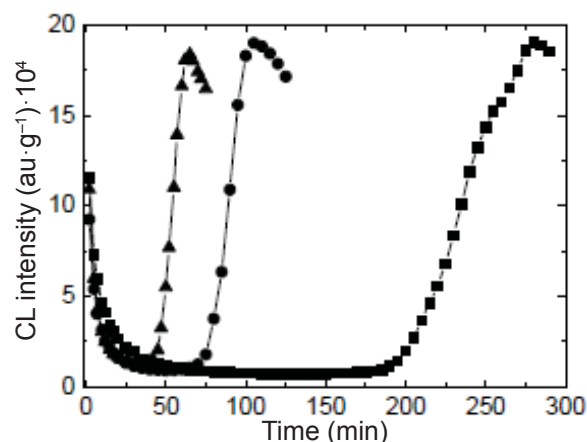
Fig.9. The time dependence of CL intensity with the treatment temperature for irradiated EVA copolymer at 12 kGy. Measurement temperatures: (■) 200°C, (●) 210°C, (▲) 220°C [30].

Combining several of the surface property methods is recommended in order to achieve reliable results.

3. METHODOLOGIES FOR THE CHARACTERIZATION OF SOME BULK PROPERTIES

Industry uses ionizing radiation to modify the properties of polymers for use in many areas. The irradiation of polymers can lead to crosslinking and/or chain scissioning reactions, depending on the chemical structure of the polymer and the irradiation conditions. Generally, crosslinking results in an increase in tensile strength, hardness, softening temperature, solvent resistance, abrasion resistance, dimensional stability, and a decrease in elongation at break [31, 32].

Chain scissioning most often leads to reduced tensile strength, hardness and softening temperature, and increased solubility and elongation. Crosslinking and scissioning occur simultaneously in a polymer during irradiation and the overall change in properties depends on which process predominates.

For a given polymer, the irradiation conditions that most affect the relative amounts of crosslinking and chain scissioning are the dose rate, and the presence of oxygen, additives and solvents and the irradiation temperature.

Several important bulk properties of polymers are affected by irradiation: chemical composition and structure, average molecular weight, solubility, mechanical properties (Young's modulus, tensile, impact, hardness, fatigue, flexural modulus, *etc.*), electric and optical properties, crystallinity, transition temperatures (mainly glass transition related to Vicat softening point and

brittleness temperature), gas permeability across a polymer film or a membrane, water absorption, melt viscosity and rheological properties, polymer stability under aging, biological factors, temperature and UV resistance, weathering (environmental stress), *etc.* Descriptions of many methods used to determine the bulk properties of irradiated materials can be found in Refs. [33, 34].

Several important properties of polymers are related to their bulk morphology. Methods used to evaluate surface morphology have been discussed above. In food packaging, the crystallinity, the glass transition temperature and barrier properties are of interest including migration phenomena from packaging materials to food, as possible with the use of nanoparticles. Methods to characterize these properties are described below.

3.1. GLASS TRANSITION TEMPERATURE

The glass transition temperature (T_g) is the temperature at which several physical characteristics of polymers change, such as: specific heat capacity (c_p), coefficient of thermal expansion, mechanical modulus, dielectric constant.

The glass-liquid transition or glass transition is the reversible transition in amorphous materials (or in amorphous regions within semicrystalline materials) from a hard and relatively brittle "glassy" state into a molten or rubber-like state, as the temperature is increased. The reverse transition, achieved by cooling a liquid into the glass state, is called vitrification. The temperature at which the transition in a material changes between a glassy, hard state to a rubbery or liquid state is called the glass transition temperature.

Three techniques are generally used for determining T_g:
• differential scanning calorimetry (DSC),
• thermomechanical analysis (TMA),
• dynamic mechanical analysis (DMA).
In each of these techniques, a change in a sample is determined as a function of temperature.

Differential scanning calorimetry is a traditional and widely used technique with many polymeric materials. Depending on the equipment capability, DSC can be used for a wide range of thermoplastic and thermoset polymers. The glass transition, as illustrated in Fig.10, appears as a step in the DSC curve and shows the change of the specific heat capacity (c_p) from the glassy/vitreous to the rubbery phase.

T_g can be calculated by using a half-height technique in the transition region. This procedure is described in the ISO standard 11357-2:1999 [35].

For a given polymer, the glass transition temperature depends on polymer morphology that includes molecular weight, branching, crystallinity, the amount and type of additives and traces of solvents/water. For irradiated polymers, T_g also depends on dose [36, 37].
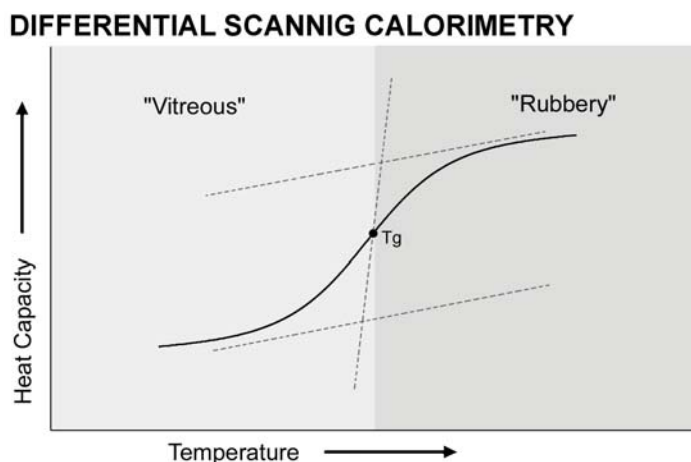
DIFFERENTIAL SCANNIG CALORIMETRY

Fig.10. Typical DSC curve.

Carswell-Pomerantz *et al.* [38] evaluated the glass transition of fluoropolyimide (FPI) samples at different gamma irradiation doses. Before irradiation, the T_g of FPI was 280°C. After irradiation to 600 and 1800 kGy, the T_g of FPI increased to 295 and 310°C, respectively. These temperature changes in T_g were attributed to crosslinking of the FPI, which hinders molecular mobility. The higher T_g also indicates an increase in crosslinked density. Different properties can be obtained if the polymer is irradiated below or above its glass transition temperature, as it was reported by Sun and Zhong [39] in their study of tacticity changes of isotactic poly(methyl methacrylate) (PMMA) and syndiotactic PMMA samples.

3.2. DEGREE OF CRYSTALLINITY

The crystallization of polymers is a more complicated process than the crystallization of low molecular weight materials. This is related to the wide distribution of chain lengths of macromolecules, the high interfacial free energy associated with the basal plane of the crystallites and to the difficulty in extracting ordered sequences of macromolecules of sufficient length from the disordered melt in a finite or reasonable time. The crystallization of long chain, higher molecular weight molecules will only occur during long cool down cycles, which gives rise to a complex arrangement of molecules with a polycrystalline character and to the coexistence of crystalline and amorphous components.

The degree of crystallinity of a polymer is the relative amount of crystalline and amorphous components and can be expressed on either a volume or mass basis. The degree of crystallinity depends on the crystallization conditions, the degree of polymer branching, polymer side chain bulkiness, and the regu-

larity of molecular configuration. The dependence on irradiation dose should be taken into account when examining irradiated polymers. In particular, the degree of crystallinity will increase in following order:
- slow cooling more than fast cooling (this allows time for diffusion to occur and for polymer chains or segments to align),
- linear more than branched more than crosslinked polymers,
- isotactic and syndiotactic more than atactic polymers,
- simple repeat units more than bulky side chains in repeat units.

For polymers that crystallize, the crystallinity influences many properties of some manufactured products (Table 4). More crystalline polymers tend to be mechanically stronger and more resistant to chemical attack and to softening by heat.

Table 4. Effect of increase in crystallinity on different polymer properties [40]. ↑ represents increase and ↓ represents decrease (with increasing crystallinity).

S/N	Property	Effect of crystallinity
1	Density	↑
2	Tensile strength	↑
3	Clarity	↓
4	Permeability	↓
5	Opacity	↑
6	Compressive strength	↑
7	Impact strength	↓
8	Tear resistance	↓
9	Toughness	↓
10	Ductility	↓
11	Ultimate elongation	↓

The degree of crystallinity can be determined using several methodologies based on density measurement, X-ray diffraction, and the determination of melting enthalpy. All these methodologies are based on a two-phase model, having crystalline and amorphous phases.

Using volume (x_v) and mass (x_m), the degree of crystallinity can be determined from density measurements using the following equations:

$$x_v = [(\rho - \rho_a)/(\rho_c - \rho_a)] \times 100 \tag{10a}$$
$$x_m = [\rho_c(\rho - \rho_a)/\rho(\rho_c - \rho_a)] \times 100 \tag{10b}$$

where ρ, ρ_a and ρ_c are the densities of the sample, of the same material in amorphous phase and in the crystalline phase, respectively.

A typical wide-angle X-ray diffraction (WAXD) curve for a semicrystalline polymer has sharp diffraction peaks resulting from the crystalline phase

of a sample material and a broad diffuse halo corresponding to the amorphous phase of that material. The areas under the "amorphous" halo and the "crystalline" peaks are used to determine degree of crystallinity:

$$\% \text{ Crystallinity} = \frac{\text{Area under crystalline peaks}}{\text{Total area under all peaks}} \times 100\% \qquad (11)$$

The degree of crystallinity can also be obtained measuring the melting enthalpy of the sample and comparing its value with the melting enthalpy of the polymer having nearly 100% crystallinity. The usual procedure in determining the degree of crystallinity by DSC involves drawing an arbitrary linear baseline from the onset of melting to the last trace of crystallinity and determining the enthalpy of fusion from the area under this endotherm, as illustrated in Fig.11. The degree of crystallinity is then defined as:

$$\% \text{ Crystallinity} = [\Delta H_f / \Delta H_f^\circ] \times 100 \qquad (12)$$

where ΔH_f is the enthalpy of fusion measured at the melting point (T_m), and ΔH_f° is the enthalpy of fusion of the 100% crystalline polymer measured at the equilibrium melting point (T_m°).
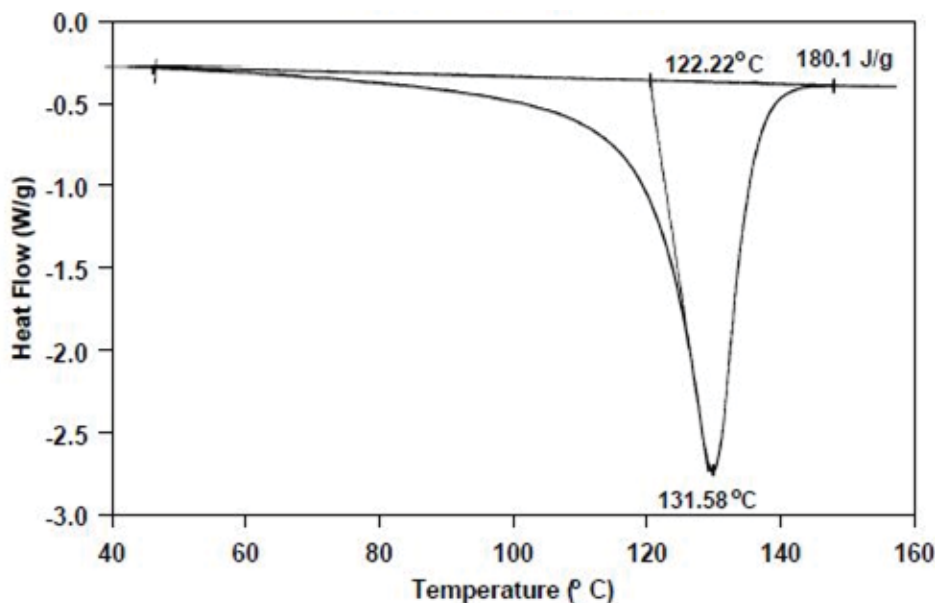

Fig.11. Melting endotherm for a polyethylene sample after heating.

The relative degree of crosslinking and scissioning in polymers when irradiated are effected by the degree of crystallinity of the polymer. Since crosslinking usually takes place in the amorphous phase, increased crystallinity in a polymer reduces its ability to crosslink [41]. At the same time, irradiation may alter the crystallinity in polymers. Increased crosslinking reduces the ability of a polymer to recrystallize because the three-dimensional polymer network produced by crosslinking inhibits crystallite formation. Under certain irradia-

tion conditions some crystalline polymers can undergo radiation-induced chain scissioning followed by recrystallization which stops the degradation process and generates a sample with increased crystallinity.

Table 5. Crystallinity by X-ray diffraction in PLA nanocomposites containing clay (Dellite D67G) nanoparticles before and after irradiation to 1 and 10 kGy [41].

Sample	Xc [%]
PLA/D67G 1%	–
PLA/D67G 1%_1 kGy	2
PLA/D67G 1%_10 kGy	3
PLA/D67G 3%	4
PLA/D67G 3%_1 kGy	6
PLA/D67G 3%_10 kGy	5
PLA/D67G 5%	8
PLA/D67G 5%_1 kGy	9
PLA/D67G 5%_10 kGy	7

The admixture of clay nanoparticles and the influence of irradiation on the crystallinity of poly(lactic acid) (PLA)-based nanocomposites was investigated using WAXD [42, 43]. Unmodified PLA remains amorphous after irradiation to the doses of 1 and 10 kGy [41, 42]. For the nanocomposites containing clay nanoparticles, however, the X-ray diffraction patterns showed the formation of a crystalline phase. Some crystals of the α-form were observed in PLA nano-composite containing 1 wt% of clay (Dellite D67G) and the crystallinity increased for nanocomposites containing 3 and 5 wt% of Dellite D67G. The values of crystallinity are reported in Table 5.

3.3. BARRIER PROPERTIES

Barrier properties are of importance in food packaging because they control the ability of a package to preserve its contents from the deleterious effects of gases, aromas, humidity, *etc.* UNI (UNI 10534 12/94) defines the limits of permeability associated with low and high barrier properties (Table 6).

Permeability (P) is defined as the quantity of gas passing through a unit surface area, of given thickness, under a partial and unitary difference of pressure in the unit of time. The permeability of plastic films is a function of several polymer characteristics (chemical type, morphology, and crystallinity), of environmental factors (temperature, relative humidity, difference of pressure), of thickness and geometry of the packaging, and the kind and size of permeant

Table 6. Barrier properties range.

Barrier	Permeability $[cm^3/(m^2 \cdot 24\ h)] \cdot (cm/bar)$
Very high	< 0.5
High	0.5-3.0
Medium	3.1-30
Low	31-150
Very low	> 150

gas molecules or particles. Permeability is also influenced by the amount, distribution, and size of such particles because the presence of these particles affects the path of gas molecules.

Barrier properties are linked to the diffusion parameters. Fick's laws are used to study the diffusion parameters of polymers. Fick's first law is an empirical expression. It states that the flux (mass per unit time per unit area) traveling through a material is equal to $-D$ (the diffusion coefficient or diffusivity) times the concentration gradient (dc/dx) with respect to the distance traveled (x) [44]:

$$j = -D\ (dc/dx) \tag{13}$$

Fick's first law applies strictly to neutral, non-interacting particles only. For other situations, the coefficient D is not a constant.

Fick's law in terms of permeability (P) and the pressure gradient (dp/dx) can be written as:

$$j = -D\ (dc/dx) = -P\ (dp/dx) \tag{14}$$

Converting dp/dx gradient into actual values, the following equation can be obtained for the permeability:

$$P = Q \times x\ /A \times (p_1 - p_2) \tag{15}$$

where: Q – the fluid flow rate defined as the quantity of fluid or gas (O_2, N_2, CO_2, water vapor) passing through a unit area in the unit of time with the
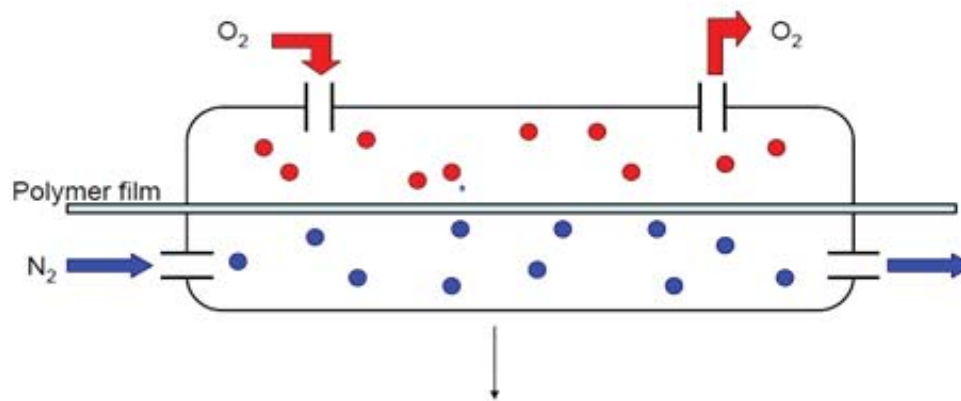

Fig.12. Operating principle of a gas permeability tester.

difference of pressure ($p_1 - p_2$), A – the sample surface, and x – the sample thickness. This equation can be used to calculate P from the measurements performed using a permeability testing apparatus, as shown in Fig.12. The permeability testing apparatus consists of a double diffusion chamber with the test film inserted between the two chambers. For the evaluation of oxygen permeability, oxygen enters into the upper chamber, while anhydrous nitrogen enters the bottom one as a carrier gas. The chambers are conditioned at 23°C. As the oxygen gas permeates through the specimen (polymer film) into the carrier gas, it is transported to the coulometric detector where it creates an electric current which is proportional to the number of oxygen atoms flowing into the detector.

This test is performed in accordance with ASTM D3985 which determines the amount of oxygen that passes through the surface (50 cm^2) of the film of a given thickness, in a certain time (24 h), with precise relative humidity conditions (0%) and temperature (23°C).

3.4. PARTICLES MIGRATION

Packaging protects foodstuff from spoilage. However, the transfer of chemicals from packaging to food may have a negative impact on the quality and safety of the food since no food contact material is completely inert and there is a need to ensure the safety of such materials. The main consumer demand is that the packaging should not be a source of contamination in the food.

Any mass transfer from an external source into food by particle migration is important when developing a new packaging material for the market. Such migration may impact on food in two ways: (i) causes safety problems related to the migration of harmful substances and (ii) causes quality problems related to the migration of substances which impart taint or odor. To overcome some of these problems, polymer-based food packaging is irradiated. When a polymer packaging materials is subjected to irradiation not only the migration of the typical additives must be taken into consideration but also the radiolytic products (RPs) generated during the irradiation process. The RPs from some commonly used polymers consist of low molecular weight aldehydes, acids and olefins. In the case on packaging based on nanomaterials the migration of the nanoparticles must be also assessed.

Typical additives for plastics are: stabilizers, UV absorbers, preservatives, optical brighteners, foaming agents, release agents, antioxidants, plasticizers, lubricants, emulsifiers, fillers, flame retardants, impact modifiers.

The migration ability of particles increases with temperature and decreases with the dimension of the migrating substance.

Migration tests are usually performed by using food simulants that are intended to mimic the migration properties of different categories of foods. This

methodology was introduced in the early 1980s along with the rules for using simulants. The basics for migration tests are reported in the following European Community (EC) documents:

* 82/711/EEC – Basic rules for testing migration,
* 93/8/EEC – 1st amendment,
* 97/48/EEC – 2nd amendment,
* 85/572/EEC List of simulants,
* 10/2011/EU List of simulants.

According to the regulations the following steps need to be performed:

* selection of simulant which is based on a food type (Table 7),
* selection of the exposure type,
* selection of the exposure time and temperature.

Table 7. Types of simulants used for food packaging testing.

Simulant	Abbreviation	Food
Ethanol 10% (v/v) in water	Simulant A	Aqueous foods
Acetic acid 3% (w/v) in water	Simulant B	Acidic foods (< pH 4.5)
Ethanol 20% (v/v) in water	Simulant C	Alcoholic foods (< 20% alcohol)
Ethanol 50% (v/v)	Simulant D1	Foods with an alcohol content of above 20% and for oil in water emulsions
Vegetable oil	Simulant D2	Foods with an alcohol content of above 20% and for oil in water emulsions
Modified poly(phenylene oxide)s, particle size – 60-80 mesh, pore size – 200 nm	Simulant E	Dry foods

The migration models in different food stuffs are set in EC regulations and are normally quoted from migration tests using the following values: 600 cm^2 of print, 1 kg of food, 10 days at 40°C.

Migration tests may be performed in four ways depending on the form and the dimensions of the material or article to be tested:

* by using a migration test cell,
* by preparation of a pouch,
* by total immersion,
* by article filling.

For most of the samples the total immersion method is used: the sample (1 dm^2) is immersed in the simulant.

For total immersion tests, different procedures have been adopted according to the type of the selected food simulant. In the case of aqueous simulants,

the overall migration is calculated by determining the mass (M) of the residue after evaporation of the water in the food simulant.

For fatty food the determinations, the overall migration into vegetable oil is more complicated. The value of the overall migration is measured by determining the weight loss from the sample. Taking into account that the sample might have absorbed components of the fatty simulant during contact, the weight loss of the sample must be corrected for the amount of absorbed fat [45].

The effect of irradiation on the migration behavior of particles from packaging to food is reported in the literature. Zygoura *et al.* [46] compared the effect of irradiation type and dose on the specific migration behavior of poly(vinyl chloride) (PVC) films. The migration levels of a plasticizer (acetyl tributyl citrate – ATBC) from PVC into the European Union (EU) aqueous food simulants (distilled water, 3% w/v acetic acid and 10% v/v ethanol) after PVC films were irradiated to 5, 15 and 25 kGy doses using an electron beam or gamma rays (Co-60 unit) were studied. The electron beam irradiated films had significantly higher ATBC migration as compared to gamma treatment, although for both types of ionizing radiation the values defining ATBC migration into the aqueous food simulants were far below the EU limits (1 mg·kg^{-1} body weight). Because of these results, it was concluded that irradiated PVC cling films may be used in contact with aqueous foodstuffs.

Jeon *et al.* [47] evaluated the effect of gamma irradiation on the migration levels of two antioxidants, tris-(2,4-di-tert-butylphenyl) phosphite (Irgafos 168) and octadecyl-3-(3,5-di-tert-butyl-4-hydroxyphenyl) propionate (Irganox 1076), on linear low density polyethylene (LLDPE) films treated at doses ranging from 0 to 200 kGy. The migration of Irgafos 168 from a LLDPE pouch into food simulants, distilled water, acetic acid (4 ml/100 ml distilled water) or ethanol (20 ml/100 ml distilled water), was not detected at dose levels up to 200 kGy while Irganox 1076 was detected in a decreasing mode with increasing doses.

4. CONCLUSIONS AND FUTURE TRENDS

The use of the main methods to study the changes in the surface and bulk properties of irradiated polymers was presented, emphasizing the advantages and limitations of each method. As instrumentation and theory continue to develop, methods will also improve to facilitate the understanding of the effects of radiation on polymer structure and morphology which subsequently influence the final properties of products.

REFERENCES

[1]. Vasile, C., & Pascu, M.C. (2007). *Surface properties of polymers*. Kerala, India: Research Signpost.

[2]. StJohn, H.A.W., Gengenbach, T.R., Hartley, P.G., & Grisser, H.J. (2003). Surface analysis of polymers. In D.J. O'Connor, B.A. Sexton & R.St.C. Smart (Eds.), *Surface analysis methods in materials science* (pp. 519-553). Berlin, Heidelberg: Springer. (Springer Series in Surface Sciences 23).

[3]. Murray, K.A., Kennedy, J.E., McEvoy, B., Vrain, O., Ryan, D., Cowman, R., & Higginbothama, C.L. (2013). Characterisation of the surface and structural properties of gamma ray and electron beam irradiated low density polyethylene. *International Journal of Material Science (IJMSCI)*, *3*(1), 1-8.

[4]. Klauber, C., & Smart, R.St.C. (2003). Solid surfaces, their structure and composition. In D.J. O'Connor, B.A. Sexton & R.St.C. Smart (Eds.), *Surface analysis methods in materials science* (pp. 3-81). Berlin, Heidelberg: Springer. (Springer Series in Surface Sciences 23).

[5]. Israelachvili, J.N. (1992). *Intermolecular and surface forces*. London: Academic Press.

[6]. Garbassi, F., Morra, M., & Occhiello, E. (1994, 1998). *Polymer surfaces. From physics to technology*. Chichester: John Wiley & Sons.

[7]. Ratner, B.D. (1988). *Surface characterization of biomaterials*. Amsterdam: Elsevier Science Publishers.

[8]. Goessl, A., Jung, L., Bowen-Pope, D., & Hoffman, A.S. (2002). Affinity patterning of biomaterials using plasma gas discharge. In *Radiation synthesis and modification of polymers for biomedical applications. Final results of a co-ordinated research project, 1996-2000.* Vienna: IAEA. (IAEA-TECDOC-1324).

[9]. Onyiriuka, E.C. (1993). The effects of high-energy radiation on the surface chemistry of polystyrene: A mechanistic study. *J. Appl. Polym. Sci.*, *47*(12), 2187-2194.

[10]. Jenkins, S. (2016, January). *Principle of SIMS (Secondary Ion Mass Spectrometry)*. Retrieved January 14, 2016, from http://www.lpdlabservices.co.uk/analytical_techniques/surface_analysis/sims/index.php.

[11]. Leggett, G.J., & Vickerman, J.C. (1992). An empirical model for ion formation from polymer surfaces during analysis by secondary-ion mass spectrometry. *Int. J. Mass Spectrom. Ion Processes*, *122*, 281-319.

[12]. SurfaceSpectra Ltd. (2012). Retrieved January 14, 2016, from http://www.SurfaceSpectra.com/.

[13]. Parparita, E., Zaharescu, T., Darie, R.N., & Vasile, C. (2015). Biomass effect on gamma-irradiation behavior of some polypropylene biocomposites. *Ind. Eng. Chem. Res.*, *54*(8), 2404-2413.

[14]. Gupta, R., Kumar, V., Goyal, P.K., Kumar, S., Kalsi, P.C., & Lata Goyal, S. (2011). Effect of γ-irradiation on thermal stability of CR-39 polymer. *Adv. Appl. Sci. Res.*, *2*(1), 248-254. Retrieved January 14, 2016, from http://pelagiaresearchlibrary.com/advances-in-applied-science/vol2-iss1/AASR-2011-2-1-248-254.pdf.

[15]. Briggs, D., & Seah, M.P. (1983). *Practical surface analysis.* New York: John Wiley.

[16]. Andrade, L.D. (1985). *Surface and interfacial aspects of biomedical polymers.* New York: Plenum Press.

[17]. Beamson, G., & Briggs, D. (1992). *High resolution XPS of organic polymers: The Scienta ESCA300 Database.* Chichester: Wiley.

[18]. Bradley, R.H., Ling, X., & Sutherland, I. (1993). An investigation of carbon fibre surface chemistry and reactivity based on XPS and surface free energy. *Carbon*, *31*(7), 1115-1120.

[19]. Russell, T.P. (1990). X-ray and neutron reflectivity for the investigation of polymers. *Mater. Sci. Rep.*, *5*, 171-271.

[20]. Nathawat, R., Kumar, A., & Vijay, Y.K. (2007). Morphological changes of electron-beam irradiated PMMA surface. In C. Petit-Jean-Genaz (Ed.), *Particle accelerator*. *Proceedings, 22nd Conference, PAC'07, Albuquerque, USA, June 25-29, 2007* (pp. 2745-2747). Piscataway, USA: IEEE.

[21]. Stoleru (Paslaru), E., Tsekov, Y., Kotsilkova, R., Ivanov, E., & Vasile, C. (2015). Mechanical behavior at nano-scale of chitosan-coated PE surface. *J. Appl. Polym. Sci.*, *132*(31), 42344.

[22]. Kodama, Y., Oishi, A., Nagasawa, N., Nakayama, K., Tamada, M., & Machado, L.D.B. (2013). Atomic force microscopy investigation of electron beam (EB) irradiated composites based on biodegradable polymers and coconut fiber. *Nukleonika*, *58*(4), 459-468.

[23]. Pai, D.Z., Ostrikov, K., Kumar, S., Lacoste, D.A., Levchenko, I., & Laux, C.O. (2013). Energy efficiency in nanoscale synthesis using nanosecond plasmas. *Sci. Rep.*, *3*, 1221. DOI: 10.1038/srep01221.

[24]. Laurer, J.H., & Winey, K.I. (1998). Direct imaging of ionic aggregates in Zn-neutralized poly(ethylene-co-methacrylic acid) copolymers. *Macromolecules*, *31*(25), 9106-9108.

[25]. Pascu, M., Vasile, C., & Gheorghiu, M. (2003). Modification of polymer blend properties by argon plasma/electron beam treatment: surface properties. *Mater. Chem. Phys.*, *80*, 2, 548-554.

[26]. Wu, S. (1971). Calculation of interfacial tension in polymer systems. *J. Polym. Sci. C*, *34*, 19-30.

[27]. Jimenez A.M., & Navas, M.J. (2002). Chemiluminescence methods (present and future). *Grasas y Aceites*, *53*(1), 64-75.

[28]. Ishigaki, I., & Yoshii, F. (1992). Radiation effects on polymer materials in radiation sterilization of medical supplies. *Int. J. Radiat. Appl. Instrum. C: Radiat. Phys. Chem.*, *39*(6), 527-533.

[29]. Yoshii, F., Sasaki, T., Makuuchi, K., & Tamura, N. (1986). Durability of radiation-sterilized polymers III. Oxidation layer determined by chemiluminescence. *J. Appl. Polym. Sci.*, *31*(5), 1343-1350.

[30]. Jipa, S., Zaharescu, T., Senescu, R., & Kappel, W. (2007). Chemiluminescence study on the endurance of ethylenevinylacetate (EVA) under radiation and thermal degradation. *J. Opt. Adv. Mater.*, *9*(6), 1623-1625.

[31]. Bruce, M.B., & Davis, M.V. (1981). *Radiation effects on organic materials in nuclear plants*. Electric Power Research Institute. (Final Report EPRI NP-2129).

[32]. Drobny, J.G. (2012). *Ionizing radiation and polymers principles, technology and applications*. Oxford: Elsevier.

[33]. Sperling, L.H. (1992). *Introduction to physical polymer science* (2nd ed.). New York: Wiley-Interscience.

[34]. van Krevelen, D.W. (1990). *Properties of polymers* (3rd ed.). Amsterdam: Elsevier Science.

[35]. ISO. (1999). *Plastics – Differential scanning calorimetry (DSC) – Part 2: Determination of glass transition temperature*. ISO 11357-2:1999. Retrieved January 14, 2016, from http://www.iso.org/iso/iso_catalogue/catalogue_ics/catalogue_detail_ics.htm?csnumber=25545.

[36]. Davenas, J., Stevenson I., Celette, N., Cambon, S., Gardette, J.L., & Rivaton, A. (2002). Stability of polymers under ionising radiation: The many faces of radiation interactions with polymers. *Nucl. Instrum. Meth. B.*, *191*(1), 653-661.

[37]. Sasuga, T., & Hagiwara, M. (1986). Mechanical relaxation of crystalline poly (aryl-ether-ether-ketone) (PEEK) and influence of electron beam irradiation. *Polymer*, 27, 821-826.

[38]. Carswell-Pomerantz, T., Babanalbandi, A., Dong, L., Hill, D.J.T., Perera, M. C.S., Pomery, P.J., Saadat, G., & Whittaker, A.K. (1999). Changes in molecular structure and properties of irradiated polymers of different compositions. ESR and NMR study. In *Stability and stabilization of polymers under irradiation*. Vienna: IAEA. (IAEA-TECDOC-1062). Retrieved January 14, 2016, from www-pub.iaea.org/mtcd/publications/pdf/te_1062_prn.pdf.

[39]. Zhong, X., & Sun, J. (1999). Studies on radiation stability of polymers. In *Stability and stabilization of polymers under irradiation*. Vienna: IAEA. (IAEA-TECDOC-1062). Retrieved January 14, 2016, from www-Pub.Iaea.Org/Mtcd/Publications/Pdf/Te_1062_Prn.Pdf.

[40]. Selke, S., Culter, J., & Hernandez, R. (2004). *Plastics packaging: Properties, processing, applications, and regulations* (2nd ed.). Munich: Hanser Publications.

[41]. Drobny, J.G. (2010). *Radiation technology for polymers* (2nd ed.). Boca Raton: CRC Press.

[42]. Salvatore, M., Marra, A., Duraccio, D., Shayanfar, S., Pillai, S.D., Cimmino, S., & Silvestre, C. (2016). Effect of electron beam irradiation on the properties of polylactic acid/montmorillonite nanocomposites for food packaging applications. *J. Appl. Polym. Sci.*, 133, 42219.

[43]. Shayanfar, S., Smith, B., Pillai, S., Duraccio, D., & Silvestre, C. (2014). Bioplastics and MAP to enhance sustainable packaging and food quality: The role of electron beam (eBeam) technology as a platform technology for enhancing packaging materials and food quality. IFT'14, New Orleans, USA.

[44]. Zeman, S., & Kubík, L. (2007). Permeability of polymeric packaging materials technical sciences. *Techn. Sc.*, *10*. DOI 10.2478/v10022-007-0004-6.

[45]. Simoneau, C. (2009). *Guidelines on testing conditions for articles in contact with foodstuffs*. European Communities. (JRC Scientific and Technical Reports). Retrieved January 14, 2016, from http://www.iss.it/binary/moca/cont/guide-lines_test_conditions.pdf.

[46]. Zygoura, P., Paleologos, E., & Kontominas, M. (2011). Effect of ionizing radiation treatment on the specic migration characteristics of packaging – food simulant combinations: Effect of type and dose of radiation. *Food Addit. Contam.*, *28*, 686-694.

[47]. Jeon, D.H., Park, G.Y., Kwak, I.S., Lee, K.H., & Park, H.J. (2007). Antioxidants and their migration into food simulants on irradiated LLDPE film. *LWT*, 40(1), 151-156.